Investigation of Oxygen Rebound Utilizing a Novel Mononuclear Nonheme Complex: Kinetic and Structural Investigations

By
Thomas M. Pangia

A dissertation submitted to Johns Hopkins University in conformity with the requirements for the degree of Doctor of Philosophy

Baltimore, Maryland
January 2019

Abstract

Many heme and nonheme enzymes contain iron ligated in their respective active sites, which is key to the facilitation of vital biological transformations. Both enzymes are known to enact common pathways in the incorporation of dioxygen into various substrates. Common intermediates such as iron-oxo and iron-hydroxo species have been investigated using model complexes, as to allow the study of bond-forming and bond-breaking reactivity which occurs at the metal centers. This dissertation contains reactivity studies on a novel iron(III)-methoxo complex to better understand the mechanism of oxygen radical rebound in nonheme iron enzymes. An overview of key high-valent iron intermediates and complexes is featured in Chapter 1, as well as the introduction to the rebound mechanism.

In Chapter 2, the synthesis of the novel iron(III)-methoxo complex is discussed. The material culminated from the synthesis of a new organic ligand with structural modification to encourage mononuclearity. The ferric material forms from its ferrous precursor when open to atmospheric oxygen, and provides a platform from which an analog of rebound could be directly investigated.

Chapter 3 discusses the measure of reactivity of the iron(III)-methoxo complex with a stable carbon-based radical. The organic product was identified and quantified, while the one-electron reduced iron material was also observed and quantified. This observation of rebound in the iron(III)-methoxo system provided valuable information regarding oxygen rebound in a mononuclear nonheme iron complex.

Chapter 4 utilizes the iron(III)-methoxo material in reaction with several additional organic radicals, to investigate whether the observed rebound reactivity occurs in a

concerted or stepwise fashion. Hammett and Marcus analysis was employed, indicating that the transformation was concerted, as would be expected of a rebound reaction.

Chapter 5 gives the synthesis of several other iron complexes, with the potential for further investigation of rebound reactivity with regards to chlorine and fluorine. Preliminary reactivity indicates some success, providing a possible avenue toward the study of halogen rebound.

Committee Members:

Dr. David Goldberg

Dr. Ken Karlin

Dr. John Toscano

Acknowledgements

I express my sincerest gratitude to all of those who have contributed either directly, or inspirationally, to the completion of this dissertation. I would like to thank my research advisor, David Goldberg, for accepting me into his research group at Johns Hopkins University, and for the support he's given me during my time here. I've learned many things from him, and I am especially grateful for his ability to guide me in my research projects. I'm also thankful to Professor Karlin and Professor Toscano for being on my thesis committee, and for the examples they've provided for me of successful research faculty.

Many of the people working in the Chemistry Department also deserve special thanks, and without their work, this dissertation could not have been possible. I particularly thank Max Siegler, who solved each of the crystal structures described in this dissertation, Joel Tang for the help with EPR experiments, and Phil Mortimer for the mass spectrometry instrument help. I would also like to thank others in the department who tirelessly work behind the scenes: Lauren McGee, John Kidwell, Joe Russell, Indira Jones, Jasmine Harris, Jean Goodwin, Rosalie Elder, and particularly Boris Steinberg.

During my graduate work it was a privilege to collaborate with some of the premier experts in the scientific field, and I have benefited tremendously from their knowledge. Professor Guy Jameson (University of Melbourne) and his students Casey Davies and Joshua Prendergast collected and analyzed Mössbauer data for materials in Chapters 3 and 4. Professor Sam de Visser (University of Manchester) and his students Emilie Gérard and Yen-Ting Lin provided valuable DFT calculations for the experiments in Chapter 4.

I also thank Sumit Sahu, Alex Confer, and Jesse Gordon for their help, either providing guidance with synthetic techniques, or helping with collection and analysis of Mössbauer spectroscopy. I'm also grateful to Alex for the great discussions on research, ideas for project development, and future goals beyond graduate school. I thank the rest of the Goldberg Lab, both past and current members: Alison, Heather, Gina, Evan, Paulo, Alex, Nick, Jesse, Jireh, Jeremy, Aniruddha, Vishal, Geoff, Jithin, David, and James for making the lab a fun place to work in these past years. I'm going to miss the great research discussions and group meetings, punctuated periodically with birthday celebrations.

Finally I'd like to thank the most important people of all, my family. I'd like to thank my parents, Michael and Laura, for their encouragement in pursuing these academic goals, and for teaching me many of the things that I would need for this journey. I also thank my wife, Tori, for her unending support and encouragement over the years, and for helping me to take time to relax and enjoy myself. I'm also thankful to Tori's parents, Bob and Mary Ulich, for their guidance and encouragement, even when I was speaking the sometimes foreign language of chemistry. I'm grateful to Tori's entire family as well for including me in so many of their traditions, especially the annual ski vacation. I'm incredibly thankful that Tori's late grandmother Joan Ulich traveled to attend my dissertation defense, shortly before she passed away. And last of all, I want to thank my grandfather, Michael Pangia. Whether I was successful in my various projects or not, he reminded me that the education that I was receiving was the greatest gift I could give to myself, and can never be taken away. It's been a tremendous blessing to have all of this support and to have partaken in the journey of graduate school, and I'm thankful for the experience.

For my wife,

Thanks for your faith in me

Table of Contents

Index of Tables

Chapter 3. Observation of Rebound in a Nonheme Mononuclear Iron Model Complex

Chapter 4. Kinetic Investigation of Rebound in a Nonheme Model Complex

Chapter 5. Evaluation of Oxygen Reactivity and Halogen Rebound in Additional Compounds

Index of Figures

Chapter 1. Introduction

Chapter 2. Synthesis and Characterization of a Terminal $Fe^{III}(OCH_3)$ Complex

Chapter 3. Observation of Rebound in a Nonheme Mononuclear Iron Model Complex

Chapter 5. Evaluation of Oxygen Reactivity and Halogen Rebound in Additional Compounds

Index of Schemes

Chapter 1. Introduction

Chapter 2. Synthesis and Characterization of a Terminal $Fe^{III}(OCH_3)$ Complex

Chapter 3. Observation of Rebound in a Nonheme Mononuclear Iron Model Complex

Chapter 4. Kinetic Investigation of Rebound in a Nonheme Model Complex

Chapter 5. Evaluation of Oxygen Reactivity and Halogen Rebound in Additional Compounds

Chapter 1 Introduction

1.1. Dioxygen Activation in Nonheme Enzymes

An ongoing focus in the inorganic, bioorganic, and bioinorganic and chemical arenas is the investigation of the nature and ability of both heme and nonheme enzymes to activate molecular and atmospheric oxygen in order to incorporate oxygen atoms into various substrates. Oxygen incorporation into organic substrates, either in the form of one or both of the dioxygen atoms, is done by many of these heme and nonheme enzymes.[1-3] Thus dioxygen is a key biosynthetic building block due to its ubiquity (roughly 20.94% of the planetary atmosphere), and is vital in the sustenance of aerobic life and biological cycles.[4]

Oxygen is a bit of a paradox, existing in a stable state and incapable of reacting with many organic compounds in spite of its inherent diradical nature (Scheme 1.1), and the barrier to its activation is quite high. However, the cleavage of the oxygen-oxygen bond is exothermic and energetically-favorable in spite of the stable nature of the molecule.

Scheme 1.1. Representation of diradical forms of dioxygen.

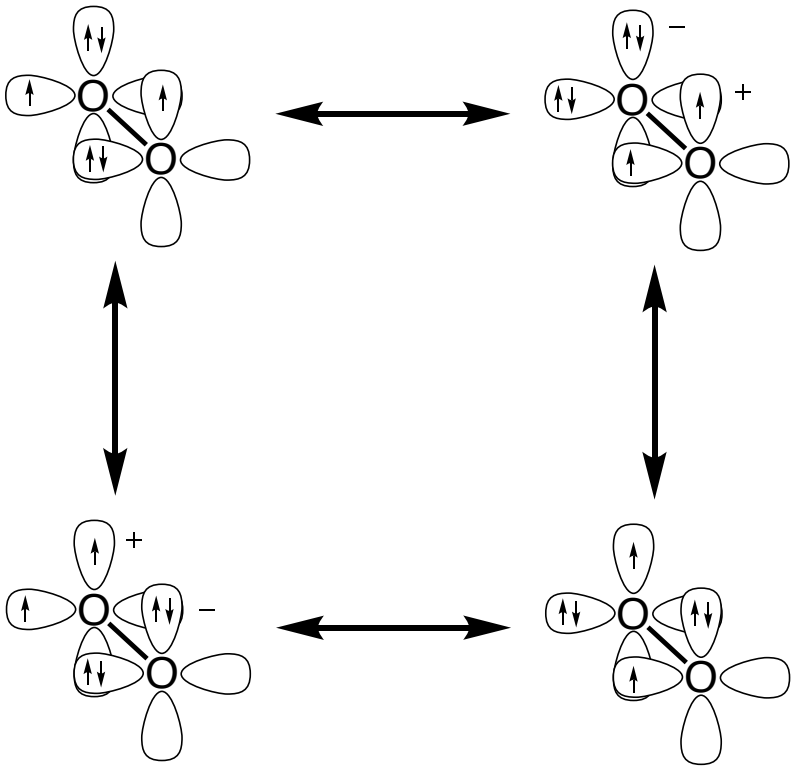

To access inherent reactivity of O_2, metalloenzymes are useful. They are capable of facilitating incorporation of O_2 into substrate molecules. Unaided incorporation of dioxygen at ambient temperatures is low. This low level of reactivity results from the diradical triplet ground state of dioxygen. The two oxygen atoms of the molecule share six electrons in their 2p orbitals, while the remaining two unpaired electrons reside in a set of degenerate antibonding orbitals (Scheme 1.1). This then would describe dioxygen as having a formal bond order of two, with the lowest energy orbitals capable of accepting electrons being antibonding. Furthermore while the dioxygen possesses a triplet ground state, stable organic substrates are normally comprised of singlet (paired) ground states, and interaction between these ground states are spin-forbidden.[1] Nature accomplishes the biological addition of dioxygen by utilization of transition metals (e.g. Fe, Cu, Mn) in appropriate oxidation states that are capable of forming adducts directly with O_2 (Scheme

1.2).[2-3] This dissertation will focus on some of the mechanistic transformations that are implicated in these reactions in nonheme iron oxygenase enzymes.

Scheme 1.2. Dioxygen activation pathway in nonheme iron model complexes

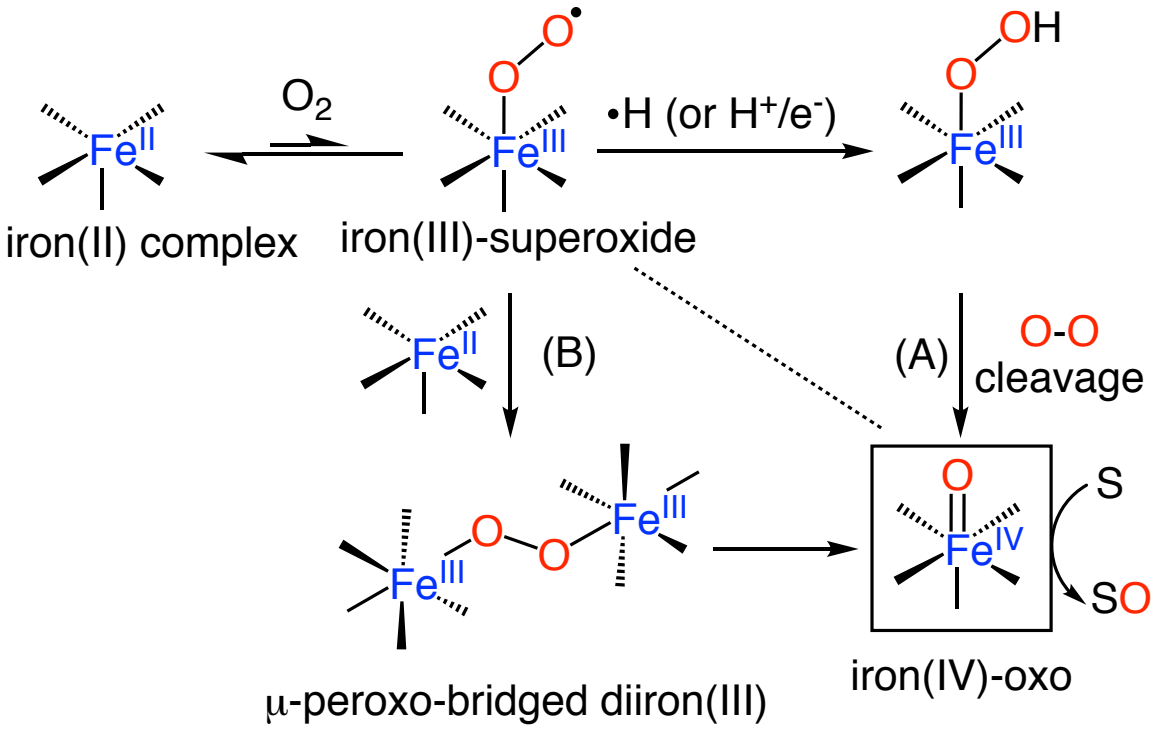

Of primary interest here is the nonheme class of these enzymes. Some of the examples that are shown here incorporate atmospheric oxygen into organic substrates by hydroxylation of C–H bonds (Scheme 1.3).[5] The presence of iron in these nonheme enzymes combined with iron's ability to attain multiple redox states increases iron's utility as an O_2-activation aid. While heme and nonheme enzymes have large variations in active site structure, the iron-oxygen intermediates generated during their respective transformations are often similar (Scheme 1.2).[3]

Activation of dioxygen in a synthetic nonheme iron model complex may occur through either of the proposed pathways shown in Scheme 1.2. Initial coordination of dioxygen to an Fe^{II} complex coupled with charge transfer gives what is commonly

proposed to be a ferric–superoxo adduct, the first intermediate in the dioxygen activation cycle.[3] The characterization of this intermediate has proven challenging, and there have been little evidence of the intermediate observed in a mononuclear nonheme iron enzyme, save for some indication in isopenicillin N synthase (IPNS).[6] Additionally in the dinuclear *myo*-inositol oxygenase (MIOX) there has been found evidence of a ferric–superoxo complex.[3, 7] Addition of a source of protons/electrons can further induce the reactivity along pathway (A) (Scheme 1.2). To explain the loss of one of the oxygen atoms, both homolytic and heterolytic cleavage mechanisms have been proposed for the subsequent step. The final product in this case is often an $Fe^{IV}(O)$ species. An additional option for reactivity may occur when another ferrous center takes the place of the proton/electron source of pathway (A), as shown in pathway (B). This results in a peroxo-bridged dinuclear species, which by homolytic cleavage gives the same terminal mononuclear $Fe^{IV}(O)$ as in pathway (A). The $Fe^{IV}(O)$ complex is an effective oxidant in substrate oxidation reactions.

Scheme 1.3. Nonheme iron enzymes. Adapted from Reference 3.

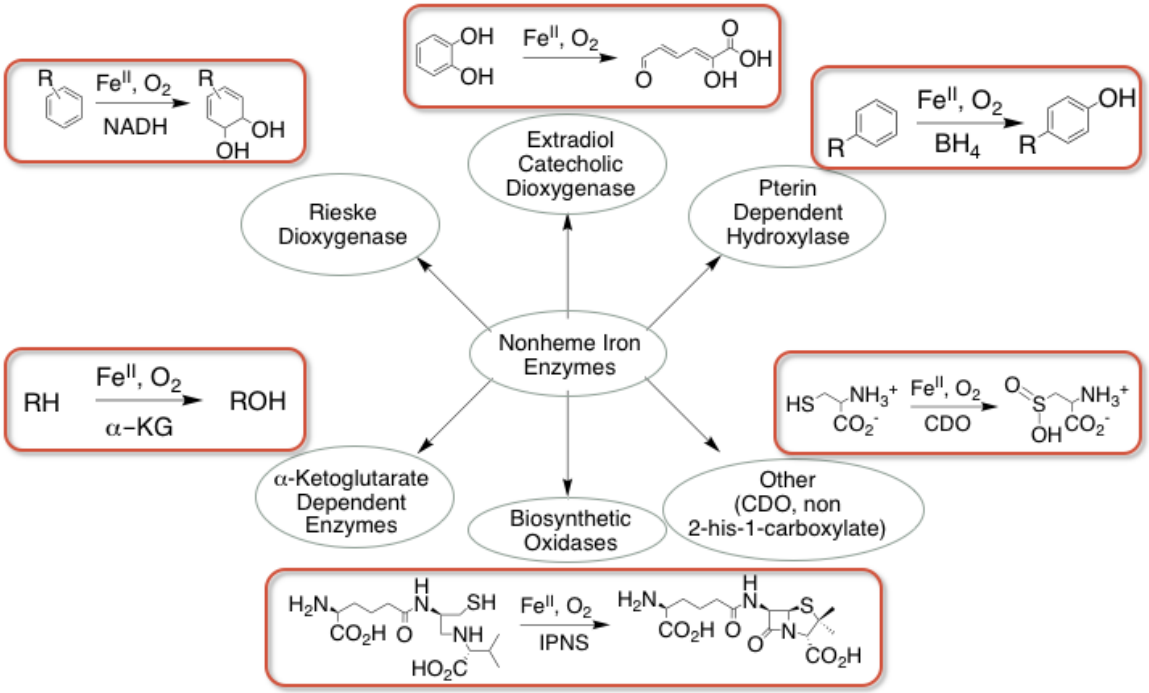

As noted, hydroxylation of C-H bonds is one key area of focus. Nonheme iron enzymes are able to carry out the valuable functionalization of substrates in order to produce biologically-relevant transformations and signals. The environment around the metal center plays a large part in the transformations that are allowed. Coordination by N, O, and S donors from amino acids such as histidine, tryptophan, and cysteine are common motifs. Additional amino acids surrounding the active site may also introduce important hydrogen-bond donors or acceptors that interact with oxygen adducts formed during these catalytic transformations.[2] One well-known heme-type enzyme Cytochrome P450 carries out such transformations (Scheme 1.4).[5, 8-9] The distal S-donor cysteinate is significant in the reactivity of the enzyme toward dioxygen.

Scheme 1.4. Cytochrome P450 hydroxylation of alkane substrate.

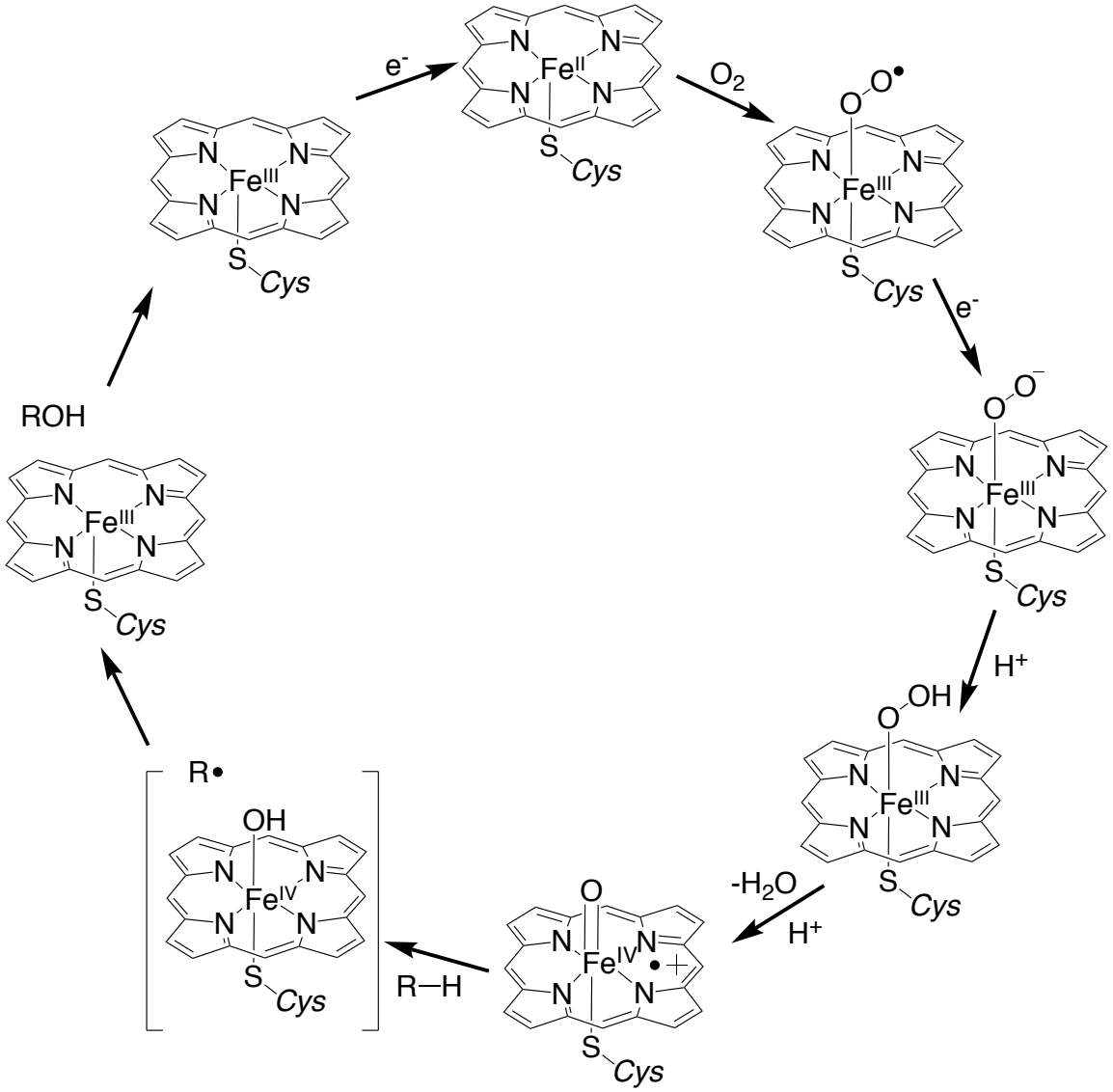

The enzyme contains a labile site, and activation of dioxygen begins with the binding of substrate, followed by an electron transfer, which produces a ferrous center that affords binding of dioxygen. The ferric–superoxo species undergoes an additional electron transfer, and protonation to form a hydroperoxide species, which is again protonated to induce dehydration. The dehydration product, $Fe^{IV}(O)$ cation radical, carries out hydrogen atom transfer on the captive substrate. The resulting $Fe^{IV}(OH)$ intermediate transfers the hydroxyl portion to the adjacent substrate radical during the rebound portion of the

mechanism, resulting in the formation of the new C-O bond and the one-electron reduced iron center.

A nonheme example of such a transformation comes from the enzyme taurine αKG dioxygenase (TauD), which is capable of hydroxylating the α-CH_2 adjacent to the sulfate on taurine (Scheme 1.5).[3, 5, 10] A six-coordinate mononuclear ferrous center is coordinated with two histidine ligands, an aspartate/glutamate ligand provided by the protein backbone. Dioxygen is used by this enzyme to hydroxylate unactivated carbon atoms in taurine and other organosulfonates.

Scheme 1.5. TauD hydroxylation of taurine substrate.

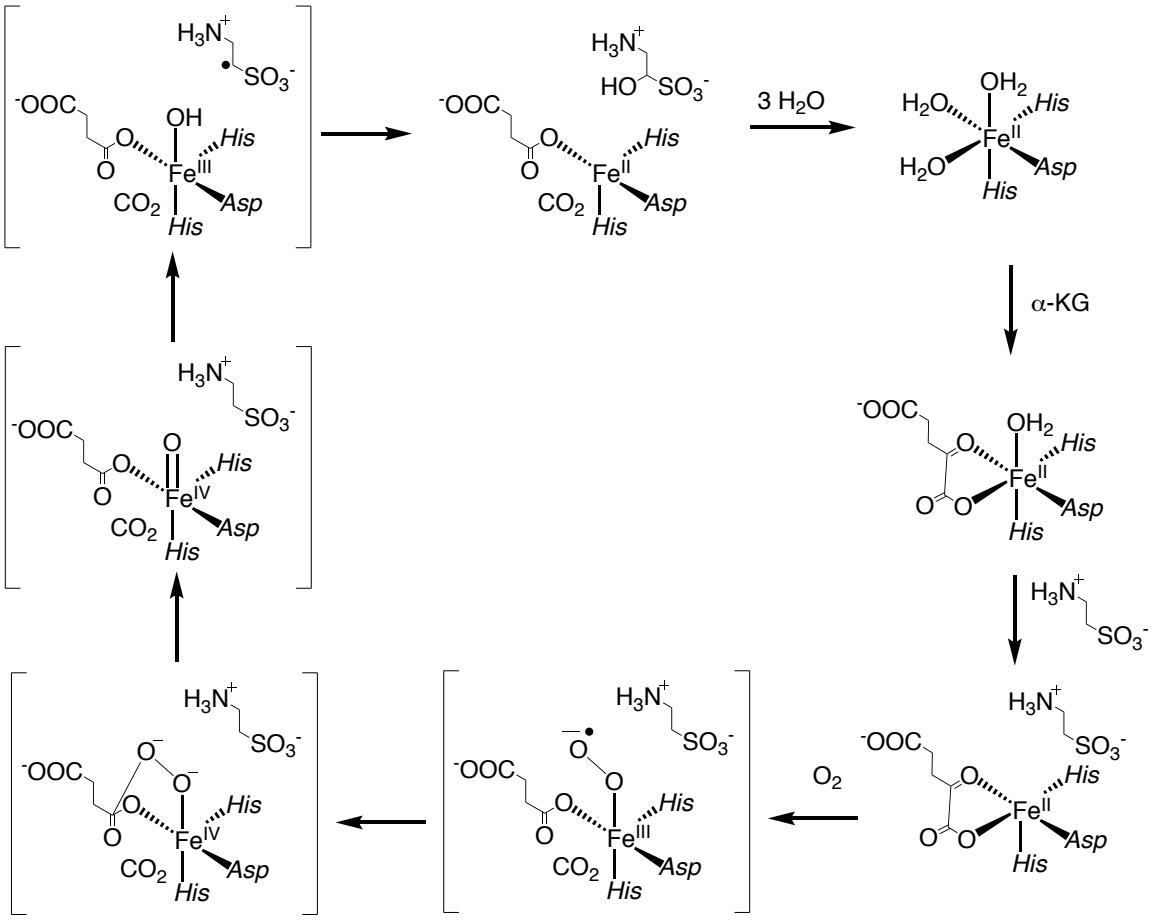

The initial complex becomes bound by αKG, which induces substrate to associate with the complex (although not in a coordinating manner). It is proposed that the conformational triggers of H_2O dissociation from the active site and binding of the substrate greatly increases the reactivity of the enzyme toward dioxygen, favoring formation of the reactive intermediates only when substrate is present. The necessary presence of the substrate likely reduces the possibility of any self-oxidation reactions that could inhibit the enzyme.[11] The dioxygen binding leads to a ferric–superoxo complex, which is thought to form a bicyclic complex by attack on αKG. This leads to the cleavage of the O–O bond and subsequent formation of an $Fe^{IV}(O)$ intermediate. This intermediate interacts with and abstracts a hydrogen atom from the adjacent substrate to form what has been proposed as an intermediate $Fe^{III}(OH)$ and radical. These species then undergo what has been dubbed "oxygen rebound" to transfer the hydroxyl moiety to the radical, yielding the hydroxylated substrate product as well as the one-electron reduced Fe^{II} center.[10-11]

In addition to the mechanistic understanding obtained from the study of these enzymes, insight has also been brought about from the synthesis of small molecule active-site model-complexes. Through the understanding of the enzymatic processes applied using small molecule complexes, a great deal of catalytic or therapeutic benefit also exists. On an industrial scale, it can be valuable to functionalize raw hydrocarbon materials in order to obtain useful products from potentially cheap and abundant feedstocks. The advent of hydraulic fracturing ("fracking") has allowed for development of shale oil formations which have until now been inaccessible by traditional crude oil pumping methods. A large amount of hydrocarbon-based fuels and fuel precursors have been made accessible due to the increased functionality and usage of fracking, particularly in the Midwestern United

States, as well as parts of Canada and Alaska. Such hydrocarbons, previously encased in shale formations which were not accessible by conventional pumping and extraction techniques, are now readily available and have contributed greatly to the United States' larger role in global energy (Figure 1.1).

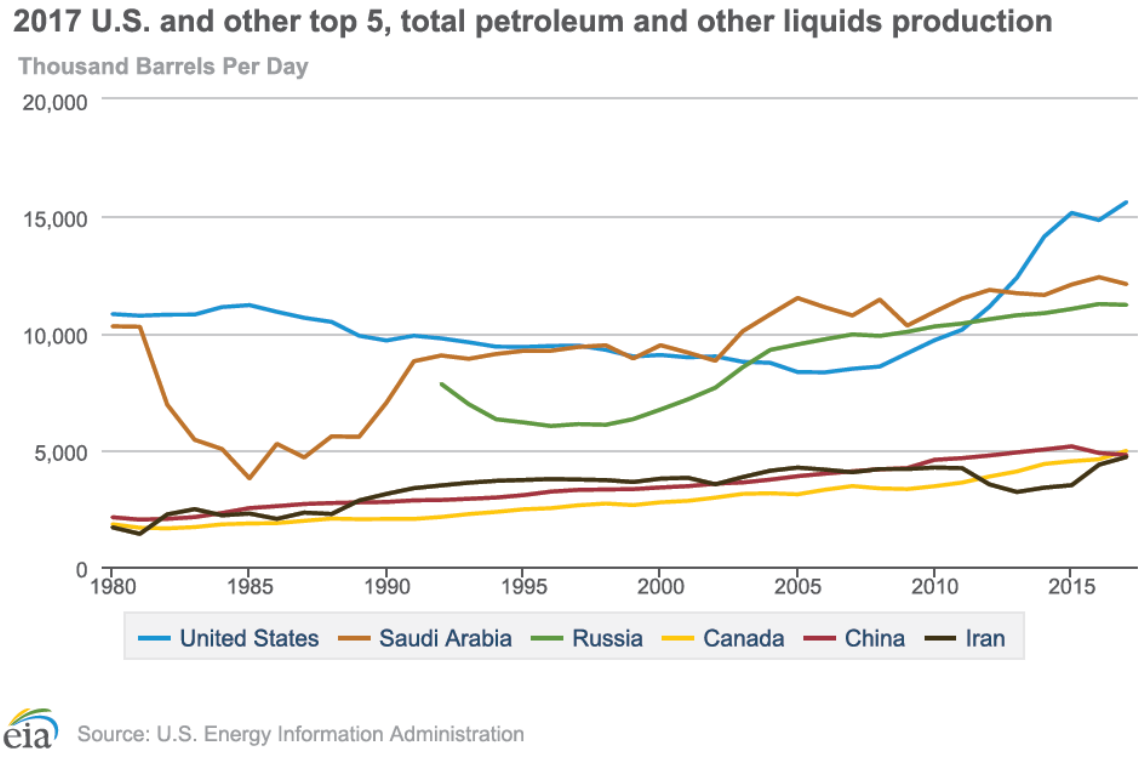

Figure 1.1. Global top-five oil producing nations, production levels since 1980 (https://www.eia.gov).

The natural gas (lighter and more volatile hydrocarbons such as methane and ethane) element of such extracted compound is of a particular interest since large portions of these lighter hydrocarbons commonly escape from the crude fuel mixtures when extracted or transported. Such hydrocarbons, including the volatile and gaseous methane, are classified as greenhouse gases,[12-13] and have the potential to contribute significantly to climate change. Large amounts of heat could be trapped by these gases due to their C-H bond vibrations in the infrared absorbance range (3000-3500 cm^{-1}), compared to the lower-

energy absorbance at 2350 cm^{-1} exhibited by carbon dioxide.[14] The net result of this "climate forcing" effect is that energy irradiated into the earth's atmosphere is absorbed by components of the atmosphere, which results in an increase of energy present, and subsequent temperature increase.

To avoid releasing large amounts of these hydrocarbons into the atmosphere, companies burn most of these gaseous or volatile hydrocarbons directly upon extraction to produce the much less-effective greenhouse gas, carbon dioxide. Unfortunately, this is a practice that is both wasteful and consumes valuable fuel without deriving any benefit (energy) from the consumption, while still producing greenhouse gas. Were there an effective and widely accessible method of activating the C–H bonds of methane and other volatile hydrocarbons, these bonds might be hydroxylated to produce methanol or other solvents, which would be liquid and more readily transportable. Additionally such recaptured liquid combustibles could then be utilized as sources of energy production, or else feedstocks for other industrial processes. The use of C–H hydroxylators such as those mentioned above potentially serve as models which might be capable of activating oxygen and inserting it into an alkane C–H bond, which would make accessible portions of natural gas which are more difficult to utilize using current technological means.

There are significant advances which could also be made in medical treatments from research into nonheme enzymes. For example, cysteine dioxygenase (CDO) is responsible for S-oxygenation of cysteine to generate cysteine sulfinic acid.[3] The mononuclear active site contains a facial triad of three histidine ligands, which is less common than the two-histidine-one-carboxylate binding environment that is more likely to be found in a mononuclear nonheme iron enzyme. CDO is responsible for the regulation

of cysteine in the body, which is necessary for human life and development. Cysteine, as one of the two sulfur-containing amino acids present in the human body, is one of the primary components in protein synthesis, and is a precursor for several other biologically-relevant molecules of glutathione and coenzyme A.[15] Additionally, cysteine present in the body at extreme concentrations has also been implicated as a cause of neurological damage that may result in Alzheimer's or Parkinson's.[15-16] The regulation of cysteine at proper concentrations by synthesis into subsequent metabolites of sulfate, taurine, and hypotaurine is of interest in medicinal chemistry,[15, 17] and increased understanding of the mechanism has potential to treat some of these neurodegenerative disorders.[15-16]

It has been proposed that during the activation of dioxygen by CDO (Scheme 1.6) the initial ferrous species, bound by water in the open coordination sites,[18-19] is subsequently coordinated by the nitrogen and sulfur of a cysteine amino acid.[16-17, 20] Dioxygen becomes bound at the 6th coordination site, and gives a single electron transfer which leads to the formation of a ferric–superoxo species. The distal oxygen radical is proposed to bind to the sulfur and give a 4-membered ring, then to undergo homolytic cleavage. The sulfur-oxygen bond undergoes rearrangement to result in sulfenato oxygen binding to the iron center. The oxygen of the $Fe^{IV}(O)$ species then binds to the sulfur to form the cysteine sulfinic acid product, which is displaced by water to reform the starting complex.

Scheme 1.6. Mechanism of dioxygen activation by CDO.

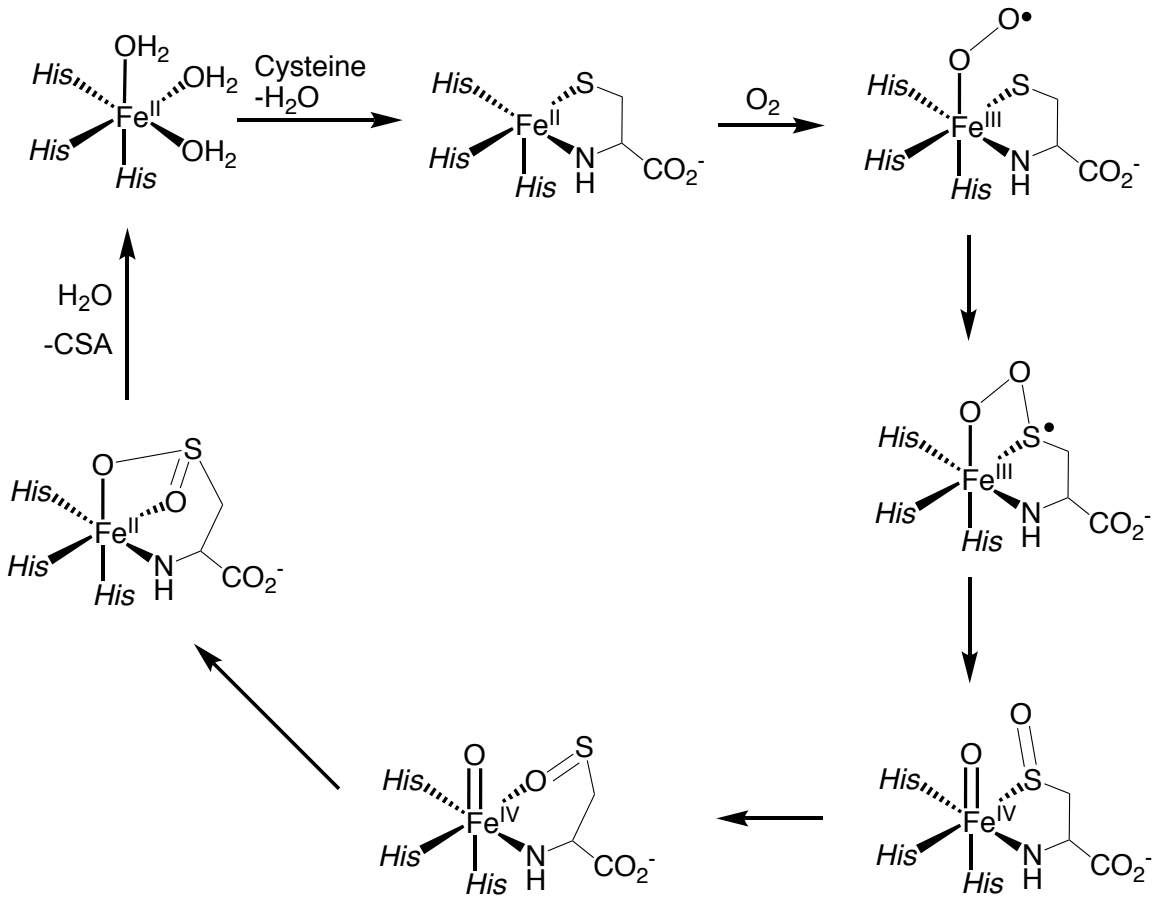

Both the heme and nonheme hydroxylases are related in that they possess high-valent oxo intermediates, which are drivers of their respective hydroxylations or oxidations.[5] These intermediates are proposed to carry out the key hydroxylation oxygen transfer step using what has been dubbed the "rebound mechanism".[5] First, the high valent oxo species abstracts a hydrogen from the substrate. The resulting substrate radical, initially closely associated with the metal-hydroxo product of hydrogen atom abstraction (HAT), is then capable of reacting, by different mechanisms (Scheme 1.7).[5] On remaining closely associated the oxygen atom "rebounds" to attach to the alkyl radical and form a new hydroxylated product, which is free to dissociate and give rise to the free alcohol and

one-electron-reduced metal product. This transformation occurs rapidly and with retention of stereochemistry.

Scheme 1.7. Possible reaction mechanisms for a nonheme iron-oxo.

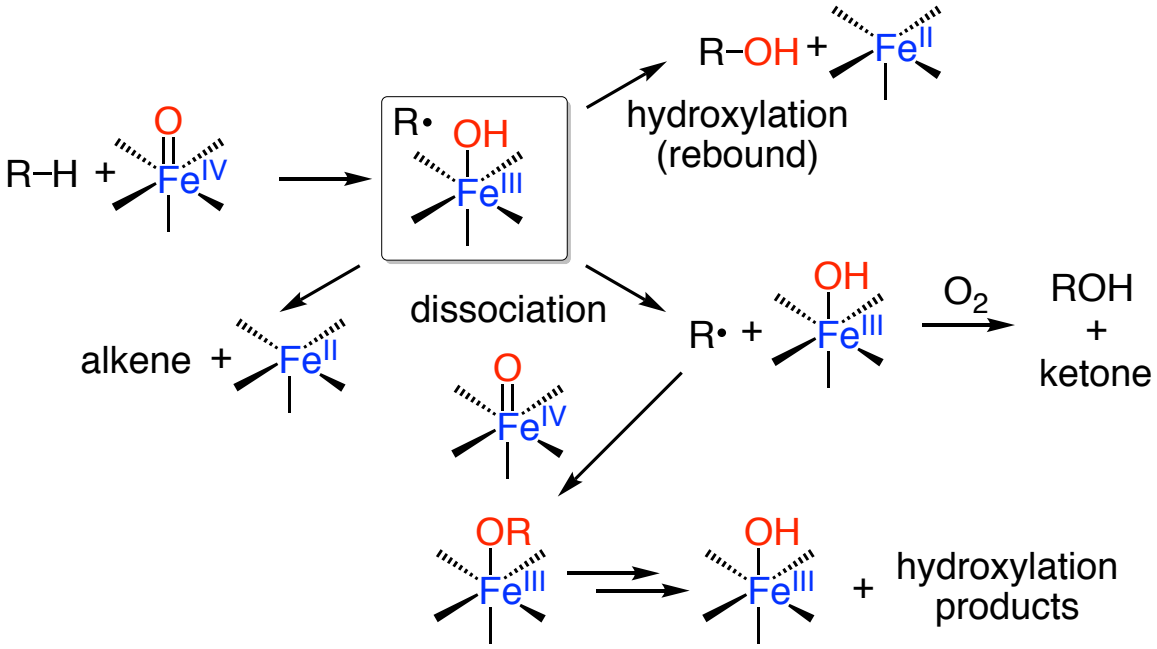

While the rebound is the desired outcome in many cases, there are reaction pathways which may occur. The radical may undergo a transformation which results in alkene-type products/desaturation and the 1-electron-reduced metal center (Scheme 1.7).[21-23] When considering synthetic catalyst systems modeling the analogous reactivity, the proximity of the substrate radical and metal center must also be considered. In these synthetic models, it is also possible for the radical and Fe(OH) components to dissociate and drift apart. If the radical dissociates from the solvent cage, exposure to errant oxygen can form radical oxidation products of alcohols and ketones/aldehydes.[24] The radical might also interact with other metal-oxo compounds to eventually give new hydroxylated products.

While oxygen rebound is an area of mechanistic relevance in oxygenase enzymes, there are other atoms which are capable of rebound in a similar fashion. Other enzymes

where radical rebound is an important concept include the halogenases.[25] The halogenase class of enzymes, particularly SyrB2 and WelO5, perform the installation of halogen (Cl or Br) atoms onto saturated carbon centers.[25] An iron (II) center coupled with 2-oxoglutarate (2OG), along with O_2, produce an iron (IV) intermediate similar to those discussed above (Scheme 1.8). However, following abstraction of the substrate hydrogen, there remains a ferric complex possessing both halogen and hydroxo ligands, each of which is theoretically able to combine with the carbon radical R• ("rebound" step) (Scheme 1.8).

Scheme 1.8. Halogenation vs hydroxylation in halogenase enzymes.

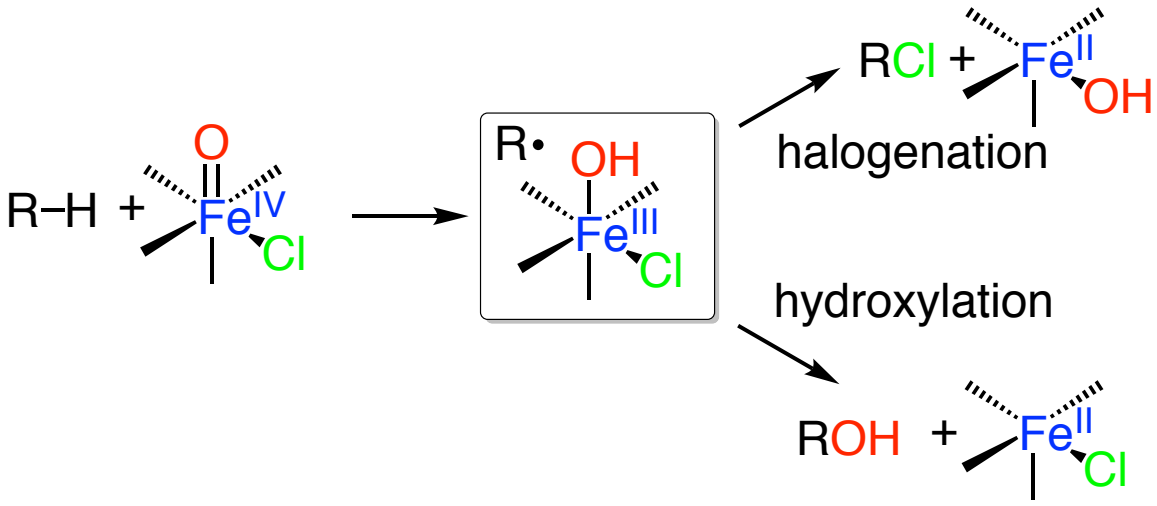

Aside from the potential competition between the possibility of halogen rebound and hydroxyl rebound, alternative mechanisms are also possible. Rearrangement of the radical may produce similar mechanistic alternatives as in the above oxygen-only rebound mechanism. Considering synthetic model complexes, dissociation of the solvent cage complex may also result in alternative pathways.

The potential for competition between halogen and hydroxyl rebound occurs with enzymes capable of both pathways. Halogenases that are capable of enacting halogen rebound exclusively are therefore of considerable mechanistic interest.[25] The orientation

of the halogen within the enzyme active site appears to be a major driver of the halogenation, as opposed to hydroxylation (Scheme 1.8).

1.2. Dioxygen Activation and Iron-Oxygen Adducts

Synthetic complexes have been utilized as well as enzymes to understand the steps responsible for oxygen transfer. Efforts have been made to model, isolate, and characterize several of these species, such as the Fe(OH) and Fe(O). One of the intermediates of primary interest in the dioxygen activation mechanism is the initial ferric–superoxo complex that. The formation of a synthetic species capable of stabilizing such a ferric–superoxo has been shown to be challenging, with only few examples existing in nonheme investigations.[3] While a goal has been to characterize the mononuclear nonheme species, there was previously some success in the characterization of a dinuclear dioxygen adduct in 2005.[26] The complex was composed around a substituted TPA-based framework which had been shown on earlier occasion to interact with dioxygen under separate conditions.[27]

Scheme 1.9. Generation and reaction of a dinuclear ferric–superoxo complex.[26]

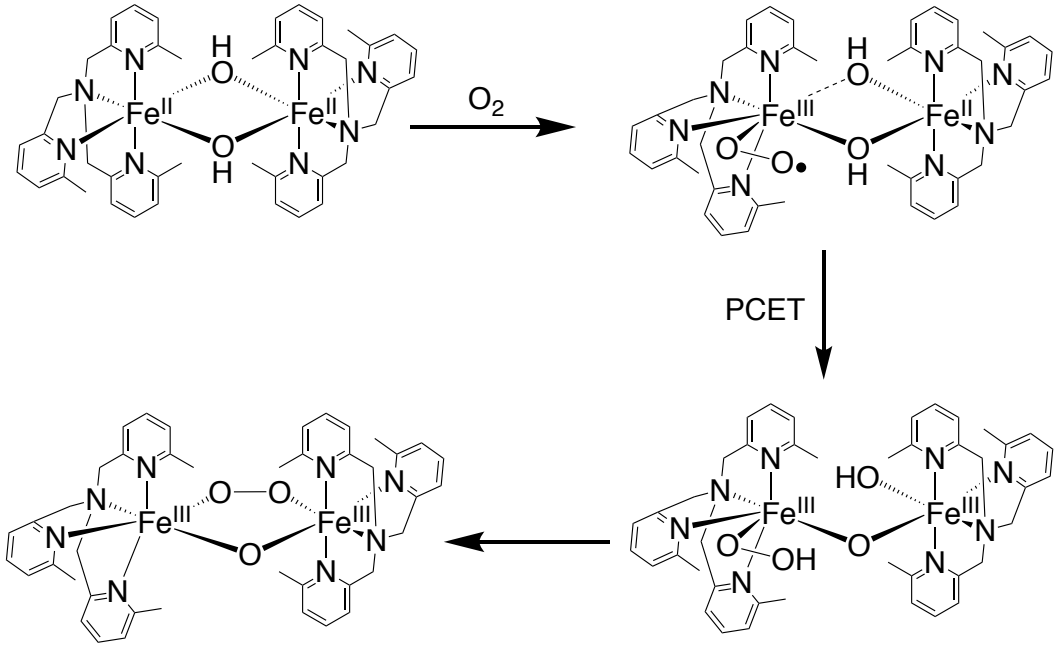

Both difficult to synthesize and isolate, the diferric–superoxo intermediate was formed at low temperature (-80 °C) and persisted only long enough to obtain some spectroscopic characterization. Some of the prominent features of the complex consisted of intense absorbance features at 325 nm (ε = 10,300 M^{-1} cm^{-1}), as well as features at 500 nm (ε = 1,400 M^{-1} cm^{-1}) and 620 nm(ε = 1,200 M^{-1} cm^{-1}). When warming the solution to higher temperatures (-60 °C), a species formed that was characterized as a (μ-oxo)(μ-1,2-peroxo)diiron(III), a dark-green complex with some additional distinct UV characteristics at 494 nm (ε = 1,100 M^{-1} cm^{-1}), 648 nm (ε = 1,200 M^{-1} cm^{-1}), and 846 nm (ε = 230 M^{-1} cm^{-1}). When bubbling inert gas through the solution of the diferric–superoxo complex using $Ar_{(g)}$, there was no reversal of superoxo formation by putative displacement of O_2, even after prolonged exposure. Additionally, attempts to form the diferric complex by alternative methods were unsuccessful. Generation of the oxo–peroxo species at -60 °C and cooling to -80 °C did not form the diferric–superoxo complex. However during

oxygenation experiments of the precursor compound, the formation of the intermediate diferric–superoxo was possible at -75 °C and -90 °C. Characterization by resonance Raman spectroscopy showed evidence of $\upsilon(O–O)_{superoxo}$ at 1310 cm^{-1}, giving valuable insight into the characteristics of the diferric–superoxo complex and subsequently its mechanism of O_2 activation.[26]

To further underline the difficulty in investigating the reactivity between mononuclear Fe–complexes and dioxygen and observing formed intermediates, it was not until 2014 that any subsequent mononuclear ferric–superoxo compounds were fully characterized.[3, 28] A monuclear ferric–superoxo complex bearing a sterically-encumbered yet efficiently-synthesized dialkylate-bearing ligand was isolated and characterized. While there had been several heme-type superoxo complexes previously obtained, and dinuclear nonheme iron–superoxo materials observed, this was the first example of a synthetically-generated nonheme monuclear ferric–superoxo complex.[28]

Scheme 1.10. Reaction of a mononuclear nonheme iron complex with dioxygen.[28]

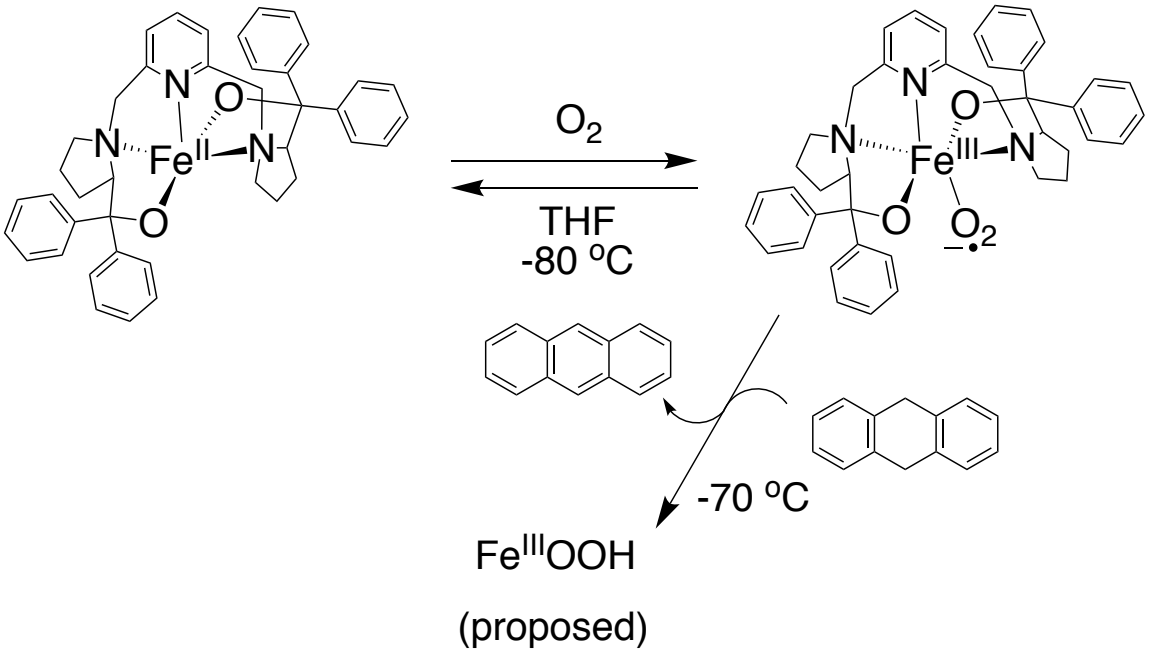

The Fe^{II} complex (characterized by XRD) was observed to be 5-coordinate, with an open site available for dioxygen binding. The ferric–superoxo complex was observed when dioxygen was bubbled through a solution of the ferrous complex at –80 °C, with intense UV-absorption at 330 nm (ε = 9,400 M^{-1} cm^{-1}), similar to what was previously observed in the diferric–superoxo complex $[Fe^{II}(\mu\text{-}OH)_2(6\text{-}Me_3TPA)_2]^{2+}$.[26] The ferrous complex regenerates when the solution of the newly-formed ferric–superoxo complex is purged with N_2 while maintaining –80 °C, indicating a reversible O_2 binding to the iron(II) center. Excitation of the ferric–superoxo with visible irradiation produced a resonance-enhanced vibration of 1,125 cm^{-1}. The open coordination site combined with the observed vibrational frequency attributed to the superoxo O-O stretch was evidence of an end-on superoxide binding moiety. Under further investigation, the ferric–superoxo was found capable of oxidizing dihydroanthracene, which is consistent with t hydrogen atom abstraction from the C–H substrate.[28]

A few other illusive nonheme ferric–superoxo complexes have been characterized. A mononuclear side-on ferric–superoxo complex stabilized with a tetraamido macrocyclic ligand (TAML) was formed upon exposure of the parent ferrous complex to KO_2.[29] The species was found to remain stable at -20 °C, showed a UV absorbance band at 490 nm (ε = 2,600 M^{-1} cm^{-1}), an absorbance markedly different than previously observed end-on-bound superoxo complexes. The stability at low temperature afforded by the TAML framework allowed for isolation of crystals for structural analysis.

Scheme 1.11. Generation of a side-on ferric–superoxo complex.[29]

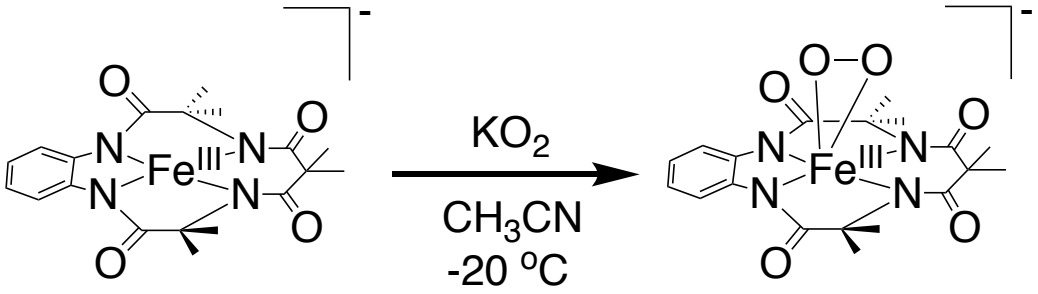

Appropriate mass shifts of four mass units upon labelling with $K^{18}O_2$ indicated incorporation of the O_2 into the ferric–superoxo complex. Appropriate shifts are also observed when infrared spectroscopy was employed, an O–O stretching vibration of 1,260 cm^{-1} for the unlabeled compound which shifts to 1,183 cm^{-1} upon labelling, consistent with previously observed complexes.[3] Mössbauer spectroscopy showed features (δ = 0.096 mm s^{-1}, ΔE_Q = 2.696 mm s^{-1}) consistent with intermediate-spin Fe(III) when bound to the TAML framework. Examination of the EPR spectrum showed no observed signal, which could have indicated either an iron(IV)–peroxo (S = 1 or 2), or an iron(III)–superoxo (S = 1/2, 3/2, or 5/2) coupled with a superoxide unit (S = 1/2). The observed infrared spectrum with an O-O stretching vibration at 1,260 cm^{-1} was consistent with the range of 1,125-1,310 cm^{-1} reported for other iron(III)–superoxo complexes,[26, 28, 30-31] and confirmed the assignment of the compound as a ferric–superoxo. Observed reactivity indicated that the superoxo moiety was capable of nucleophilic reactivity, as well as intermolecular O_2-transfer. A series of substituted phenols was used to demonstrate O-H bond activation, and a linear relationship was shown, with electronegativity of *para*-phenol substituents greatly affecting reactivity. The kinetics of aldehyde deformylation showed a linear relationship with the identity of the *para*-substituents on a series of benzaldehydes, indicating that the ferric–superoxo was an active nucleophilic agent. These results, taken together, gave

valuable insight into the formation of the ferric–superoxo complex, as well as information on its reactivity.

Shortly after, in 2015, another ferric–superoxo complex was isolated, this time consisting of a mixed-ligand system of tridentate hydrotris(3,5-dimethylpyrazolyl)borate (Tp^{Me2}) and bidentate imidazolyl-containing borate ligands $[B\text{-}(Im^{N\text{-}Me})_2MePh)]^-$.[3, 32] While such Tp^R-based frameworks had been previously used in conjunction with other bidentate ligands in iron(II) complexes to activate O_2, there had been no detection of any putative mononuclear ferric–superoxo complexes. Formation of dinuclear iron(III)–μ–peroxo complexes, resulting from ligand isomerization or immediate reaction of dioxygen with ligands, precluded the mononuclear ferric–superoxo formation in previous experiments. The above mixed ligand system which successfully formed an observable mononuclear ferric–superoxo complex was selected for both robustness toward oxygenation as well as strong chelating nature, which prevented the above rearrangements and reactions that result in dinuclear iron(III)–μ–peroxo formation.

Scheme 1.12. Reaction of a mixed-ligand mononuclear iron complex with dioxygen.[32]

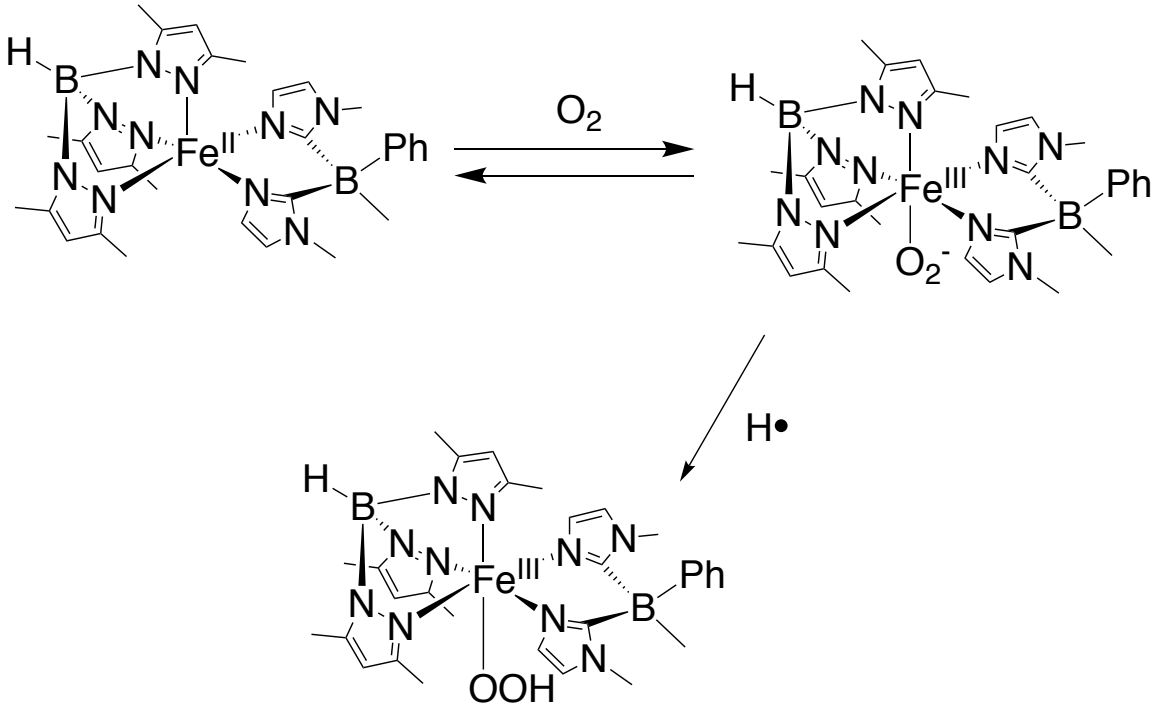

The ferric–superoxo species was formed at low temperatures (-60 °C), and was relatively stable at that temperature, however reverted to starting material when temperatures were raised to -20 °C. The observed ferric–superoxo also reverted to its ferrous precursor on bubbling of Ar gas, and repeated addition of O_2 and Ar gases showed reversible changes, similarly to the behavior observed for the above-mentioned [Fe^{II}(BDDP)] complex.[28, 32] UV/Vis absorbance at 350 nm (ε = 4800 M^{-1} cm^{-1}) was similar to the previous complex, which indicated that the observed superoxo was an end-on species, as opposed to a side-on ferric–superoxo. Previous work with another mononuclear ferric system produced a side-on superoxo orientation, with UV/Vis absorbance at 490 nm.[29] The ferric–superoxo exhibited an (O–O) resonance Raman band at 1168 cm^{-1} which shifted to 1090 cm^{-1} on substitution of $^{18}O_2$ for $^{16}O_2$. The ferrous complex was also capable of binding with CO to form a low-spin iron(II)–carbonyl complex with a υ(C–O) feature at 1967 cm^{-1} consistent

with heme iron(II) centers and Fe-Bleomycin. However, the isolation and structural determination of the complex was not successful, so additional structural information was obtained using cobalt analogues. The ferric–superoxo species was capable of hydrogen atom abstraction from weak X-H (X = O or N) bonds to form what was characterized as a ferric–hydroperoxo compound (Scheme 1.12).[32] Although the final structure of the ferric–superoxo complex was not isolated, there was sufficient characterization to fully assign the compound, providing valuable structural insight into the formation and reactivity of a mononuclear ferric–superoxo complex.

There have been relatively few ferric–superoxo complexes observed and characterized, but another O_2-activation intermediate, the Fe(O) species which forms following the reaction of the ferric–superoxo, has been characterized to a greater extent.[3] The high-valent $Fe^{IV}(O)$ is hypothesized to be the key intermediate responsible for oxidation of substrates in enzymes bearing nonheme iron in their active sites. While not the first example of an $Fe^{IV}(O)$, the first example of nonheme $Fe^{IV}(O)$ observed from a reaction between a ferrous starting material and dioxygen was reported in 2005.[33] The starting material, $[Fe(II)(TMC)(CF_3SO_3)_2]$, was unreactive toward dioxygen when in solution with CH_3CN. However, upon inclusion of several additional solvents mixed with CH_3CN (v/v = 1:1) (ethanol, THF, or butyl ether), the solution changed color and produced what was identified as $[Fe(IV)(O)(TMC)(CF_3SO_3)]^+$ (Scheme 1.13), an intermediate compound in the reaction.[33]

Scheme 1.13. Formation of an $Fe^{IV}(O)$ complex and cycle of reactivity.[33]

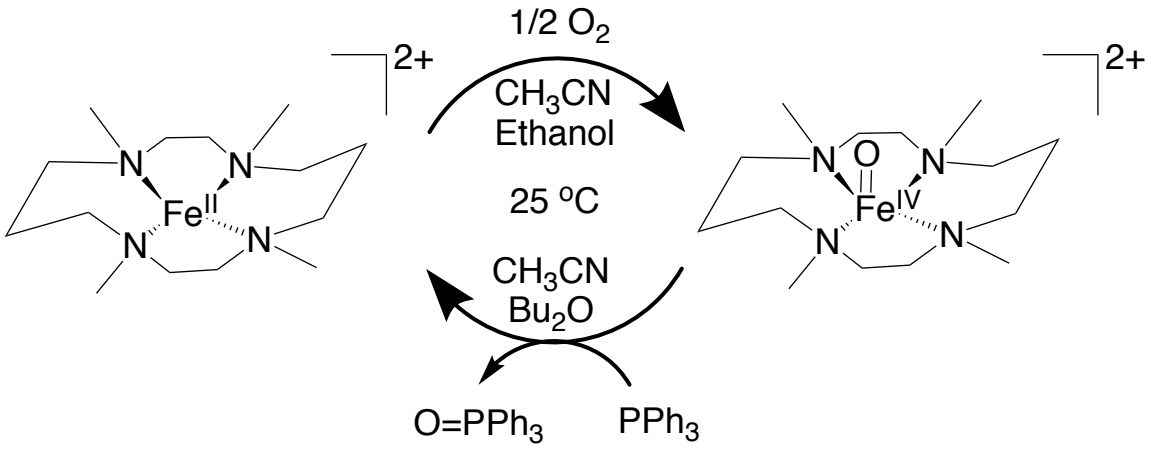

The mass of the complex was shown to shift appropriately when generated in the presence of $^{18}O_2$. Additionally, when $[Fe(IV)(^{16}O)(TMC)(CF_3SO_3)]^+$ was exposed to $H_2{}^{18}O$, the oxygen atoms rapidly exchanged to produce $[Fe(IV)(^{18}O)(TMC)(CF_3SO_3)]^+$. These data provided evidence for the formation of an $Fe^{IV}(O)$ generated from Fe^{II} and O_2. The complex was also capable of transferring oxygen to Ph_3P to form Ph_3PO catalytically when conducted in the presence of O_2. Thioanisole and benzyl alcohol were also oxidized under the same aerobic conditions. Examination of solvent effects found that there was some correlation between the reaction of the Fe^{II} complex with oxygen and the $Fe^{III/II}$ redox potential in the solvent system. For solvents in which a low $Fe^{III/II}$ redox potential (< -0.1 V) was observed, reactions with O_2 to form iron-oxygen adducts were also observed. However, for solvents where higher $Fe^{III/II}$ redox potentials were measured, there was no reaction with O_2. This indicated that a more electron-rich Fe^{II} is more likely to react with O_2 to bring about an $Fe^{IV}(O)$ species, which was a valuable observation in conjunction with the understanding that solvent effects have roles in the dioxygen activation of nonheme ferrous complexes.[3, 33]

Additional insight into the formation of $Fe^{IV}(O)$ from dioxygen and Fe^{II} was obtained when observing behavior of a modified TMC ligand. A methyl arm of TMC was replaced by a pyridylmethyl segment to give the modified ligand (TMC-py) an axial substituent. The ligand was formulated based on the success of the previous unsubstituted TMC ligand, and observations that axially-coordinated ligands in *trans* positions to the labile open site are capable of encouraging iron-oxygen adduct formation and formation of the $Fe^{IV}(O)$ complex.[34] The complex was capable of forming an isolated $Fe^{IV}(O)$ from reaction with its ferrous precursor $[Fe^{II}(TMC\text{-}py)]^{2+}$ with external oxidants (PhIO, H_2O_2), and with addition of a proton and electron source in the presence of O_2, also formed the $[Fe^{IV}(O)(TMC\text{-}py)](OTf)^{+}$ complex (Scheme 1.14).

Scheme 1.14. Proton and electron-mediated formation of $Fe^{IV}(O)$ from a ferrous nonheme complex.[34]

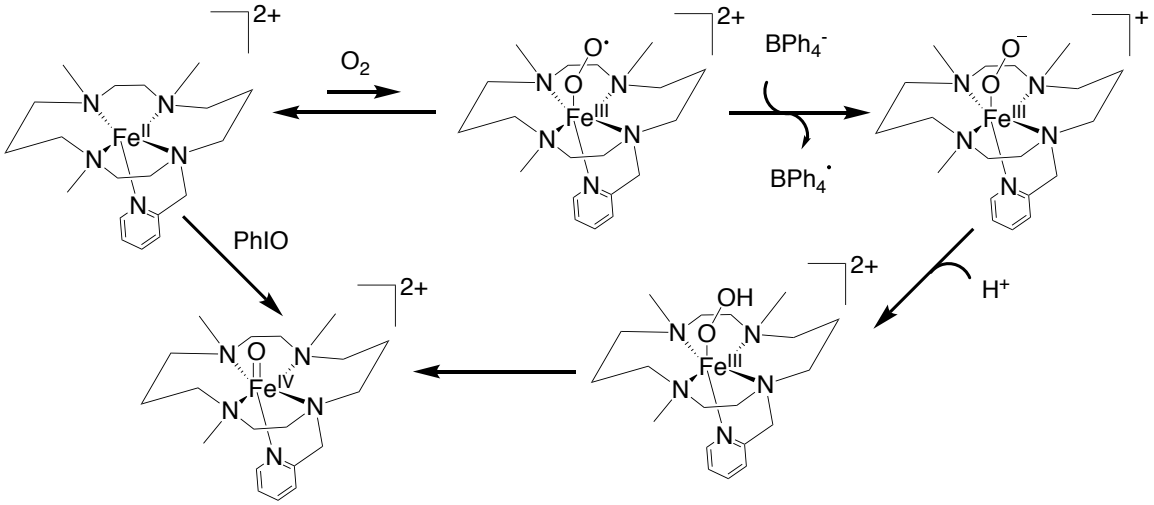

The greater electron density afforded by the axial pyridine moiety likely encouraged the stability of the $Fe^{IV}(O)$ complex, which was crystallographically characterized. However, the complex was not O_2-active when exposed to just O_2. Additional proton/electron sources were necessary for reaction with O_2. This gave validation to the above proposed mechanism (Scheme 1.14), and indicated that the superoxo intermediate was likely too

unstable for isolation. Furthermore the requirement of a 1:1:1 ratio of metal complex, electron donor, and proton donor indicated the likely formation of a ferric–hydroperoxo intermediate, although the intermediate was not isolated for characterization. Nonetheless, isolation of an O_2-derived $Fe^{IV}(O)$ with an axial pendant electron-donating ligand indicated the value of a higher electron density metal center for stabilization of $Fe^{IV}(O)$ complexes.

Work continued on isolation of the ferric–hydroperoxo and $Fe^{IV}(O)$ complexes generated from the activation of O_2 and ferrous complexes. More success was found in the addition of another electron donor (BNAH) and proton donor ($HClO_4$).[35] When low-spin ferrous complexes of N4Py and Bn-TPEN were exposed to oxygen, BNAH, and $HClO_4$ in acetonitrile, no reactions were observed. However on the transference of the reaction to methanol, ferric–hydroperoxo complexes were detected (Scheme 1.15).[35]

Scheme 1.15. Generation and isolation of $Fe^{III}(OOH)$ species using proton and electron donors.[35]

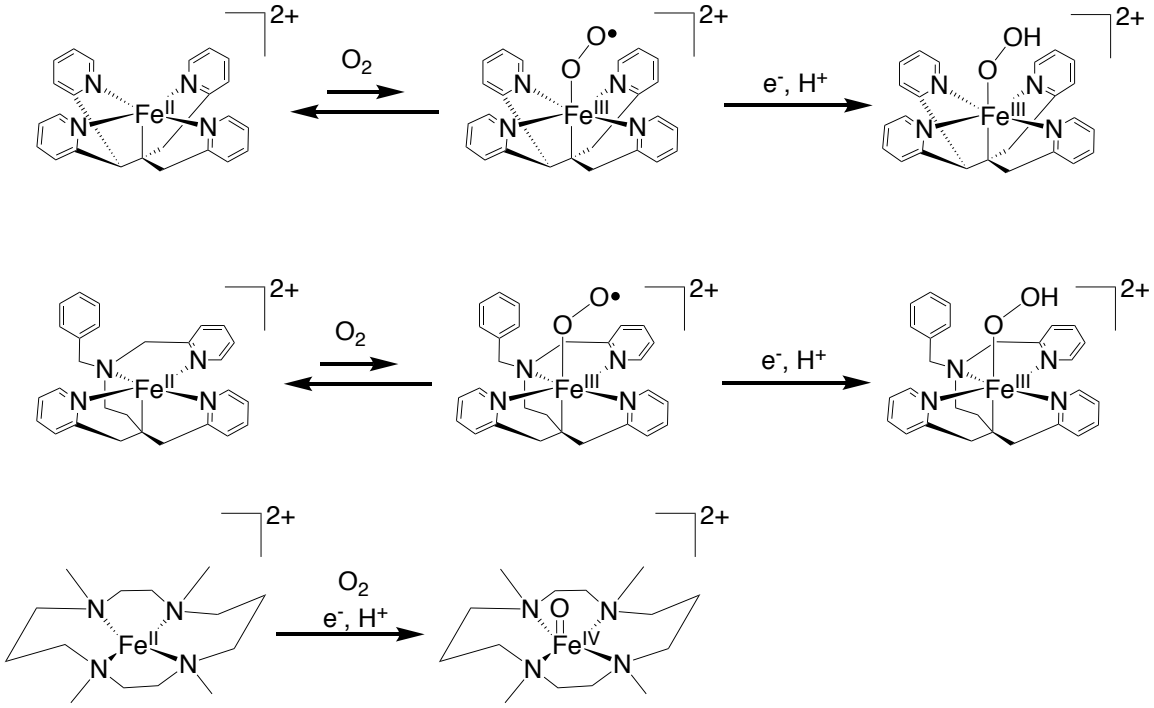

When reacting $[Fe^{II}(TMC)]^{2+}$ with BNAH and $HClO_4$ in the presence of dioxygen, the reaction proceeds in acetonitrile without any requirement for methanol. However, the ferric–hydroperoxo is not observed and instead only $[Fe^{IV}(O)(TMC)]^{2+}$ is formed. Upon increased scrutiny into the nature of solvent effects on the reactivity, it was found that $[Fe^{II}(N4Py)]^{2+}$ and $[Fe^{II}(Bn\text{-}TPEN)]^{2+}$ complexes are low-spin in MeCN, but high-spin in CH_3OH. The $[Fe^{II}(TMC)]^{2+}$ complex is also high-spin in CH_3CN. Lower Fe^{III}/Fe^{II} redox potentials were also displayed by these high-spin complexes, further corroborating the observation that such lower redox potentials favored the dioxygen-driven oxidation.[33, 35] This correlation of observation of O_2 reactivity with high-spin ferrous complexes matches what is seen for biological heme and nonheme enzymes.

Activation of O_2 using Fe^{II} complexes was also achieved replacing Brönsted acids with Lewis acids, while still utilizing an electron donor.[36] The aforementioned $[Fe^{II}(TMC)]^{2+}$ complex has been shown to activate dioxygen in the presence of H^+ and BPh_4^- to give $[Fe^{IV}(O)(TMC)]^{2+}$. When substituting H^+ for Sc^{3+} under aerobic conditions, production of $[Fe^{IV}(O)(TMC)]^{2+}$ was also observed.

Scheme 1.16. Dioxygen activation using Lewis acid.[36]

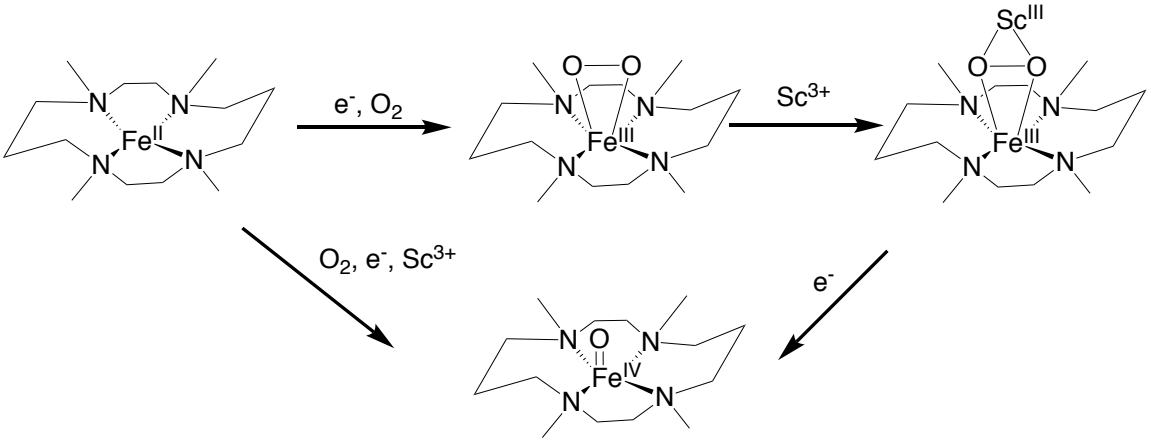

When both Sc^{3+} and BPh_4^- were not present during the aerobic reaction, there was no transformation observed, indicating the necessity for the BPh_4^- electron source. Although not crystallographically characterized, it was proposed that the Sc^{3+} ion was bound to the peroxo intermediate in an η^2 fashion, promoting O–O cleavage to form the final $[Fe^{IV}(O)(TMC)]^{2+}$ complex, or perhaps via a radical chain pathway. The investigation of the effect of a Lewis acid extended the knowledge in the field on dioxygen activation and iron-oxygen bond formation.

While there have been several examples of proton and electron sources used in the dioxygen activation complex, with ferrous complexes, replacement of these external sources with a hydrogen-atom donor has the same effect.[37] When olefinic substrates were added to the air-stable solution of $[Fe^{II}(TMC)]^{2+}$ in acetonitrile, the complex was found to activate O_2.

Scheme 1.17. Hydrogen-atom donation in activation of dioxygen with a mononuclear nonheme complex.[37]

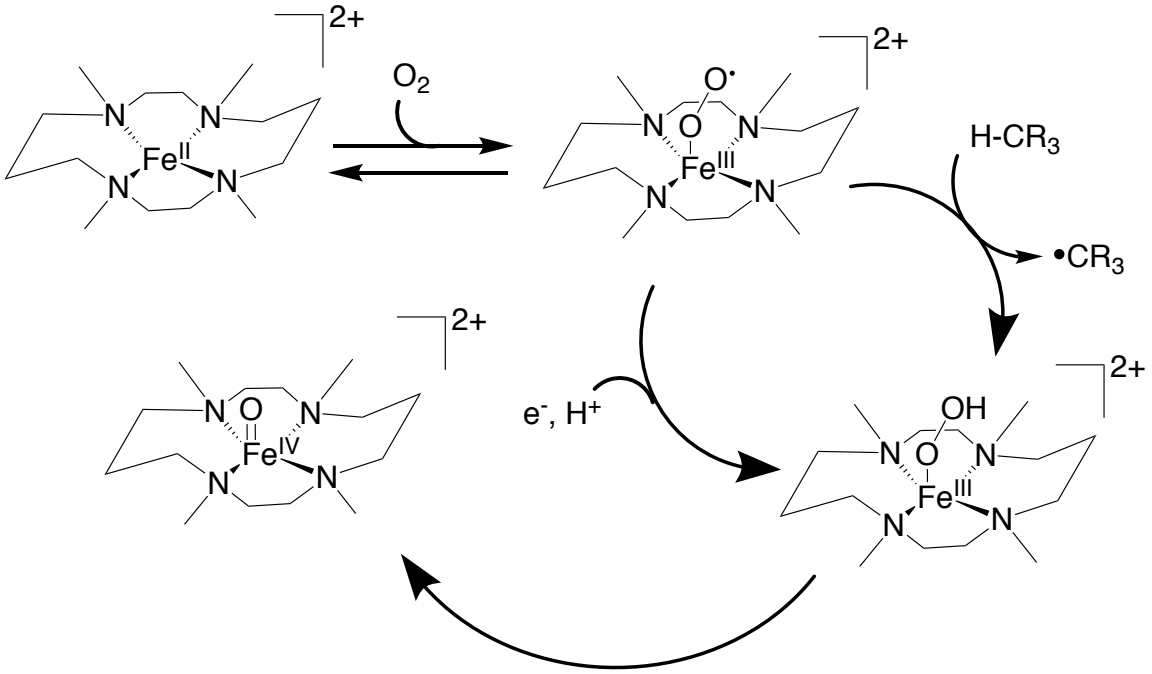

When adding olefinic compounds (cyclohexene, -heptene, and -octene) to the CH_3CN solution of $[Fe^{II}(TMC)]^{2+}$, rapid formation of $[Fe^{IV}(O)(TMC)]^{2+}$ was observed, and accumulation was possible due to low reactivity of the product toward the olefinic compounds used in formation. By incorporation of deuterated-cyclohexene, a KIE (kinetic isotope effect) of 6.3 was observed, indicating the dependence of the rate-determining step on C–H bond activation. The nature of the rate-determining step gave credence to the proposed pathway that a ferric–superoxo species forms and abstracts the added hydrogen atom, which then produces an iron(III)–hydroperoxo intermediate that subsequently decays into the $Fe^{IV}(O)$ complex (Scheme 1.17). A ferric–superoxo species was not directly observed, but some evidence for its formation was obtained. Observation of an iron(III)–peroxo complex when performing the reaction in the presence of a base provided an indirect result supporting the formation of a ferric–superoxo.

There has additionally been some success in development of synthetic compounds capable of enacting the above biologically inspired C-H oxidations, particularly the precursor species of Fe(O). A notable result was produced by Bouchu and others,[38] with the H_2O_2-mediated reaction between an iron dinuclear μ-nitrido-bridged phthalocyanine complex and methane, which was shown to produce methanol and subsequent oxidation products.

Scheme 1.18. Proposed mechanism for C-H activation.[38]

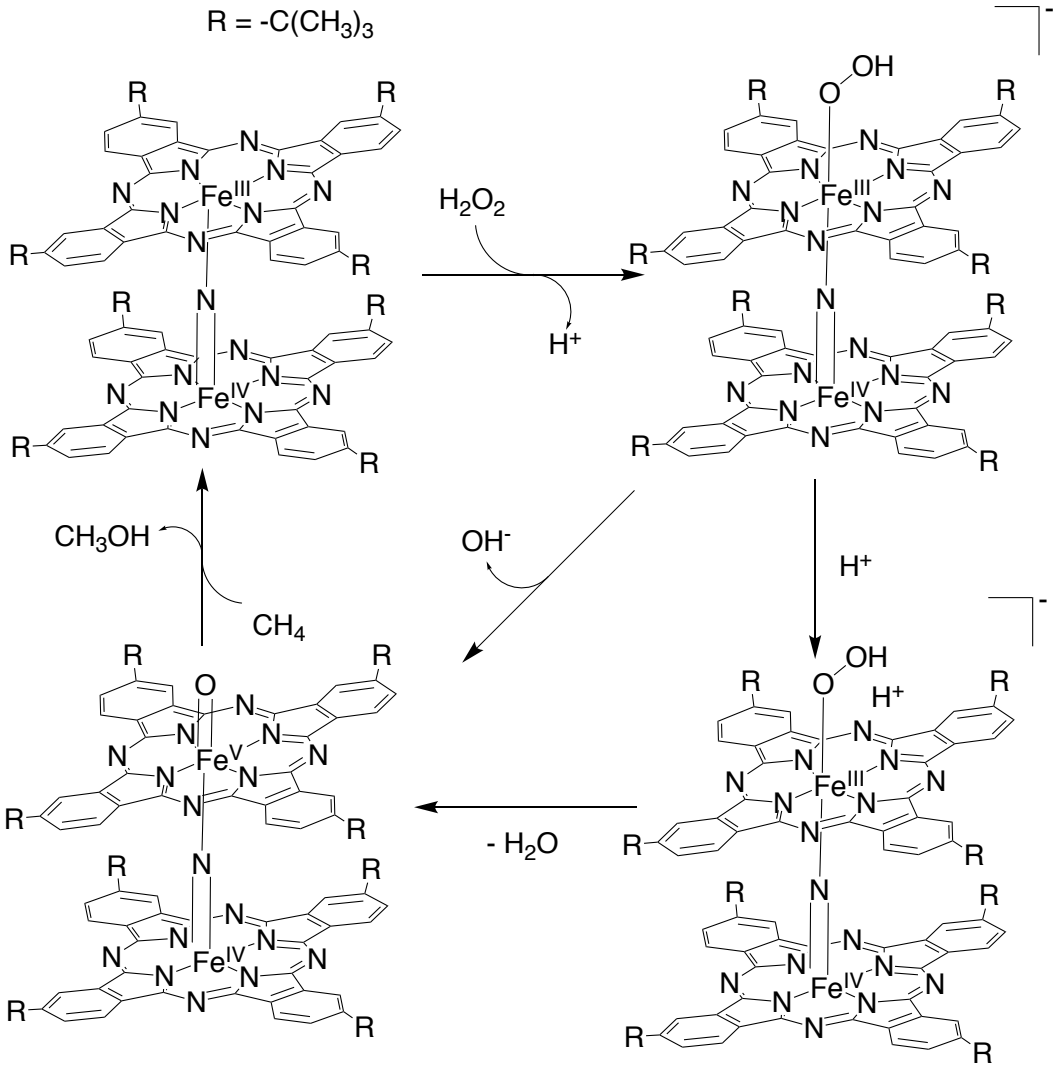

Initial first-stage oxidation products were observed as methanol, however the high reactivity of the system produced formaldehyde and formic acid as the major products. Such a method was found to proceed at far more gentle conditions than had previous oxidation methods of methane (40–80 ºC, vs ~200 ºC), and with higher turnover. It was proposed that the initial H_2O_2 reacted with the ($Fe^{IV}Pc^tBu_4$)N($Fe^{III}Pc^tBu_4$) (Pc^tBu_4 = tetra-*tert*-butylphtalocyanine) complex form a hydroperoxo complex, which whether by exposure to acid or base would homolytically cleave to form an oxo complex (Scheme 1.18). The oxo complex is expected to be the agent responsible for the observed C-H

activation, and when in the presence of excess oxidant, one that is capable of producing up to 436 turnovers.[38] However, the reactivity of the complex was on the level such that none of the proposed intermediates were isolable.

Following the success of the above μ-nitrido-bridged phthalocyanine complex in the oxidation of methane in a biologically-inspired manner, work was continued targeting the characterization of the intermediates in the oxidation mechanism.[39] Since the reactivity of the phthalocyanine-based complex prevented the direct observation of the putative oxo intermediate, the complex was modified via the incorporation of a porphyrin ligand in the manner of cytochrome c peroxidases, which contain two heme compounds that generate $Fe^{IV}(O)$ intermediates during the decomposition of peroxides.

Scheme 1.19: Generation of a C-H activation intermediate.[39]

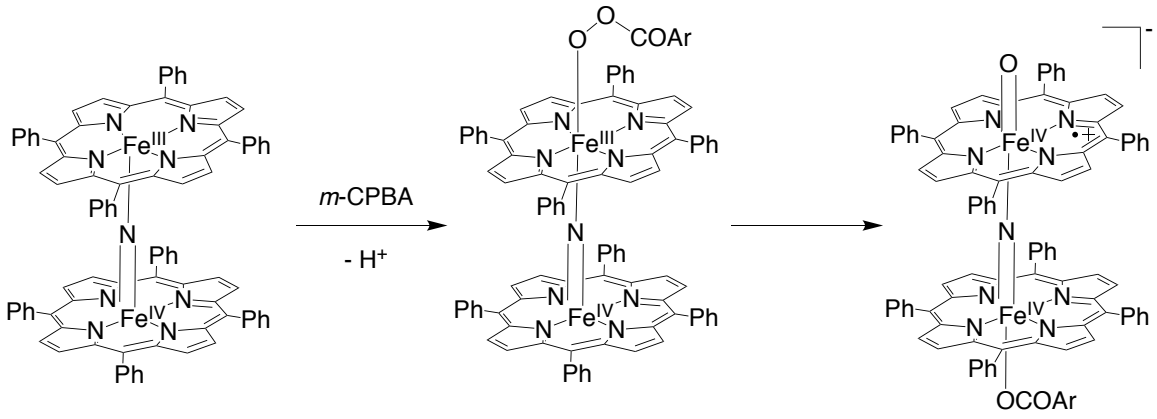

Modification of the complex did not prevent methane reactivity, as the complex was capable of similar methane oxidations in the manner of its predecessor while supported on silica.[39] The incorporation of the porphyrin moiety allowed for the observation and characterization of the $Fe^{IV}(O)$ cation radical responsible for the oxidation.

1.3. Iron-Mediated Dioxygen Activation Versus S-Oxygenation

Because of the relevance of biological O_2 activation by nonheme enzymes which incorporate cysteinate ligands, there has been significant exploration into iron complexes which incorporate sulfur-based moieties into their coordination spheres.[3] One of these iron–thiolate enzymes, CDO (cysteine dioxygenase), consists of a mononuclear iron site with a facial triad of histidine ligands, and is part of a group of enzymes classified as thiol dioxygenases. Each of these enzymes is capable of activating dioxygen in order to convert sulfur-containing substrates into sulfinic (dioxygenated) acid compounds. Recent research has been undertaken to understand the mechanism of oxygen reactivity with iron–thiolate complexes, however there is little known about reaction intermediates. There have been recent examples of S-oxygenation in such complexes, with a notable example in 2010.[40] A CDO model complex bearing a thiolate donor was found to react with O_2 to produce a new S-oxygenated complex.

Scheme 1.20. Reaction of O_2 to produce an S-oxygenated product.[40]

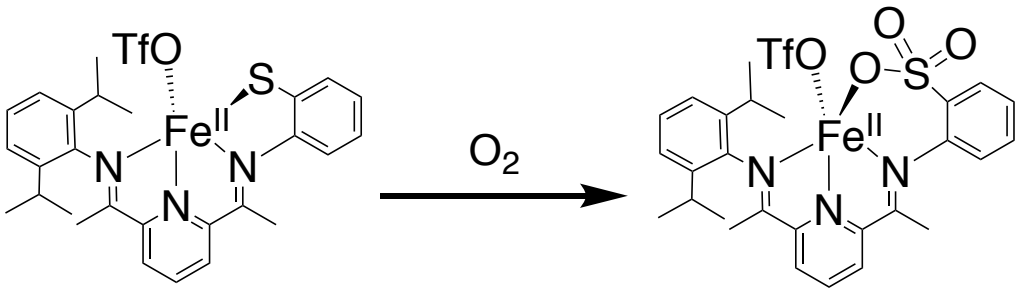

On exposure to O_2, the formation of a triply-oxygenated ferrous–sulfonate complex was isolated and crystallographically characterized. Isotopic labelling of O_2 showed full isotope incorporation, while there was no ^{18}O incorporation when the reaction was performed in the present of $H_2{}^{18}O$, indicating that O_2 is the sole source of the S-oxygenation. Further examination indicated that, while no metal-oxygen intermediates were observed, a dioxygenation occurs initially, followed by the

incorporation of a third oxygen atom on the sulfur donor. The incorporation of dioxygen resulting in S-oxygenation provided additional insight into the nature of nonheme iron dioxygen activation.

Additional success in incorporating dioxygen into ferrous thiolate systems was obtained using more complexes with similar bis(imino)pyridine (BIP) frameworks.[41] As opposed to a previous complex where the thiolate moiety was tethered to the BIP scaffold, additional asymmetric BIP complexes were formed with thiolate ligands unbound to the primary part of the framework. Separate complexes [(^{iPr}BIP)Fe^{II}(SPh)(Cl)] and [(^{iPr}BIP)Fe^{II}(SPh)(OTf)] were reacted with dioxygen in order to examine whether iron-oxygen intermediates could be detected (Scheme 1.21).

Scheme 1.21. Dioxygen reactivity of mononuclear nonheme iron BIP complexes.[41]

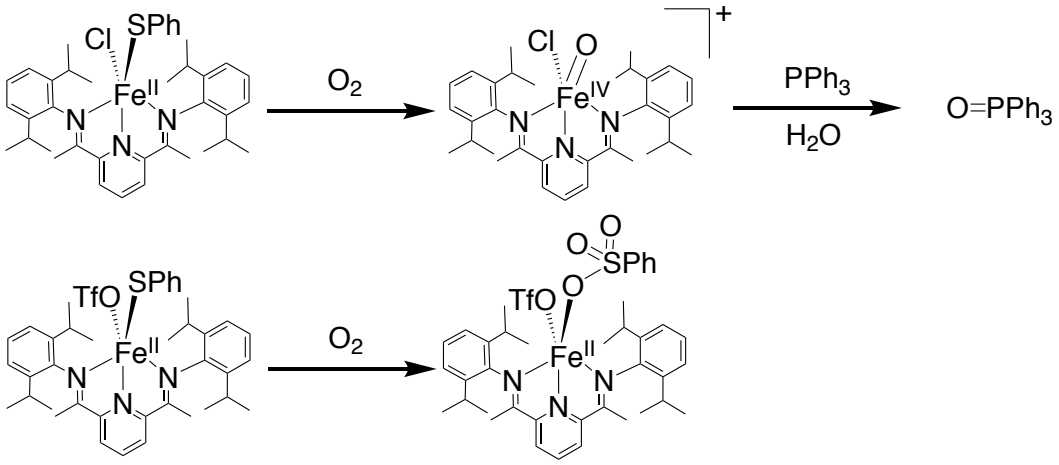

When [(^{iPr}BIP)Fe^{II}(SPh)(Cl)] was exposed to O_2, an intermediate Fe^{IV}(O) complex was detected, and observed to transfer an oxygen atom to PPh_3. However, the analogous [(^{iPr}BIP)Fe^{II}(SPh)(OTf)] did not form a detectable Fe^{IV}(O) species, and instead underwent S-oxygenation to produce what was detected as [(^{iPr}BIP)Fe^{II}($PhSO_3$)]$^+$. The thiolate ligand was required for O_2 reactivity, as neither Fe^{II}(^{iPr}BIP)(OTf)$_2$ nor Fe^{II}(^{iPr}BIP)Cl$_2$ were reactive under aerobic conditions. The positioning of the thiolate ligand may also have an

effect. The thiolate of [(^{iPr}BIP)Fe^{II}(SPh)(Cl)] lies trans to the open coordination site, while the thiolate of [(^{iPr}BIP)Fe^{II}(SPh)(OTf)] is cis to the open site, which indicates that S-oxygenation is encouraged when the S-donor is trans to the open coordination site. The redox potentials for the unreactive complexes were 0.613 V and 0.025 V respectively, while those of [(^{iPr}BIP)Fe^{II}(SPh)(Cl)] and [(^{iPr}BIP)Fe^{II}(SPh)(OTf)] were -0.173 V and -0.372 V respectively. This indicated that the O_2 reactivity only appears to occur when $E_{1/2}(Fe^{III/II}) < -0.1$ V, which may have some solvent-dependence.[41] However, because these oxygenations led only to triply-S-oxygenated products (beyond that of the biological reaction), additional investigation continued.

Synthesis of a complex which produced a doubly-S-oxygenated product met with success when a 5-coordinate N4Py-based ligand was supplemented with a thiolate moiety.[17] Reaction with O_2 in a methanolic solution formed an Fe^{II}-sulfinate complex, a rare example of a structurally-characterized doubly-S-oxygenated ferrous complex.

Scheme 1.22. Activation of dioxygen with a monunuclear nonheme complex.[17]

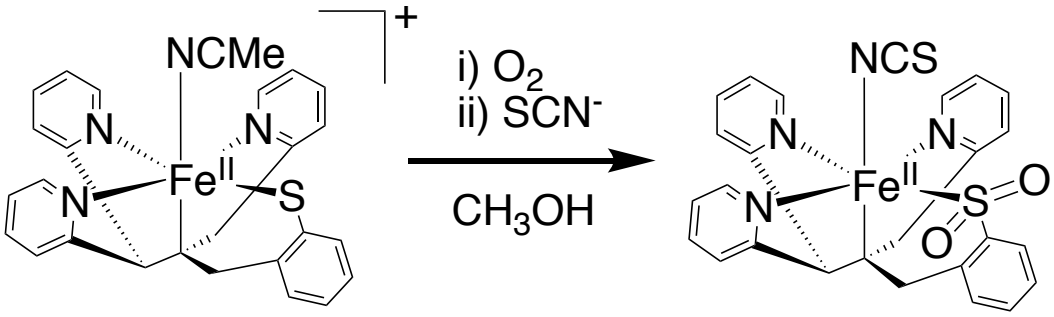

While the initial ferrous complex is low-spin when dissolved in acetonitrile, the complex converts to a high-spin Fe^{II} complex when solubilized in methanol. As was previously observed, this solvent-dependence of spin-state allows for the reaction of O_2 with the ferrous material.[3, 17, 35, 37, 40-41] Capture of the product with KSCN showed that the reaction yielded a doubly-S-oxygenated complex, which is similar to the reactivity of biological

CDO. It was proposed, based on observation of oxygen transfer and reactivity with dimedone, that an intermediate S-oxygenated species was a sulfenate (mono-oxygenated). Control reactions with the ferrous sulfinate product were unsuccessful under both of the testing conditions.

There has also been success at observing double-S-oxygenation in another CDO-type model complex based on a tris(pyrazolyl)borate framework (Tp) containing a cysteine analog.[42]

Scheme 1.23. S-oxygenation of a cysteine analog by a mononuclear nonheme iron complex.[42]

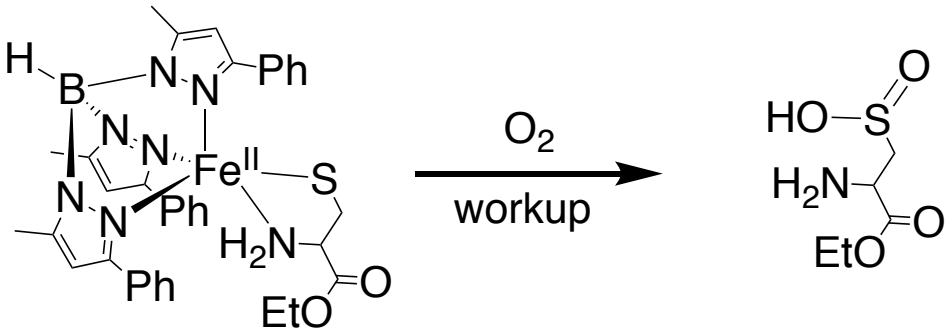

$[Fe^{II}(Tp^{Me,Ph})CysOEt]$ was found to react with O_2, albeit much more slowly than some of the previous examples. The product mixture was worked up to yield the sulfinic acid product. When labelling studies were utilized, analysis indicated that the S-oxygenation occurs with the transference of one O_2 molecule to yield the doubly-oxygenated product. This model matched closely with both the structure and behavior of the CDO enzyme.

1.4. Radical Rebound in Iron Complexes

Examination of the reaction between the high-valent Fe(O) species and the substrate during the cytochrome P450-catalyzed hydroxylation indicated that there was

loss of stereochemistry in substrates, or inversion of stereochemistry (Scheme 1.4).[43] This inversion indicated formation of a radical intermediate. These results indicated that the high-valent Fe(O) is capable of abstracting a hydrogen atom from the substrate, generating a radical which rapidly recombines with the hydroxide equivalent on the metal. Deuterium labeling studies showed that these transformations have a large kinetic isotope effect (k_H/k_D = 11.5), indicating that the proposed hydrogen atom transfer step is rate-limiting. However, these studies have mostly been based on the competitive hydroxylation between equivalent sites of substrates, since it was not possible to directly measure the isotope effect on the reaction of the activated hydroxylating species.

The rate-determining nature of the formation of an Fe(OH) species, proposed as the key intermediate in the radical rebound reaction, has made it difficult to observe the direct rebound step due to the rapid consumption of the Fe(OH) intermediate once formed. In spite of the difficulty in observing the key rebound step directly, some insight has been obtained by the study of "radical clock" substrates. Radical clock substrates are capable of forming radicals by hydrogen atom abstraction (Scheme 1.24). These radicals then are able to react in multiple pathways. One way of reacting is to collapse into an unrearranged product, while a second pathway involves the rearrangement to form another radical, which will then lead to an entirely different and distinct product. The knowledge of the rates of these rearrangements may give an estimate of the rate of radical rebound, based on the ratio of rearranged to unrearranged products. The first successful experiment utilizing this radical clock technique gave a rate constant of radical rebound $k_1 = 1.4 \times 10^{10}$ s^{-1}.[43]

Scheme 1.24: Utilization of radical clock reactions to probe hydroxylation. Adapted from Reference 43.

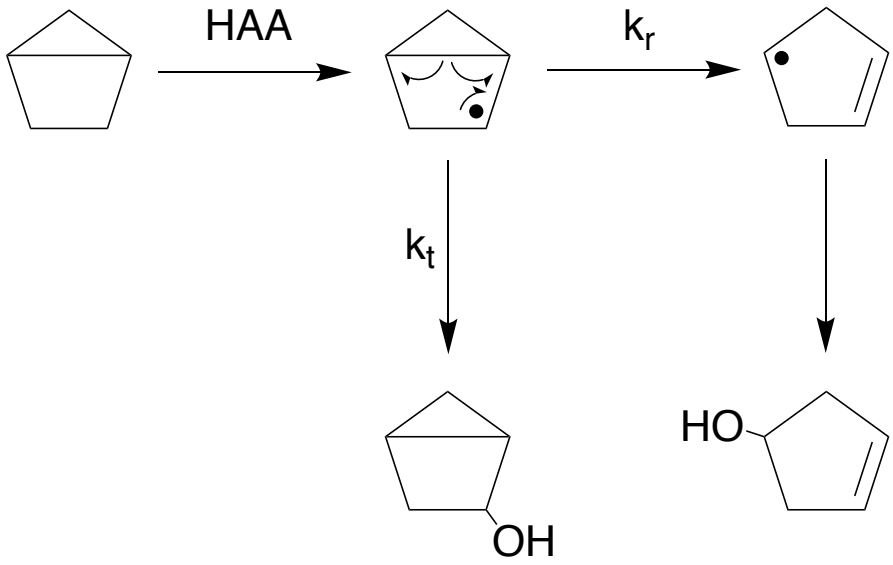

Other radical clock probes gave comparable rate constants, with the estimated rates of radical rebound falling on the scale of ~10^{10}-10^{11} s^{-1}.[43]

Further information was obtained about the mechanism of hydroxylation by investigations into the reactivity of the C-H bonds that are employed as substrates. Quantification of isomers indicates that C-H oxidation is preferred in the following order: tertiary > secondary > primary.[43] Further studies have indicated that the stability of the generated carbon radical and the strength of the C-H bond may be used to predict reactivity toward substrate hydroxylation. The earlier experimental results were corroborated by computational studies yielding that the order of reactivity and subsequently radical stability is as follows: benzylic/allylic > tertiary > secondary > primary.[43]

The mechanism of cytochrome P450 was further investigated by Rittle and Green, obtaining additional data on the kinetics of C-H hydroxylation.[44] One of the key intermediates proposed in C-H hydroxylation by P450, compound I (Cpd-I), was hypothesized to exist as an $Fe^{IV}(O)$ cation radical delocalized over the ligated thiolate and

porphyrin.[44] However, because Cpd-I does not accumulate during the cycle of the enzyme, its role in the hydroxylation pathway had been disputed.[44] CYP119, an example of P450, was used in the generation and isolation of Cpd-I (Scheme 1.25).[44]

Scheme 1.25: Generation of Cpd-I and reaction with substrate.

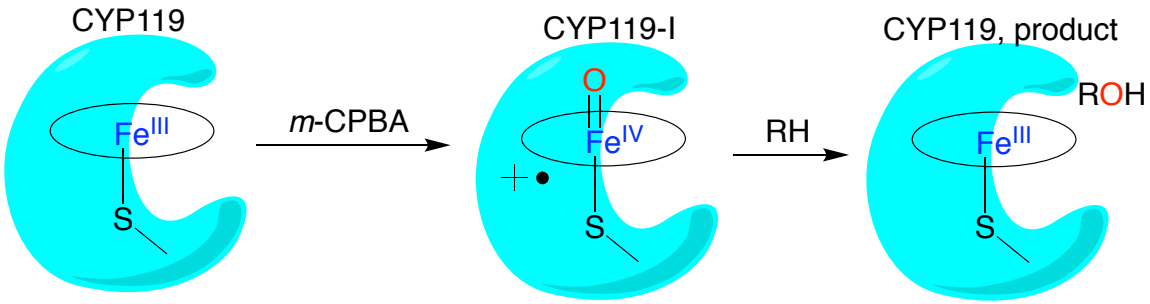

Cpd-I was generated in high yield (~75%) and characterized. Further experiments were performed to ascertain the complex's reactivity as a hydroxylating agent. Reactions with long-chain fatty acids were examined and indicated that Cpd-I was efficient as a hydroxylating agent, particularly in the case of lauric acid ($k_2 = 1.1 \times 10^7$ M^{-1} s^{-1}). The reactivity of Cpd-I toward organic substrates indicated that it likely is an active agent in the rebound mechanism, while at the same time pointing more evidence toward the formation and mechanistic significance of a Fe(OH) reactive species. The concrete identification of Cpd-I contributed much to the understanding of the hydroxylation mechanism in heme enzymes, however without the observation of the implicated Fe(OH) intermediate, or the formation of an analog of the complex, the direct rebound mechanism remained unobserved.

Until recently, the difficulty in observing the key rebound step has arisen from the challenges in synthesizing and isolating the Fe^{IV}(OH) complex implicated in the cytochrome P450 oxidation mechanism, Compound II.[45] There has also been additional difficulty in identification of suitable radicals which are stable enough to react in an

observable fashion with Cpd-II models. More recent attempts to observe rebound in heme-type systems have produced some success, particularly in a recent iron-hydroxide complex synthesized by Goldberg and others (Scheme 1.26).[45] The design of a model for the direct observation of radical rebound would involve the isolation of the high valent Fe(OH), and the use of a stable carbon-based radical capable of reaction with the high valent Fe(OH) species. A particular difficulty in the preparation of a mononuclear Fe(OH) complex suitable for the observation of the key rebound step lies in the tendency of such complexes to dimerize rather than remain in a monomeric state. It was proposed that a high level of steric barrier might preclude the dimerization and allow for the isolation and characterization of such a mononuclear Fe(OH) species.

Scheme 1.26. Previously observed hydroxyl rebound in a heme iron model complex.[45]

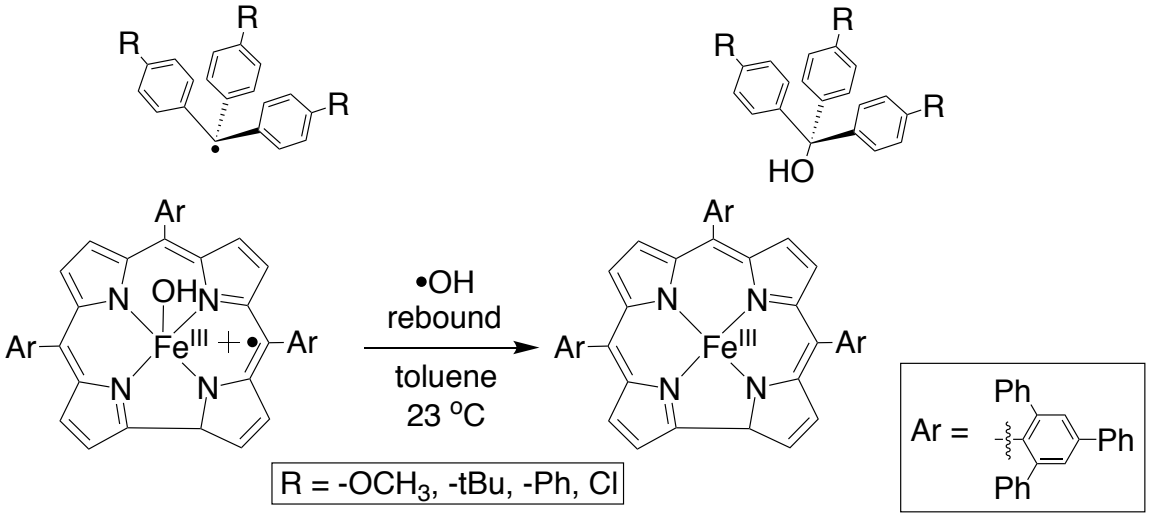

The modification of a known ligand framework allowed for the synthesis of a model for Cpd-II. This was the first direct observation in a heme iron model complex of the key rebound step, which is proposed to follow he HAT with the high valent oxo center. The synthesis and isolation of the formal Fe^{IV}(OH) heme complex allowed for the direct reaction of the iron center with several organic carbon-centered radicals which are stable

in solution.[45] According to knowledge of radical stabilization, a benzylic/allylic-type radical would be the most stable and readily reactive toward the isolated Fe(OH). Combining these characteristics of radical stability, it was deemed that a tertiary benzylic radical might be suitable for the observation of rebound. The triphenylmethyl and related radicals were selected, due to their relatively long-lived nature in solution, and ease of preparing substituted derivatives. The longer-lived (although still reactive) nature of these organic radicals allowed for reaction on an observable scale. Companion kinetic experiments yielded rate constants for the rebound reaction, giving second-order rate constants ranging from 12.6 to 357 M^{-1} s^{-1}.[45] The organic product and one-electron reduced metal complex were isolated and quantified, which gave indication of the expected rebound reaction. Hammett analysis of the reaction showed a small slope (ρ = -0.55), which pointed to a small separation of charges in the reaction transition state. Further Marcus analysis showed a likewise linear correlation with a small slope of -0.15. This slope can be compared to the Marcus cross-relation,[46] which indicates that a simple rate-limiting electron-transfer process holds a slope of ~-0.5. Thus the reaction is likely to proceed as the proposed concerted rebound process. Additionally the small slope obtained compares well to the small slope (-0.05) that is seen for the reaction between the cumylperoxyl radical and various phenols, which is considered to be an effective model of a concerted hydrogen atom transfer as opposed to an ET mechanism.[47-48] The mechanistic information acquired through Marcus and Hammett analysis of the above reaction proceeded in the manner consistent with a concerted rebound process.

Little direct evidence for radical rebound has been obtained from nonheme model complexes. The rebound process in nonheme systems may be in fact more complicated

than in that of the heme systems.. Through a variety of both computational and experimental investigations utilizing nonheme Fe(O) model systems, some evidence for both rebound and nonrebound pathways of C-H oxidation has been observed. Particularly, some evidence for hydroxyl rebound has been previously obtained in a non-iron nonheme model complex system, in which a ruthenium-bound product of the expected C-O bond formation was observed (Scheme 1.27).[49]

Scheme 1.27: Putative oxygen rebound in a nonheme complex.[49]

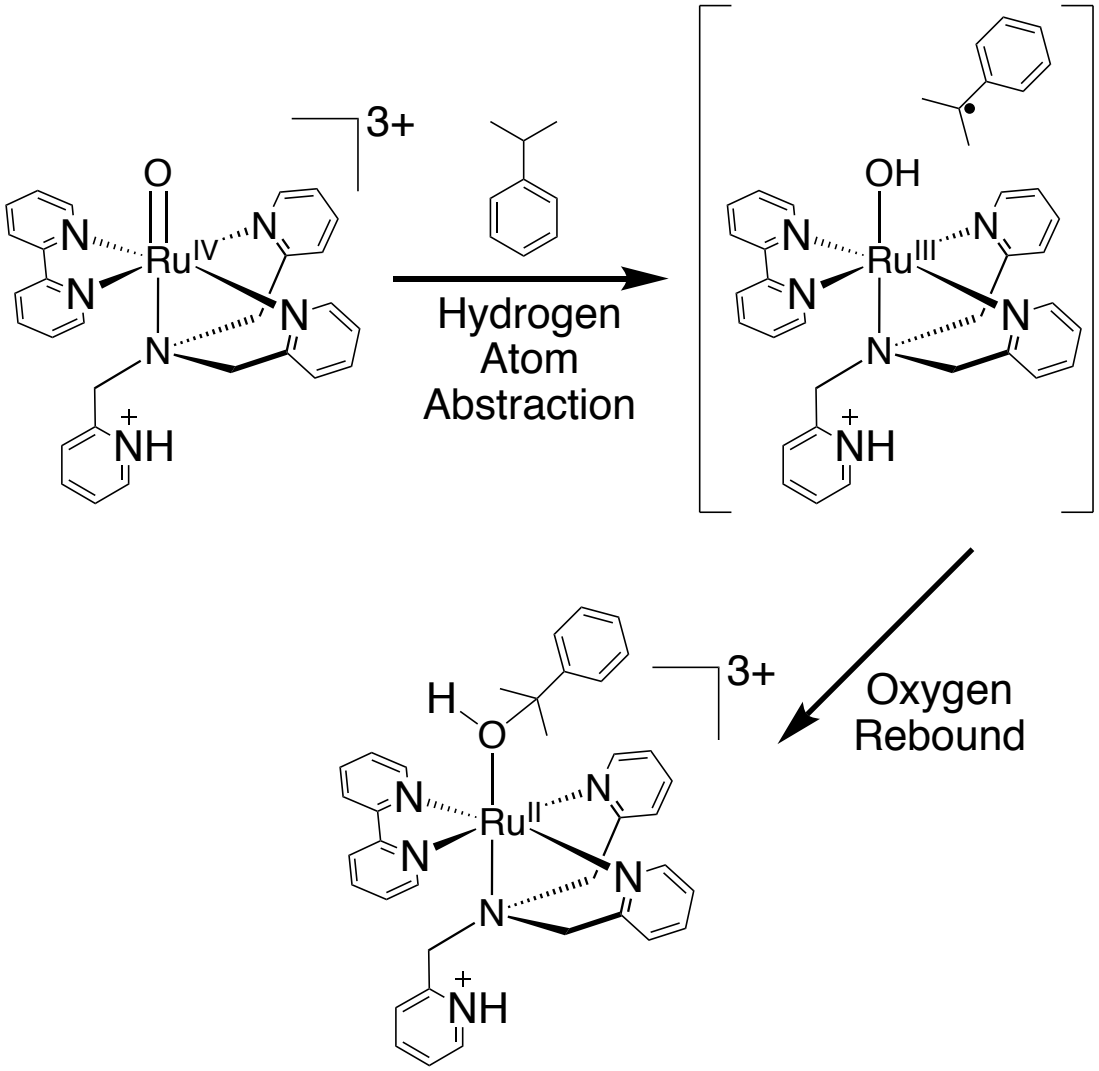

Evidence of a bound product of C-O bond formation was detected by ESI-MS. However, the isolated Ru^{III} products had already undergone oxidation at the metal center due to

further interaction with remaining $Ru^{IV}(O)$ material. Nonetheless, the evidence that was obtained indicated that C-O bond formation results from a radical that does not escape from the solvent cage. However, lack of more concrete evidence (detection and isolation of the product of C-O bond formation and proper one-electron-reduced metal complex) has indicated that it might be possible, at least in the case of certain model complexes, that hydroxylation of substrates might occur by a nonrebound pathway.[5] This being the case, the radical would more than likely dissociate from the solvent cage and then become hydroxylated by an alternate mechanism as opposed to the concerted rebound mechanism (Scheme 1.7). Some computational studies have indicated that when the dissociation rates for a radical from the solvent cage are competitive with the rates of rebound itself, the nonrebound type mechanism might predominate.[5]

There has additionally been investigation into synthetic nonheme complexes in order to investigate the nature of the first-coordination sphere in influencing the reactivity of oxygen transfer versus halogenation.[50] Exploration of the driving force of halogenation as opposed to hydroxylation is of interest in the understanding of key features of the nonheme iron halogenase enzymes (WelO5, SyrB2, CytC3, etc.).[25, 51-53] Maiti and others have observed a selectivity of above 99% for aromatic halogenation as opposed to methoxylation (isoelectronic to hydroxylation).[50] Generation of a putative $[(TPA)Fe(III)(OCH_3)(X)]^+$ (X = Cl, Br) species was proposed as the reactive species responsible for the observed reaction products (Scheme 1.28).

Scheme 1.28. Halogenation vs methoxylation in a nonheme iron model complex.[50]

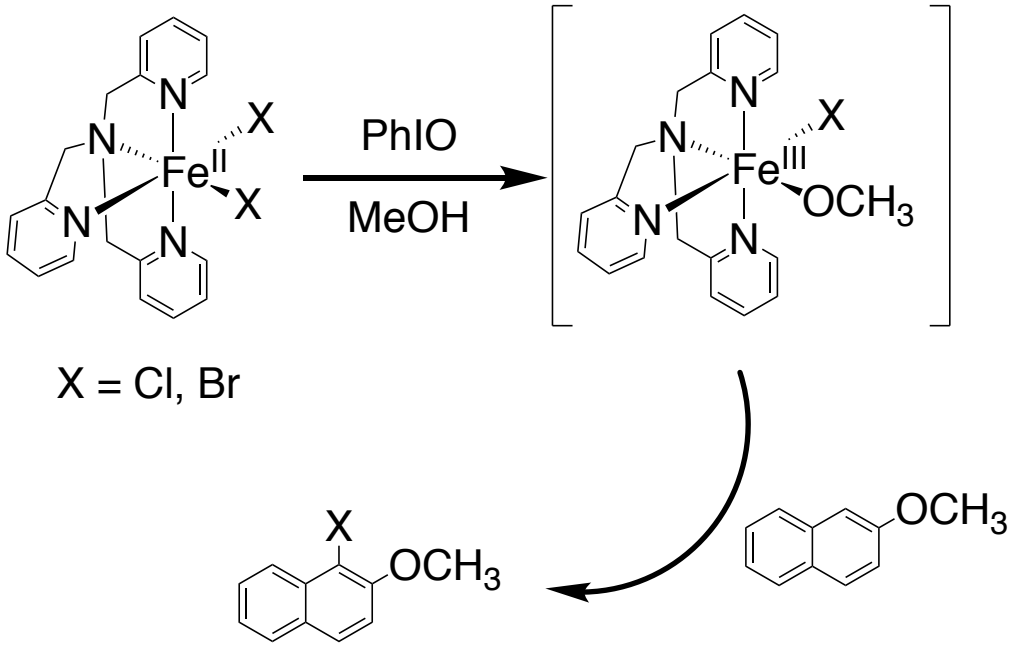

While not fully characterized, the proposed metal intermediate was found to work in a catalytic manner when external halide (KCl or KBr) was added, increasing the utility of the reaction.

The nature of the coordination sphere in the influence of halogenation compared to a competing hydroxylation was also explored by Costas and others.[54] An example of a rare $Fe^{IV}(O)$ with a *cis*-available labile site was generated and used in the preparation of *cis*-halogen compounds (Scheme 1.29).

Scheme 1.29: Formation of *cis*-available labile $Fe^{IV}(O)$ complex.[54]

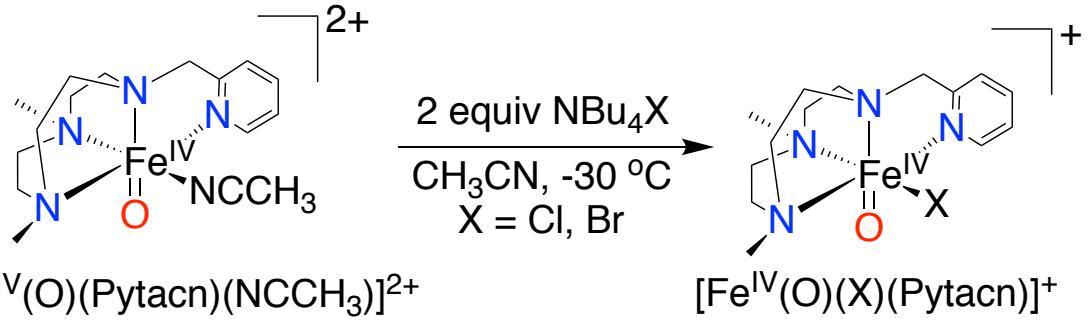

Generation of the above $[Fe^{IV}(O)(X)(Pytacn)]^{+}$ allowed for the examination of the reaction with organic substrates and radical generators. The complex was reactive toward both oxygen atom transfer and hydrogen atom abstraction. Reaction of the complex with triphenylmethane (Ph_3CH) formed triphenylmethanol (Ph_3COH) and Fe^{III} products (resulting from excess oxidant used during the reaction). There were no halogenated organic products observed, which for this system indicated a preference for hydroxylation over halogenation (Scheme 1.30). It was proposed that the hydroxylation product was formed by a rebound-like mechanism of hydroxyl transfer following hydrogen atom abstraction by the $Fe^{IV}(O)$ complex. It was also proposed that the radical may be capable of dissociating from the solvent cage, reacting with oxygen to form the alcohol product and the ferric complex.

Scheme 1.30: Proposed mechanism for hydroxylation by $[Fe^{IV}(O)(X)(Pytacn)]^{+}$.[54]

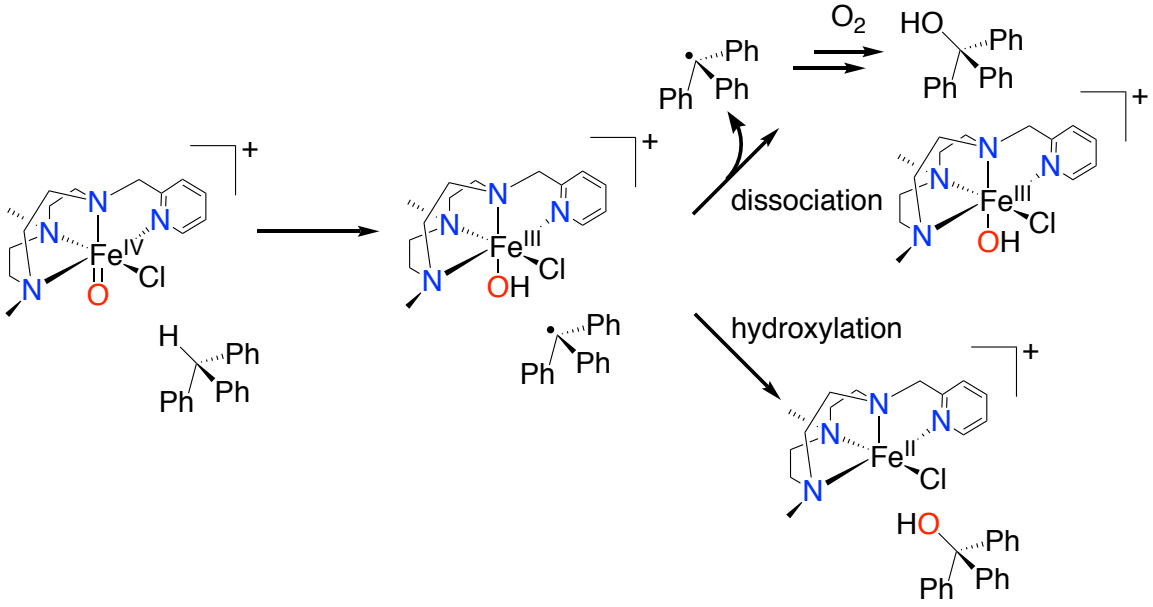

The modification of the study by incorporation of ^{18}O-labelled $Fe^{IV}(O)$ complex confirmed that the anaerobically-generated hydroxylated product contained 90% labelled ^{18}O, indicating that the Ph_3COH was generated by a rebound-like process. Unfortunately it was

not accompanied by the one-electron-reduced metal complex, attributed to the use of excess oxidant in the reaction. Instead a ferric complex was observed. While evidence of a rebound-like process was observed, the lack of observation of both the organic rebound product and one-electron-reduced metal complex did not allow for a definitive conclusion regarding the occurrence of a rebound reaction. Generation and isolation of the purported intermediate $Fe^{III}(OH)Cl$ complex would be a valuable future focus for investigation, allowing the potential for direct comparison between hydroxide and halogen rebound processes, and determination of the likelihood of the dominance of one over the other.

In the investigation of the mechanism of C-H activation by another $Fe^{IV}(O)$ complex, there was additional observation of rebound-like behavior by Maiti and others.[55] Formation of the $Fe^{IV}(O)$ complex and reaction with benzyl alcohol indicated that the initial step in the reaction was a rate-determining hydrogen atom transfer. Deuterium labeling of the C-H methylene positions of benzyl alcohol gave a KIE of 11, further indicating the rate-limiting nature of the hydrogen atom abstraction. The reaction between the $Fe^{IV}(O)$ complex and C-H donors ethylbenzene and cumene afforded ferric hydroxide and ferric-alcohol complexes (Scheme 1.31).

Scheme 1.31: Proposed radical rebound pathway.[55]

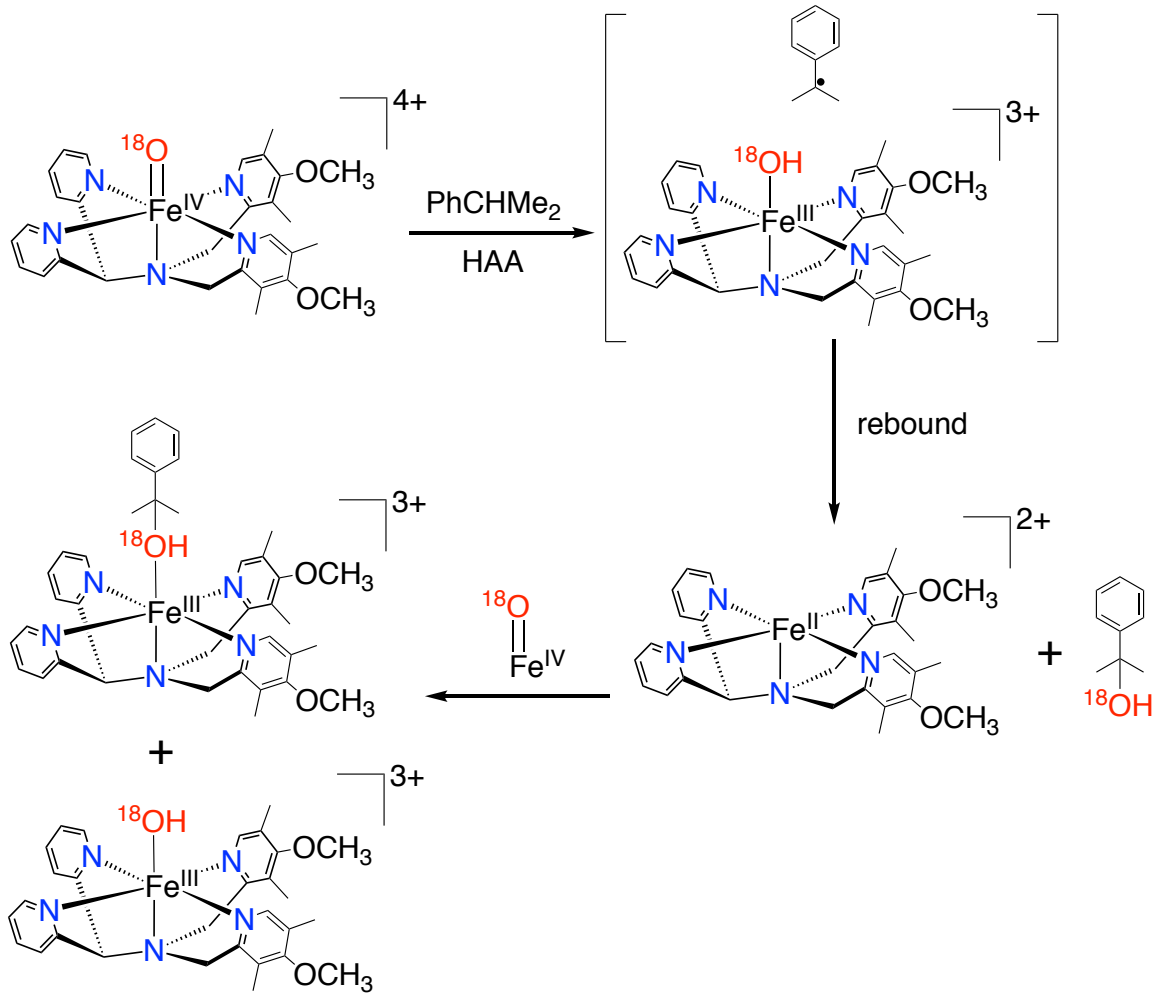

While expected as the metal product of the rebound reaction, the proposed one-electron-reduced ferrous material was not observed in significant portion. To explain the reactivity and observed products, it was instead proposed that reaction of ferrous material with additional $Fe^{IV}(O)$ oxidized the ferrous product in the presence of the hydroxyl rebound product, forming the observed ferric compounds.[55] Further investigation was undertaken by addition of radical trapping reagents, which did not form the requisite products during the reactions of the $Fe^{IV}(O)$ material with cumene and ethylbenzene. The lack of radical-trapped intermediates indicated that the *in situ* generated radicals were incapable of escaping the solvent cage, which is expected during the rebound process, so as to allow the

reaction of the radical and intermediate metal-hydroxyl complex. The observed product mixture gave additional credence to the occurrence of a rebound-type reaction, although not directly observed.

My work in this research group has been focused on the directly observation of the same rebound in a nonheme counterpart. The above series of reactions provided evidence of the feasibility of observation of oxygen and halogen rebound within nonheme iron model complexes. With the same difficulties anticipated in synthesizing a mononuclear nonheme $Fe^{III}(OH)$ analog as to synthesize a mononuclear heme $Fe^{IV}(OH)$, such as Fe-O-Fe formation,[45, 56] additional steric encumbrance was added to a known framework.[57] The N4Py framework was selected as a basic template for its ability to stabilize iron-oxygen intermediates,[58] and was modified with a phenolate moiety to add additional electronic properties. The unsubstituted analogous N3PyO system is known to coordinate with iron and form oxygen adducts, however stable mononuclear iron-oxygen adducts of this complex are not known.[56] The tendency toward dimerization of this compound was addressed by the incorporation of phenyl substituents in the secondary coordination sphere, which was been shown to eliminate dimerization of compounds in similar N4Py-based frameworks.[59-60]

Scheme 1.32: Synthesis of a mononuclear rebound analog precursor.[57]

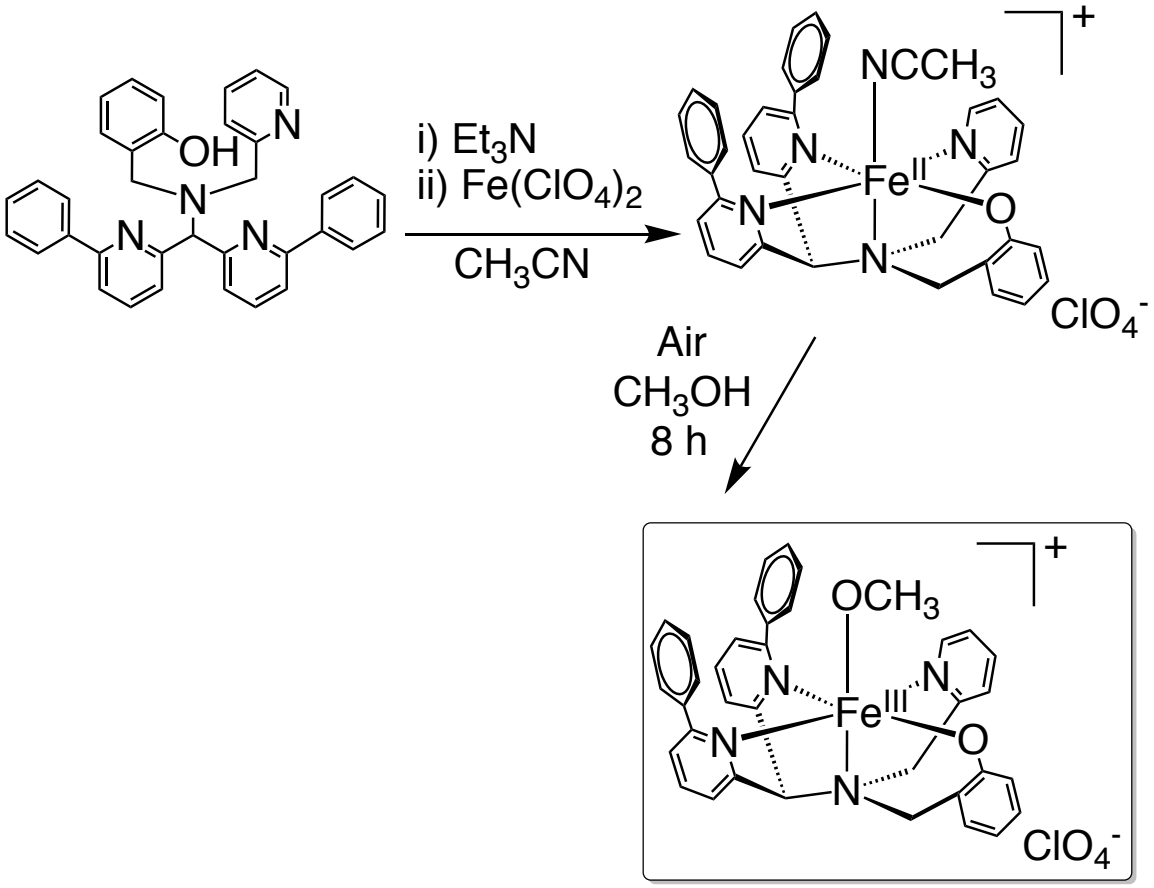

The synthesis of the designed N3PyOH^{2Ph} framework allowed for metalation and isolation of a mononuclear ferrous complex. Further reaction of this compound brought about the isolation of a mononuclear ferric terminal methoxide. The acquisition of this compound was the formation of a stable platform on which the rebound mechanism could be examined.[57] The trityl radical (consisting of multiple benzylic groups surrounding a tertiary, triply benzylic, carbon-based radical) was selected as a potential reactant with the $Fe^{III}(OCH_3)$ complex. Reaction between trityl radical and $Fe^{III}(OCH_3)$ produced the organic rebound product Ph_3COCH_3 and one-electron reduced Fe^{II} complex. UV-vis and EPR spectroscopies were employed to observe the consumption of ferric material.

Scheme 1.33: Rebound between a carbon-based radical and an $Fe^{III}(OCH_3)$ complex.[57]

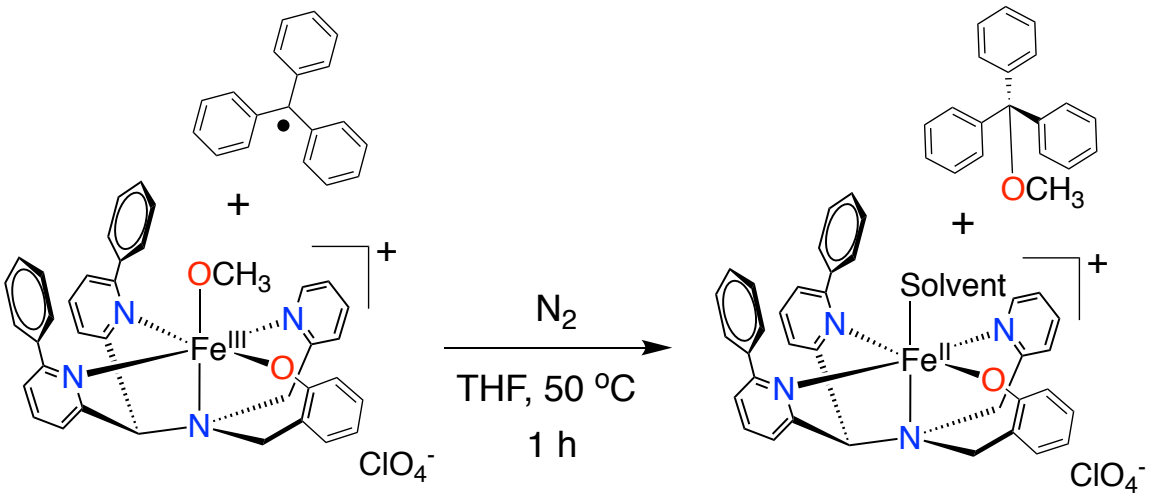

Mössbauer spectroscopy was employed to definitively observe the formation of the Fe^{II} complex. The Fe^{II} complex was also observed by ^1H NMR spectroscopy, which was additionally utilized in the observation of the organic product. The organic rebound product was also observed by GC-FID. This data taken together indicated that radical rebound had been observed between the ferric-methoxo complex and trityl radical.

Additional study was undertaken with substituted trityl-type radicals to gain information on the reactivity and mechanism with the $Fe^{III}OCH_3$ complex. Reaction of a series of radicals (R = -*p*-OCH_3, -*p*-*t*Bu, -*p*-Ph, -*p*-CN) was performed to obtain respective pseudo-first order rate constants that were used in a Hammett analysis.

Scheme 1.34. Rebound reactions of a series of organic radicals.

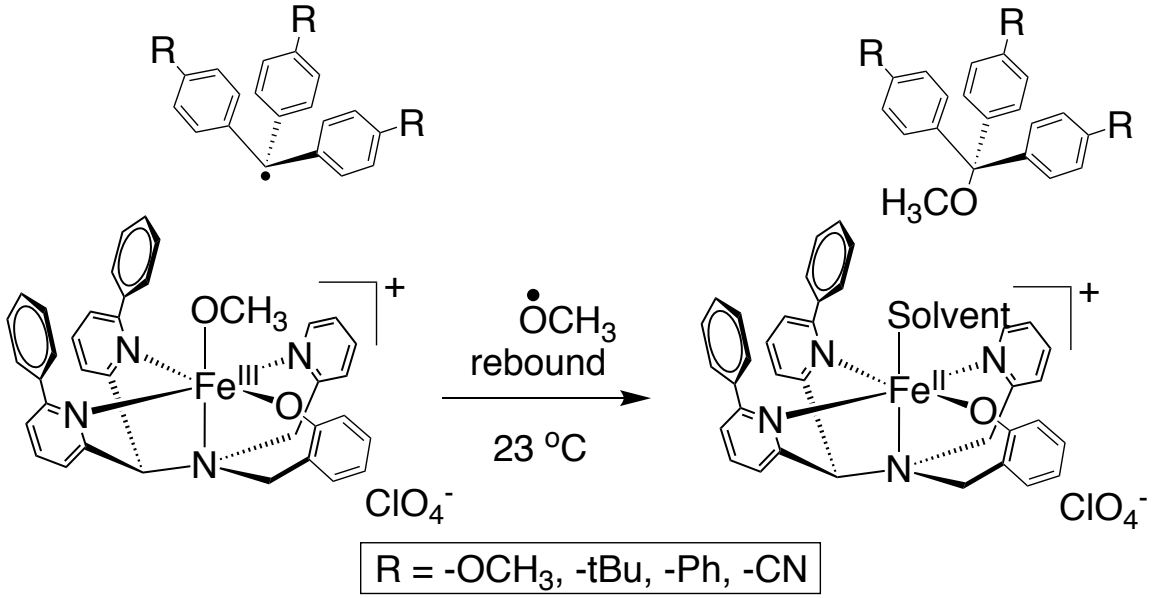

Hammett analysis of the reaction series showed a slope of -0.25, a small slope which indicated small charge separation in the transition state.[45, 61] Continued analysis was performed using Marcus theory to determine the nature of the rebound reaction, whether a concerted process or else a stepwise electron-transfer/action transfer. The likewise small slope of the Marcus plot (ρ = -0.098) compares well to other concerted proton-coupled electron transfer processes.[45, 47-48] These data indicate that not only are the proper one-electron reduced metal and the organic product produced, but the reaction occurs in a concerted fashion, in the manner of proposed enzymatic rebound processes.

The concept of radical rebound has long been used to explain the hydroxylation mechanism observed in heme enzymes, and has additionally been directly observed in a recent model complex.[45] The radical rebound concept has also been applied in the explanation of the analogous hydroxylation and halogenation mechanisms enacted in some nonheme enzymes. Experiments with several nonheme model complexes have produced additional information regarding the nature of rebound in nonheme complexes, as well as

additional experiments which have yielded direct evidence of the rebound step.[57] Having obtained direct observation of the rebound mechanism in a nonheme model complex, further investigation of the nature of halogenation or desaturation versus hydroxylation presents a point for future analysis.

1.5. References

1. Sono, M.; Roach, M. P.; Coulter, E. D.; Dawson, J. H., *Chem. Rev.* **1996,** *96*, 2841-2887.

2. Baglia, R. A.; Zaragoza, J. P. T.; Goldberg, D. P., *Chem. Rev.* **2017,** *117*, 13320-13352.

3. Sahu, S.; Goldberg, D. P., *J. Am. Chem. Soc.* **2016,** *138*, 11410-11428.

4. Borden, W. T.; Hoffmann, R.; Stuyver, T.; Chen, B., *J. Am. Chem. Soc.* **2017,** *139*, 9010-9018.

5. Cho, K. B.; Hirao, H.; Shaik, S.; Nam, W., *Chem. Soc. Rev.* **2016,** *45*, 1197-210.

6. Peck, S. C.; Donk, W. A. v. d., *J. Biol. Inorg. Chem.* **2017,** *22*, 381-394.

7. Xing, G.; Diao, Y.; Hoffart, L. M.; Barr, E. W.; Prabhu, K. S.; Arner, R. J.; Reddy, C. C.; Krebs, C.; J. Martin Bollinger, J., *Proc. Natl. Acad. Sci.* **2006,** *103*, 6130-6135.

8. Huang, X.; Groves, J. T., *Chem. Rev.* **2018,** *118*, 2491-2553.

9. Liang, Y.; Wei, J.; Qiu, X.; Jiao, N., *Chem. Rev.* **2018,** *118*, 4912-4945.

10. Price, J. C.; Barr, E. W.; Hoffart, L. M.; Krebs, C.; Bollinger, J. M. J., *Biochemistry* **2005,** *44*, 8138-8147.

11. Bollinger, J. M., Jr.; Price, J. C.; Hoffart, L. M.; Barr, E. W.; Krebs, C., *Eur. J. Inorg. Chem.* **2005,** *2005*, 4245-4254.

12. Laurenzi, I. J.; Jersey, G. R., *Environ. Sci. Technol.* **2013,** *47*, 4896-4903.

13. Etminan, M.; Myhre, G.; Highwood, E. J.; Shine, K. P., *Geophys. Res. Lett.* **2016,** *43*, 12614-12623.

14. Yvon-Durocher, G.; Allen, A. P.; Bastiviken, D.; Conrad, R.; Gudasz, C.; St-Pierre, A.; Thanh-Duc, N.; Giorgio, P. A. d., *Nature* **2014,** *507*, 488-495.

15. Gardner, J. D.; Pierce, B. S.; Fox, B. G.; Brunold, T. C., *Biochemistry* **2010,** *49*, 6033-6041.

16. Kumar, D.; Thiel, W.; Visser, S. P. d., *J. Am. Chem. Soc.* **2011,** *133*, 3869-3882.

17. McQuilken, A. C.; Jiang, Y.; Siegler, M. A.; Goldberg, D. P., *J. Am. Chem. Soc.* **2012,** *134*, 8759-8761.

18. Tchesnokov, E. P.; Faponle, A. S.; Davies, C. G.; Quesne, M. G.; Turner, R.; Fellner, M.; Souness, R. J.; Wilbanks, S. M.; Visser, S. P. d.; Jameson, G. N. L., *Chem. Commun.* **2016,** *2016*, 8814-8817.

19. Fellner, M.; Siakkou, E.; Faponle, A. S.; Tchesnokov, E. P.; Visser, S. P. d.; Wilbanks, S. M.; Jameson, G. N. L., *JBIC, J. Biol. Inorg. Chem.* **2016,** *21*, 501-510.

20. Ye, S.; Wu, X. a.; Wei, L.; Tang, D.; Sun, P.; Bartlam, M.; Rao, Z., *J. Biol. Chem.* **2007,** *282*, 3391-3402.

21. Chang, W.-c.; Li, J.; Lee, J. L.; Cronican, A. A.; Guo, Y., *J. Am. Chem. Soc.* **2016,** *138*, 10390-10393.

22. Liao, H.-J.; Li, J.; Huang, J.-L.; Davidson, M.; Kurnikov, I.; Lin, T.-S.; Lee, J. L.; Kurnikova, M.; Guo, Y.; Chan, N.-L.; Chang, W.-c., *Angew. Chem. Int. Ed.* **2018,** *57*, 1831-1835.

23. Dunham, N. P.; Chang, W.-c.; Mitchell, A. J.; Martinie, R. J.; Zhang, B.; Bergman, J. A.; Rajakovich, L. J.; Wang, B.; Silakov, A.; Krebs, C.; Boal, A. K.; J. Martin Bollinger, J., *J. Am. Chem. Soc.* **2018,** *140*, 7116-7126.

24. Bigi, M. A.; Reed, S. A.; White, M. C., *Nat. Chem.* **2011,** *3*, 216-222.

25. Mitchell, A. J.; Zhu, Q.; Maggiolo, A. O.; Anath, N. R.; Hillwig, M. L.; Liu, X.; Boal, A. K., *Nat. Chem. Biol.* **2016,** *12*, 636-640.

26. Shan, X.; Jr., L. Q., *Proc. Natl. Acad. Sci.* **2005,** *102*, 5340-5345.

27. MacMurdo, V. L.; Zheng, H.; Lawrence Que, J., *Inorg. Chem.* **2000,** *39*, 2254-2255.

28. Chiang, C.-W.; Kleespies, S. T.; Stout, H. D.; Meier, K. K.; Li, P.-Y.; Bominaar, E. L.; Lawrence Que, J.; Münck, E.; Lee, W.-Z., *J. Am. Chem. Soc.* **2014,** *136*, 10846-10849.

29. Hong, S.; Sutherlin, K. D.; Park, J.; Kwon, E.; Siegler, M. A.; Solomon, E. I.; Nam, W., *Nat. Commun.* **2014,** *5*, 5440-5446.

30. Momenteau, M.; Reed, C. A., *Chem. Rev.* **1994,** *94*, 659-698.

31. Kundu, S.; Matito, E.; Walleck, S.; Pfaff, F. F.; Heims, F.; Rábay, B.; Luis, J. M.; Company, A.; Braun, B.; Glaser, T.; Ray, K., *Chem. Eur. J.* **2012,** *18*, 2787-2791.

32. Oddon, F.; Chiba, Y.; Nakazawa, J.; Ohta, T.; Ogura, T.; Hikichi, S., *Angew. Chem. Int. Ed.* **2015,** *54*, 7336-7339.

33. Kim, S. O.; Sastri, C. V.; Seo, M. S.; Kim, J.; Nam, W., *J. Am. Chem. Soc.* **2005,** *127*, 4178-4179.

34. Thibon, A.; England, J.; Martinho, M.; Victor G. Young, J.; Frisch, J. R.; Guillot, R.; Girerd, J.-J.; Münck, E.; Lawrence Que, J.; Banse, F., *Angew. Chem. Int. Ed.* **2008,** *47*, 7064-7067.

35. Hong, S.; Lee, Y.-M.; Shin, W.; Fukuzumi, S.; Nam, W., *J. Am. Chem. Soc.* **2009,** *131*, 13910-13911.

36. Li, F.; Heuvelen, K. M. V.; Meyer, K. K.; Münck, E.; Lawrence Que, J., *J. Am. Chem. Soc.* **2013,** *135*, 10198-10201.

37. Lee, Y.-M.; Hong, S.; Morimoto, Y.; Shin, W.; Fukuzumi, S.; Nam, W., *J. Am. Chem. Soc.* **2010,** *132*, 10668-10670.

38. Sorokin, A. B.; Kudrik, E. V.; Bouchu, D., *Chem. Commun.* **2008**, 2562-2564.

39. Kudrik, E. V.; Afanasiev, P.; Alvarez, L. X.; Dubourdeaux, P.; Clémancey, M.; Latour, J.-M.; Blondin, G.; Bouchu, D.; Albrieux, F.; Nefedov, S. E.; Sorokin, A. B., *Nat. Chem.* **2012,** *4*, 1024-1029.

40. Jiang, Y.; Widger, L. R.; Kasper, G. D.; Siegler, M. A.; Goldberg, D. P., *J. Am. Chem. Soc.* **2010,** *132*, 12214-12215.

41. Badiei, Y. M.; Siegler, M. A.; Goldberg, D. P., *J. Am. Chem. Soc.* **2011,** *133*, 1274-1277.

42. Sallmann, M.; Siewert, I.; Fohlmeister, L.; Limberg, C.; Knispel, C., *Angew. Chem. Int. Ed.* **2012,** *51*, 2234-2237.

43. Ortiz de Montellano, P. R., *Chem. Rev.* **2010,** *110*, 932-948.

44. Rittle, J.; Green, M. T., *Science* **2010,** *330*, 933-937.

45. Zaragoza, J. P. T.; Yosca, T. H.; Siegler, M. A.; Moënne-Loccoz, P.; Green, M. T.; Goldberg, D. P., *J. Am. Chem. Soc.* **2017,** *139*, 13640-13643.

46. Marcus, R. A.; Sutin, N., *Biochim. Biophys. Acta., Rev. Bioenerg.* **1985,** *811*.

47. Osako, T.; Ohkubo, K.; Taki, M.; Tachi, Y.; Fukuzumi, S.; Itoh, S., *J. Am. Chem. Soc.* **2003,** *125*.

48. Lee, J. Y.; Peterson, R. L.; Ohkubo, K.; Garcia-Bosch, I.; Himes, R. A.; Woertink, J.; Moore, C. D.; Solomon, E. I.; Fukuzumi, S.; Karlin, K. D., *J. Am. Chem. Soc.* **2014,** *136*, 9925-9937.

49. The observation of metal-bound C-O products following a related rebound process for a nonheme $Ru^{IV}(O)$ complex was described. Kojima, T.; Nakayama, K.; Ikemura, K.; Ogura, T.; Fukuzumi, S., *J. Am. Chem. Soc.* **2011,** *133*, 11692-11700.

50. Rana, S.; Bag, S.; Patra, T.; Maiti, D., *Adv. Synth. Catal.* **2014,** *356*, 2453-2458.

51. Matthews, M. L.; Neumann, C. S.; Miles, L. A.; Grove, T. L.; Booker, S. J.; Krebs, C.; Walsh, C. T.; Bollinger, J. M., Jr., *Proc. Natl. Acad. Sci.* **2009,** *106*, 17723-17728.

52. Martinie, R. J.; Livada, J.; Chang, W.; Green, M. T.; Krebs, C.; Bollinger, J. M., Jr.; Silakov, A., *J. Am. Chem. Soc.* **2015,** *137*, 6912-6919.

53. Wong, C.; Fujimori, D. G.; Walsh, C. T.; Drennan, C. L., *J. Am. Chem. Soc.* **2009,** *131*, 4872-4879.

54. Planas, O.; Clemancey, M.; Latour, J.-M.; Company, A.; Costas, M., *Chem. Commun.* **2014,** *50*, 10887-10890.

55. Rana, S.; Dey, A.; Maiti, D., *Chem. Commun.* **2015,** *51*, 14469-14472.

56. Ligtenbarg, A. G. J.; Oosting, P.; Roelfes, G.; La Crois, R. M.; Lutz, M.; Hage, R.; Spek, A. L.; Feringa, B. L., *Chem. Commun.* **2001**, 385-386.

57. Pangia, T. M.; Davies, C. G.; Prendergast, J. R.; Gordon, J. B.; Siegler, M. A.; Jameson, G. N. L.; Goldberg, D. P., *J. Am. Chem. Soc.* **2018,** *140*, 4191-4194.

58. Lubben, M. M., Auke; Wilkinson, Elizabeth C.; Feringa, Ben; Que Jr., Lawrence, *Angew. Chem. Int. Ed. Engl.* **1995,** *34*, 1512-1514.

59. Sahu, S.; Zhang, B.; Pollock, C. J.; Dürr, M.; Davies, C. G.; Confer, A. M.; Ivanović-Burmazović, I.; Siegler, M. A.; Jameson, G. N. L.; Krebs, C.; Goldberg, D. P., *J. Am. Chem. Soc.* **2016,** *138*, 12791-12802.

60. Sahu, S.; Widger, L. R.; Quesne, M. G.; de Visser, S. P.; Matsumura, H.; Moënne-Loccoz, P.; Siegler, M. A.; Goldberg, D. P., *J. Am. Chem. Soc.* **2013,** *135*, 10590-10593.

61. Colclough, N.; Smith, J. R. L., *J. Chem. Soc. Perkin Trans. 2* **1994**, 1139-1149.

Chapter 2 Synthesis and Characterization of a Terminal $Fe^{III}(OCH_3)$ Complex

Parts of the following chapter were adapted from a work co-written with the following authors:

Pangia, Thomas M.; Davies, Casey G.; Prendergast, Joshua R.; Gordon, Jesse B.; Siegler, Maxime A.; Jameson, Guy N. L.; Goldberg, David P. *J. Am. Chem. Soc.*, **2018**, 140, 4191-4194.

2.1. Introduction

Synthetic complexes of both heme and nonheme frameworks have also been utilized to study C-H hydroxylation.[1-3] A typical C-H hydroxylation mechanism involves the abstraction of a hydrogen atom from a C–H bond by a high-valent metal-oxo species. This initial step is then followed by recombination of the carbon radical (R•) with the newly formed metal-bound hydroxide ligand (Scheme 2.1). The iron–hydroxide intermediate is not observed because the cleavage of the C-H bond is rate-determining.[4] In order to study this key recombination step, the synthesis of an analog of the ferric–hydroxide compound was undertaken.

Scheme 2.1. Hydroxide versus halogen rebound in nonheme complexes.[5]

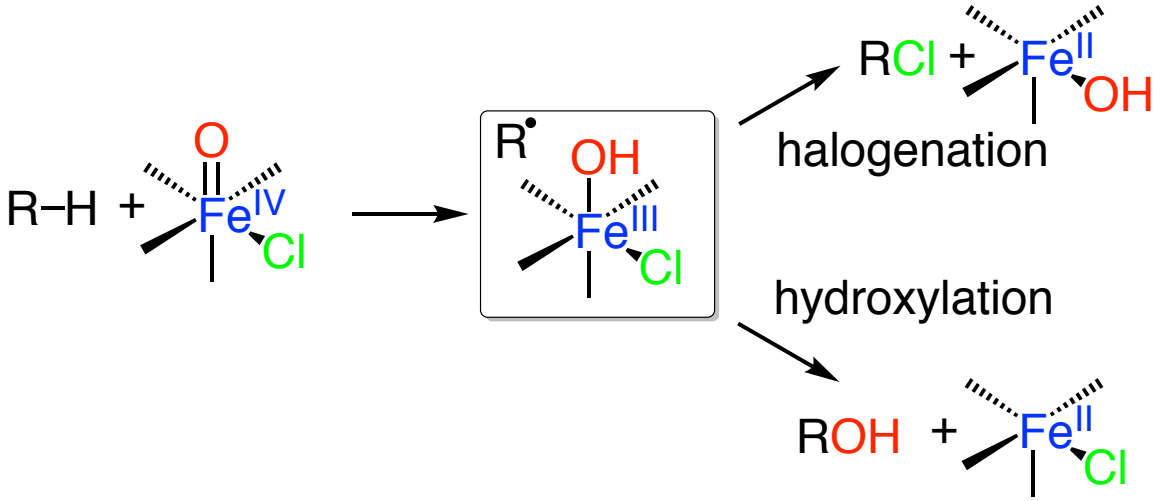

The rebound process is controlled by numerous factors that are critical in determining the final outcome of these nonheme iron mediated oxidations. Substrate orientation is particularly important, and plays a primary role in the understanding of the rebound process in the class of nonheme iron halogenases.[6-9] In addition to the orientation of the substrate, which may be responsible for the selective halogenation as opposed to possible hydroxylation in halogenase enzymes. Other factors may also have a significant influence on the reactivity. First-coordination sphere and metal-O bond strengths may be important for reactivity. Of further consideration is the redox potential of the complex, as well as the electronic structure. These different factors could influence the preference of rebound vs non-rebound reactivity in both enzymes and synthetic catalysts.

Efforts have been underway to produce complexes that could be used to examine the factors that control the rebound reaction. One notable example was produced earlier by our research group, in which a heme-type iron-hydroxide complex was employed to observe a rebound reaction.[4] However there have been few examples of direct observation of the radical rebound process in a nonheme iron complex that produces a new C-O bond,

beyond that which will be discussed later.[5] There have been some additional nonheme complexes wherein similar processes have been observed, however the direct transference of oxygen from iron for form a new C-O bond was not reported.[10-13] Some complexes made use of hydrogen atom abstraction by an $Fe^{IV}(O)$ complex which is purported to form the ferric–hydroxide responsible for the oxygen addition to the substrate.[14]

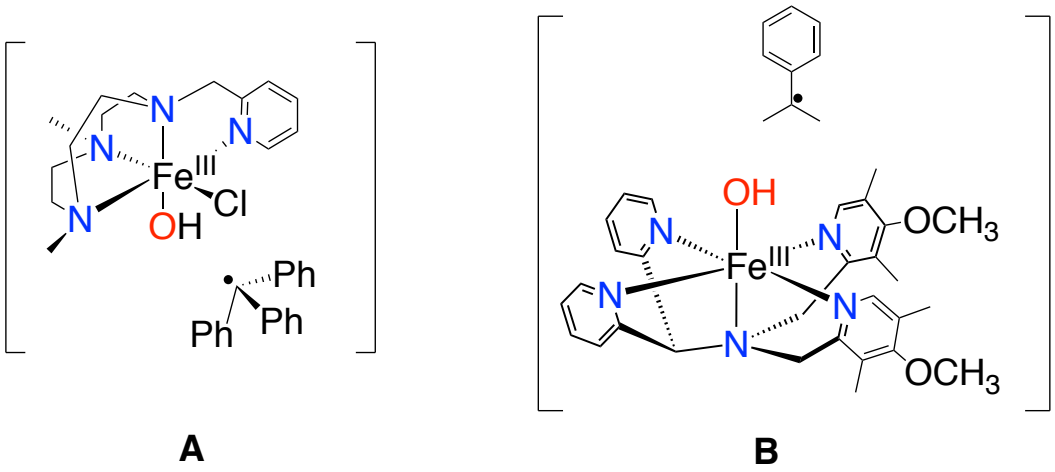

Figure 2.1. Putative ferric–hydroxide intermediates during proposed rebound reactions.[14-15]

Intermediate **A** was proposed during the study of an analog complex of CytC3 and SyrB2, halogenase enzymes.[14] Kinetic and spectroscopic studies of CytC3 have revealed evidence of Cl-$Fe^{IV}(O)$ intermediates, which react by hydrogen atom abstraction to form a Cl-$Fe^{III}(OH)$ compound accompanied by a carbon-based radical from the substrate. However in the case of these halogenase enzymes, there is no rebound involving the hydroxide moiety. Instead the halogen undergoes the rebound interaction to afford the chlorinated substrate and the one-electron-reduced metal center, purportedly due to the *cis* position of the halide with respect to the oxo functionality.[7, 14, 16] When the initial Cl-$Fe^{IV}(O)$ precursor of **A** reacted with selected substrates, the proposed Cl-$Fe^{III}(OH)$ was not observed,

however, the product formation of a hydroxylated substrate indicated transfer of the hydroxyl group rather than the halide group for this type of complex.

Intermediate **B** was proposed during the course of a similar reaction, between an $Fe^{IV}(O)$ complex and cumene, which performed functions closely related to the rebound process.[15] The starting material, $[Fe^{IV}(O)(N4Py)^{OMe,2Me}]^{2+}$ reacted with an introduced cumene substrate, resulting in a hydrogen atom abstraction to lead to the proposed intermediate. Under rebound conditions, a hydroxylated organic compound, bound to the one-electron-reduced ferrous center, was detected by ESI-MS. While the putative rebound product was detected, it was only fleeting and underwent rapid comproportionation to form oxidized ferric materials (Scheme 2.2). When tested, no trapped radical materials were detected, which indicated that there was little to no radical escape from the solvent cage and thus the observed reaction by-products are obtained by rebound and subsequent oxidation.[15]

Scheme 2.2. Oxidation of rebound products.[15]

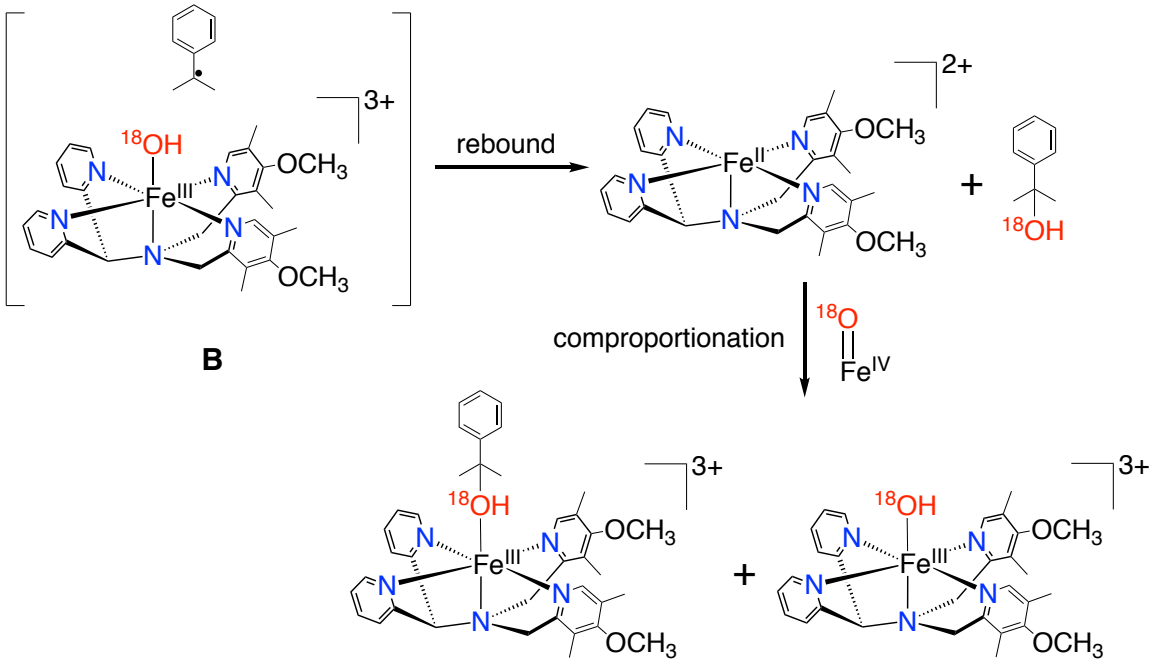

Several compounds have been characterized with terminally-bound iron(III)–methoxide ligands, which are relatively stable analogs of $Fe^{III}(OH)$.[17-21] In 1997 a complex was synthesized as a model for the ferric–hydroxide species purported to be the active hydrogen atom transfer agent in the rate-determining step of the lipoxygenase oxidative conversion reaction.[17] The complex, $[Fe(Py5)(OCH_3)](OTf)_2$, was generated by oxidation of the precursor ferrous material $[Fe(Py5)(CH_3OH)](OTf)_2$.

Scheme 2.3. Generation of a ferric-methoxide complex.[17]

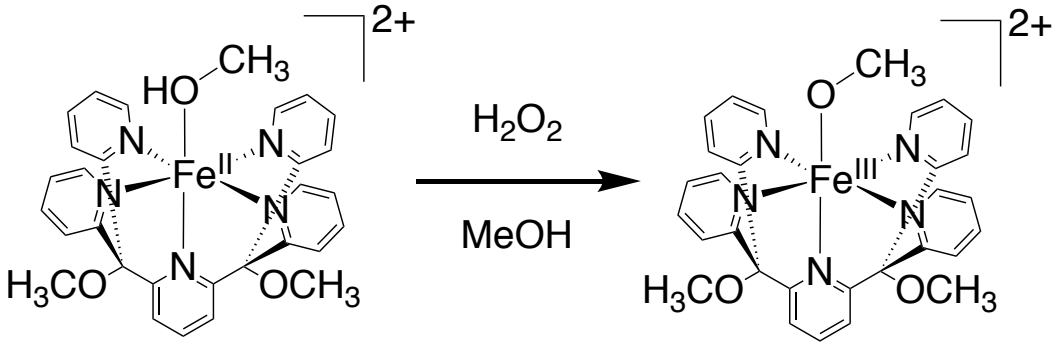

The bond length of the Fe–O bond (1.78 Å) in the $[Fe(Py5)(OCH_3)](OTf)_2$ material is notably short as is expected of the ferric oxidation state coupled with the deprotonated methoxide ligand, and is fairly close to the analogous bond length (1.88 Å) of the ferric–hydroxide species implicated in activated lipoxygenase. The compound $[Fe(Py5)(OCH_3)](OTf)_2$ was capable of abstracting hydrogen from weak C–H bonds, forming benzene from 1,4-cyclohexadiene. This compound was also estimated to be capable of abstracting hydrogen from any substrate with a C–H BDE of up to 84 kcal/mol. The potential for undergoing oxygen rebound by this complex was not investigated.

Additional complexes capable of forming such terminal ferric–methoxide were also investigated. In 1999,[19] the venerable N4Py ligand was used to stabilize an iron center to form $[(N4Py)Fe^{III}(OCH_3)](ClO_4)_2$, which was investigated for its structural characteristics

as a model for activated bleomycin, and for its ability to react with H_2O_2 to give a $Fe^{III}(OOH)$ intermediate.

Scheme 2.4. Reaction of a ferric–methoxo complex to form an intermediate ferric–hydroperoxo complex.[19]

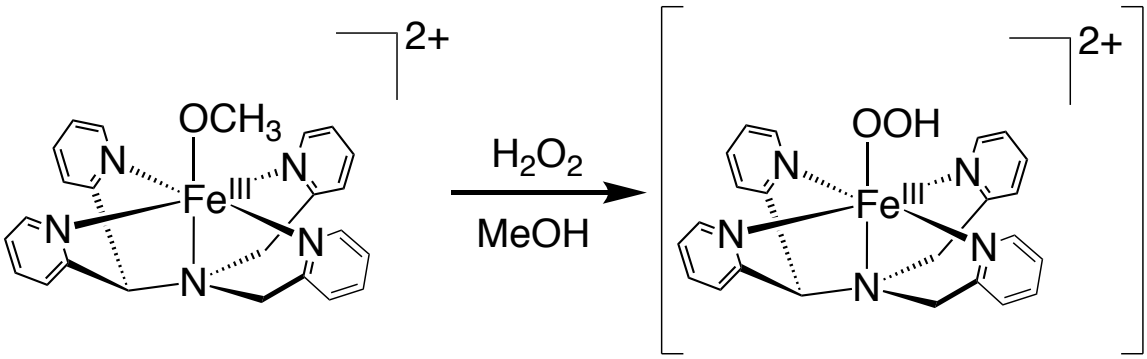

The spin state of $[(N4Py)Fe^{III}(OCH_3)](ClO_4)_2$ was found to be temperature-dependent, with lower temperatures favoring the low-spin state. The complex also formed two distinct structures when characterized crystallographically, one with an Fe–OCH_3 bond length of 1.772 Å, and one with a slightly longer Fe–OCH_3 bond length of 1.789 Å.[19] Both bond lengths are comparable to the 1.78 Å of the related $[Fe(Py5)(OMe)](OTf)_2$ complex.[17] When cooling the $[(N4Py)Fe^{III}OCH_3](ClO_4)_2$ complex to -20 °C and adding H_2O_2, the complex was converted to a hydroperoxo intermediate.

Shortly after in 2002, a set of compounds were synthesized as models for superoxide dismutase.[18, 22] The ligand was deprotonated to encourage metal coordination and stabilize the ferric oxidation state. A complex bearing two methoxide ligands was isolated and characterized.

Scheme 2.5. Formation of ferric–dimethoxide complex.[18]

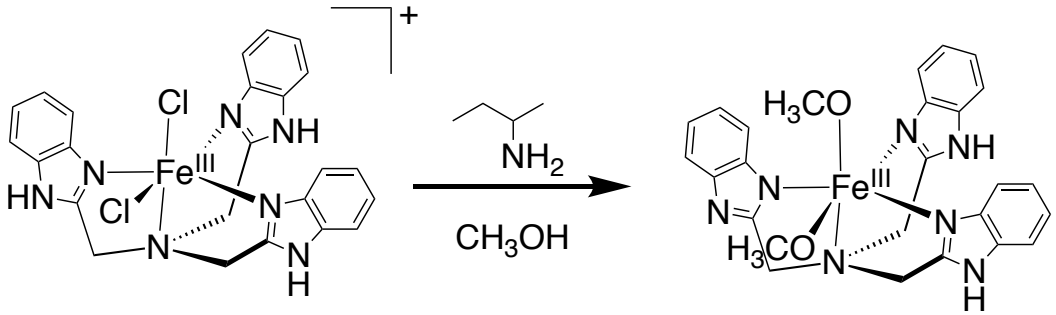

The single deprotonation of the chloride-bound starting material resulted in the formation of a doubly-bound methoxide complex, which was crystallographically characterized. The two methoxide ligands exhibited bond lengths that were more elongated than those of previous ferric–methoxide complexes, 1.861 Å and 1.902 Å.

During 2014 as part of an investigation into the pH-dependence of ferric TPA-based complexes, an additional ferric–methoxide was isolated and characterized.

Scheme 2.6. Generation of ferric–methoxide with naphtholate.[20]

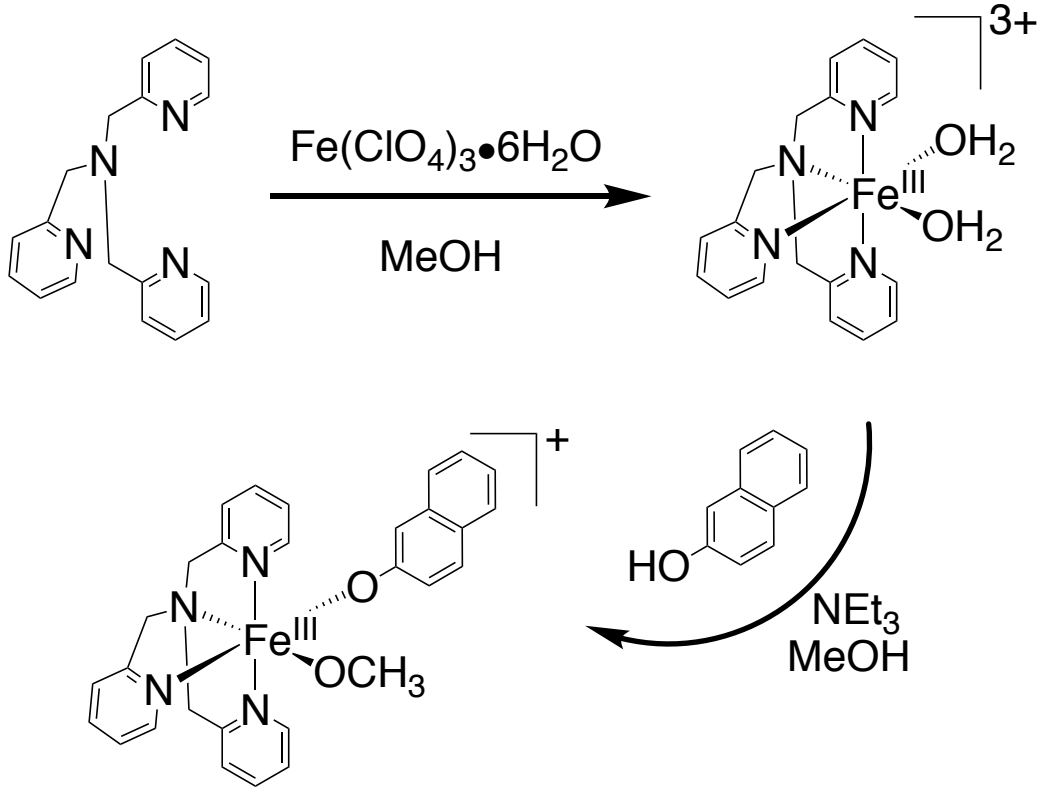

The TPA ligand was metallated in a methanolic solution, and subsequently combined with 2-naphthol and triethylamine base to afford the [Fe(TPA)(2-naphtholate)(OCH_3)]ClO_4 complex, which was crystallographically characterized. The Fe-OCH_3 bond length of 1.833 Å was also a bit longer than some of what had been previously observed, approximately in the middle of the range of 1.77-1.992 Å.

Further observation of a ferric–methoxide complex was obtained in 2016, when a tripodal thiolate-ligated complex was synthesized and isolated.[21] The complex was generated as a model of ferric–hydroxide/alkoxide species recognized as key in lipoxygenase and other enzymes, particularly as agents for hydrogen atom abstraction.

Scheme 2.7. Generation of a thiolate-bound ferric–methoxide complex.[21]

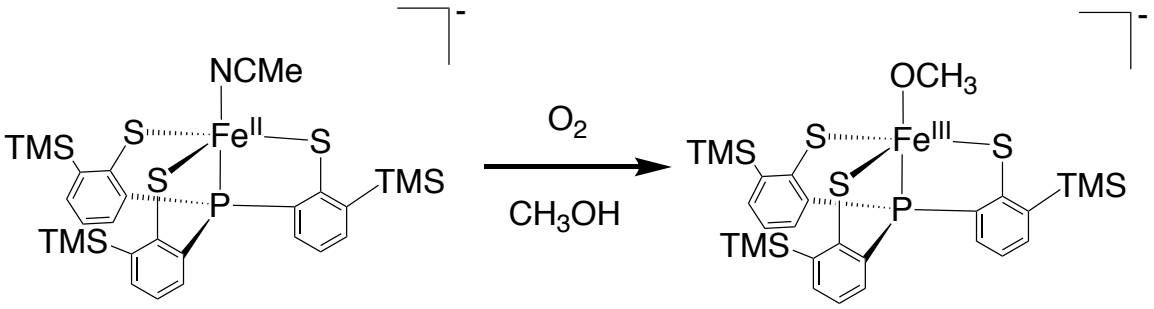

A tetradentate tris(benzenethiolato)phosphine ligand was utilized to stabilize the metal complex, and exposure of the ferrous material to dioxygen in methanol resulted in the acquisition of a $Fe^{III}(OCH_3)$ compound. Following formation of the ferric–methoxide material, the complex was explored as a potential rare nucleophilic ferric center. When dissolved in dichloromethane, the ferric center is capable of activating the C–Cl bond of CH_2Cl_2 to yield an analogous ferric–chloride.

Scheme 2.8. Formation of a ferric–chloride complex by nucleophilic iron(III) attack.[21]

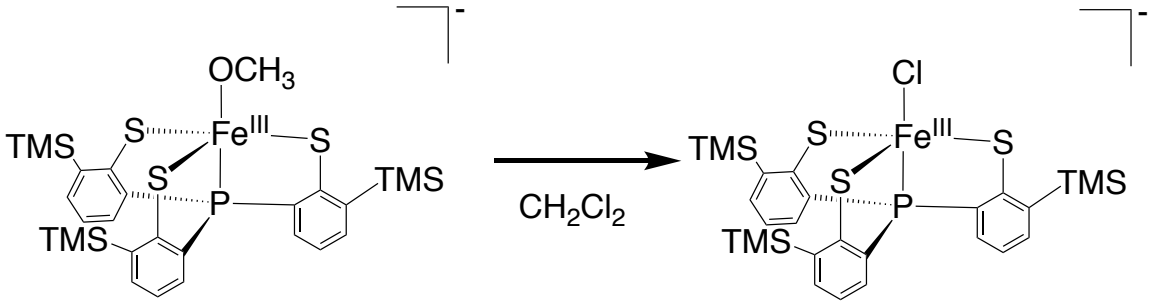

The ferric–methoxide complex was crystallographically characterized, revealing the Fe–OCH_3 bond length to be 1.866 Å, roughly in the middle of the range of previously characterized ferric–methoxide complexes. The observation of nucleophilic attack by a ferric–methoxide material expanded knowledge on the capabilities of these complexes, and points to potential new directions for ferric–methoxide reactivity investigations. However, although the stable ferric–methoxide compound was formed, there was no investigation into potential for rebound activity.

In order to design a complex through which the direct rebound step might be interrogated, several structural factors were considered. Past work from our lab produced a pentadentate ligand based on the N4Py framework, the N3PyS ligand.[23] When bound with iron(II), a mononuclear compound was formed that readily reacted with both O_2 and NO. The single thiolate donor was capable of encouraging and facilitating dioxygen reactivity of the complex.[24] Observation of the dioxygen-activating capabilities of $[Fe^{II}(N3PyS)](BF_4)$ and characterization of the resulting compounds showed S-oxygenation of the thiolate ligand.

Based on the activity of the phenyl thiolate moiety of the N3PyS system, it was proposed to modify the ligand framework with a phenolate as opposed to the phenyl thiolate, as the phenolate would be inert to dioxygen reactivity in the manner of S-

oxygenation. The ligand framework N3PyO was previously characterized, and an Fe complex with this ligand reacts with H_2O_2 to oxidize alcohols.[25] However, the Fe complex is prone to dimerization when in the ferric state.

Scheme 2.9. Dimerization of N3PyO complex.[25]

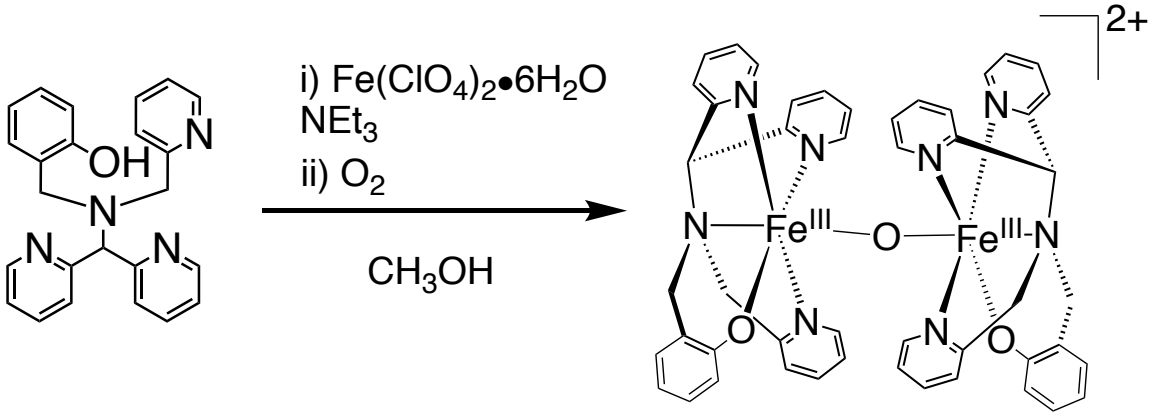

The generated μ-oxo dimer was examined as a catalyst for substrate oxidation in concert with H_2O_2. The complex was capable of mediating the rapid oxidation of secondary and primary alcohols. The system was fairly stable as a catalyst, producing up to 96 turnovers for each iron center, a process which the system was able to repeat at least three times without any loss of activity. The dimerization of the complex prevented any putative hydroxide or methoxide intermediates from being observed, although the complex in conjunction with H_2O_2 is fairly effective at oxidizing alcohol substrates.

The phenolate functionality was selected as a target for effective coordination with an iron center for further study, however tendency to dimerize would need to be negated to form the desired mononuclear model complex. For this study, it was proposed to modify an N4Py framework with a phenoxo donor, while adding steric encumbrance to prevent dimerization. Diphenyl substituents modifying an N4Py framework have been shown to

negate dimerization, while also offering opportunity to observe unique reactivity in nonheme systems.[26-27]

One of the key intermediates in the nonheme-type oxygenase reaction mechanism is an $Fe^{IV}(O)$ species, and much effort has been placed into generating $Fe^{IV}(O)$ models. Special efforts have been made in designing ligands that are capable of stabilizing this high-valent species for observation and characterization. Our group has in the past utilized secondary coordination sphere modifications to increase stability of these species. One such modification has been to apply an increased amount of steric hindrance to the basic N4Py framework by utilization of a diphenyl substituent system.

Scheme 2.10. Generation of an intermediate $Fe^{IV}(O)$ species in a nonheme iron complex.[26]

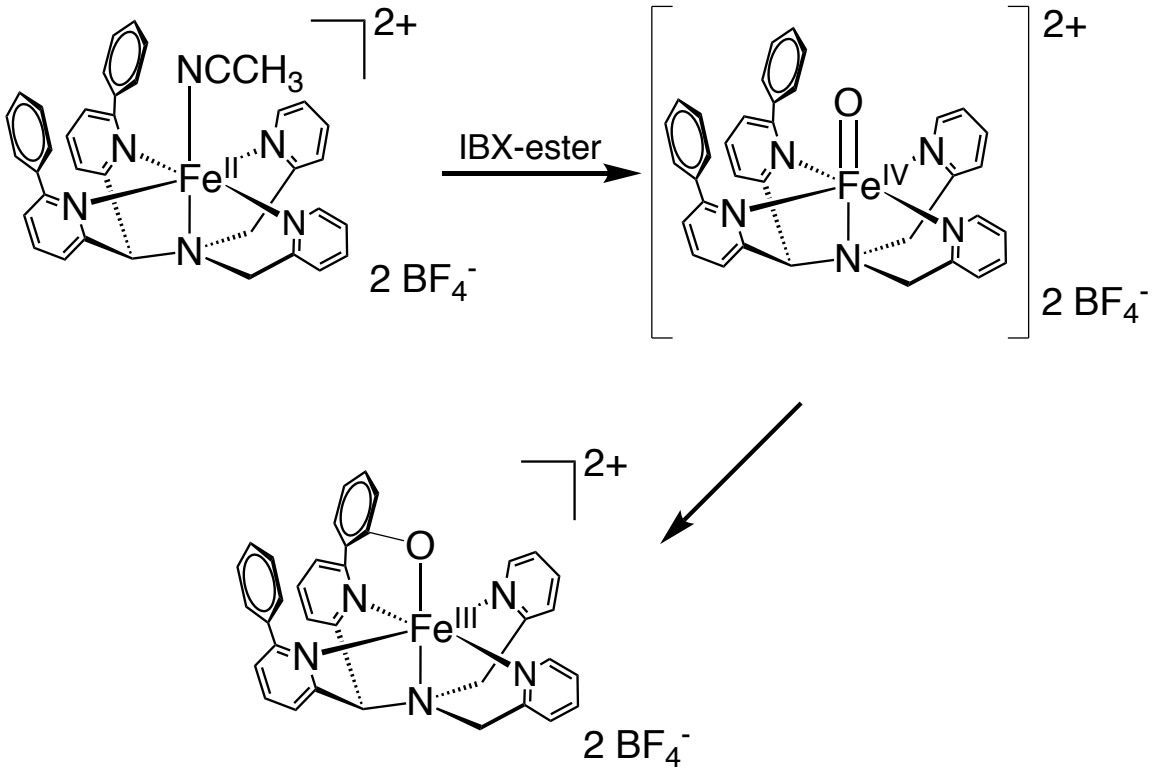

The additional phenyl substituents were found to significantly alter the spin state. While $[Fe^{II}(N4Py)(CH_3CN)]^{2+}$ is known to exist in a low-spin state, the analogous $[Fe^{II}(N4Py^{2Ph})(CH_3CN)]^{2+}$ resides in the high-spin state. When adding IBX ester or other

suitable oxygen transfer agents, a surprising ferric–hydroxide compound was isolated, showing evidence of arene hydroxylation (Scheme 2.10). The single *ortho*-hydroxylated product, observed in several different cases, showed selectivity that indicated a common intermediate in each pathway, which was proposed as $[Fe^{IV}(O)(N4Py^{2Ph})]^{2+}$. Oxygen transfer by $PhI^{18}O$ formed the appropriate product with 88% incorporation, indicating that the hydroxylation results from the labeled source and likely $Fe^{IV}(O)$ intermediate. Although efforts to trap the intermediate at low temperatures (-35 °C and -60 °C) were unsuccessful, the rapid nature of the hydroxylation even at low temperatures is in stark contrast to the lack of benzene/arene reactivity of $[Fe^{IV}(O)(N4Py)]^{2+}$.

The ligand set was further modified by addition of *ortho*-substituents on the phenyl groups, in an attempt to decrease likelihood of arene hydroxylation.[27] Elimination of arene hydroxylation was proposed to be key in stabilizing the intermediate $Fe^{IV}(O)$ species.

Scheme 2.11. Generation and isolation of a mononuclear nonheme $Fe^{IV}(O)$ species.[27]

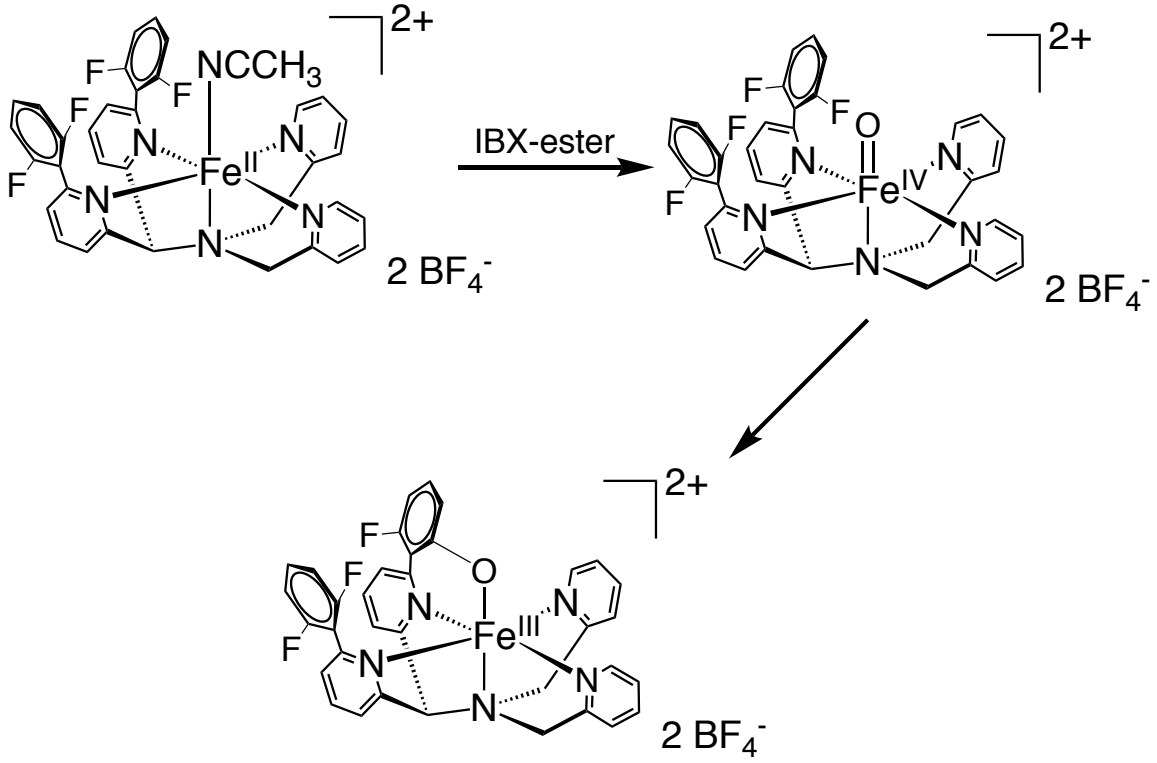

When reacted with IBX-ester, the $Fe^{IV}(O)$ material was generated and isolated at low temperature (-20 °C), indicating that the fluoride substituents deter reaction enough for isolation. The compound was crystallographically characterized to provide valuable information on this catalytic intermediate. However, on warming, the $Fe^{IV}(O)$ underwent arene hydroxylation as was previously observed in the similar precursor complex, in spite of the presence of the fluoride substituents.[27]

Based on the previous successes individually observed in the incorporation of phenolate in the primary coordination sphere and phenyl substituents in the secondary coordination sphere, both modifications were selected in the generation of a new complex (Scheme 2.12).

Scheme 2.12. Formation of a high-spin ferrous phenolate complex.[5]

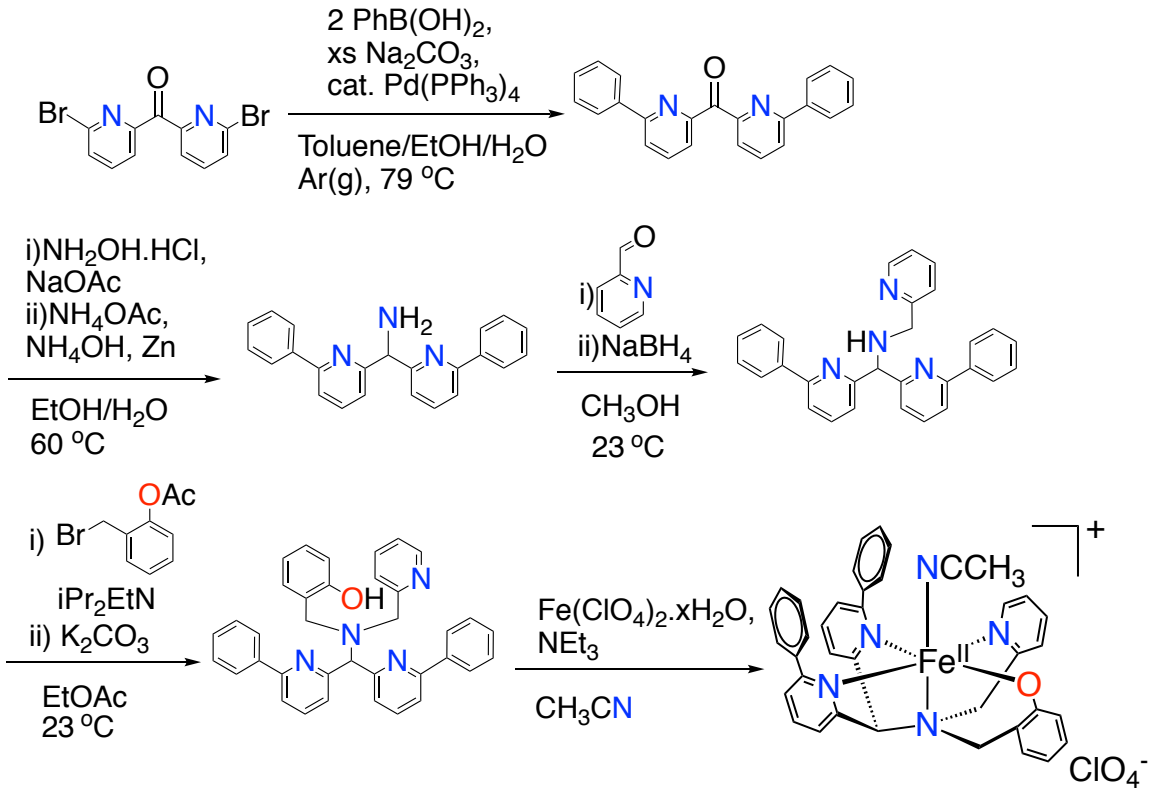

2.2. Experimental

General Methods and Materials. All chemicals and reagents were purchased from Sigma- Aldrich, Fisher Scientific, Acros Organics, Merck, Fluka Analytical, or Alfa Aesar and were used without further purification unless noted otherwise. Solvents (methanol, diethyl ether, acetonitrile, and tetrahydrofuran) used in organic synthesis were purified via Pure-Solv Solvent Purification System from Innovative Technology, Inc. Carbon tetrachloride was purchased from Fisher Scientific and used without further purification. For Mössbauer spectroscopy, ^{57}Fe (95.93% isotope-enriched) was purchased from Cambridge Isotope Laboratories. Solvents used in the reactions of the iron(II) and iron(III) complexes were subjected to additional purification after initial purification via a Pure-Solv Solvent Purification System. Acetonitrile was distilled over calcium hydride. THF was distilled from sodium/benzophenone. All solvents were degassed by freeze-pump-thaw cycles and stored in a N2 filled dry box. Reactions involving inert atmosphere were performed using either standard Schlenk techniques or in a dry box. The compounds 1,1-bis(6-phenylpyridin-2-yl)-*N*-(pyridin-2-ylmethyl)methanamine,[26] and 2-(bromomethyl)phenyl acetate[28] were synthesized according to literature procedures. *Caution: Perchlorate salts of metal complexes are potentially explosive. Care should be taken when handling these compounds.*

Analytical Methods. Kinetic UV-vis measurements were performed on a Hewlett-Packard Agilent 8453 diode-array spectrophotometer with a 3.5 mL quartz cuvette (path length = 1 cm) equipped with a septum. Other UV-visible spectra were recorded on a Varian Cary 50 Bio spectrophotometer. NMR spectra were collected on a Bruker Avance 400 MHz FT-NMR spectrometer. Electron paramagnetic resonance (EPR) spectra were

obtained on a Bruker EMX EPR spectrometer controlled with a Bruker ER 041 X G microwave bridge. The EPR spectrometer was equipped with a continuous-flow liquid He cryostat and an ITC503 temperature controller made by Oxford Instruments, Inc. Elemental analyses on air-stable compounds were performed by Atlantic Microlab Inc., Norcross, GA. Elemental analyses on air-sensitive compounds were performed by Midwest Microlabs, Indianapolis, IN.

Scheme 2.13. Synthesis of N3Py^{2Ph}OH.

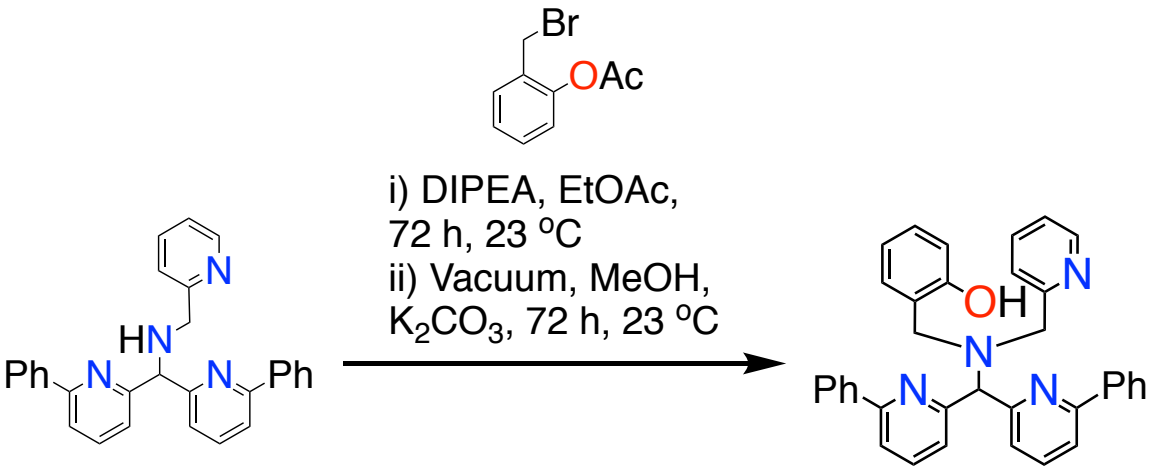

Synthesis of 2-(((bis(6-phenylpyridin-2-yl)methyl)(pyridin-2-ylmethyl)amino)methyl)phenol (N3Py^{2Ph}OH). The synthesis was adapted from a previous literature procedure.[25] An amount of 1,1-bis(6-phenylpyridin-2-yl)-*N*-(pyridin-2-ylmethyl)methanamine (1.21 g, 2.82 mmol) was dissolved in ethyl acetate (20 mL) in a 100 mL round bottom flask (Scheme S2.1). An amount of 2-(bromomethyl)phenyl acetate (0.77 g, 3.37 mmol) was dissolved in ethyl acetate (10 mL) and added to the amine solution, followed by addition of diisopropylethylamine (1.0 mL, 5.9 mmol). The reaction was stirred for 72 h at 23 °C. The organic solvent was removed under vacuum, and methanol (30 mL) was added, followed by potassium carbonate (2.21 g, 16 mmol) and stirring for

72 h at 23 °C. The resulting slurry was filtered through Celite and the filtrate concentrated under vacuum. The crude product was purified by column chromatography on silica gel with CH_2Cl_2/MeOH gradient as eluent. The compound was obtained as a yellow solid (0.518 g, 34%). ^{1}H NMR ($CDCl_3$) (Figure 2.9): δ 11.31-11.20 (br s, 1H), 8.74-8.60 (m, 1H), 8.10-8.01 (m, 4H), 7.79-7.65 (m, 4H), 7.64-7.56 (m, 1H), 7.53-7.33 (m, 9H), 7.24-7.14 (m, 2H), 7.13-7.07 (m, 1H), 6.96-6.87 (m, 1H), 6.82-6.75 (m, 1H), 5.56-5.50 (s, 1H), 4.25-4.17 (s, 2H), 4.11-4.03 (s, 2H). ^{13}C NMR ($CDCl_3$) (Figure 2.10): δ 159.0, 158.9, 158.0, 156.5, 148.7, 139.4, 137.0, 136.8, 130.6, 128.9, 128.8, 128.7, 127.1, 123.6, 123.0, 122.8, 122.2, 118.9, 118.7, 116.6, 69.6, 56.3, 54.6. FAB-MS: *calcd* for $[M+H]^+$ 535.2498, observed mass: 535.2486.

Synthesis of $[Fe^{II}(N3PyO^{2Ph})(CH_3CN)](ClO_4)$ (1). Under an inert atmosphere, $N3Py^{2Ph}OH$ (40 mg, 0.07 mmol) was dissolved in 5 mL of acetonitrile, to which was added triethylamine (10 μL, 0.07 mmol). The reaction mixture was stirred for 5 min. To this solution was added $Fe(ClO_4)_2 \bullet xH_2O$ (18 mg, 0.07 mmol), resulting in an instant change from yellow to dark brown. The solvent was removed in vacuo and the brown residue redissolved in methanol (2 mL) and filtered through Celite. Vapor diffusion of diethyl ether gave red-brown crystalline prisms of **1** after 1-2 weeks (15 mg, 27%) suitable for X-ray diffraction (Figure 2.2). ^{1}H NMR (CD_3CN): δ 72.6, 61.5, 51.2, 49.4, 45.5, 36.1, 31.8, 25.3, 19.2, 15.1, -8.2, -24.1, -27.3 (Figure 2.11). *Anal. Calcd* for $(C_{38}H_{32}ClFeN_5O_5) \bullet (CH_3OH) \bullet 0.5(CH_3CN)$: C, 61.47, H; 4.76; N, 9.19. Found: C, 60.48; H, 4.65; N, 8.76. UV-Vis (CH_3CN) (23 °C): Slight shoulder, λ = 450 nm (ε = 900 M^{-1} cm^{-1}). (Figure 2.7).

Synthesis of [Fe^{III}(N3PyO^{2Ph})(OCH_3)](ClO_4) (2). Under an inert atmosphere, a solution of **1** was generated in situ following the above procedure (0.05 mmol scale). Following filtration through Celite, the resulting solution of **1** was placed under vacuum to remove the organic solvent. The remaining brown residue was dissolved in 5 mL methanol and filtered through Celite an additional time. The brown methanol solution was removed from the inert atmosphere and exposed to air for 8 h, forming a purple solution (Figure 2.3, Figure 2.8). The purple solution was concentrated under vacuum and redissolved in methanol (1 mL). Vapor diffusion of diethyl ether formed dark purple crystalline rods of **2** after 2 days (17 mg, 41%) suitable for X-ray diffraction (Figure 2.6). ^{1}H NMR (THF-d_8): δ 88.2, 72.0, 63.0, 60.0, 55.4, 51.3, 48.3, 39.4, 38.6, 28.2, 27.0, 25.5, 16.6, -9.5, -15.5,-20.9 (Figure 2.13). *Anal. Calcd* for ($C_{37}H_{32}ClFeN_4O_6$)•(H_2O)•0.4($C_4H_{10}O$): C, 60.89, H; 4.93; N, 7.21. Found: C, 60.70; H, 4.74; N, 8.08. UV-vis (CH_3OH) (room temperature): λ = 550 nm (ε = 1290 M^{-1} cm^{-1}) (Figure 2.7). EPR (THF, 13 K): g = 4.26 (Figure 2.4).

Evans method measurement of the solution magnetic moment of 2. A stock solution of toluene in THF-d_8 (9% toluene) was prepared by mixing toluene (50 μL) into THF-d_8 (500 μL). A 75 μL aliquot was injected into a glass capillary which was flame sealed and inserted into an NMR tube. A solution of **2** (1.4 mM) was prepared in THF-d_8 (500 μL)/ toluene (50 μL), then transferred to the NMR tube containing the sealed capillary tube, and an ^{1}H NMR spectrum was recorded (Figure 2.5). The chemical shift of the singlet assigned to the -CH_3 peak for toluene in the presence of the paramagnetic complex was compared with that of the same peak in the inserted capillary tube. The effective spin-only magnetic

moment was calculated by simplified Evans method[22-23] using the equation $\mu_{eff} = 0.0618(\Delta\nu T/2fM)^{1/2}$, where f is the oscillator frequency (MHz) of the superconducting spectrometer, T is temperature (K), M is the molar concentration of the paramagnetic metal complex, and $\Delta\nu$ is the frequency difference (Hz) between the two reference toluene $-CH_3$ signals. The data shown in Figure 2.5 gave $\Delta\nu = 28.01$ Hz, $\mu_{eff} = 5.3\ \mu_B$, which is close to the calculated spin-only value for high-spin Fe^{III} (d^5), $\mu_{eff} = 5.9\ \mu_B$.

Single Crystal X-Ray crystallography. All reflection intensities were measured at 110(2) K using a SuperNova diffractometer (equipped with Atlas detector) with Mo *K*α radiation (λ = 0.71073 Å) for **1** or with Cu *K*α radiation (λ = 1.54178 Å) for **2** under the program CrysAlisPro (Version 1.171.36.32 Agilent Technologies, 2013). The same program was used to refine the cell dimensions and for data reduction. Both structures were solved with the program SHELXS-2014 (Sheldrick, 2008) and were refined on F^2 with SHELXL-2014 (Sheldrick, 2008).[29] Analytical numeric absorption correction based on a multifaceted crystal model was applied using CrysAlisPro. The temperature of the data collection was controlled using the system Cryojet (manufactured by Oxford Instruments). The H atoms were placed at calculated positions using the instructions AFIX 13, AFIX 23, AFIX 43, AFIX 137 or AFIX 147 with isotropic displacement parameters having values 1.2 *U*eq or 1.5 of the attached C or O atoms. For **2**, the H atoms attached to O1W/O1W' (disordered lattice water molecule) could not be retrieved from difference Fourier maps.

Crystal Structure of 1. The ClO_4^- counterion is found to be disordered over two orientations, and the occupancy factor of the major component refines to 0.780(7). The

asymmetric unit also contains one site occupied with a disordered mixture of solvent molecules (MeOH with occupancy factor of 0.618(2) and MeCN with occupancy factor of 0.382(2)).

1, Fw = 765.47, orange block, 0.41 × 0.35 × 0.22 mm^3, monoclinic, $P2_1/n$, a = 10.1120(3), b = 22.0629(6), c = 16.4935(4) Å. α = 90, β = 104.954(3), γ = 90°, V = 3555.08(17) $Å^3$, Z = 4, μ = 0.56 mm^{-1}, abs. corr. range: 0.838-0.915. 28564 Reflections were measured up to a resolution of $(\sin \theta/\lambda)_{max}$ = 0.650 $Å^{-1}$. 8157 Reflections were unique (R_{int} = 0.0244), of which 7099 were observed [$I > 2\sigma(I)$]. 542 Parameters were refined with 123 restraints. R1/wR2 [I >2σ(I)]: 0.0361/0.0884. *R*1/*wR*2 [all refl.]: 0.0436/0.0927. S = 1.04. Residual electron density found between -0.32 and 0.52 e $Å^{-3}$.

Crystal Structure of 2. The asymmetric unit contains one Fe complex, one ClO_4^- counterion and some amount of lattice solvent molecules (water and diethyl ether). The perchlorate counterion is disordered over three orientations, and the occupancy factors of the three components refine to 0.465(3), 0.231(2) and 0.304(3). One molecule of diethyl ether is found at sites of inversion symmetry, and thus is disordered with an occupancy factor refining to 0.381(4). The lattice water solvent molecule is disordered over two orientations, and the occupancy factor of the major component refines to 0.769(7).

2, Fw = 764.13, black rod, 0.32 × 0.09 × 0.05 mm^3, triclinic, *P*-1 (no. 2), *a* = 10.0679(4), *b* = 12.6568(4), *c* = 15.6766(5) Å, α = 98.834(3), β = 106.858(3), γ = 104.372(3)°, *V* = 1796.30(11) $Å^3$, *Z* = 2, D_x = 1.413 g cm^{-3}, μ = 4.527 mm^{-1}, T_{min}-T_{max}: 0.383–0.816. 23559 Reflections were measured up to a resolution of $(\sin \theta/\lambda)_{max}$ = 0.62 $Å^{-1}$. 7075 Reflections were unique (R_{int} = 0.0255), of which 6418 were observed [$I > 2\sigma(I)$]. 591 Parameters were

refined using 426 restraints. $R1/wR2$ [$I > 2\sigma(I)$]: 0.0504/0.1410. $R1/wR2$ [all refl.]: 0.0555/0.1461. S = 1.026. Residual electron density found between −0.49 and 0.90 e $Å^{-3}$. The crystallographic data for **1** and **2** can be obtained free of charge from the Cambridge Crystallographic Data Centre (www.ccdc.cam.ac.uk/data_request/cif).

2.3. Results and Discussion

The challenges of dimerization in the nonheme complexes **1** and **2** were avoided through the successful synthesis of the $N3PyOH^{2Ph}$ ligand. The synthesis of the precursor complex 1,1-bis(6-phenylpyridin-2-yl)-*N*-(pyridin-2-ylmethyl)methanamine ($N3Py^{2Ph}$) was already known to our group,[30] and this precursor was chosen for modification based on its phenyl group substituents. Addition of a phenolate was proposed through addition of an alkyl halide under basic conditions, however protection to the phenol moiety was needed to avoid unwanted interaction between the phenolate and alkyl halide. The compound, 2-(bromomethyl)phenyl acetate, was chosen for its acetate protecting group which was removed through addition of K_2CO_3 following the reaction with $N3Py^{2Ph}$. The successful synthesis of this compound was confirmed by ^{1}H and ^{13}C NMR analysis. The high-spin ferrous complex $[Fe^{II}(N3PyO^{2Ph})(CH_3CN)](ClO_4)$ (**1**) formed dark yellow crystals suitable for X-ray crystallography when grown from $MeOH/Et_2O$, shown in Figure 2.2. This ferrous complex was mononuclear, as expected from the steric encumbrance afforded by the phenyl substituents.

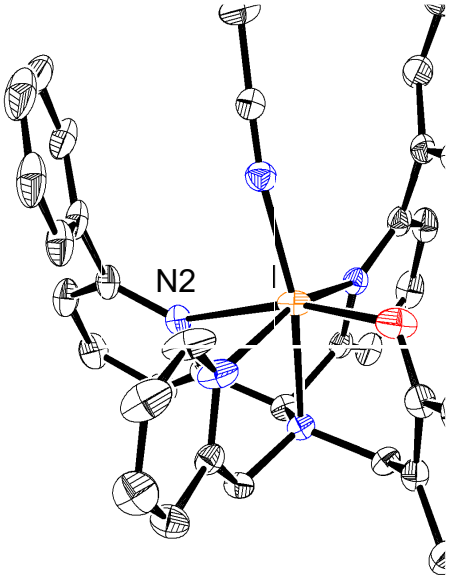

Figure 2.2. Displ evel) of the cation of **1**. H atoms, lattice solvent molecules, and ClO_4^- counterion have been omitted for clarity. Selected bond distances (Å) and angles (°): Fe1-N1 2.2633(13), Fe1-N2 2.473(3), Fe1-N3 2.1699(13), Fe1-N4 2.1598(14), Fe1-O1 1.9560(13), Fe1-N5 2.0769(14), N3-Fe1-N5 163.95(5), N1-Fe1-N4 155.78(5), O1-Fe1-N2 164.43(5), N5-Fe1-N4 101.54(5), N4-Fe1-N3, 79.02(5), O1-Fe1-N1 99.71(5), N4-Fe1-N2 85.40(5), N2-Fe1-N1 80.41(5), N4-Fe1-O1 88.82(6), N5-Fe1-O1 103.96(6), N5-Fe1-N1 98.34(5), N3-Fe1-N2 72.63(5), N5-Fe1-N2 91.37(5), N3-Fe1-N1 78.06(5), N3-Fe1-O1 92.08(5).

The phenolate ligand was bound in a pentadentate manner to the Fe^{II} center, while the phenolate arm was deprotonated. The labile sixth coordination site is occupied by an acetonitrile molecule. The Fe-N distances in **1** are fairly similar to analogous Fe-N distances in high-spin ferrous complexes of related N3PyS and $N4Ph^{2Ph}$ derivative ligands, with exception being made for the phenyl-substituted substituent pyridine trans to the phenolate moiety, which showed a fairly elongated distance of 2.473(3) Å. Another

similarly elongated bond distance can be observed for a phenyl-pyridyl donor of $[Fe^{II}(N4Py^{2Ph})(CH_3CN)]^{2+}$ (Fe-N = 2.378(13) Å).[26]

Scheme 2.14. Aerobic oxidation of a mononuclear nonheme iron complex.[5]

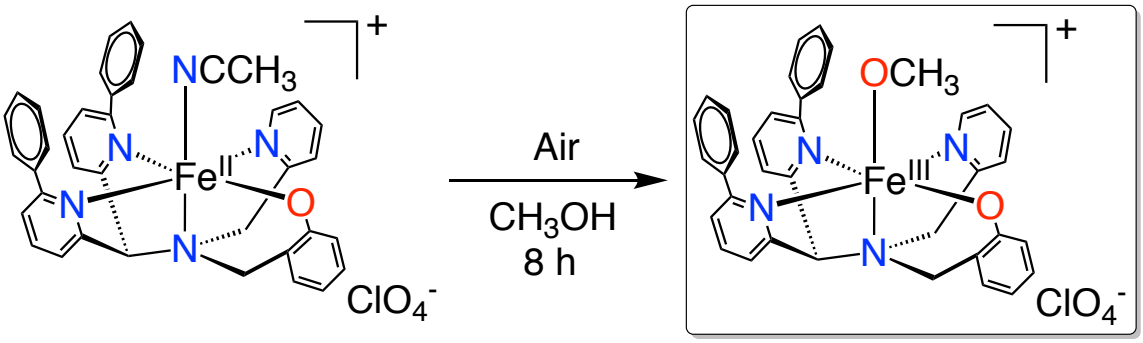

When **1** was reacted with air in methanol, the reaction produces a slow color change from dark yellow **1** to form a new dark purple species. When this reaction was monitored by UV-vis spectroscopy, the conversion of the spectrum for **1** was observed to form a new spectrum with a broad absorbance band at 550 nm (ε = 1290 M^{-1} cm^{-1}). The band is consistent with the formation of a phenolate-to-iron(III) transition associated with charge transfer.[31]

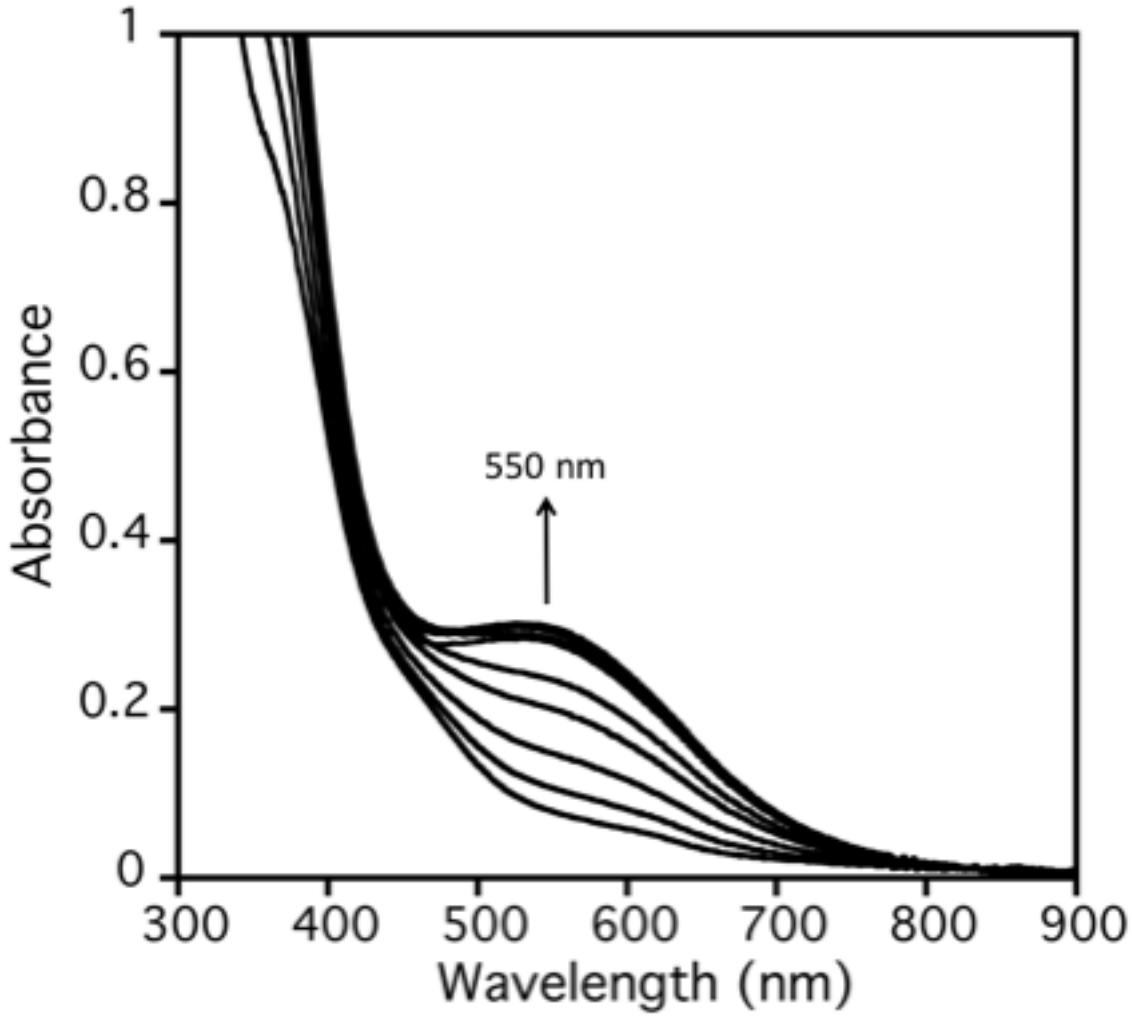

Figure 2.3. Formation of **2** from **1** (0.25 mM) in methanol at 23 °C under aerobic conditions, monitored by UV-vis spectroscopy over 8 h.

The purple complex was crystallized from CH_3OH/Et_2O, leading to crystals which were suitable for X-ray crystallographic structural determination (Figure 2.6). Analysis of the structure revealed a mononuclear iron(III) complex containing a terminal methoxide ligand occupying the open site, having a formula of $[Fe^{III}(N3PyO^{2Ph})(OCH_3)](ClO_4)$ **(2)**.

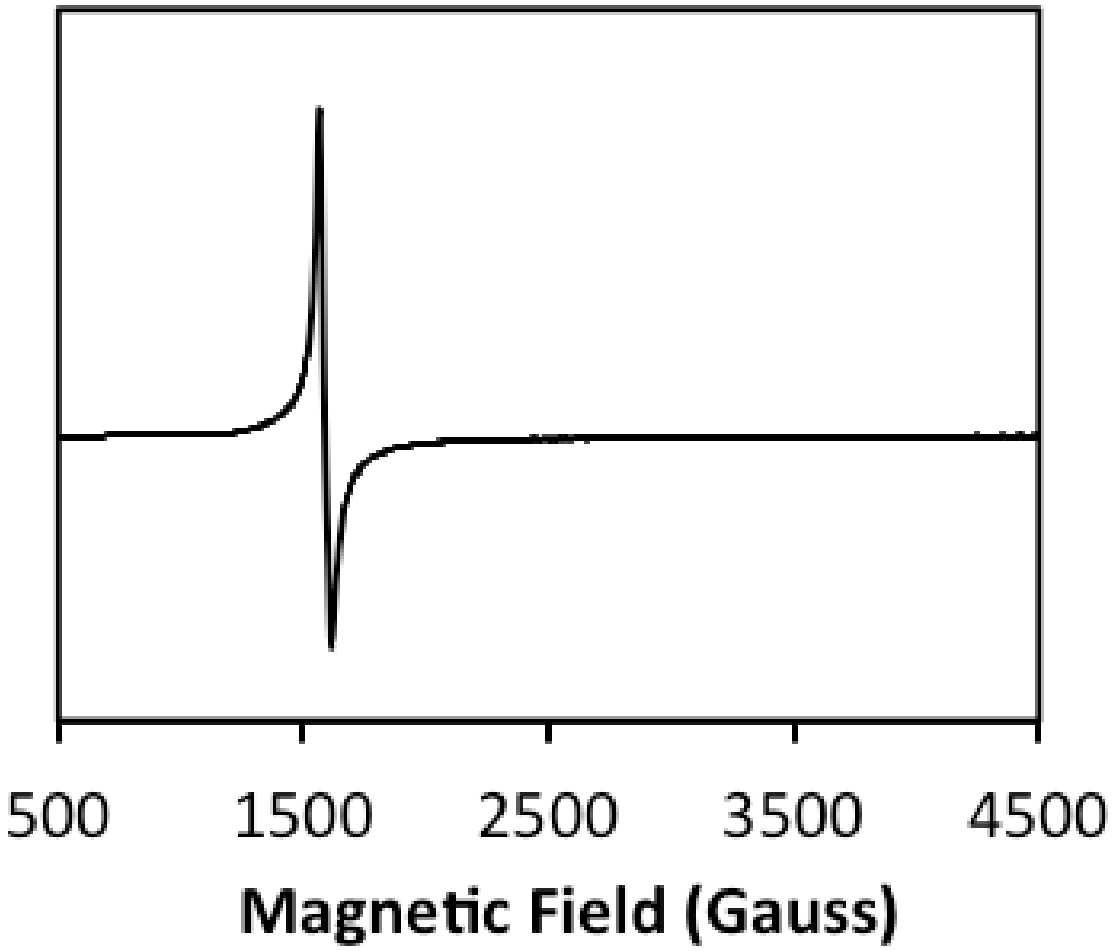

Figure 2.4. EPR spectrum of **2** in THF at 13 K. Frequency 9.2617 GHz, modulation amplitude 10 G, modulation frequency 100 KHz, attenuation 20 dB, receiver gain 5.02 x 10^3.

Crystals of the compound were observed by EPR spectroscopy, and found to have a relatively sharp feature at g = 4.26 when examined in frozen solution (THF, 13 K). This spectrum shows consistence with that expected of a high-spin Fe^{III} (S = 5/2) ground state for **2** (Figure 2.4).

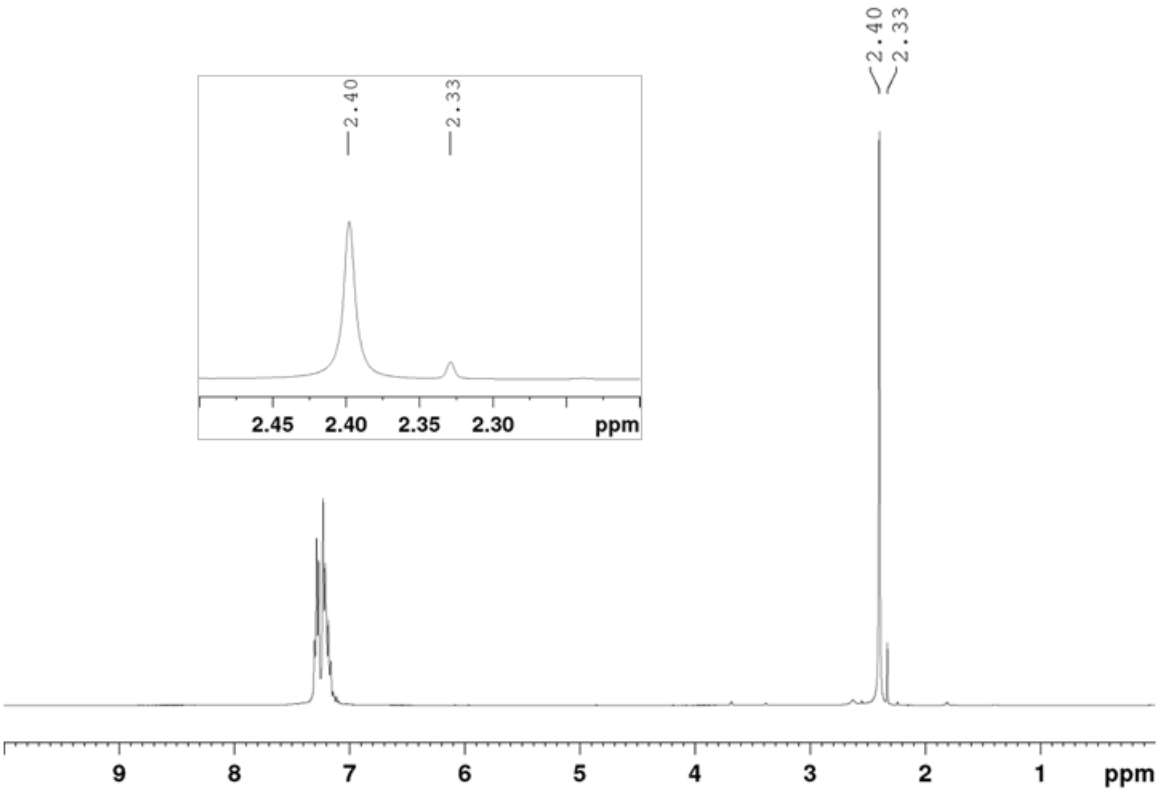

Figure 2.5. The ^{1}H NMR spectrum for the Evans method determination of the solution magnetic moment for **2** (0.0014 M) in THF-d_8 with toluene added as the internal standard. Inset: Expanded region of the spectrum showing the toluene –CH_3 peaks. $\Delta\nu$ = 28.01 Hz; f = 400.13 MHz; T = 294.8 K. The equation $\mu_{eff} = 0.0618(\Delta\nu T/2fM)^{1/2}$ was used to calculate the effective magnetic moment for **1**, where f is the oscillator frequency (MHz) of the superconducting spectrometer, T is temperature (K), M is the molar concentration of the paramagnetic metal complex, and $\Delta\nu$ is the frequency difference (Hz) between the two standard toluene -CH_3 signals.

Investigation by Evans method[32-33] measurement of **2** in THF-d_8 at 21 °C gave a measurement of μ_{eff} = 5.3 μ_B, which was close to the expected spin-only value of 5.91 μ_B expected for a mononuclear high-spin ferric ion (Figure 2.5).

When considering bond distances for **2**, the distance of the Fe-N bond held by the phenyl-substituted pyridine moiety in the trans position to the phenolate donor is shorter than the same bond in **1** (2.341(2) Å vs. 2.473(3) Å) as would be expected for the increase in oxidation state. Considering the Fe-OCH_3 bond length of **2**, the length of 1.784(2) Å is fairly similar to the same bond in the close analog $Fe^{III}(N4Py)(OCH_3)]^{2+}$ (1.772(3) Å). [19] Comparing to the range of values observed for such bonds in previously characterized complexes (Fe^{III}-OCH_3: 1.77-1.90 Å), the same bond in **2** is on the short end of the range.

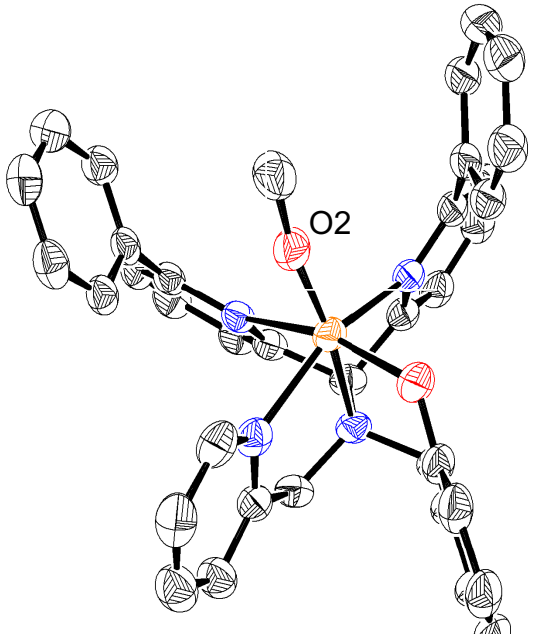

Figure 2.6. Displacement ellipsoid plot (50% probability level) of the cation of **2**. H atoms, lattice solvent molecules, and ClO_4^- counterion have been omitted for clarity. Selected bond distances (Å) and angles (°): Fe1-N1 2.341(2), Fe1-N2 2.249(2), Fe1-N3 2.202(2), Fe1-N4 2.156(2), Fe1-O1 1.9279(18), Fe1-O2 1.785(2), N1-Fe1-N2 81.41(7), N1-Fe1-N3 73.69(8), N1-Fe1-N4 87.28(7), N1-Fe1-O1 162.73(8), N1-Fe1-O2 94.40(9), N2-Fe1-N3 75.91(8), N2-Fe1-N4 152.29(8), N2-Fe1-O1 98.27(8), N2-Fe1-O2 102.40(9), N3-Fe1-N4

76.67(8), N3-Fe1-O1 89.43(8), N3-Fe1-O2 168.08(9), N4-Fe1-O1 85.26(9), N4-Fe1-O2 103.63(9), O1-Fe1-O2 102.48(9).

2.4. Conclusions

Isolation and characterization of **2** gave an analog of the $Fe^{III}(OH)$ rebound intermediate species, which provided opportunity to probe the key transfer step of the rebound process directly. Although previous complexes have existed by which such a mechanistic investigation might be possible, **2** was the first nonheme iron complex to our knowledge which was used in a direct examination of the rebound step.

2.5. Supporting Information

Contents

I. Supporting Figures.

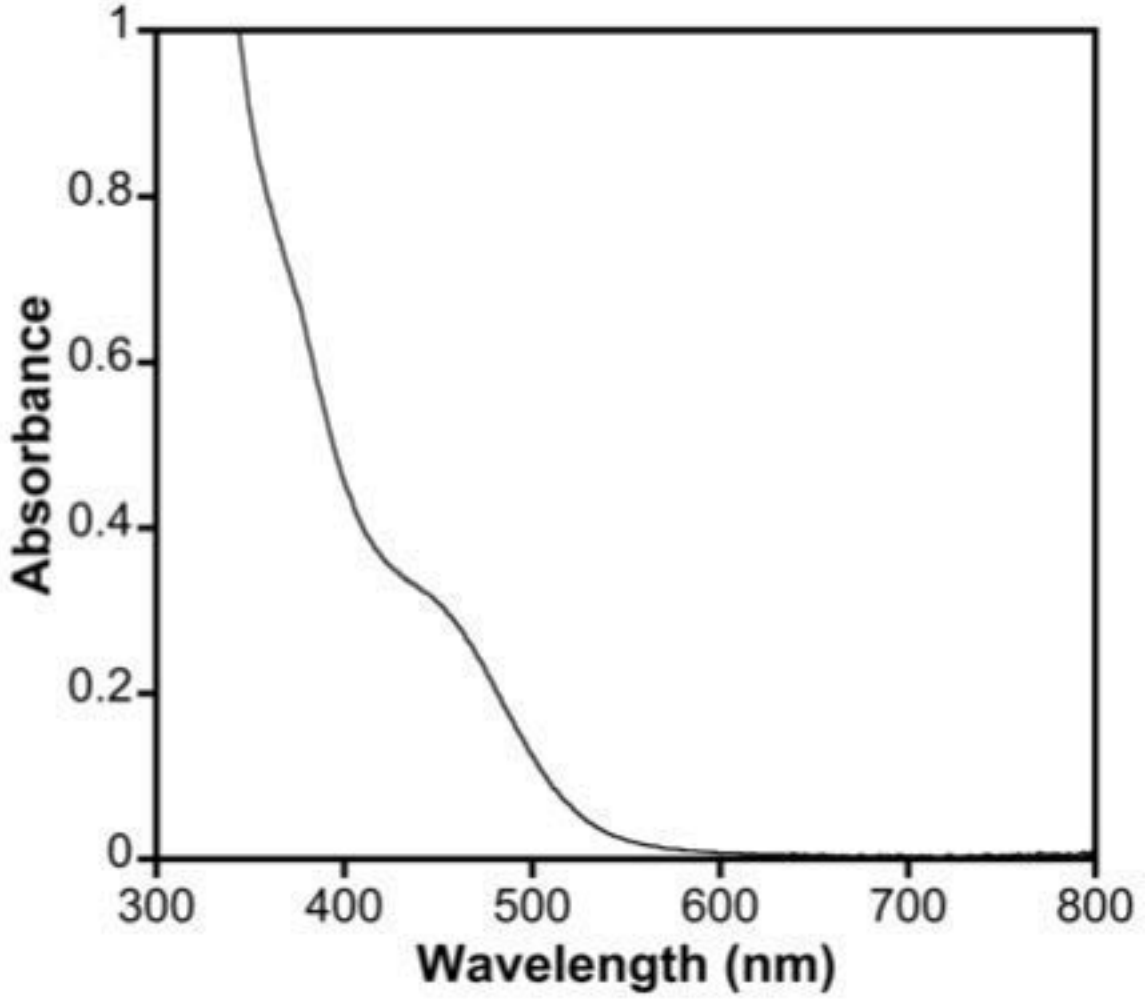

Figure 2.7. UV-vis spectrum of **1** (0.3 mM) in acetonitrile.

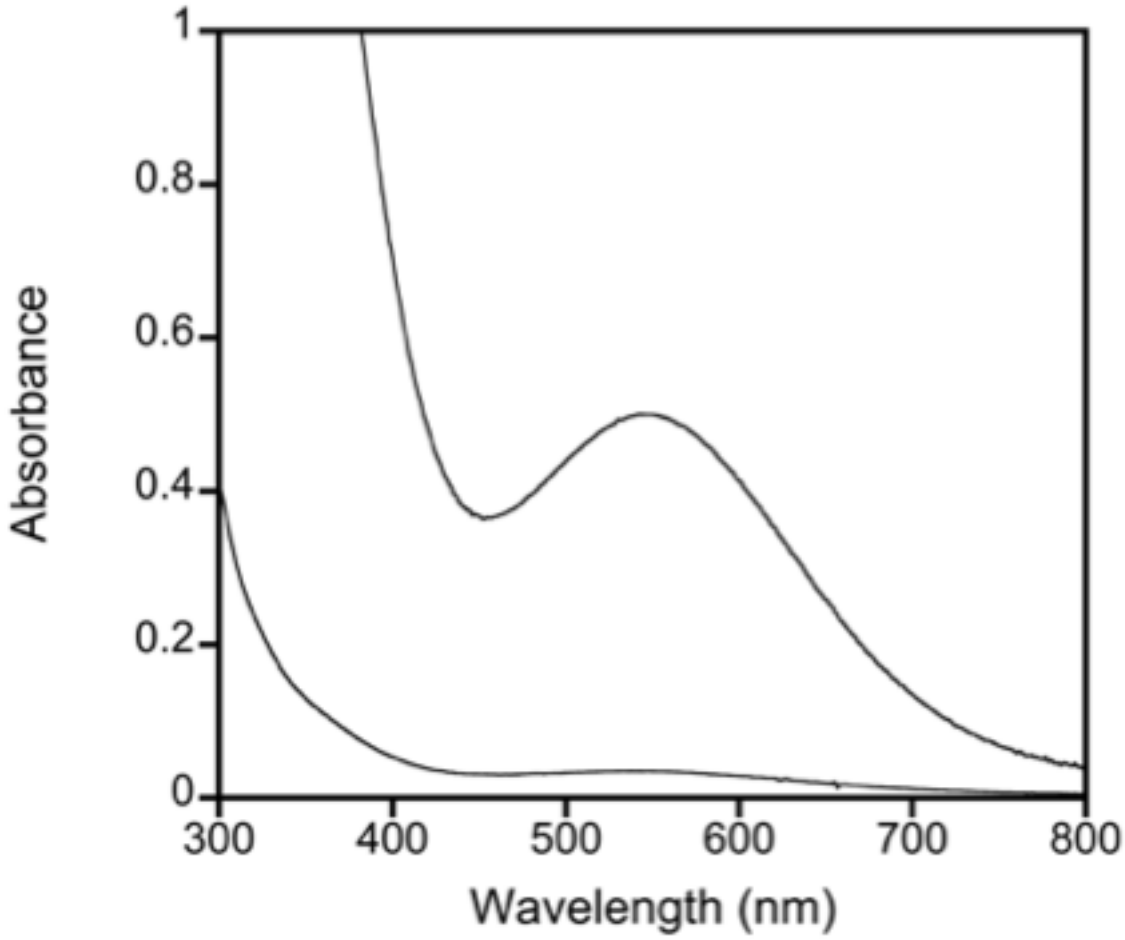

Figure 2.8. UV-vis spectra of **2** in methanol. Concentrated spectrum: 0.4 mM. Dilute spectrum: 0.03 mM.

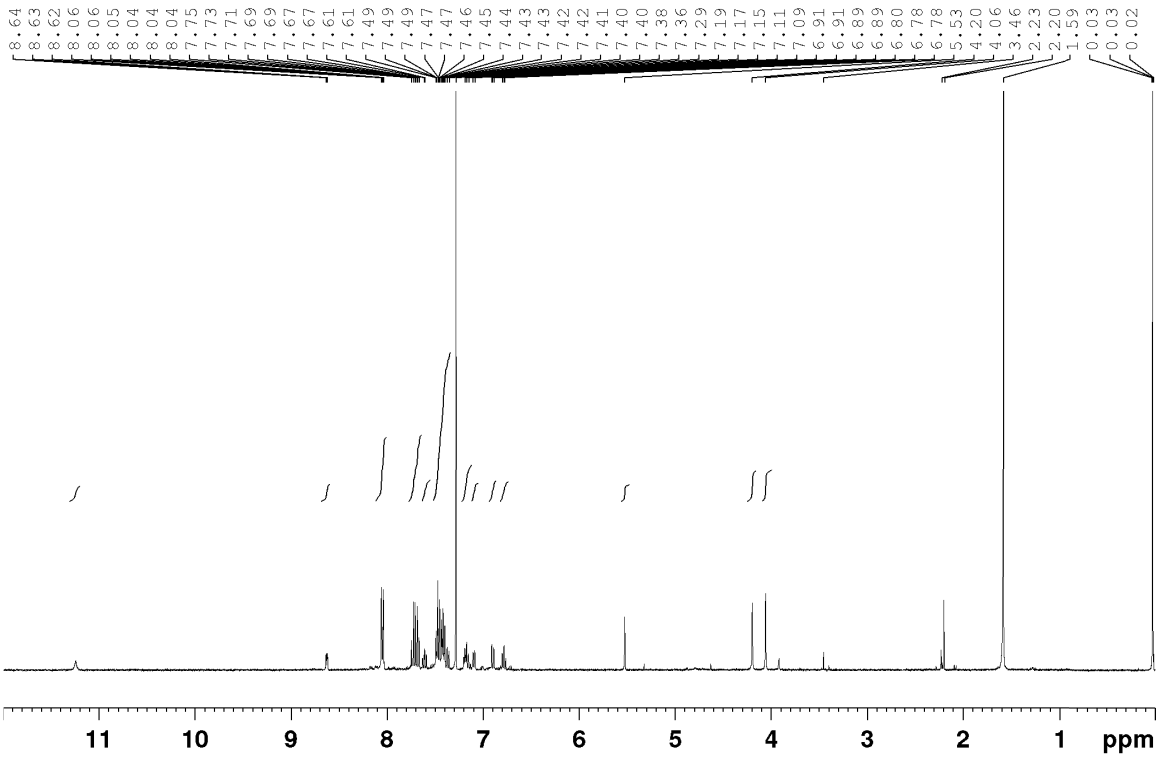

Figure 2.9. ^{1}H NMR spectrum of N3PyOH^{2Ph} in $CDCl_3$.

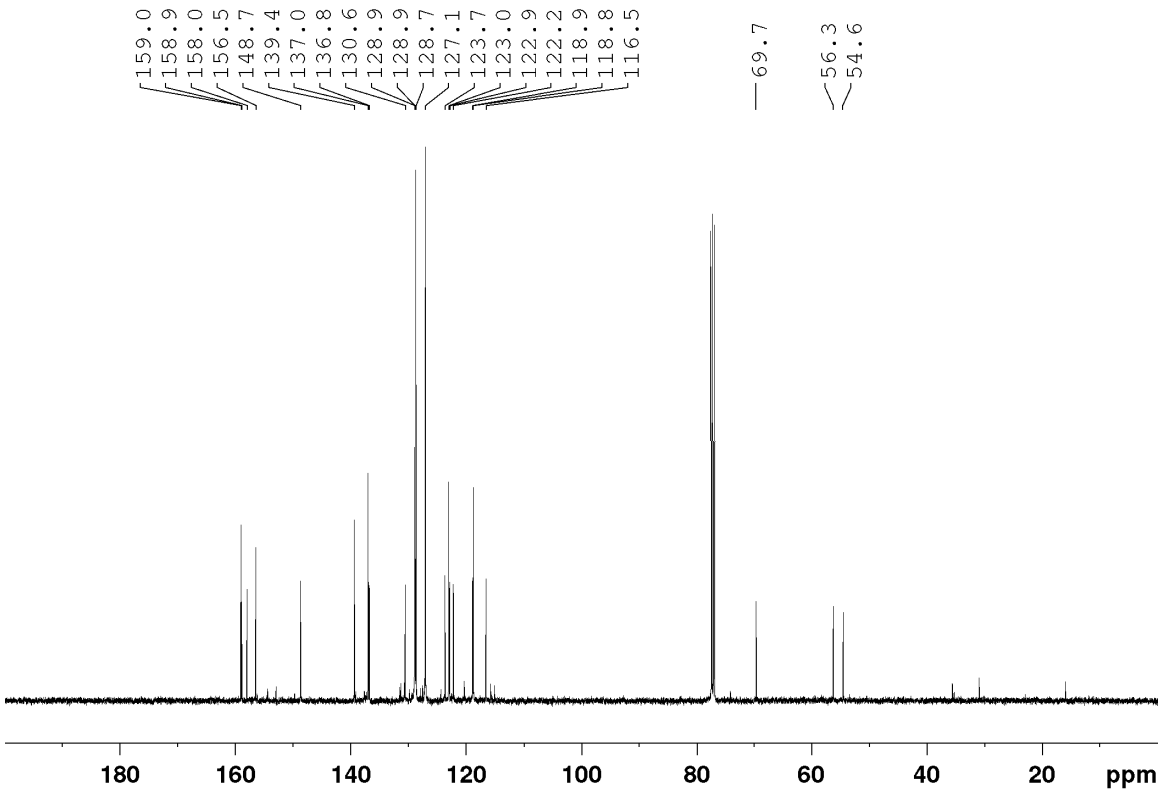

Figure 2.10. ^{13}C NMR spectrum of N3PyOH^{2Ph} in $CDCl_3$.

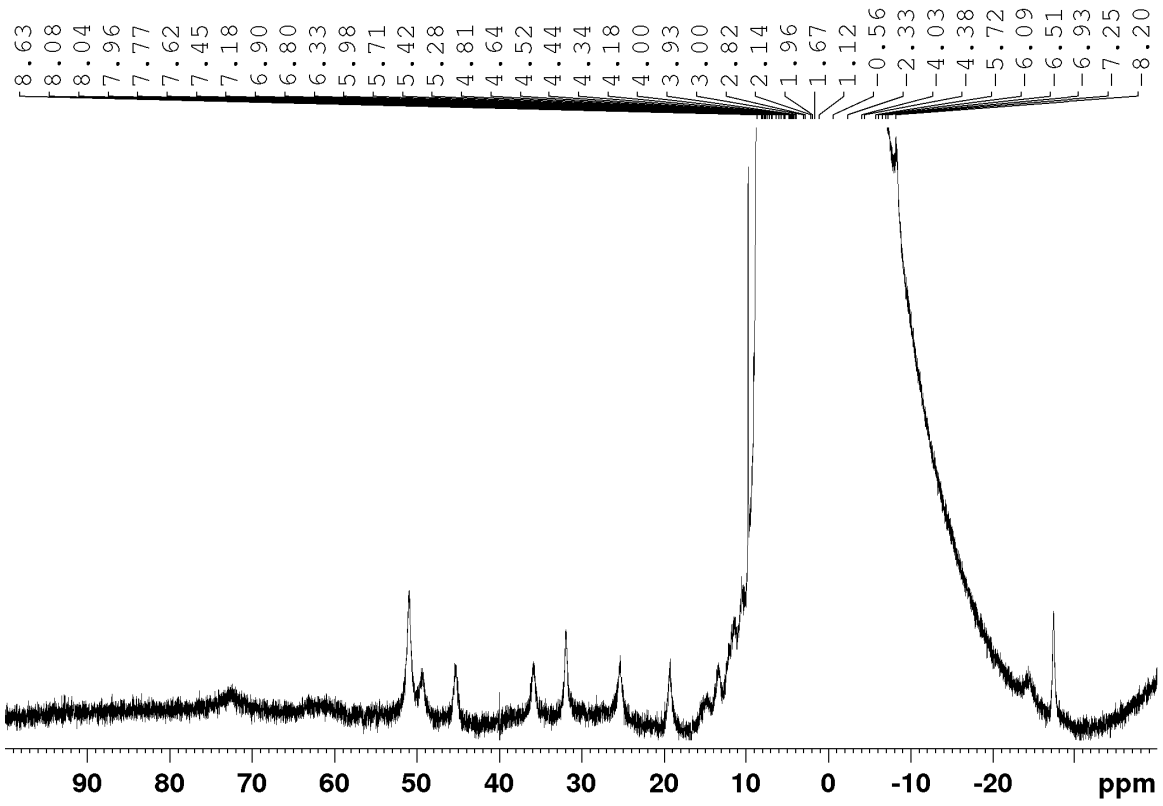

Figure 2.11. ^{1}H NMR spectrum of $[Fe^{II}(N3PyO^{2Ph})(CH_3CN)](ClO_4)$ (**1**) in CD_3CN.

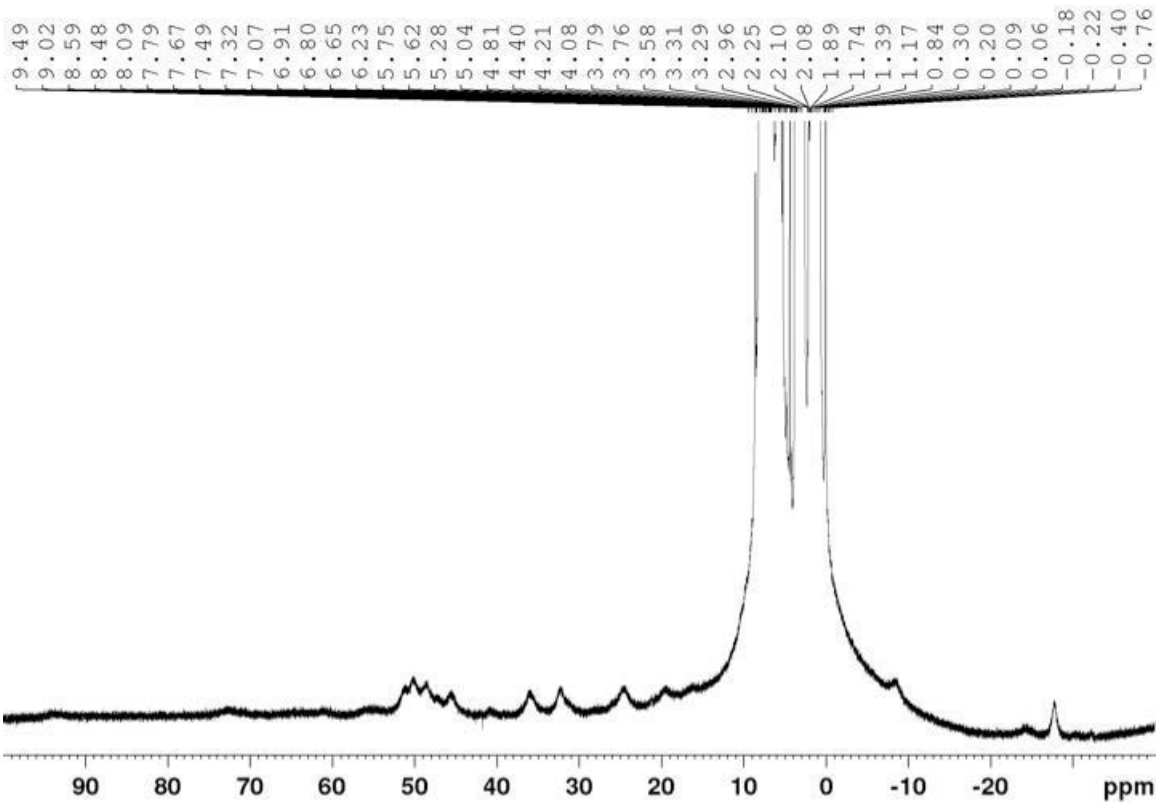

Figure 2.12. ^{1}H NMR of [Fe^{II}(N3PyO^{2Ph})(CH_3CN)](ClO_4) (**1**) in THF-d_8/CD_3CN.

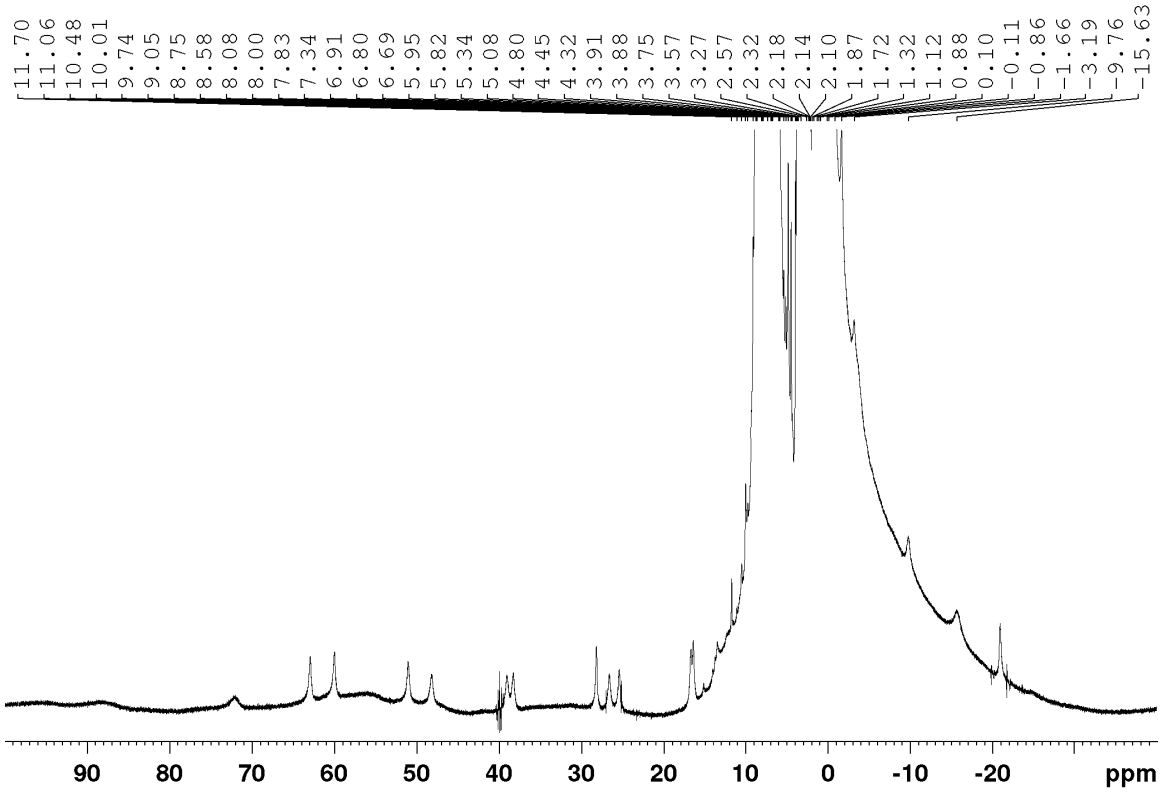

Figure 2.13. ^{1}H NMR of ([Fe^{III}(N3PyO^{2Ph})(OMe)]ClO_4) (**2**) in THF-d_8.

2.6. References

1. Huang, X.; Groves, J. T., *JBIC, J. Biol. Inorg. Chem.* **2017,** *22*, 185-207.

2. Ortiz de Montellano, P. R., *Chem. Rev.* **2010,** *110*, 932-948.

3. Kovaleva, E. G.; Lipscomb, J. D., *Nat. Chem. Biol.* **2008,** *4*, 186-193.

4. Zaragoza, J. P. T.; Yosca, T. H.; Siegler, M. A.; Moënne-Loccoz, P.; Green, M. T.; Goldberg, D. P., *J. Am. Chem. Soc.* **2017,** *139*, 13640-13643.

5. Pangia, T. M.; Davies, C. G.; Prendergast, J. R.; Gordon, J. B.; Siegler, M. A.; Jameson, G. N. L.; Goldberg, D. P., *J. Am. Chem. Soc.* **2018,** *140*, 4191-4194.

6. Mitchell, A. J.; Zhu, Q.; Maggiolo, A. O.; Anath, N. R.; Hillwig, M. L.; Liu, X.; Boal, A. K., *Nat. Chem. Biol.* **2016,** *12*, 636-640.

7. Matthews, M. L.; Neumann, C. S.; Miles, L. A.; Grove, T. L.; Booker, S. J.; Krebs, C.; Walsh, C. T.; Bollinger, J. M., Jr., *Proc. Natl. Acad. Sci.* **2009,** *106*, 17723-17728.

8. Martinie, R. J.; Livada, J.; Chang, W.; Green, M. T.; Krebs, C.; Bollinger, J. M., Jr.; Silakov, A., *J. Am. Chem. Soc.* **2015,** *137*, 6912-6919.

9. Wong, C.; Fujimori, D. G.; Walsh, C. T.; Drennan, C. L., *J. Am. Chem. Soc.* **2009,** *131*, 4872-4879.

10. The observation of metal-bound C-O products following a related rebound process for a nonheme $Ru^{IV}(O)$ complex was described. Kojima, T.; Nakayama, K.; Ikemura, K.; Ogura, T.; Fukuzumi, S., *J. Am. Chem. Soc.* **2011,** *133*, 11692-11700.

11. Smith, J. M.; Mayberry, D. E.; Margarit, C. G.; Sutter, J.; Wang, H.; Meyer, K.; Bontchev, R. P., *J. Am. Chem. Soc.* **2012,** *134*, 6516-6519.

12. Jang, E. S.; McMullin, C. L.; Kass, M.; Meyer, K.; Cundari, T. R.; Warren, T. H., *J. Am. Chem. Soc.* **2014,** *136*, 10930-10940.

13. Iovan, D. A.; Betley, T. A., *J. Am. Chem. Soc.* **2016,** *138*, 1983-1993.

14. Planas, O.; Clemancey, M.; Latour, J.-M.; Company, A.; Costas, M., *Chem. Commun.* **2014,** *50*, 10887-10890.

15. Rana, S.; Dey, A.; Maiti, D., *Chem. Commun.* **2015,** *51*, 14469-14472.

16. Wong, S. D.; Srnec, M.; Matthews, M. L.; Liu, L. V.; Kwak, Y.; Park, K.; III, C. B. B.; Alp, E. E.; Zhao, J.; Yoda, Y.; Kitao, S.; Seto, M.; Krebs, C.; J. Martin Bollinger, J.; Solomon, E. I., *Nature* **2013,** *499*, 320-323.

17. Jonas, R. T.; Stack, T. D. P., *J. Am. Chem. Soc.* **1997,** *119*, 8566-8567.

18. Moon, D.; Lah, M. S.; Sesto, R. E. D.; Miller, J. S., *Inorg. Chem.* **2002,** *41*, 4708-4714.

19. Roelfes, G.; Lubben, M.; Chen, K.; Ho, R. Y. N.; Meetsma, A.; Genseberger, S.; Hermant, R. M.; Hage, R.; Mandal, S. K.; Young, V. G., Jr.; Zang, Y.; Kooijman, H.; Spek, A. L.; Que, L., Jr.; Feringa, B. L., *Inorg. Chem.* **1999,** *38*, 1929-1936.

20. Kerber, W. D.; Perez, K. A.; Ren, C.; Siegler, M. A., *Inorg. Chem.* **2014,** *53*, 11507-11516.

21. Chang, K.-C.; Huang, C.-J.; Chang, Y.-H.; Wu, Z.-H.; Kuo, T.-S.; Hsu, H.-F., *Inorg. Chem.* **2016,** *55*, 566-572.

22. Kwak, B.; Cho, K. W.; Pyo, M.; Lah, M. S., *Inorg. Chim. Acta.* **1999,** *290*, 21-27.

23. McQuilken, A. C.; Jiang, Y.; Siegler, M. A.; Goldberg, D. P., *J. Am. Chem. Soc.* **2012,** *134*, 8759-8761.

24. Draksharapu, A.; Li, Q.; Roelfes, G.; Browne, W. R., *Dalton Trans.* **2012,** *41*, 13180-13190.

25. Ligtenbarg, A. G. J.; Oosting, P.; Roelfes, G.; La Crois, R. M.; Lutz, M.; Hage, R.; Spek, A. L.; Feringa, B. L., *Chem. Commun.* **2001**, 385-386.

26. Sahu, S.; Widger, L. R.; Quesne, M. G.; de Visser, S. P.; Matsumura, H.; Moënne-Loccoz, P.; Siegler, M. A.; Goldberg, D. P., *J. Am. Chem. Soc.* **2013,** *135*, 10590-10593.

27. Sahu, S.; Zhang, B.; Pollock, C. J.; Dürr, M.; Davies, C. G.; Confer, A. M.; Ivanović-Burmazović, I.; Siegler, M. A.; Jameson, G. N. L.; Krebs, C.; Goldberg, D. P., *J. Am. Chem. Soc.* **2016,** *138*, 12791-12802.

28. Ghosh, S.; Das, J., *Tetrahedron Lett.* **2011,** *52*, 1112-1116.

29. Sheldrick, G. M., *Acta Cryst.* **2008,** *A64*, 112-122.

30. Sahu, S.; Widger, L. R.; Quesne, M. G.; de Visser, S. P.; Matsumura, H.; Moenne-Loccoz, P.; Siegler, M. A.; Goldberg, D. P., *J Am Chem Soc* **2013,** *135*, 10590-3.

31. Shakya, R.; Allard, M. M.; Johann, M.; Heeg, M. J.; Rentschler, E.; Shearer, J. M.; McGarvey, B.; Verani, C. N., *Inorg. Chem.* **2011,** *50*, 8356-8366.

32. Evans, D. F.; Jakubovik, D. A., *J. Chem. Soc. Dalton Trans.* **1988**, 2927-2933.

33. Confer, A. M.; McQuilken, A. C.; Matsumura, H.; Moënne-Loccoz, P.; Goldberg, D. P., *J. Am. Chem. Soc.* **2017,** *139*, 10621-10624.

Chapter 3 Observation of Rebound in a Nonheme Mononuclear Iron Model Complex

Parts of the following chapter were adapted from a work co-written with the following authors:

Pangia, Thomas M.; Davies, Casey G.; Prendergast, Joshua R.; Gordon, Jesse B.; Siegler, Maxime A.; Jameson, Guy N. L.; Goldberg, David P. *J. Am. Chem. Soc.*, **2018**, 140, 4191-4194.

3.1. Introduction

A mechanism involving hydroxide "rebound" has been utilized to explain C-H hydroxylation reactions that are performed by heme and nonheme oxygenases, as well as some related synthetic complexes.[1-3] The key process utilizes an initial abstraction of a hydrogen atom contained within a C-H bond, abstracted by a high-valent metal-oxo compound, followed by recombination of the carbon radical with the resulting metal-hydroxide. The new C-O bond is formed accompanied by the one-electron reduction of the metal center (Scheme 3.1), however, due to the rate-determining nature of the C-H cleavage process, this step is typically too fast for direct observation. There has been indirect evidence from some experimental and computational studies,[4-5] providing valuable information on this mechanistic paradigm. There are alternative pathways by which a radical might react instead of the rebound pathway, including dissociation of the radical in a synthetic system, or else trapping of the radical by an additional reactive species (e.g.

O_2).[4] Additionally the rebound mechanism has been invoked in the case of carbon-halogen bond formations driven by nonheme iron halogenase enzymes (SyrB2, CytC3, WelO5).[6-9]

Scheme 3.1. Oxygen and halogen mechanisms of radical rebound. Adapted from reference 10.[10]

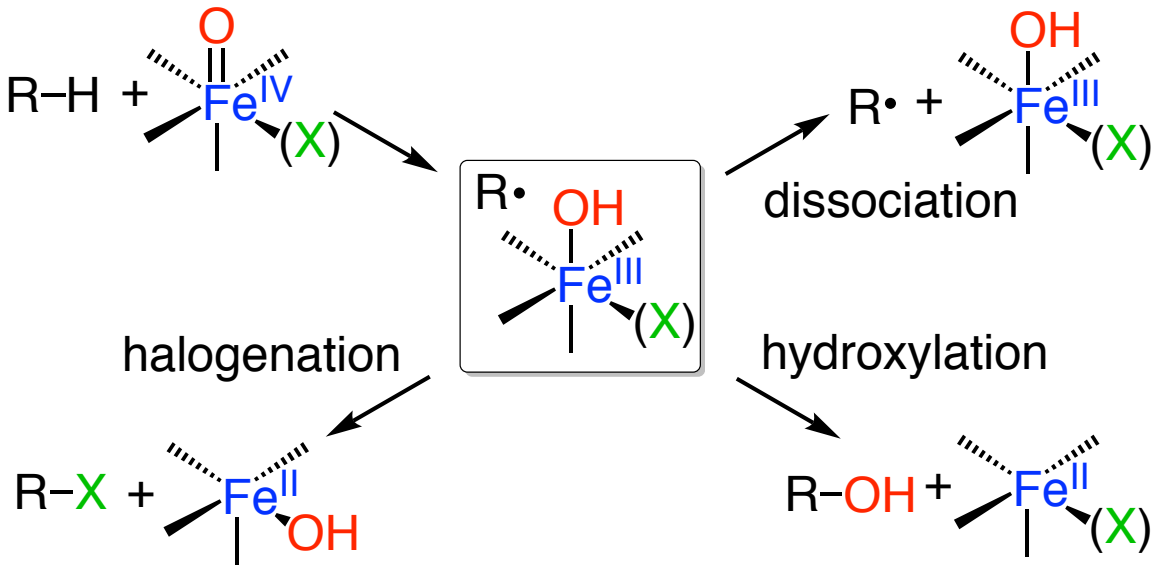

Nonheme iron model complexes of high-valent Fe(O) species have also provided evidence for rebound and non-rebound-type pathways in C-H oxidation reactions.[11-13] Related, computationally-centered studies have also shown that during the radical reaction, when rates of radical dissociation are such that competition with the rate of rebound is possible, a non-rebound mechanism may predominate, and causes for the non-rebound process have been suggested.[4]

Efforts undertaken by this lab have been directed toward observation of the rebound reaction. As a measure of our success, the first known example of such a system was described in a heme-type iron-hydroxide complex.[14] However, there has not been reported any direct observation of the analogous radical rebound reaction with a nonheme iron complex to give a new C-O bond.[15-18]

Recently, Cu complexes have been used in C-H amination processes which induce radical-driven formation of C-N bonds.[17] Accompaniment of a copper catalyst by peroxide oxidants allowed activation of C-H bonds and incorporation into amines to generate additional C-N bonds.

Scheme 3.2. Copper-mediated formation of C-N bonds.[17]

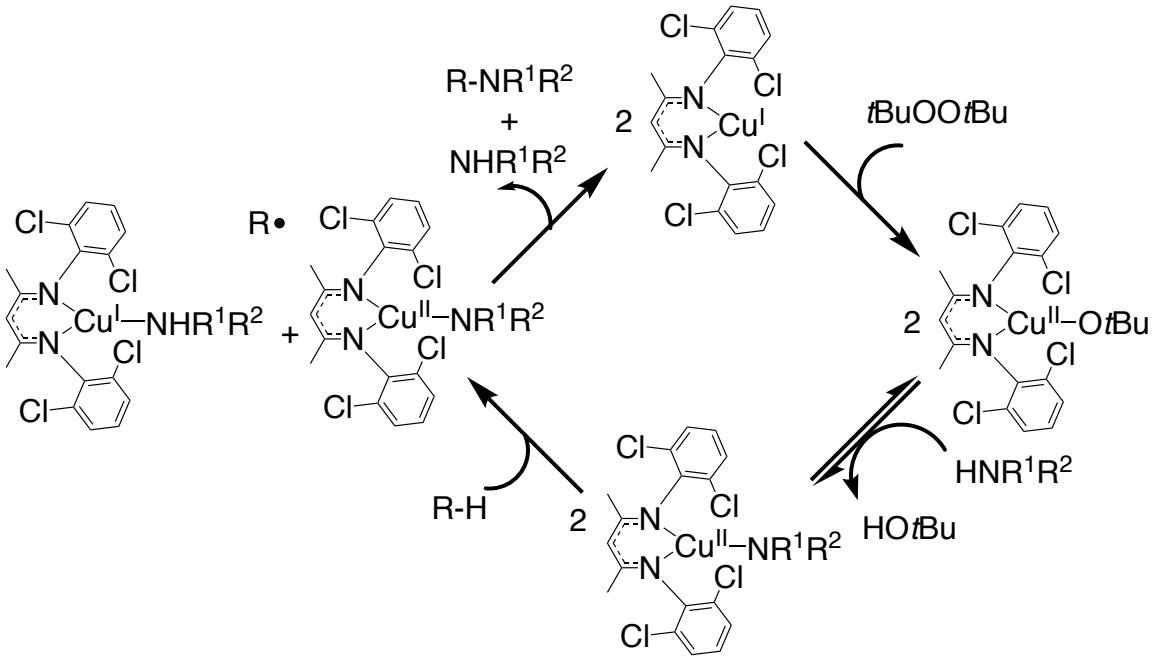

The system in Scheme 3.2 was found effective at catalyzing the formation of primary and secondary amines from R-H substrates. The mild oxidant *t*BuOO*t*Bu was employed to generate the active intermediate Cu^{II} complex. Hydrogen atom transfer was shown by kinetic studies to be rate-limiting in the formation of a radical which recombines with the $Cu^{II}NHR_2$ intermediate to form the new C-N bond and the one-electron reduced copper complex. Successful observation of this C-H activation provided additional evidence that such rebound-type chemistry would likely be observable in model complexes using other metals.

Scheme 3.3. Formation of a terminal iron (III)-methoxide.[10]

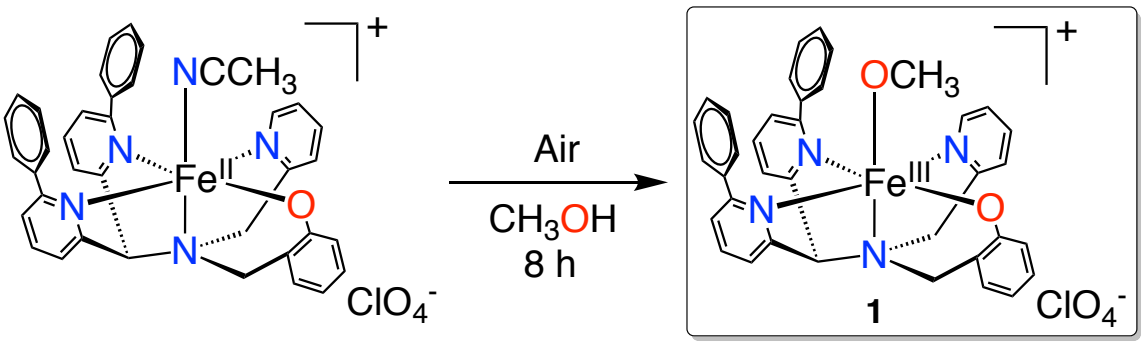

Work in this arena by our lab produced a terminal iron (III)-methoxide compound $[Fe^{III}(N3PyO^{2Ph})(OCH_3)](ClO_4)$ (**1**) (Scheme 3.3). This complex is a high-spin Fe^{III} complex (S = 5/2) and a potential analog of the ferric-hydroxide involved in nonheme iron rebound. It was proposed that **1** would be capable of reacting with a suitable carbon-based radical (R•) to yield a methoxy-ether ($ROCH_3$) organic product, as well as the one-electron reduced iron(II) complex.

3.2. Experimental

General Methods and Materials. All chemicals and reagents were purchased from Sigma- Aldrich, Fisher Scientific, Acros Organics, Merck, Fluka Analytical, or Alfa Aesar and were used without further purification unless noted otherwise. Solvents (methanol, diethyl ether, acetonitrile, and tetrahydrofuran) used in organic synthesis were purified via Pure-Solv Solvent Purification System from Innovative Technology, Inc. For Mössbauer spectroscopy, ^{57}Fe (95.93% isotope-enriched) was purchased from Cambridge Isotope Laboratories. Solvents used in the reactions of the iron(II) and iron(III) complexes were subjected to additional purification after initial purification via a Pure-Solv Solvent Purification System. Acetonitrile was distilled over calcium hydride. THF was distilled from sodium/benzophenone. All solvents were degassed by freeze-pump-thaw cycles and

stored in a N2 filled dry box. Reactions involving inert atmosphere were performed using either standard Schlenk techniques or in a dry box. *Caution: Perchlorate salts of metal complexes are potentially explosive. Care should be taken when handling these compounds. Note: trityl radical is O_2 and light-sensitive. Measures should be taken to avoid exposure of the radical to light and air.*

Analytical Methods. Kinetic UV-vis measurements were performed on a Hewlett-Packard Agilent 8453 diode-array spectrophotometer with a 3.5 mL quartz cuvette (path length = 1 cm) equipped with a septum. Other UV-visible spectra were recorded on a Varian Cary 50 Bio spectrophotometer. NMR spectra were collected on a Bruker Avance 400 MHz FT-NMR spectrometer. Electron paramagnetic resonance (EPR) spectra were obtained on a Bruker EMX EPR spectrometer controlled with a Bruker ER 041 X G microwave bridge. The EPR spectrometer was equipped with a continuous-flow liquid He cryostat and an ITC503 temperature controller made by Oxford Instruments, Inc. Gas Chromatography (GC-FID) was carried out on an Agilent 6890 gas chromatograph fitted with a DB–5 5% phenylmethyl siloxane capillary column (30 m x 0.32 mm x 0.25 μm) and equipped with a flame–ionization detector. FAB-MS was obtained using a VG analytical VG-70SE magnetic sector mass spectrometer. Mössbauer spectroscopy was performed on a spectrometer from SEE Co. (Science Engineering & Education Co., MN) equipped with a closed cycle refrigerator system from Janis Research Co. and SHI (Sumitomo Heavy Industries Ltd.) Spectra were measured with a small magnetic field (47 mT) applied parallel to the gamma radiation. Fitted parameters are presented in Table 3.1.

[Fe^{II}(N3PyO^{2Ph})(CH_3CN)](ClO_4). Mössbauer Spectroscopy. A solution of ^{57}Fe enriched **1** (4 mM) in THF was produced anaerobically in a glove box and frozen in a Mössbauer cup. The Mössbauer spectrum was collected at 5.2 K.

Reaction of 1 with Gomberg's dimer. UV-vis Spectroscopy. A solution of **1** (3 mL, 0.5 mM) in THF was placed in a quartz cuvette (1 cm pathlength) under inert atmosphere. The solution was heated to 50 °C and an initial spectrum recorded. Gomberg's dimer, $(Ph_3C)_2$, (1.6 equiv in 0.1 mL THF) was added and the UV-vis bands at λ_{max} = 516 nm (triphenyl methyl radical in THF) and λ_{max} = 570 nm (**1** in THF) were monitored over 1 h. Decay (~80%) of the peak at 570 nm was observed over the time period, denoting the consumption of the Fe^{III} starting material (Figure 3.1). Heating **1** in THF over 1 h with no $(Ph_3C)_2$ produces a slow background decomposition when monitored by UV-vis, accounting for ~25% loss of **1** (Figure 3.7).

Reaction of 2 with $(Ph_3C)_2$. EPR Spectroscopy. A solution of **1** (2 mM) in THF was heated to 50 °C. An amount of $(Ph_3C)_2$ (1.6 equiv) was added. Aliquots (0.5 mL) were removed at the following time points: 0 min, 1 min, 5 min, 30 min, and 60 min and placed in separate 4 mm inner diameter quartz EPR tubes and frozen in liquid nitrogen. Each aliquot was then analyzed by X-band EPR at 13 K. A decrease in the signal at g = 4.26 was observed over time, consistent with consumption of **1** and formation of an EPR-silent Fe^{II} species equivalent to [Fe^{II}(N3PyO^{2Ph})(CH_3CN)](ClO_4) (Figure 3.2).

Reaction of 2 with $(Ph_3C)_2$. ^1H NMR Spectroscopy. A solution of **2** (0.6 mL, 3.5 mM) in THF-d_8 was heated to 50 °C in a sealed NMR tube and an initial spectrum was recorded. An amount of $(Ph_3C)_2$ (4 equiv) was added and the solution manually mixed in the NMR tube. A spectrum recorded after 60 min at 50 °C showed formation of a peak at 3.04 ppm matching the $–OCH_3$ signal of Ph_3COCH_3, the expected rebound product. Integration against an internal standard (Ph-C_6H_4-OCH_3, 3.2 mM) gave a yield of 60% for Ph_3COCH_3 (based on **2**, Figure 3.3). The paramagnetic spectrum of **2** with peaks between +100 to -40 ppm disappeared after 60 min and a new spectrum with peaks between +90 and -40 ppm was observed. Removal of the reaction solvent and dissolution of the brown residue in CD_3CN resulted in a spectrum that could be assigned to **1**. Control experiments between $(Ph_3C)_2$ and sodium methoxide (10 equiv and 100 equiv) produced no detectable Ph_3COCH_3. Control experiments between $(Ph_3C)_2$ and methanol (10 equiv and 100 equiv) also did not produce Ph_3COCH_3.

Reaction of 2 with $(Ph_3C)_2$. Gas Chromatography. A solution of **2** in THF (4 mM, 1 mL) was combined with $(Ph_3C)_2$ (3 equiv) and the internal standard Ph-C_6H_4-OCH_3 (2.2 mM). The solution was heated for 60 min at 50 °C. An aliquot (100 μL) was combined with 100 μL of oxygenated THF to quench the reaction. The resulting solution was injected (2 μL) onto the GC-FID. The Ph_3COCH_3 (R_T = 12.4 min) was quantified from a calibration curve with the Ph-C_6H_4-OCH_3 internal standard (R_T = 8.1 min) (Figure 3.4). Each reaction was injected twice, obtaining an average yield of 58%.

Reaction of 2 with $(Ph_3C)_2$. Mössbauer Spectroscopy. A solution of **2-^{57}Fe** was made in THF in a glove box under an inert atmosphere (N_2(g)). To the resulting dark purple solution was added 1.6 equiv $(Ph_3C)_2$ dissolved in THF. Equal volumes of each solution, preheated to 50 °C, were added to give final concentrations of 4 mM of **2-^{57}Fe** and 6.4 mM of $(Ph_3C)_2$. The reaction was kept at 50 ± 1 °C in a water bath. The dark purple solution rapidly turned light yellow-brown and was incubated for a total of 70 min. The reaction mixture was then frozen anaerobically at 77 K in a Mössbauer cup and stored until spectra could be collected (Table 3.1). Mössbauer spectra of **2-^{57}Fe** and the final reaction mixture were recorded (Figure 3.5). Additional measurements of a solid-phase crystalline sample of **2** (35 mg in boron-nitride) were made at 100 K for comparison with solution-phase samples (Figure 3.8, Table 3.1).

DFT Computational Studies.

All calculations were performed in the *ORCA-3.0.2* program package.[19] Initial geometries were obtained from X-ray crystallographic models. Optimized geometries were calculated using the BP86 functional.[20-21] Geometries were also calculated using the TPSSh functional,[22-23] which yielded similar geometries to those with BP86. The 6-311g* basis set was used for all Fe, N, O, and Cl atoms and the 6-31g* basis set was for all C and H atoms. A continuum solvation model was included (COSMO) with acetonitrile used for **$[Fe^{II}(N3PyO^{2Ph})(CH_3CN)]^+$** and **1**, and THF for **$[Fe^{II}(N3PyO^{2Ph})(THF)]^+$** and **$[Fe^{II}(N3PyO^{2Ph})]^+$**. Due to SCF convergence difficulties in **$[Fe^{II}(N3PyO^{2Ph})(CH_3CN)]^+$** damping parameters were altered using the Slowconv function in ORCA. Frequency calculations at the same level of theory confirmed that all optimizations had converged to

true minima on the potential energy surface (i.e., no imaginary frequencies). The optimized structures using the BP86 functional were used for Mössbauer calculations for **[Fe^{II}(N3PyO^{2Ph})(CH$_3$CN)]$^+$**, **[Fe^{II}(N3PyO^{2Ph})(THF)]$^+$**, and **[Fe^{II}(N3PyO^{2Ph})]$^+$** because of the close match between the X-ray crystallographic and calculated metrics for **[Fe^{II}(N3PyO^{2Ph})(CH$_3$CN)]$^+$**. However, we were unable to obtain a geometry optimization of **1** using BP86 and instead employed the TPSSh functional. Mössbauer parameters were computed using the B3LYP[24-27] functional and the def2-TZVP[28-29] basis set for all atoms, or a combination of CP(PPP)[30] for Fe and def2-TZVP for all other atoms. The angular integration grid was set to Grid4 (NoFinalGrid), with increased radial accuracy for the Fe atom (IntAcc 7). To simulate solid state effects, a continuum solvation model was included (COSMO) with a solvent of intermediate dielectric (methanol).The isomer shift was obtained from the electron density at the Fe nucleus, using a linear fit function previously reported: $\delta = \alpha(\rho(0) - c) + \beta$.[31] For the methodology described here, $\alpha = -0.424$ au^3 mm s^{-1}, $\beta = 7.55$ mm s^{-1}, and $c = 11800$ au^{-3}.

3.3. Results and Discussion

The trityl radical (triphenylmethyl, Ph$_3$C•) is known to be stable in organic solvents. It is prepared in a dimeric, non-radical form ((Ph$_3$C)$_2$ Gomberg's dimer), which dissociates in solution to give a known amount of monomeric trityl radical (~2% at 25 °C).[32-33] When **1** was allowed to react with (Ph$_3$C)$_2$ in THF at 23 °C, a process of slow decay of the Fe^{III}-OCH$_3$ material (~48 h) was observed by monitoring with UV-vis spectroscopy.

Scheme 3.4. Radical rebound reaction between **1** and trityl radical.[10]

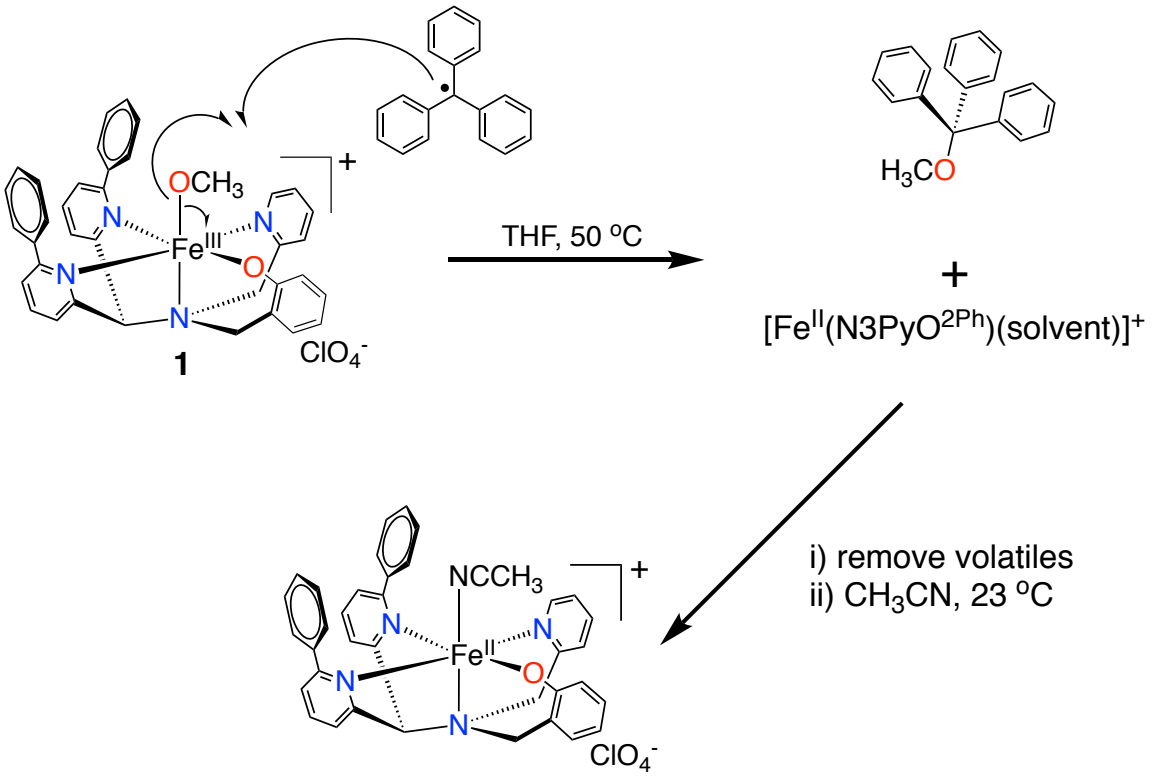

When heated to higher temperatures, Gomberg's dimer is capable of dissociating to a greater extent.[32-33] Making use of this, heating the former reaction to 50 °C induced roughly ~80% decay of the 570 nm absorbance of **1** within the course of 1 h (Figure 3.1).

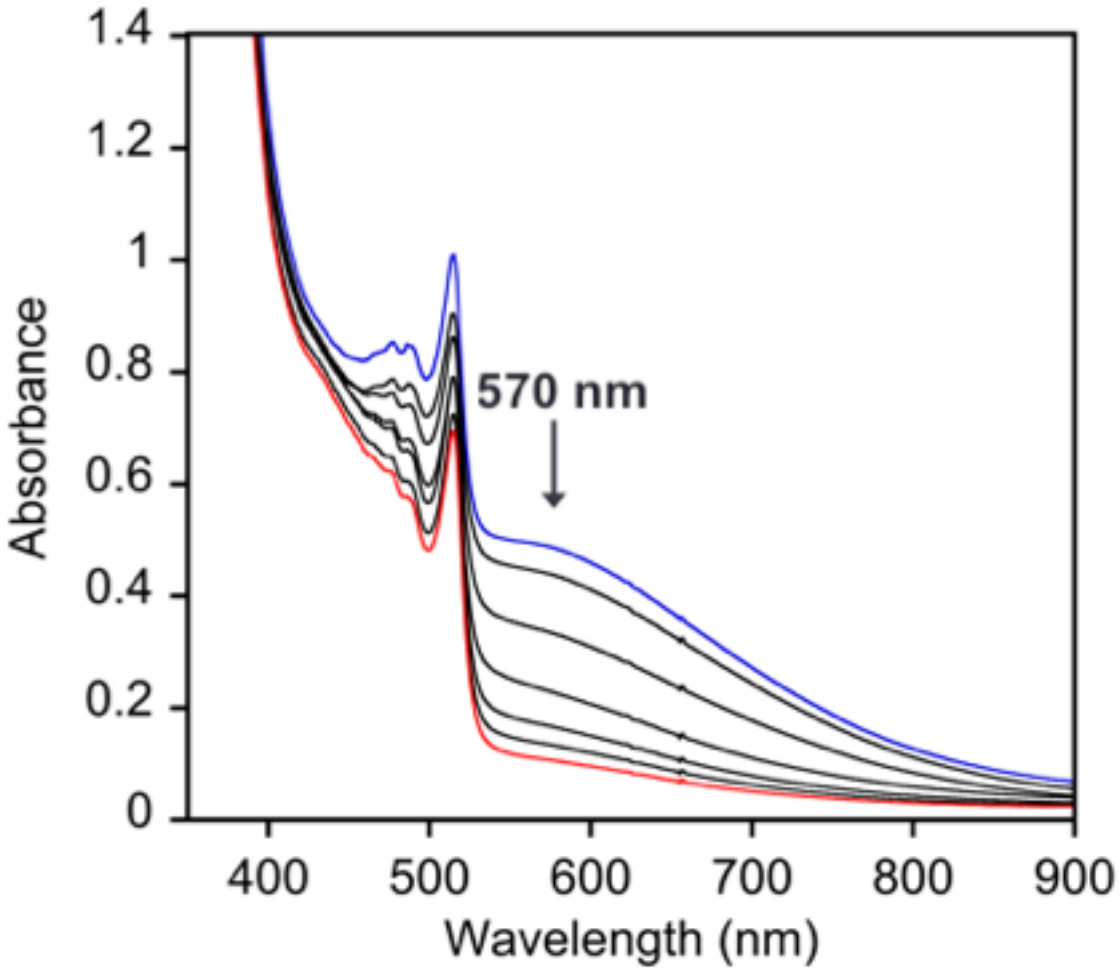

Figure 3.1. Reaction of **1** and $(Ph_3C)_2$ in THF at 50 °C, monitored by UV-vis spectroscopy. **1** (570 nm) is consumed over the course of 1 h. Initial spectrum (blue): combination of **1** and $(Ph_3C)_2$. Final spectrum (red): **1** has been consumed while excess $(Ph_3C)_2$ is still present.

The same reaction was monitored using EPR spectroscopy (Figure 3.2). The peak positioned at g = 4.26 showed loss of 80% of **1** after 1 h when heated at 50 °C, which coincided well with the observations afforded by the UV-vis data. Observations of the final product of the reaction were EPR-silent, as would be consistent with an integer-spin iron(II), the expected one-electron reduced product.

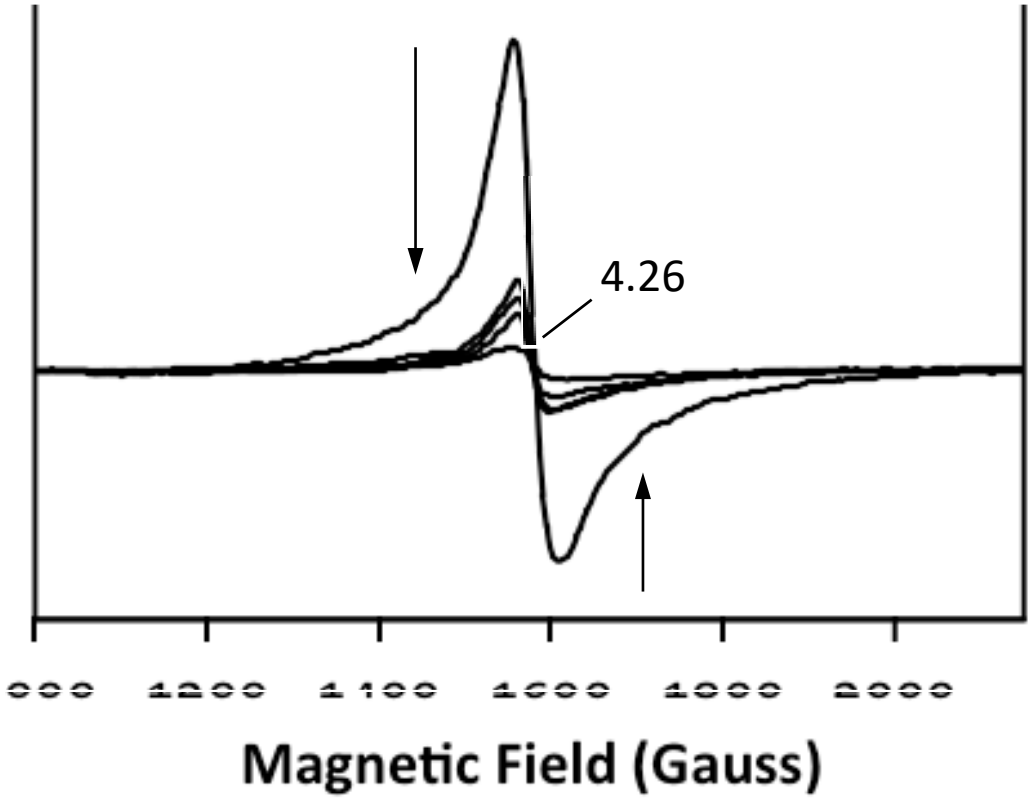

Figure 3.2. X-band EPR spectra at 15 K of the reaction of **2** and $(Ph_3C)_2$ (1.6 equiv) over 60 min in THF at 50 °C. Spectra were taken at 0, 1, 5, 30, and 60 min, showing up to 80% consumption of **2**. Frequency 9.2464 GHz, modulation amplitude 10 G, modulation frequency 100 KHz, attenuation 20 dB, power = 2.0 mW, receiver gain 5.02 x 10^3.

The reaction performed in THF-d_8 showed formation of a signal at δ 3.04 ppm after 60 min, which can be assigned to Ph_3COCH_3, the expected organic rebound product (Figure 3.3). When this peak was quantified by integration and comparison using an internal standard, the yield of methoxy ether product was found to be 60% (based on total **1** present).

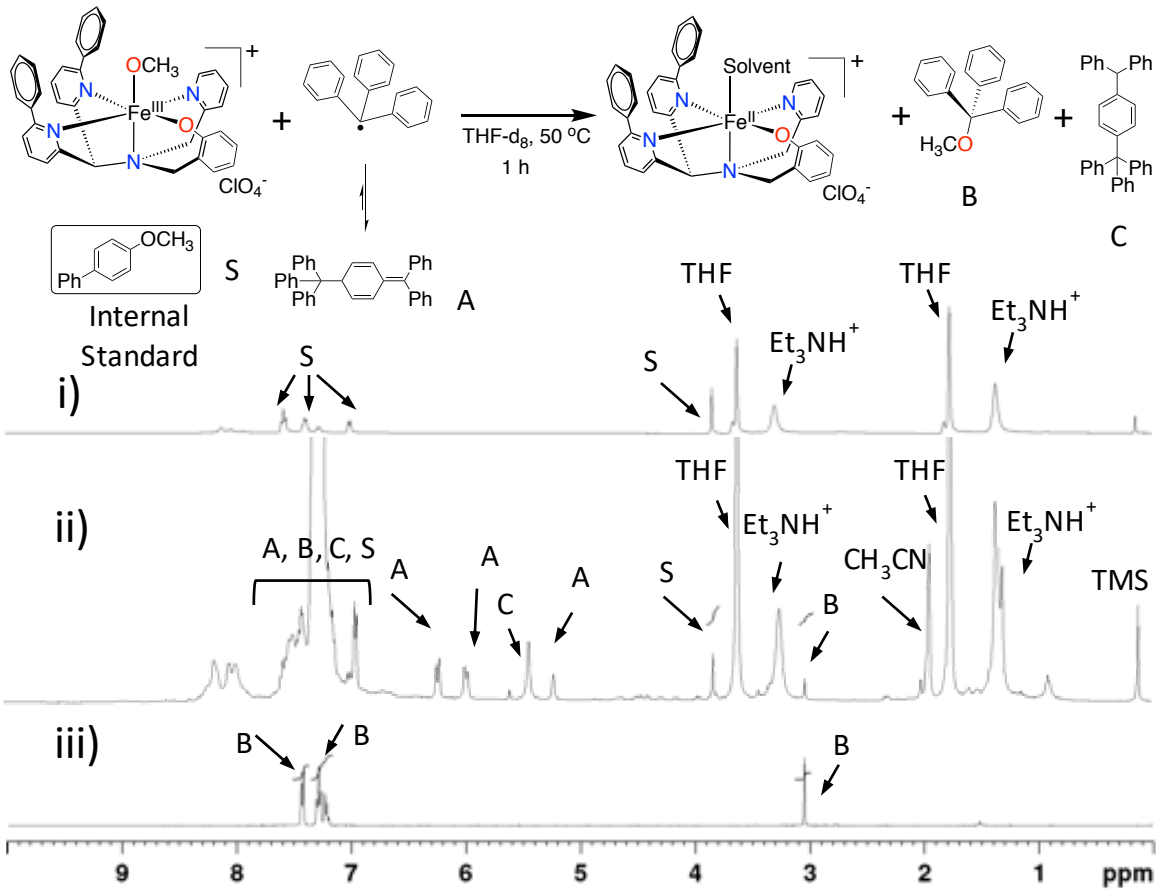

Figure 3.3. Reaction of **1** and $(Ph_3C)_2$ in THF-d_8 for 60 min at 50 °C as monitored by ^{1}H NMR spectroscopy. i) **1** and 4-Ph-C_6H_4-OCH_3 (internal standard S) before addition of $(Ph_3C)_2$. ii) **1** and $(Ph_3C)_2$ after 60 min. iii) Ph_3COCH_3 reference spectrum. Following the reaction, the –OCH_3 peak of the product Ph_3COCH_3 at 3.04 ppm was integrated against the internal standard (4-Ph-C_6H_4-OCH_3) –OCH_3 peak at 3.83 ppm. Peaks at 5.2, 6.0, and 6.2 ppm were from unreacted $(Ph_3C)_2$. The peak at 5.4 ppm is assigned to Ph_3-C_6H_4-$CHPh_2$, a side-product of trityl radical recombination.[34] Acetonitrile and Et_3NH^+ may be observed as residual compounds from in-situ generation of **1** (see experimental section for details).

This result was then further corroborated using GC-FID, showing production of the Ph_3COCH_3 material in 58% yield (Figure 3.4). Both GC and NMR yields are in good agreement. The yield could not be improved by increasing reaction times up to 24 h.

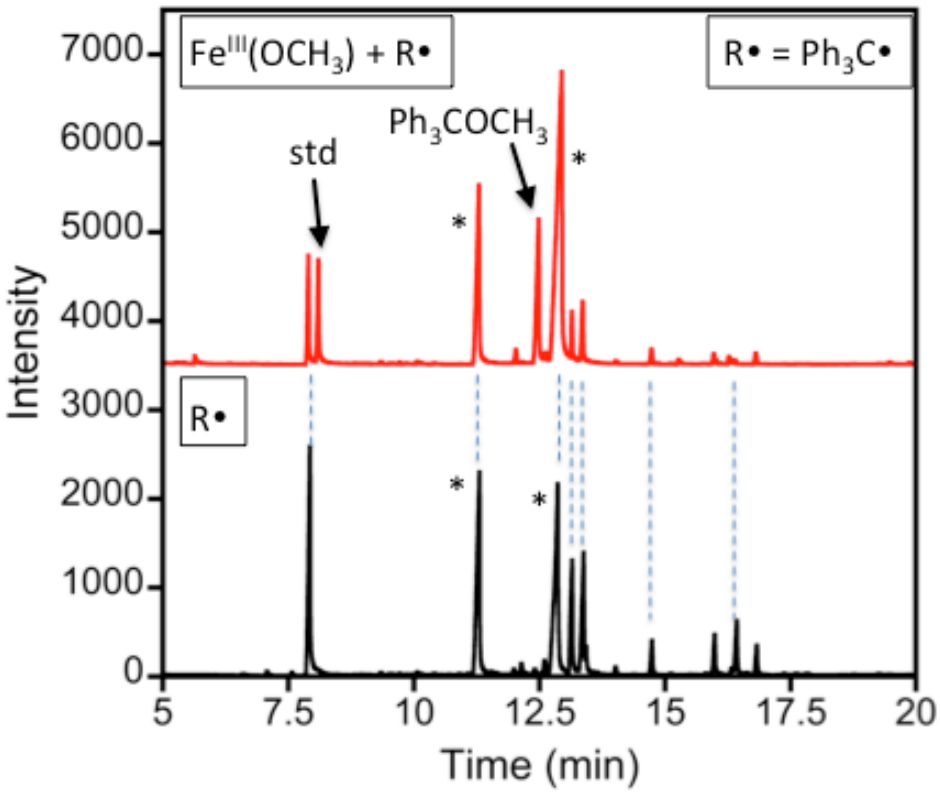

Figure 3.4. GC-FID data for the reaction of **1** (4 mM) and $(Ph_3C)_2$ (3 equiv) (red) and $(Ph_3C)_2$ alone (black). The Ph_3COCH_3 (R_T = 12.4 min) was quantified from a calibration curve with the Ph-C_6H_4-OCH_3 internal standard (R_T = 8.1 min), yield = 58%. Marked peaks at 11.3 min and 12.9 min are from triphenyl methane (Ph_3CH) and triphenyl methanol (Ph_3COH) respectively, resulting from radical decay during aerobic workup. Unlabelled peaks are unidentified decay products, also present in $(Ph_3C)_2$ (shown by dashed lines).

Yield of this reaction may be limited by the formation of a side product of trityl radical dissociation, which has been identified by ^{1}H NMR to be a tautomeric form of Gomberg's dimer that does not release trityl radical through dissociation.[34] At the high temperatures employed during this reaction, there is also a slow background decomposition

of **1** when monitored by UV-vis, which also would be a probable cause of the limitations of the yield of the organic product.

Though the former results indicated consumption of the Fe^{III} starting material and concomitant production of Ph_3COCH_3, definitive formation of the one-electron reduced iron(II) was not obtained using the above methods. The EPR-silent observations and the lack of a distinct UV-vis spectrographic identifier for the iron(II) product necessitated the application of Mössbauer spectroscopy, which was employed to give additional insight into the rebound reaction between **1** and the trityl radical. Isotopically-enriched (^{57}Fe, 95.93%) **1** was reacted with $(Ph_3C)_2$ at 50 °C for a period of 70 min, then was frozen at 77 K for analysis by Mössbauer (Figure 3.5). The spectrum of **1** before the reaction was measured at 5.2 K, and showed a 6-line pattern that is typical of an iron(III) complex which is split magnetically. The spectrum was also showed a quadrupole doublet. These signals were found to be consistent with a mixture of the Fe^{III} complex in both slow- and fast-relaxation regimes, respectively. The analysis was confirmed when the sample was again measured at 100 K. At the higher temperature, the spectrum showed that the sextet seen at 5.4 K had collapsed into only a single quadrupole doublet having parameters that were consistent with a high-spin iron(III) complex (δ = 0.50, ΔE_q = 1.29 mm s^{-1}). When the Mössbauer spectrum was taken of **1** in the solid state at 100 K, the spectrum is nearly identical (Figure 3.5), which further corroborates the analysis.

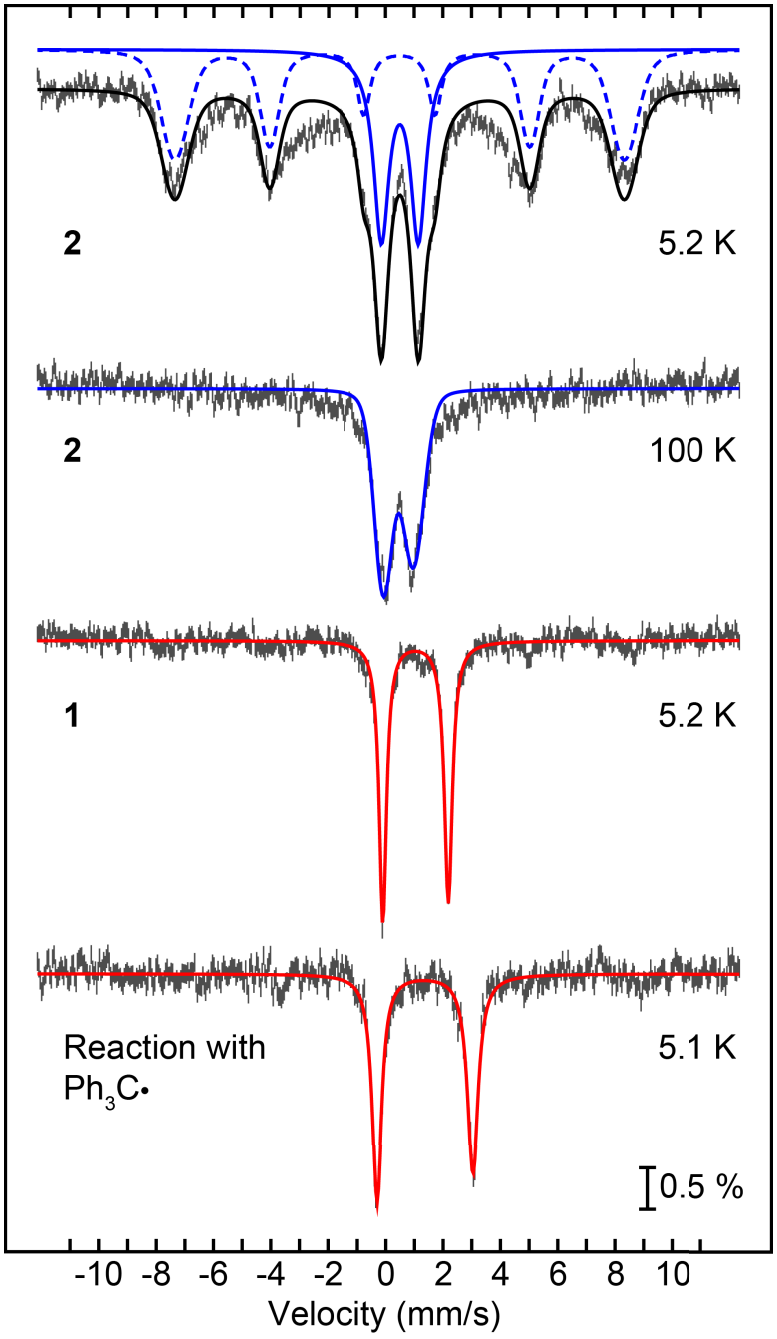

Figure 3.5. ^{57}Fe Mössbauer spectra for: complex **1 (**hatched line) in THF at 5.2 K together with the best fits for hs-Fe^{III} in both the slow-(blue dashed line) and fast-relaxing (blue solid line) regimes (top); same sample as in (top) at 100 K (hatched line) and best fit (blue line) for a fast-relaxing quadrupole doublet as the major component (top middle); **Fe^{II}** complex in THF at 5.2 K (hatched line) and best fit (red line) for a hs-Fe^{II} quadrupole

doublet (bottom middle); the reaction mixture of **1** and Gomberg's dimer in THF at 50 °C after 70 min (hatched line) and best fit (red line) for a hs-Fe^{II} quadrupole doublet (bottom).

When **1** was reacted with Ph_3C•, the iron(III) starting material was shown to disappear, while a new, sharp quadrupole doublet having parameters of $\delta = 1.38$ and $\Delta E_q = 3.35$ mm s^{-1} was observed. The parameters of the emergent doublet are clear indications of high-spin iron(II). Quantification of this signal indicated that the final Fe^{II} species makes up 90% of the total iron content.

Table 3.1. ^{57}Fe Mössbauer parameters for **[Fe^{II}(N3PyO^{2Ph})(CH_3CN)]$^+$**, **1** and reaction of **1** with Ph_3C• in THF.

	T (K)	Species	δ (mm/s)	ΔE_Q (mm/s)	$\Gamma_{L(R)}$ (mm/s)	B_{int} (T)	I (%)
Fe^{II}	5.2[a]	hs-Fe^{II}	1.05	2.29	0.31 (0.34)	-	90
1	5.2[b]	hs-Fe^{III} fast relaxing	0.50	1.29	0.66 (0.66)	-	30
		hs-Fe^{III} slow relaxing	0.50	-	0.50 (0.50)	49	70
	100[c]	hs-Fe^{III}	0.48	1.05	0.82 (0.93)	-	90
	100[d]	hs-Fe^{III}	0.45	0.84	0.54 (0.56)	-	
Reaction of **1** with Ph_3C•	5.1[a]	hs-Fe^{II}	1.37	3.34	0.40 (0.45)	-	90

[a] Spectrum contains approximately 10 % iron(III).

[b] Spectra are a mixture of the fast- and slow-relaxing regimes.

[c] Spectrum is *nearly* completely fast-relaxing HS iron(III). Both isomer shift and quadrupole splitting have decreased due to a second order Doppler effect. Line broadening shows the sample is not fully relaxed.

[d] Spectrum measured using crystalline **1** suspended in boron-nitride.

The Mössbauer spectrum taken of a recrystallized sample of [Fe^{II}(N3PyO^{2Ph})(CH_3CN)](ClO_4) also revealed a high-spin Fe^{II} quadrupole doublet with $\delta = 1.05$, and $\Delta E_q = 2.29$ mm s^{-1}, although the parameters are slightly different than those of

the final Fe^{II} product dominating the reaction mixture (Figure 3.5). The differences that were observed between this spectrum and the spectrum of the final reaction mixture are most probably due to different solvent ligands that occupy the sixth site of the $[Fe^{II}(N3PyO^{2Ph})]^{+}$ complex. A THF solvent molecule is more likely to be the solvent occupying the open site after the reaction with $Ph_3C\bullet$, as opposed to the coordination of CH_3CN that is seen in $[Fe^{II}(N3PyO^{2Ph})(CH_3CN)](ClO_4)$. For additional insight, DFT calculations were performed on optimized geometries of $[Fe^{II}(N3PyO^{2Ph})(CH_3CN)]^{+}$, $[Fe^{II}(N3PyO^{2Ph})(THF)]^{+}$, and a 5-coordinate analog. When compared, the calculated isomer shift of the 5-coordinated complex (no solvent coordination), the shift is lower than both the experimental data and the data calculated for the 6-coordinate complexes. DFT calculations of the isomer shifts for $[Fe^{II}(N3PyO^{2Ph})(CH_3CN)]^{+}$ and $[Fe^{II}(N3PyO^{2Ph})(THF)]^{+}$ also follow along with the observed experimental trend, while the isomer shift obtain for $[Fe^{II}(N3PyO^{2Ph})(THF)]^{+}$ is higher than that for $[Fe^{II}(N3PyO^{2Ph})(CH_3CN)]^{+}$. Therefor the information obtained from the DFT calculations indicate that a product of a 6-coordinate nature is formed.

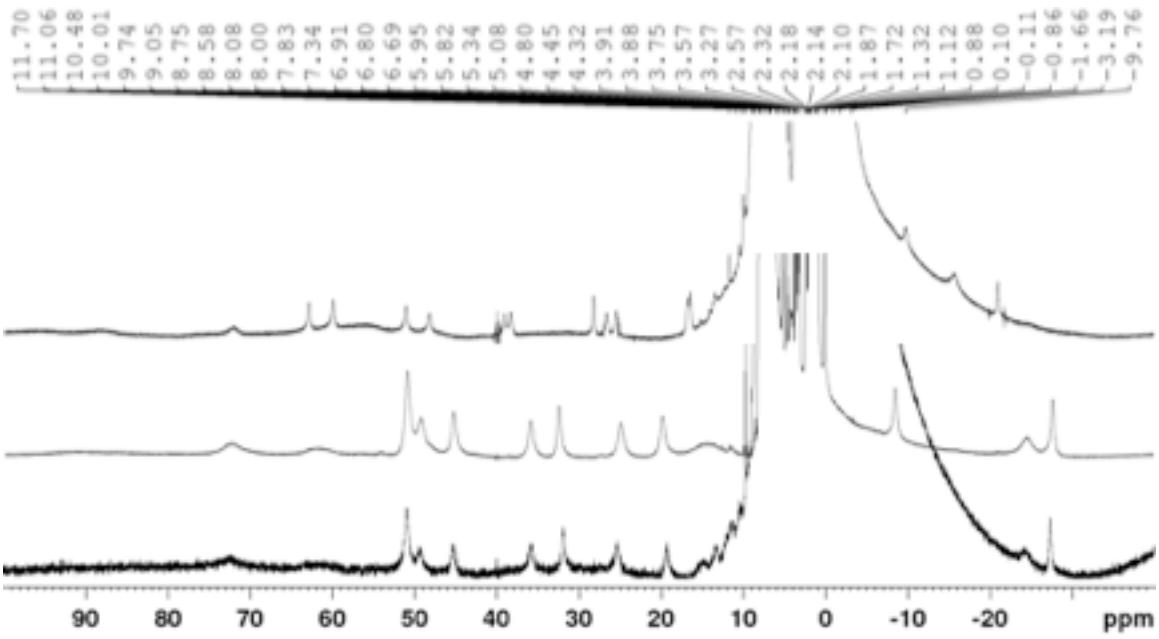

Figure 3.6. ^{1}H NMR spectra of [Fe^{III}(N3PyO^{2Ph})(OCH_3)](ClO_4) (**1**) and $(Ph_3C)_2$ in THF-d_8 for 60 min at 50 °C. Top: **1** before addition of $(Ph_3C)_2$. Middle: **1** and $(Ph_3C)_2$ after 60 min, followed by removal of THF-d_8 and dissolution in CD_3CN. Bottom: [Fe^{II}(N3PyO^{2Ph})(CH_3CN)](ClO_4) in CD_3CN.

This analysis is additionally supported by paramagnetic ^{1}H NMR (Figure 3.6), which revealed that the initial spectrum for **1** with peaks between +100 and -40 ppm disappears during the reaction with the trityl radical, and forms a spectrum with poorly-resolved features. However, upon removal of the THF, followed by dissolution of the resulting brown residue into CD_3CN, an NMR spectrum is obtained that can be assigned to the acetonitrile-bound Fe^{II} starting material.

3.4. Conclusions

The UV-vis, EPR, NMR, and Mössbauer data confirm that **1** reacts with trityl radical to produce the one-electron reduced, radical rebound product [Fe^{II}(N3PyO^{2Ph})]$^{+}$, along with a new C-O bond (Scheme 3.4). During our previous work involving the reaction

of an Fe(OH) complex with trityl radical, we showed that there was a concerted mechanism for hydroxylation, the most likely scenario.[14] As is shown in Scheme 3.4, we would suggest a similar mechanism of transformation here.

To summarize, this synthesis and characterization of a mononuclear terminal Fe^{III}-methoxide complex **1** provided a platform that would allow the first direct observation of radical oxygen rebound with a nonheme iron complex that gives a new C-O bond and free organic material. The complex **1** is capable of reacting in an efficient manner with the trityl radical in a rebound process that relies on a homolytic cleavage of the Fe-O bond and concomitant formation of the organic Ph_3COCH_3 as well as accompanying formation of the one-electron reduced Fe^{II} product. This current work provided support for the feasibility of a rebound pathway being enacted in C-H activation processes undergone by nonheme iron-oxo materials. Although the rebound reaction is feasible, the probability that would lead to rebound as opposed to solvent cage escape of the carbon radical is still a key question which presents a challenge to properly assess. Direct examination of the radical oxygen rebound reaction as described here foreshadows additional experimental approaches and methodologies that may be used to address the fundamentals of these mechanistic issues.

3.5. Supporting Information

Contents

I. Supporting Tables

Table 3.2. Comparison of the metrical parameters obtained from X-ray crystallography and DFT calculations for **Fe^{II}-MeCN**, **Fe^{II}-THF**, **Fe^{II}-5C** (the five-coordinate analog of the Fe^{II} complex without the CH_3CN ligand), and **1**.

	Fe^{II}-MeCN		**Fe^{II}-THF**	**Fe^{II}-5C**	**1**	
Bond Distances (Å)	**XRD**	**DFT**	**DFT**	**DFT**	**XRD**	**DFT**
Fe1-O1	1.956	1.945	1.955	1.907	1.928	1.933
Fe1-N1	2.263	2.253	2.281	2.152	2.341	2.390
Fe1-N2	2.473	2.522	2.479	2.267	2.249	2.259
Fe1-N3	2.170	2.186	2.162	2.133	2.202	2.214
Fe1-N4	2.160	2.178	2.211	2.160	2.156	2.157
Fe1-L (N5/O2)	2.077	2.012	2.114	-----	1.785	1.787
Bond Angles (°)						
O1-Fe1-N1	99.71	97.65	97.22	99.94	162.73	161.88
O1-Fe1-N2	164.43	165.04	168.06	173.98	98.27	96.68
O1-Fe1-N3	92.08	91.87	93.21	94.28	89.43	88.29
O1-Fe1-N4	88.82	89.25	87.42	89.42	85.26	84.62
O1-Fe1-L	103.96	102.08	95.04	-----	102.48	101.52
N1-Fe1-N4	155.78	156.36	156.25	160.73	87.28	89.46
N2-Fe1-N4	85.40	88.23	89.07	89.98	152.29	153.48
N3-Fe1-N4	79.01	78.69	78.34	80.37	76.67	77.35
N1-Fe1-L	98.34	101.56	99.66	-----	94.4	96.53
N2-Fe1-L	91.37	92.67	96.87	-----	102.4	101.53
N3-Fe1-L	163.94	165.86	171.67	-----	168.08	170.16
N4-Fe1-L	101.54	99.02	103.13	-----	103.63	104.15
N1-Fe1-N2	80.41	79.27	81.61	78.94	81.41	81.14
N1-Fe1-N3	78.07	78.51	78.15	82.16	73.69	73.69
N2-Fe1-N3	72.63	73.17	74.90	79.71	75.91	76.21

Table 3.3. Calculated Mössbauer parameters **Fe^{II}-MeCN**, **Fe^{II}-THF**, **Fe^{II}-5C**, and **1**.

Complex[a]	Isomer Shift[b] (mm/s^{-1})	Quadrupole Splitting (mm/s^{-1})
Fe^{II}-MeCN	1.05	3.62
Fe^{II}-THF	1.15	3.50
Fe^{II}-5C	1.02	2.74
1	0.61	1.60

[a] See DFT computational section for details regarding geometry optimizations

[b] $\rho(0)$ calculated using the B3LYP[24-2724-27] functional with a combination of CP(PPP) for Fe and def2-TZVP for all other atoms and calibrated as described in DFT computational section.

Table 3.4. Optimized coordinates for **Fe^{II}-MeCN**.

Fe	0.522849	2.592136	12.897903
C	-2.404920	-1.088544	14.112118
H	-3.313941	-0.739325	14.613279
C	-2.448936	-2.241543	13.315974
H	-3.390418	-2.790097	13.207107
C	-1.288104	-2.690604	12.662111
H	-1.317597	-3.599637	12.052296
C	-0.089383	-1.970257	12.800546
H	0.820109	-2.319630	12.300203
C	-0.043672	-0.805779	13.583319
H	0.894968	-0.250112	13.683761
C	-1.203581	-0.354848	14.250063
C	-1.172223	0.822142	15.161413
C	-1.758099	0.695779	16.441777
H	-2.212890	-0.255773	16.727615
C	-1.716652	1.762933	17.342384
H	-2.149608	1.667442	18.342244
C	-1.091159	2.951495	16.942126
H	-1.021685	3.812981	17.612785
C	-0.545498	3.018340	15.655042
C	0.028705	4.336591	15.128276
H	0.233046	5.008458	15.984872
C	-1.068453	4.949904	14.261072
C	-1.924962	5.921431	14.797744
H	-1.738443	6.331466	15.793551
C	-3.019969	6.337220	14.030019
H	-3.714817	7.092543	14.410005
C	-3.197366	5.780720	12.760785
H	-4.025756	6.100667	12.122859
C	-2.269175	4.834513	12.269541
C	-2.435901	4.323111	10.882292
C	-1.353934	4.322601	9.978361
H	-0.377625	4.671756	10.320478
C	-1.530843	3.891753	8.656058
H	-0.682261	3.884320	7.964865
C	-2.793679	3.454470	8.220163
H	-2.924366	3.108944	7.189794
C	-3.880937	3.458674	9.111435
H	-4.866812	3.116681	8.779468
C	-3.705851	3.896624	10.432970
H	-4.552547	3.885252	11.127993
C	1.780347	5.270410	13.626124
H	2.561755	5.771039	14.226237
H	0.956382	5.994980	13.506042

C	2.311770	4.920978	12.247629
C	3.338452	5.664741	11.644292
H	3.813798	6.483253	12.193172
C	3.742827	5.338129	10.343698
H	4.542353	5.903243	9.854768
C	3.111646	4.271412	9.683823
H	3.392203	3.979133	8.669003
C	2.097812	3.578966	10.353868
H	1.569383	2.748704	9.875275
C	2.319552	3.453628	15.199078
H	1.833266	2.624491	15.741161
H	2.644566	4.201168	15.951010
C	3.511629	2.927374	14.438092
C	4.814049	3.357777	14.747900
H	4.945178	4.146368	15.500131
C	5.937579	2.788249	14.127737
H	6.944293	3.133903	14.383458
C	5.750473	1.765324	13.178931
H	6.618037	1.306820	12.690543
C	4.462511	1.325122	12.848383
H	4.308718	0.529823	12.110454
C	3.317110	1.895277	13.464777
N	-0.578879	1.987371	14.767269
N	-1.218353	4.412616	13.026679
N	1.256465	4.069213	14.333025
N	1.694746	3.897359	11.606076
N	-0.493126	1.580438	11.486105
C	-0.980626	0.920625	10.652883
C	-1.587052	0.085057	9.631023
H	-1.528400	-0.973870	9.937337
H	-1.066382	0.213444	8.664338
H	-2.648061	0.359674	9.509123
O	2.093930	1.473002	13.149683
O	1.652538	1.107743	4.914532
O	0.221695	0.266205	6.743781
O	-0.372351	2.360462	5.570358
Cl	0.771195	1.512693	6.077439
O	1.588445	2.299419	7.076824

Table 3.5. Optimized coordinates for **Fe^{II}-THF**.

Fe	0.356471	2.649535	12.848095
C	-2.291599	-1.298712	14.430216
H	-3.219188	-0.987655	14.922256
C	-2.236414	-2.537767	13.777829
H	-3.118058	-3.187476	13.773135
C	-1.053067	-2.943783	13.136494
H	-1.003369	-3.917596	12.638845
C	0.064218	-2.091871	13.139217
H	0.991230	-2.404236	12.646812
C	0.009814	-0.841820	13.775320
H	0.887486	-0.186610	13.764513
C	-1.169190	-0.434089	14.436630
C	-1.215640	0.817721	15.241331
C	-1.789657	0.738236	16.530368
H	-2.197191	-0.217349	16.868508
C	-1.786719	1.845914	17.381385
H	-2.213967	1.783373	18.386106
C	-1.181685	3.023385	16.926067
H	-1.112119	3.911607	17.561013
C	-0.644482	3.046725	15.634287
C	-0.041199	4.341055	15.097032
H	0.194553	5.005063	15.952651
C	-1.106772	5.010999	14.235686
C	-1.859026	6.066403	14.768756
H	-1.624968	6.458439	15.761740
C	-2.898904	6.599682	13.998906
H	-3.504645	7.431117	14.371883
C	-3.125815	6.063983	12.729997
H	-3.900725	6.482179	12.082840
C	-2.316801	5.010529	12.244213
C	-2.558433	4.524587	10.860119
C	-1.485999	4.239945	9.989543
H	-0.464245	4.345807	10.357939
C	-1.723806	3.862865	8.660097
H	-0.880807	3.644877	7.996816
C	-3.041916	3.754520	8.184499
H	-3.224126	3.453021	7.148085
C	-4.119824	4.026202	9.044691
H	-5.149890	3.932820	8.684523
C	-3.882198	4.415311	10.370146
H	-4.728523	4.611066	11.037015
C	1.741110	5.242742	13.626054
H	2.533041	5.696629	14.249828
H	0.941624	5.996856	13.522884

C	2.273118	4.910163	12.247467
C	3.361552	5.602306	11.696956
H	3.874406	6.365770	12.289890
C	3.783836	5.292504	10.397543
H	4.633164	5.817419	9.949868
C	3.103217	4.290281	9.691782
H	3.387143	4.002569	8.676761
C	2.025589	3.648815	10.311754
H	1.473302	2.870930	9.779246
C	2.220325	3.340226	15.112020
H	1.709705	2.511464	15.629987
H	2.590579	4.042160	15.887739
C	3.376586	2.803175	14.303227
C	4.698251	3.175759	14.609351
H	4.868259	3.918671	15.399526
C	5.792075	2.605857	13.940324
H	6.813425	2.906807	14.194507
C	5.555973	1.641023	12.942765
H	6.399562	1.184447	12.412615
C	4.250108	1.256242	12.617262
H	4.056595	0.507906	11.841112
C	3.132002	1.825278	13.283616
N	-0.676909	1.989300	14.771350
N	-1.314982	4.473651	13.005288
N	1.172571	4.038695	14.290232
N	1.600194	3.948690	11.562675
O	1.894304	1.448457	12.970488
O	-0.696933	1.460809	11.453162
C	-2.130217	1.148284	11.503956
H	-2.310578	0.538466	12.404243
C	-2.418491	0.369778	10.219884
H	-3.281292	-0.306163	10.335505
C	-1.092533	-0.378771	9.980175
H	-1.030042	-1.271815	10.623416
H	-0.952493	-0.679229	8.930307
H	-2.624107	1.066102	9.390284
H	-2.672422	2.101129	11.578158
C	-0.052282	0.660304	10.397236
H	0.871110	0.246473	10.829855
H	0.192113	1.331320	9.556444
O	1.810482	1.615767	5.158820
O	0.587295	0.242009	6.813454
O	-0.545923	2.136048	5.699244
Cl	0.767792	1.636273	6.254020
O	1.233039	2.566556	7.361764

Table 3.6. Optimized coordinates for **Fe^{II}-5C**.

Fe	0.579904	2.883834	12.890452
C	-2.459299	-0.809284	13.449367
H	-3.224471	-0.714329	14.227514
C	-2.714531	-1.595699	12.317830
H	-3.667116	-2.129216	12.233857
C	-1.761500	-1.682171	11.288472
H	-1.966433	-2.287627	10.399307
C	-0.544365	-0.991903	11.404347
H	0.206220	-1.056109	10.609951
C	-0.282432	-0.205532	12.537145
H	0.705218	0.253577	12.649847
C	-1.243366	-0.095640	13.568532
C	-1.036457	0.781575	14.747297
C	-1.494230	0.397784	16.029483
H	-1.917103	-0.599969	16.169306
C	-1.393749	1.284716	17.103383
H	-1.736995	0.991191	18.099647
C	-0.851311	2.562671	16.884135
H	-0.779767	3.297332	17.691270
C	-0.393644	2.874268	15.602279
C	0.108068	4.272617	15.229797
H	0.259162	4.876514	16.144770
C	-0.973072	4.913987	14.355110
C	-1.756611	5.977558	14.812220
H	-1.577255	6.415598	15.797396
C	-2.755431	6.469728	13.958585
H	-3.365635	7.328564	14.253607
C	-2.965147	5.847880	12.727045
H	-3.736389	6.228574	12.054595
C	-2.171651	4.740181	12.341356
C	-2.457039	3.990375	11.089967
C	-1.511956	3.115979	10.509292
H	-0.513531	3.023609	10.958426
C	-1.794541	2.399112	9.341045
H	-1.035555	1.737621	8.913365
C	-3.047294	2.542815	8.722876
H	-3.272240	1.990461	7.805211
C	-4.008458	3.396265	9.289240
H	-4.993155	3.503471	8.822956
C	-3.720101	4.109204	10.459374
H	-4.500835	4.738251	10.896193
C	1.830041	5.441840	13.845900
H	2.662754	5.852816	14.444329
H	1.004364	6.173062	13.905512

C	2.247352	5.293081	12.392013
C	3.209959	6.140092	11.822766
H	3.698764	6.900374	12.439551
C	3.542525	5.984474	10.470877
H	4.295144	6.630141	10.007534
C	2.911324	4.973112	9.732058
H	3.155278	4.791684	8.682266
C	1.958020	4.171029	10.367997
H	1.467811	3.358163	9.822042
C	2.460174	3.430806	15.148498
H	1.997459	2.538428	15.603956
H	2.828951	4.074604	15.972127
C	3.606634	3.020371	14.252697
C	4.925779	3.405594	14.553184
H	5.102872	4.060074	15.415833
C	6.010265	2.955124	13.784593
H	7.030050	3.262942	14.036484
C	5.769480	2.104513	12.689392
H	6.606313	1.747448	12.078888
C	4.465619	1.709495	12.365843
H	4.262177	1.056737	11.510502
C	3.363198	2.153116	13.139211
N	-0.455960	2.001668	14.558132
N	-1.148845	4.328514	13.142178
N	1.360517	4.149329	14.420446
N	1.612843	4.334118	11.667743
O	2.122684	1.763749	12.831216
O	2.271341	0.040743	6.623198
O	2.361386	-0.141090	9.089365
O	0.182837	-0.201380	7.923673
Cl	1.573177	0.397671	7.918540
O	1.465246	1.907392	8.025718

Table 3.7. Optimized coordinates for **1**.

Fe	-2.723509	0.514255	10.032258
C	-6.237398	3.326358	11.936633
H	-7.141479	2.727158	12.009646
C	-6.325517	4.679803	11.604157
H	-7.298806	5.127607	11.424210
C	-5.164939	5.454754	11.504000
H	-5.233188	6.509394	11.252386
C	-3.915739	4.867634	11.735601
H	-3.012423	5.468424	11.675727
C	-3.825701	3.511507	12.056203
H	-2.862023	3.063108	12.266344
C	-4.984242	2.726618	12.154308
C	-4.918098	1.309894	12.596491
C	-5.742411	0.915295	13.665710
H	-6.406968	1.645057	14.115034
C	-5.665674	-0.378375	14.168868
H	-6.278860	-0.682646	15.011244
C	-4.769797	-1.270014	13.579378
H	-4.663176	-2.288080	13.937893
C	-4.008479	-0.822505	12.502894
C	-3.133470	-1.791297	11.723379
H	-2.918860	-2.676020	12.334821
C	-3.945330	-2.196850	10.499107
C	-4.652138	-3.394215	10.474814
H	-4.557023	-4.101692	11.292067
C	-5.477507	-3.650798	9.378681
H	-6.043552	-4.574678	9.316041
C	-5.545346	-2.709132	8.358714
H	-6.151651	-2.892559	7.478820
C	-4.788180	-1.524884	8.432521
C	-4.845159	-0.576906	7.291078
C	-6.091802	-0.285825	6.705489
H	-7.001500	-0.687136	7.144517
C	-6.170651	0.535568	5.579881
H	-7.140108	0.762697	5.145827
C	-5.004080	1.061393	5.014262
H	-5.062896	1.690819	4.130542
C	-3.762051	0.770700	5.588936
H	-2.853001	1.171452	5.149067
C	-3.677752	-0.038060	6.724682
H	-2.709953	-0.258865	7.163002
C	-1.109469	-0.546089	12.418157
H	-0.339901	-1.253917	12.744839
H	-1.786340	-0.387714	13.263815
C	-0.490263	0.780976	12.040563
C	0.692099	1.246653	12.622470
H	1.223331	0.628135	13.338813
C	1.173525	2.503311	12.260101

H	2.091215	2.884064	12.696637
C	0.467923	3.258538	11.317076
H	0.815855	4.234201	10.998014
C	-0.698225	2.726526	10.779840
H	-1.285802	3.256667	10.037912
C	-1.040069	-2.053248	10.474100
H	-1.689693	-2.463901	9.695103
H	-0.717872	-2.878988	11.122380
C	0.144445	-1.375605	9.843004
C	1.448499	-1.840066	10.048964
H	1.611290	-2.674745	10.728333
C	2.532650	-1.255013	9.387728
H	3.540032	-1.625188	9.556068
C	2.304421	-0.187728	8.508637
H	3.135914	0.282455	7.990648
C	1.012496	0.290403	8.290785
H	0.833818	1.122118	7.615395
C	-0.088448	-0.294029	8.952330
C	-4.721183	2.566346	8.781779
H	-4.703028	2.626241	7.684504
H	-4.696581	3.582779	9.196907
H	-5.662924	2.090233	9.088707
N	-4.064153	0.433528	12.008936
N	-4.003355	-1.273580	9.511804
N	-1.890783	-1.112563	11.282198
N	-1.175711	1.520926	11.147810
O	-1.320186	0.167513	8.748423
O	-3.618468	1.838895	9.233624
O	4.726014	4.428198	6.094725
O	3.010595	2.757012	6.574389
Cl	3.859221	3.361388	5.502358
O	4.721586	2.306077	4.887253
O	2.980544	3.961455	4.449706

II. Supporting Figures.

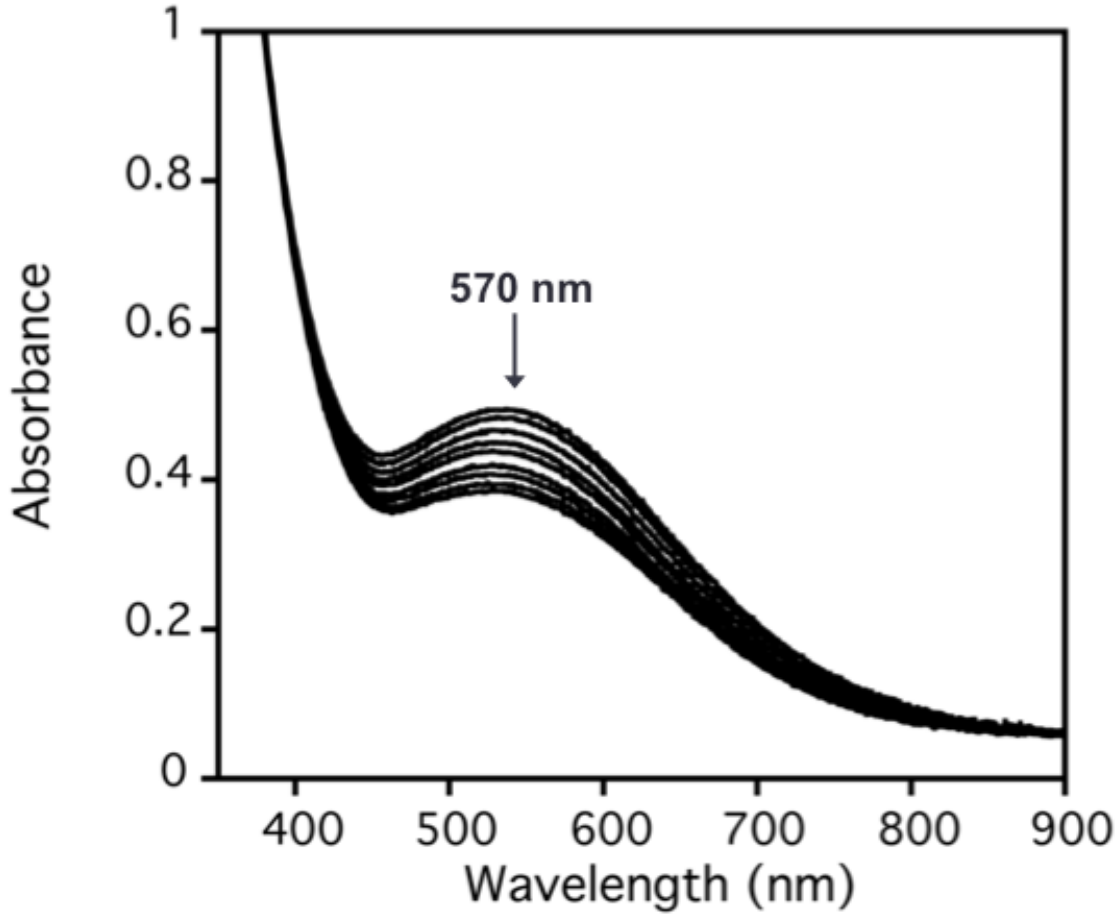

Figure 3.7. UV-vis spectra for complex **2** (0.4 mM) dissolved in THF at 50 °C over 1 h.

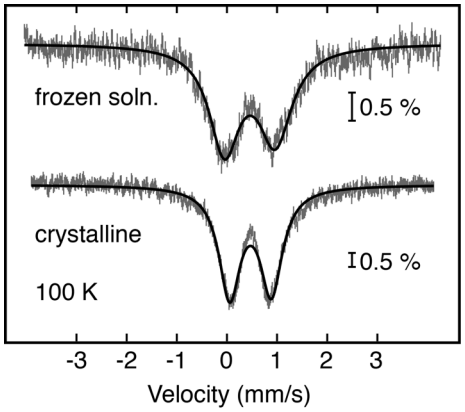

Figure 3.8. ^{57}Fe Mössbauer spectra of **1** in frozen solution (THF) (top) and as a crystalline solid dispersed in a boron nitride matrix (bottom). The two spectra are almost identical (see parameters in Table 3.1), providing strong evidence that complex **1** maintains its monomeric structure in solution.

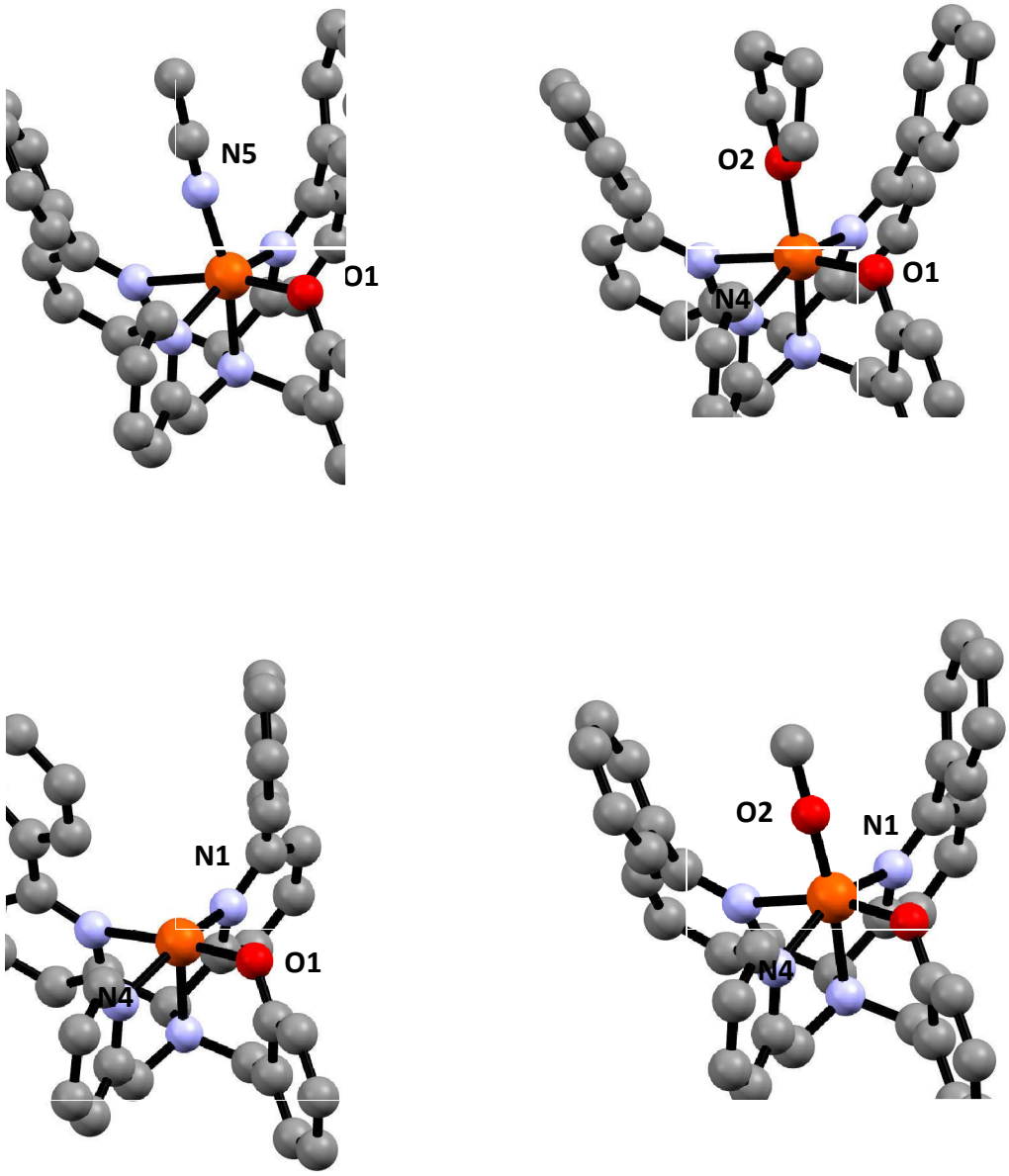

Figu mized geometry for **Fe^{II}-MeCN** (top left), **Fe^{II}-THF** (top right), **Fe^{II}-5C** (bottom left), and **1** (bottom right) with hydrogen atoms and ClO_4^- counterion omitted.

3.6. References

1. Huang, X.; Groves, J. T., *JBIC, J. Biol. Inorg. Chem.* **2017,** *22*, 185-207.

2. Ortiz de Montellano, P. R., *Chem. Rev.* **2010,** *110*, 932-948.

3. Kovaleva, E. G.; Lipscomb, J. D., *Nat. Chem. Biol.* **2008,** *4*, 186-193.

4. Cho, K. B.; Hirao, H.; Shaik, S.; Nam, W., *Chem. Soc. Rev.* **2016,** *45*, 1197-210.

5. Shaik, S.; Kumar, D.; de Visser, S. P.; Altun, A.; Thiel, W., *Chem. Rev.* **2005,** *105*, 2279-2328.

6. Mitchell, A. J.; Zhu, Q.; Maggiolo, A. O.; Anath, N. R.; Hillwig, M. L.; Liu, X.; Boal, A. K., *Nat. Chem. Biol.* **2016,** *12*, 636-640.

7. Matthews, M. L.; Neumann, C. S.; Miles, L. A.; Grove, T. L.; Booker, S. J.; Krebs, C.; Walsh, C. T.; Bollinger, J. M., Jr., *Proc. Natl. Acad. Sci.* **2009,** *106*, 17723-17728.

8. Martinie, R. J.; Livada, J.; Chang, W.; Green, M. T.; Krebs, C.; Bollinger, J. M., Jr.; Silakov, A., *J. Am. Chem. Soc.* **2015,** *137*, 6912-6919.

9. Wong, C.; Fujimori, D. G.; Walsh, C. T.; Drennan, C. L., *J. Am. Chem. Soc.* **2009,** *131*, 4872-4879.

10. Pangia, T. M.; Davies, C. G.; Prendergast, J. R.; Gordon, J. B.; Siegler, M. A.; Jameson, G. N. L.; Goldberg, D. P., *J. Am. Chem. Soc.* **2018,** *140*, 4191-4194.

11. Cho, K.-B.; Wu, X.; Lee, Y.-M.; Kwon, Y. H.; Shaik, S.; Nam, W., *J. Am. Chem. Soc.* **2012,** *134*, 20222-20225.

12. Bae, S. H.; Seo, M. S.; Lee, Y. M.; Cho, K. B.; Kim, W. S.; Nam, W., *Angew. Chem. Int. Ed. Engl.* **2016,** *55*, 8027-8031.

13. Rana, S.; Dey, A.; Maiti, D., *Chem. Commun.* **2015,** *51*, 14469-14472.

14. Zaragoza, J. P. T.; Yosca, T. H.; Siegler, M. A.; Moënne-Loccoz, P.; Green, M. T.; Goldberg, D. P., *J. Am. Chem. Soc.* **2017,** *139*, 13640-13643.

15. The observation of metal-bound C-O products following a related rebound process for a nonheme $Ru^{IV}(O)$ complex was described. Kojima, T.; Nakayama, K.; Ikemura, K.; Ogura, T.; Fukuzumi, S., *J. Am. Chem. Soc.* **2011,** *133*, 11692-11700.

16. Smith, J. M.; Mayberry, D. E.; Margarit, C. G.; Sutter, J.; Wang, H.; Meyer, K.; Bontchev, R. P., *J. Am. Chem. Soc.* **2012,** *134*, 6516-6519.

17. Jang, E. S.; McMullin, C. L.; Kass, M.; Meyer, K.; Cundari, T. R.; Warren, T. H., *J. Am. Chem. Soc.* **2014,** *136*, 10930-10940.

18. Iovan, D. A.; Betley, T. A., *J. Am. Chem. Soc.* **2016,** *138*, 1983-1993.

19. Neese, F., *Wiley Interdiscip. Rev. Comput. Mol. Sci.* **2012,** *2*, 73-78.

20. Becke, A. D., *J. Chem. Phys.* **1986,** *84*, 4524-4529.

21. Perdew, J. P., *Phys. Rev. B* **1986,** *33*, 8822-8824.

22. Tao, J.; Perdew, J. P.; Staroverov, V. N.; Scuseria, G. E., *Phys. Rev. Lett.* **2003,** *91*, 1-4.

23. Perdew, J. P.; Tao, J.; Staroverov, V. N.; Scuseria, G. E., *J. Chem. Phys.* **2004,** *120*, 6898-6911.

24. Becke, A. D., *J. Chem. Phys.* **1993,** *98*, 5648-5652.

25. Lee, C.; Yang, W.; Parr, R. G., *Phys. Rev. B* **1988,** *37*, 785-789.

26. Vosko, S. H.; Wilks, L.; Nusair, M., *Can. J. Phys.* **1980,** *58*, 1200-1211.

27. Stephens, P. J.; Devlin, F. J.; Chabalowski, C. F.; Frisch, M. J., *J. Phys. Chem.* **1994,** *98*, 11623-11627.

28. Pantazis, D. A.; Chen, X.-Y.; Landis, C. R.; Neese, F., *J. Chem. Theory Comput.* **2008,** *4*, 908-919.

29. Weigend, F.; Ahlrichs, R., *Phys. Chem. Chem. Phys.* **2005,** *7*, 3297-3305.

30. Römelt, M.; Ye, S.; Neese, F., *Inorg. Chem.* **2009,** *48*, 784-785.

31. Pápal, M.; Vankó, G., *J. Chem. Theory Comput.* **2013,** *9*, 5004-5020.

32. Gomberg, M., *J. Am. Chem. Soc.* **1914,** *36*, 1144-1170.

33. Ihde, A. J., *Pure Appl. Chem.* **1967,** *15*, 1-14.

34. Chen, C.; Lee, H.; Jordan, R. F., *Organometallics* **2010,** *29*, 5373-5381.

Chapter 4 Kinetic Investigation of Rebound in a Nonheme Model Complex

4.1. Introduction

Investigations into the radical rebound mechanism, an explanation of C–H hydroxylations that are carried out by both heme and nonheme oxygenases, have revealed valuable mechanistic insights which expand the understanding of these important biological transformations.[1] The central transformations of the mechanism involve the activation of a C–H bond via a high-valent metal-oxo species, which performs an abstraction of the C-H hydrogen atom. The newly-generated carbon radical (R•) recombines with the co-generated metal-hydroxide species to form the products. This recombination, or "rebound" step is hypothesized to occur with a homolytic cleavage along the metal–OH bond, bringing about a new C–O bond and a one-electron reduced metal center (Scheme 4.1).

Scheme 4.1. Oxygen rebound vs alternative pathway.

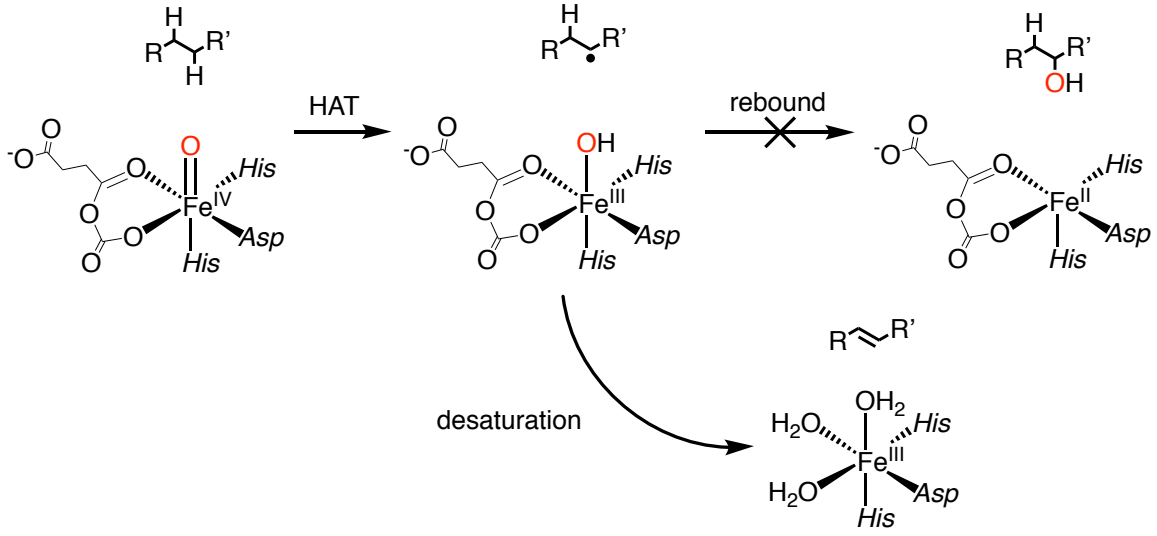

The cleavage of the C–H bond is rate-limiting, which results in the subsequent rebound step occurring too rapidly for direct observation.[2] The nonheme iron enzyme isopenicillin N synthase (IPNS) may operate using a similar pathway. A C_{Val} radical is thought to selectively combine with a coordinated thiolate ligand, rather than a bound OH group, which gives the final thiazolidine ring (Scheme 4.2).[3]

Scheme 4.2. IPNS C-S bond formation.[3]

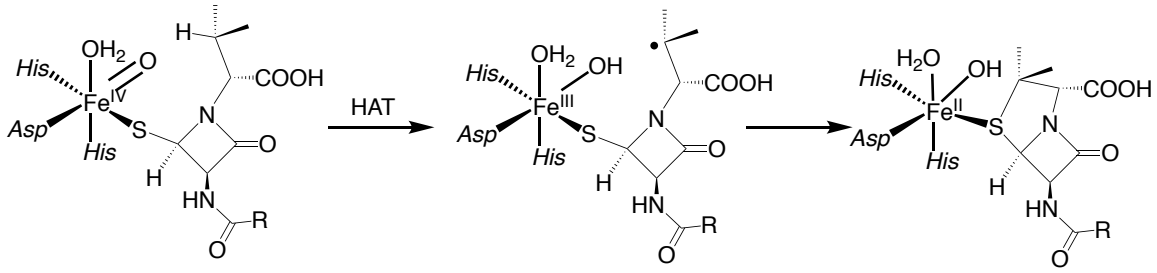

There are other processes of interest that have been observed as alternatives to the C-O bond formation step, including desaturation or decarboxylation (e.g. heme: CYP450 OleT; nonheme: AsqJ, NapI, VioC, UndA).[4-12] In the case of the nonheme iron halogenases (e.g. CytC3, WelO5, SyrB2), a halogen ligand is transferred as opposed to an OH ligand during the key rebound step. The question of how halogenation is directed remains a focus of

model studies.[13-18] In the case of some nonheme iron/oxyglutarate enzymes (e.g. AsqJ, NapI, VioC), a desaturation pathway prevails in which a C=C bond forms within the substrate.[5-6] Mechanistic studies continue to bring additional insight into the mechanisms of these transformations.

The synthesis and isolation of a recent Fe–OH complex by our group has given a platform by which the oxygen rebound mechanism may be directly measured in a heme complex (Scheme 4.3).[2] However there is to our knowledge no similar investigation on rebound in nonheme iron complexes (Scheme 4.3).[17, 19] While the reaction process in either case is similar, the oxidation state of heme rebound results in the reduction of a formal $Fe^{IV}(OH)$ to Fe^{III}, whereas the nonheme analog occurs in a $Fe^{III}(OH)$ to Fe^{II} fashion.[1, 20]

Scheme 4.3. Heme and nonheme rebound.

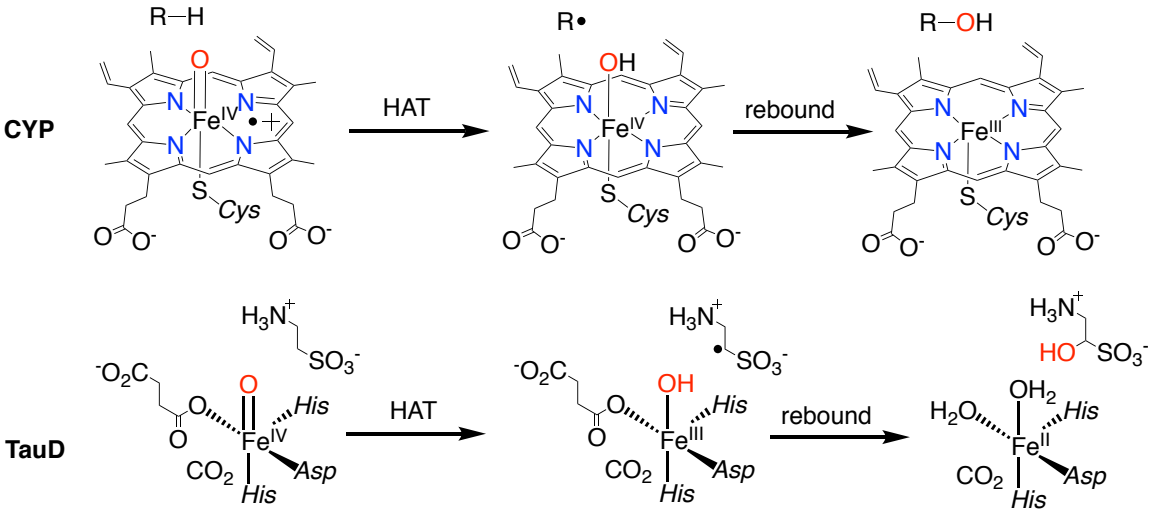

The heme-type CYP reacts utilizing a one-electron reduction process, proceeding from a formal $Fe^{IV}(OH)$(porphyrin) to an Fe^{III}(porphyrin) material product (Scheme 4.3). This reactivity was found to be well-modelled by our Fe(OH) corrole material.[2] Recently we prepared a nonheme $Fe^{III}(OCH_3)$ complex as a model for the nonheme $Fe^{III}(OH)$ intermediate.[21] The Fe–OCH_3 complex provides a stable platform to further investigate the

rebound step. The rebound reaction between [Fe^{III}(N3PyO^{2Ph})(OCH_3)](ClO_4) (**1**) and an organic radical has been examined and characterized.[21] The complex reacted with trityl radical in a process similar to the rebound process, during which the Fe-OCH_3 bond underwent homolytic cleavage to produce Ph_3COCH_3 as well as the reduced Fe^{II} product. However, there were no kinetic data obtained and the reaction mechanism was not examined in detail. As was previously shown, the reaction between a heme Fe–O complex and a series of para-substituted trityl-type radicals can be investigated to obtain mechanistic details as to the nature of the observed rebound reaction. While the rebound principle was observed by reaction of Fe–OCH_3 and unsubstituted trityl radical to form the expected rebound organic product and the one-electron reduced iron complex (observed by Mössbauer and ^{1}H NMR),[21] the mechanism was not examined to determine whether the reaction occurs in a single concerted step (Scheme 4.4). An alternative is that the transformation consists of sequential electron transfer then cation transfer.[2,4]

Scheme 4.4. Concerted and separated ET/CT transformations.

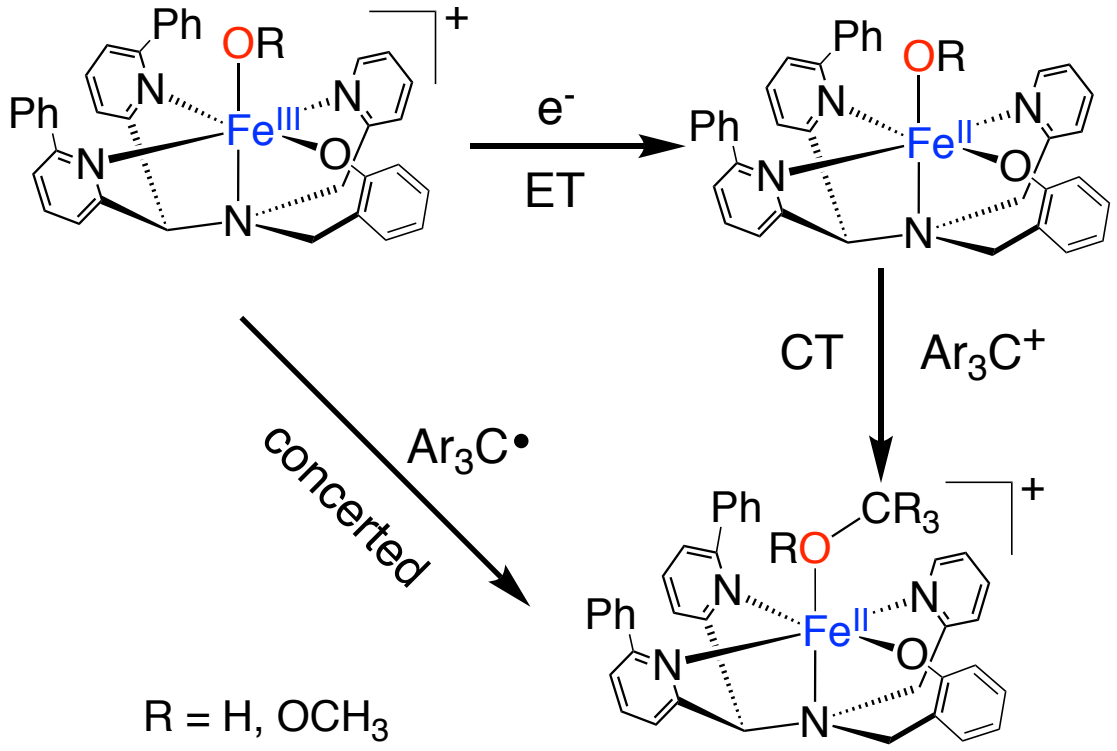

4.2. Experimental

General Methods and Materials. All chemicals and reagents were purchased from Sigma-Aldrich, Fisher Scientific, Acros Organics, Merck, Fluka Analytical, or Alfa Aesar and were used without further purification unless noted otherwise. Solvents (methanol, diethyl ether, acetonitrile, toluene, and tetrahydrofuran) used in organic synthesis were purified via Pure-Solv Solvent Purification System from Innovative Technology, Inc. Solvents used in the reactions of the iron(II) and iron(III) complexes were subjected to additional purification after initial purification via a Pure-Solv Solvent Purification System. THF and toluene were distilled from sodium/benzophenone. All solvents were degassed by freeze-pump-thaw cycles and stored in a N_2 filled dry box. Reactions involving inert atmosphere were performed using either standard Schlenk techniques or in a dry box. The compounds tris(*p*-t-butylphenyl)methyl bromide,[2, 22] tris(*p*-phenylphenyl)methyl

bromide,[2] and tris(*p*-cyanophenyl)methyl chloride[23] were prepared according to literature procedures. Tris(*p*-methoxyphenyl)methyl chloride was obtained from Alfa-Aesar and used as received. Metal complexes $[Fe^{III}(N3PyO^{2Ph})(OCH_3)](ClO_4)$ (**1**) and ^{57}**1** were prepared as previously described.[21] *Caution: Perchlorate salts of metal complexes are potentially explosive. Care should be taken when handling these compounds. Note: trityl radicals are O_2 and light-sensitive. Measures should be taken to avoid exposure of the radical to light and air.*

Analytical Methods. Kinetic UV-vis measurements were performed on a Hewlett-Packard Agilent 8453 diode-array spectrophotometer with a 3.5 mL quartz cuvette (path length = 1 cm) equipped with a septum. Other UV-visible spectra were recorded on a Varian Cary 50 Bio spectrophotometer, and also on a Varian Cary 60 Bio spectrophotometer. NMR spectra were collected on a Bruker Avance 400 MHz FT-NMR spectrometer. Mössbauer spectroscopy was performed on a spectrometer from SEE Co. (Science Engineering & Education Co., MN) equipped with a closed cycle refrigerator system from Janis Research Co. and SHI (Sumitomo Heavy Industries Ltd.) Spectra were measured with a small magnetic field (47 mT) applied parallel to the gamma radiation.

Synthesis of derivatives of trityl radical (p-X-$C_6H_4)_3$-C•. These derivatives are formed as and exist as monomers in solution,[23] and require generation *in situ*. Difficulty producing high yields of radical in solution at concentrations >10 mM limited concentration ranges in some cases.

Generation of (p-CN-C_6H_4)$_3$-C•. The compound was prepared according to a previous literature procedure.[23] To an amount of tris(p-cyanophenyl)methyl chloride (9.61 mM) was added excess zinc powder (Zn) in a scintillation vial in a glove box unit. Toluene (5.5 mL) was added to the mixture and was stirred at 75 °C in darkness for 90 minutes. The pink solution was cooled to 23 °C, filtered through Celite®, then immediately used for kinetics experiments. UV-vis (toluene): λ_{max} (ε, M^{-1} cm^{-1}): 568 (290). Radical yield (EPR) = 6.3 mM, 65%. The yield was obtained from quantification of the radical concentration by EPR spectroscopy at 23 °C (parameters: frequency = 9.75 GHz, power = 0.2 mW, receiver gain = 5.02 x 10^3, mod freq = 100 kHz, mod amp = 0.1 G). The EPR signal was quantified through double integration and comparison with TEMPO radical standard calibration curve under nonsaturating conditions. Beer's Law (ε = A/bc), was used to calculate the extinction coefficient, where A is absorbance of the stock solution at the maximum wavelength determined by the UV-vis spectroscopy, b is the path length of the UV-vis cuvette (1 cm), and c is the radical concentration in M.

Kinetic study of reactions between 1 and trityl radical derivatives. In an inert-atmosphere dry glovebox under light-limiting conditions, trityl derivatives (p-X-C_6H_4)$_3$-C• (X = -OMe, -tBu, -Ph, -CN) were freshly prepared in toluene according to literature procedure.[2] Concentrations of radicals were determined by measuring the UV-vis spectrum and using the known extinction coefficient. Varying amounts of stock solutions were prepared (200-1000 μL) and diluted to 2 mL. Solution of **1** was added (100 μL, 4 mM) to begin the reaction. Spectral changes showed consumption of **1** (λ_{max} = 570 nm). Pseudo-first-order rate constants (k_{Obs}) for these reactions were obtained using the software

Kaleidograph 4.5 through nonlinear least-squares fitting of plots of absorbance at 570 or 590 or 680 nm (Abs_t) versus time (t) according to the equation $Abs_t = Abs_f-(Abs_f-Abs_0)exp(-k_{obs}*t)$, where Abs_0 is the initial absorbance and Abs_f is the final absorbance. Second-order rate constants were found from the best-fit line from the plot of k_{Obs} versus concentration of radical.

Reaction of 1 with (4-tBu-C_6H_4)$_3$C•. ^{1}H NMR Spectroscopy. A solution of **1** (0.7 mL, 3 mM) in THF-d8 was made and an initial spectrum was recorded. Freshly prepared (4-tBu-C_6H_4)$_3$C• (5 equiv) was added and a subsequent spectrum was recorded after 5 minutes. Formation of a peak at δ 3.00 indicated production of (4-tBu-C_6H_4)$_3$$COCH_3$. After the reaction, 70% (4-tBu-C_6H_4)$_3$$COCH_3$ (based on **1**) was observed (Figure 4.2).

Reaction of 1 with (4-tBu-C_6H_4)$_3$C•. Mössbauer Spectroscopy. The radical was produced in toluene over Zn metal in a glove box. The resulting yellow solution (0.4 mL) was added anaerobically to a solution of ^{57}**1** in THF at 23 °C (0.8 mL). The final concentration of ^{57}**1** and (4-tBu-C_6H_4)$_3$C• was 4 mM. An aliquot (0.5 mL) was used to obtain the Mössbauer spectrum of the resulting solution frozen after 15 min, measured at 80 K (Figure 4.3). An additional aliquot (0.5 mL) was combined with acetonitrile (0.1 mL) and frozen, producing a sample which was likewise measured at 80 K.

Reaction of 1 with Ph_3C^+. UV-vis Spectroscopy. A solution of **1** (2 mL, 0.5 mM) in THF was placed into a quartz cuvette (1 cm pathlength) and an initial spectrum recorded at 23 °C. An amount of $Ph_3(BF_4)$ (4 equiv in 0.1 mL THF) was added. The UV-vis band at λ_{max}

= 570 nm (**1** in THF) was consumed within 2 seconds and a new band at λ_{max} = 610 nm was observed (Figure 4.6).

Reaction of 1 with Ph_3C^+. ^1H NMR Spectroscopy. A solution of **1** (0.7 mL, 5.0 mM) in THF-d_8 was recorded initially at 23 °C. An amount of $Ph_3C(BF_4)$ (4 equiv) was added and the solution manually mixed in the NMR tube. A spectrum recorded after 5 min at 23 °C showed formation of a peak at 3.04 ppm matching the $–OCH_3$ signal of Ph_3COCH_3, the expected methoxide transfer product. Integration against an internal standard (Ph-C_6H_4-OCH_3, 5.0 mM) gave a yield of 80% for Ph_3COCH_3 (based on **1**, Figure 4.7).

Reaction of 1 with Ph_3C^+. Mössbauer Spectroscopy. A solution of ^{57}**1** (0.4 mL) in THF was combined with $Ph_3C(BF_4)$ in THF (0.2 mL, 4 equiv). The final concentration of ^{57}**1** was 4 mM. An aliquot was frozen after 5 minutes and measured at 80K (Figure 4.3).

DFT Computational Studies. All calculations were conducted using Gaussian-09[24] at the UB3LYP level of theory.[25-26] Geometry optimisations, frequencies and constraint geometry scans were performed at UB3LYP with the LANL2DZ basis set on iron with core potential and 6-31G* basis set on all other atoms: basis set BS1.[27-28] Single point calculations using the LACV3P+ basis set on iron and 6-311+G* on all other atoms (basis set BS2) were carried out in order to refine the quality of the energies. Further single point calculations at B3LYP/BS2 were done including the continuum polarized conductor model (CPCM) with a dielectric constant mimicking acetonitrile.[29] Free energies reported include solvent, entropic (at 298 K) and zero-point corrections. Transition states were characterized

by a single imaginary frequency for the correct mode (C–O stretch vibration), while all local minima had real frequencies only. Calculations were mostly focused on quintet spin reactant pathways, i.e. started from $^{6}[Fe(OH)(N3PyO^{2Ph})]^{+}$ and $^{6}[Fe(OCH_3)(N3PyO^{2Ph})]^{+}$, and their reactivities with doublet spin $^{2}(p\text{-}X\text{-}C_6H_4)_3C^{\bullet}$ substrates (X = OMe, tBu, Ph, H, Cl, NO_2). The reactant complexes (**Re$_X$**), C–O bond formation transition states (**TS$_X$**) and alcohol product complexes (**Pr$_X$**) were calculated in the overall quintet and septet spin states. In general, the septet spin transition states and product complexes were substantially higher in energy than the quintet spin states.

4.3. Results and Discussion

In our initial report, we employed triphenylmethyl radical ($Ph_3C\bullet$) as a convenient carbon radical with good solubility in a range of organic solvents.[21] This radical is in equilibrium with a dimeric form (Gomberg's dimer) in solution (Figure 4.1), and it is the dimeric form that is isolated as a stable solid and allows for easy storage and handling. However, the monomer-dimer equilibrium favors the dimer in solution (2% radical in toluene at 23 °C), complicating the study of kinetics with the radical. Substitution of the *para* positions of the phenyl groups in $Ph_3C\bullet$ prevents dimerization, and provides a method for varying the electronic character of the radical derivatives.[21,30] We thus prepared a series of *para-X*-substituted radicals via metal reduction of the appropriate triarylmethyl halide, as shown Figure 1. Radical yields for X = OCH_3, tBu, Ph were estimated by UV-vis spectroscopy (λ_{max} = 530 – 570 nm) from known molar absorptivities. The yield of the cyano derivative was obtained by quantitation of the radical EPR spectrum and subsequent analysis of the molar absorptivity of the UV-vis band at 568 nm.

Figure 4.1. Substituted radicals used for examination of rebound mechanism and comparison with trityl radical and dimer.

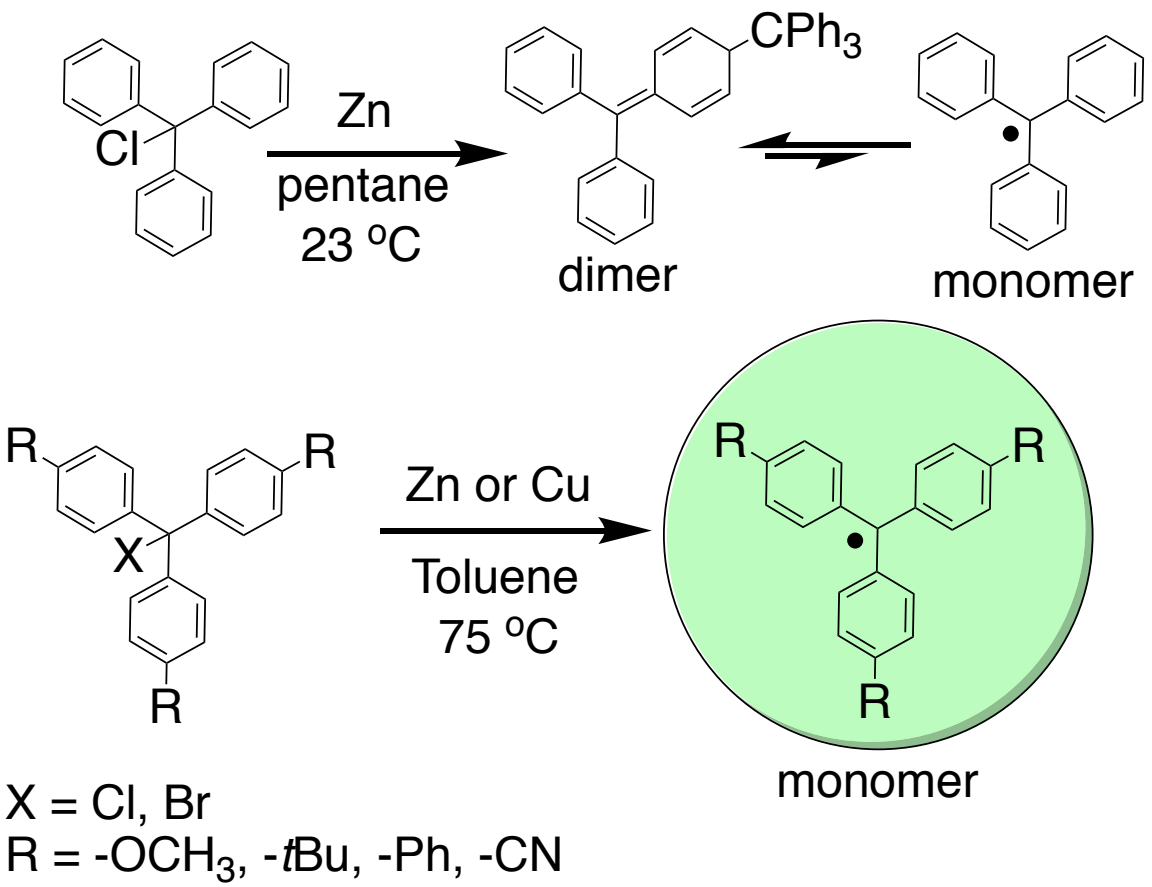

Addition of $(4\text{-tBu-}C_6H_4)_3C\bullet$ (5 equiv) to complex **1** in toluene at 23 °C led to the conversion of dark purple **1** to a yellow-orange color within 5 min. Analysis by ^1H NMR spectroscopy of the same reaction mixture showed the formation of a peak at 3.0 ppm which corresponds to the methoxy group of $(4\text{-tBu-}C_6H_4)_3COCH_3$, the expected radical recombination product (Figure 4.2). Quantitation of this peak by integration against an internal standard gave a 70% yield of the methoxy ether.

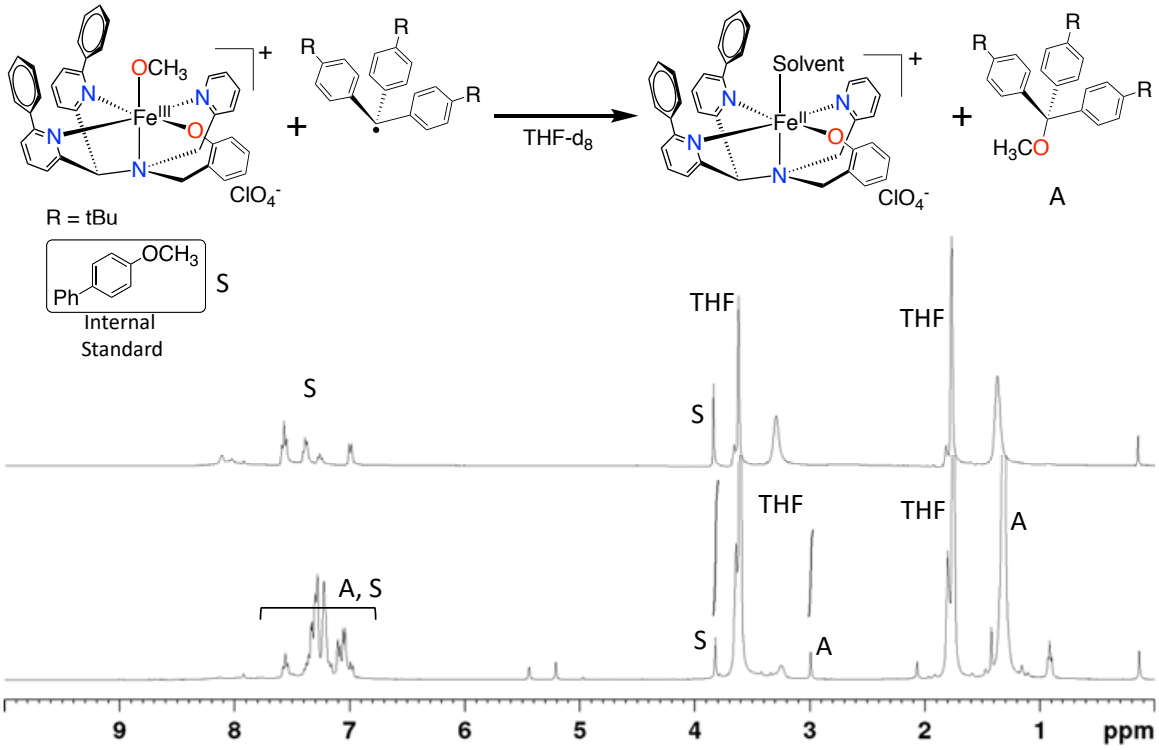

Figure 4.2. Reaction of **1** and $(4\text{-tBu-}C_6H_4)_3C\bullet$ monitored by ^1H NMR in THF-d_8 at 23 °C. Top: **1** and internal standard (S) before addition of $(4\text{-tBu-}C_6H_4)_3C\bullet$. Bottom: **1** and $(4\text{-tBu-}C_6H_4)_3C\bullet$ after 5 min. The $-OCH_3$ peak of $(4\text{-tBu-}C_6H_4)_3COCH_3$ at 3.00 ppm was integrated against the internal standard $-OCH_3$ peak at 3.83 ppm.

The same reaction was followed independently by Mössbauer spectroscopy to determine the fate of the iron complex. The ^{57}Fe-labeled **1** in THF/toluene revealed a broad doublet (0.5 mm s^{-1}, 1.29 mm s^{-1}) indicative of an Fe^{III} complex in an intermediate relaxation regime, as reported earlier.[21] This doublet disappears following addition of the tBu-substituted radical, giving rise to a new spectrum that can be fit well by two subcomponents with parameters indicative of high-spin Fe^{II} species: (species 1: δ = 1.16 mm s^{-1}, ΔE_Q = 2.68 mm s^{-1} (80% of total fit); species 2: δ = 1.34 mm s^{-1}, ΔE_Q = 3.29 mm s^{-1} (20% of total fit)) (Figure 4.3, Table 4.1).

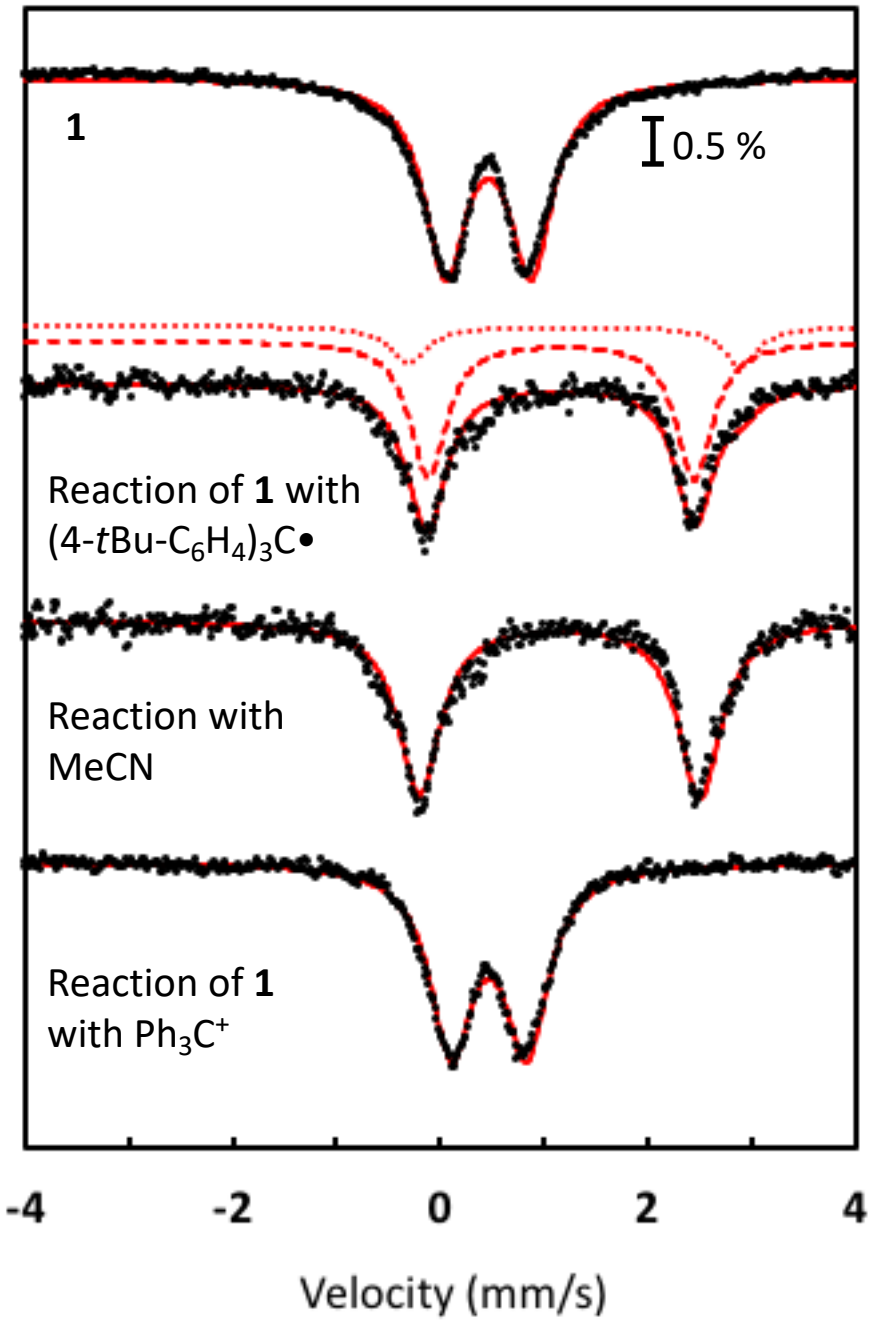

Figure 4.3. Top: ^{57}Fe Mössbauer spectrum for **1 (**dotted line) showing the experimental data (dotted line) and best fit (red line) for a fast-relaxing quadrupole doublet as the major component; Top middle: spectrum of the reaction mixture of **1** with (4-tBu-C_6H_4)$_3$C• in a ~2:1 mixture of THF:toluene reacted at 23 °C for 15 min (dotted line) and fitted with two

Fe^{II} quadrupole doublets (red dotted and dashed) in a ratio of 4:1; Bottom middle: spectrum of the reaction mixture of **1** with $(4\text{-tBu-}C_6H_4)_3C\bullet$ in a mixture of THF:toluene with addition of acetonitrile (dotted line), and the best fit for a Fe^{II} quadrupole doublet (red line). Bottom: spectrum of the reaction mixture of **1** with Ph_3C^+ (dotted line) with the best fit for a Fe^{III} quadrupole doublet (red line).

The latter component exhibits parameters that are similar to the Fe^{II} species formed after reaction with the unsubstituted $Ph_3C\bullet$,[21] although this previous reaction was run in pure THF. The solvent mixture employed here (toluene/THF 1:2) likely leads to small changes in solvent binding equilibria at the open site on the Fe^{II} product, which in turn gives rise to the two overlapping Mössbauer signals.

Table 4.1. ^{57}Fe Mössbauer parameters for **1**, and reaction of **1** with 4-**(**$(tBu\text{-}C_6H_4)_3C\bullet$.

	T (K)	Species	δ (mm/s)	ΔE_Q (mm/s)	$\Gamma_{L(R)}$ (mm/s)	I (%)
1	80	hs-Fe^{III}	0.48	0.87	0.83 (0.83)	90
1 and 4-$(tBu\text{-}C_6H_4)_3C\bullet$	80	hs-Fe^{II}	1.29	3.19	0.44 (0.44)	20
		hs-Fe^{II}	1.16	2.56	0.42 (0.42)	80
1 and 4-$(tBu\text{-}C_6H_4)_3C\bullet$, MeCN	80	hs-Fe^{II}	1.16	2.66	0.49 (0.49)	90
1 and Ph_3C^+	80	hs-Fe^{III}	0.45	0.72	0.82 (0.82)	90

When acetonitrile is added to the product mixture, the spectrum resolves to a single high-spin Fe^{II} component, δ = 1.16 mm s^{-1}, ΔE_Q = 2.66 mm s^{-1}, matching that seen for the acetonitrile-bound Fe^{II} species.[21] The ^{1}H NMR and Mössbauer data show that the tBu-substituted radical reacts with **1** in good yield via the anticipated radical rebound reaction as shown in Scheme 4.5.

Scheme 4.5. Rebound reaction between **1** and trityl radicals.

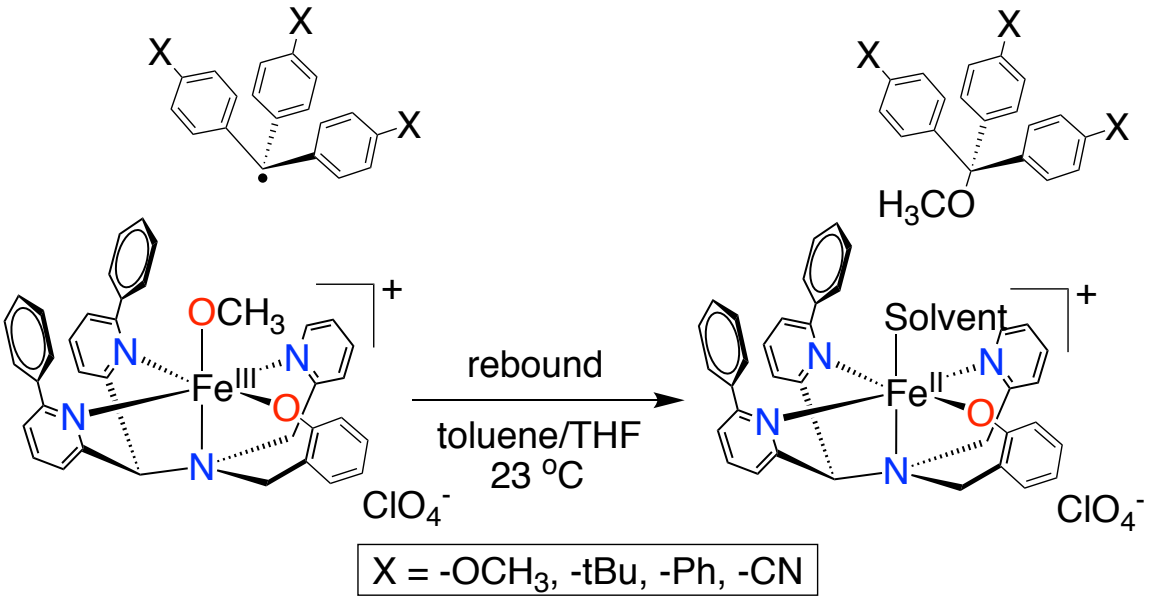

Mechanistic information about the reaction of **1** with the carbon radicals was obtained from kinetic studies. Complex **1** was reacted with the $(4\text{-X-}C_6H_4)_3C\bullet$ radical derivatives (X = -OCH_3, -tBu, -Ph, or -CN) under pseudo-first-order conditions (excess radical) in toluene at 23 °C. Reaction rates were monitored by UV-vis spectroscopy. The radical derivatives give rise to intense absorption bands in the 525 – 568 nm range, but complex **1** also exhibits a broad band with λ_{max} = 570 nm. The consumption of **1** could be followed by the loss of absorption at 570 nm, leading to good single-exponential decay that could be fit to give a pseudo-first-order rate constant (k_{obs}).

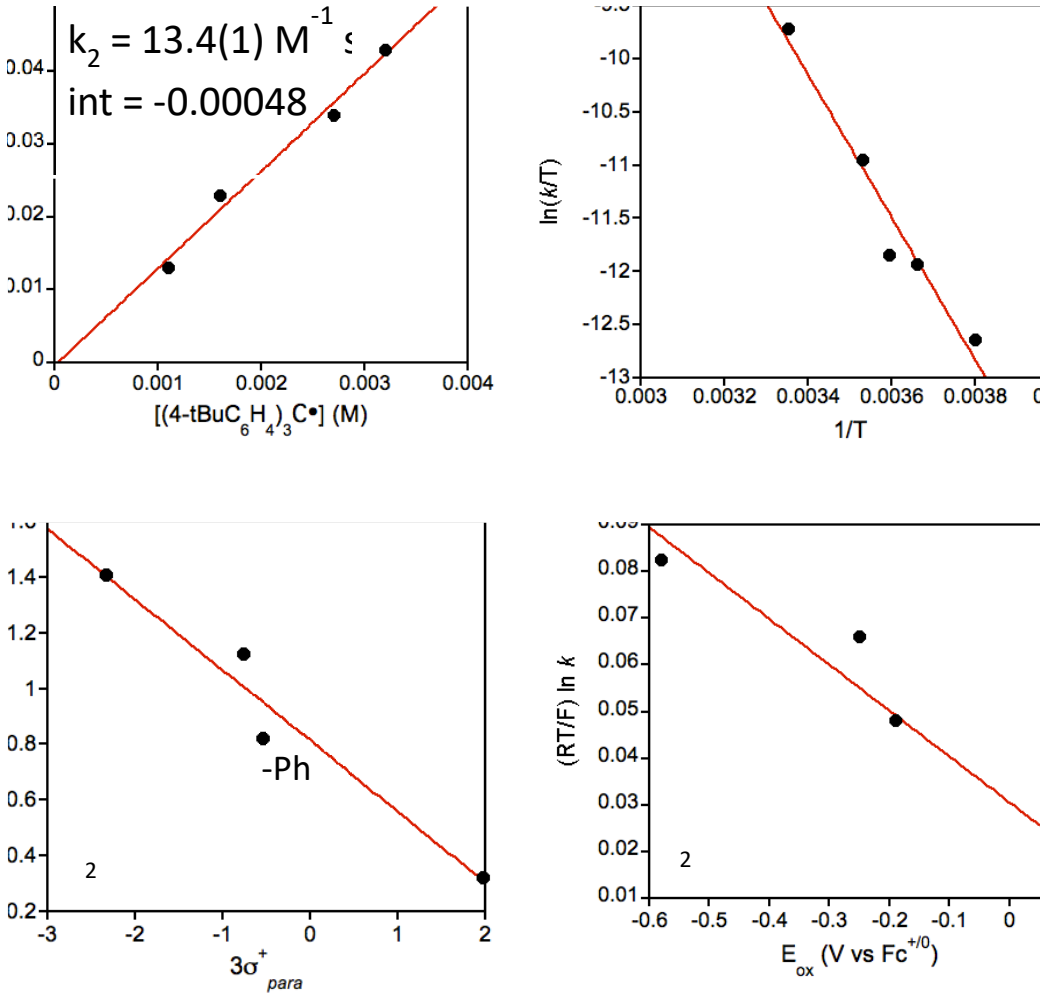

Figure 4.4. a) Plot of k_{obs} versus [(4-tBu-C_6H_4)$_3$C•], where slope of the best fit (red line) gives k_2 = 13.4(1) M^{-1} s^{-1}. b) Eyring plot of (ln(k_{obs}/T) vs 1/T for the reaction of **1** and (4-tBu-C_6H_4)$_3$-C• from -10 – 25 °C. c) Hammett plot. D) Marcus plot.

Measuring the k_{obs} values with different radical concentrations yielded a linear correlation (Figure 4.4a). The slopes of best-fit lines then gave second-order rate constants (k_2) for each different radical derivative (Table 4.2). The range of values for k_2 was found to be from 2-25 M^{-1} s^{-1} (X = CN < Ph < tBu < OMe), increasing according the electron-donating capability of the *para* substituent of the derivatives. These rate constants gave the first direct measure of rates for radical oxygen rebound in a nonheme iron(III) complex.

Table 4.2. Radicals and second-order rate constants obtained during this study.

(4-X-C_6H_4)$_3$C•	***k_2* (M^{-1} s^{-1})**
-OMe	25.5(2)
-tBu	13.4(1)
-Ph	6.8(8)
-CN	2.2(3)

Although there are no other analogous nonheme iron rebound rates available for direct comparison, we can compare these rate constants to those measured previously by some of us for a heme-like corrole complex. The iron corrole Fe^{IV}(OH)(ttppc) (ttppc = tris(2,4,6-triphenylphenyl corrole) undergoes similar radical reactivity with (4-X-C_6H_4)$_3$C•(X = -OCH_3, -tBu, -Ph, Cl) to give (4-X-C_6H_4)$_3$COH and Fe^{III}(ttppc), with rate constants from 12.6(1) to 357(4) M^{-1} s^{-1}.[2] The ttppc complex is sterically encumbered by large triphenylphenyl groups that project above and below the plane of the corrole, but reacts faster than nonheme **1**; e.g. Fe^{IV}(OH)(ttppc) reacts ~14x faster than **1** with the *para*-methoxy trityl derivative. The physical oxidation state of the iron center in the ttppc complex is not easily assigned because of the possible non-innocent behavior of the corrole ligand, but the overall redox level is one unit above the nonheme system. The iron-hydroxide corrole may be more reactive because it is one oxidation level above nonheme **1**. Alternatively, the difference in reactivity may be due to the steric demands of the axial OCH_3 versus OH ligand, or may arise from an inherent difference in Fe^{III}-OCH_3 versus Fe^{IV}-OH homolytic bond strengths. Further work is needed on both heme and nonheme systems to resolve these fundamental questions.

Mechanistic information can be obtained by analyzing the kinetic data with Hammett and Marcus correlations. A Hammett plot was constructed from the k_2 values (Figure 4.4c), consisting of a plot of log k_2 versus $3\sigma^+$, where σ^+ is the Hammett parameter for the *para*-X substituents in $(4\text{-X-}C_6H_4)_3C\bullet$. The rates decrease linearly with the σ^+ values, indicating that **1** is behaving as an electrophile, as expected. However, the slope of this plot is small (ρ = -0.25). In fact, it is less than half the slope seen for the Hammett plot for Fe^{IV}(OH)(ttppc) (ρ = -0.55) with the same trityl radical derivatives. Both of these systems exhibit rho values that suggest only a small charge separation exists in the transition state,[2, 31] and **1** is clearly even less sensitive to the electrophilicity of the radical derivatives.

The reaction for **1** with the carbon radicals could occur as a concerted process in which C-O bond formation occurs with concomitant Fe-O bond cleavage and reduction of Fe^{III} to Fe^{II}, or it could proceed in a stepwise manner following the electron-transfer/cation transfer (ET/CT) pathway shown in Scheme 4.4. The possibility of a coupled ET/CT mechanism was examined by the construction of a Marcus plot (Figure 4.4d). The plot shows reasonable linearity, but the slope (ρ = -0.098) is quite small, showing that the rates have only a weak dependence on the redox potentials of the radical substrates. In comparison, a rate-limiting, outer-sphere ET process should give slope = -0.5.[2, 32] The same plot for the reaction of Fe^{IV}(OH)(ttppc) also gave a small slope (ρ = -0.15). The Marcus analysis for nonheme **1** provides good evidence that there is little or no ET component to the radical rebound reactions, and the mechanism is best described as a concerted process (i.e. the diagonal path in Scheme 4.4). A similar conclusion was reached for the heme system. This analysis has also been applied to H-atom transfer, in order to distinguish

between concerted proton electron-transfer (CPET) and proton-coupled electron-transfer (PCET) mechanisms, with small slopes indicating a CPET process.[33-34]

A temperature-dependent study of the rate constants for the reaction of **1** and the *p*-*t*Bu-trityl derivative provided further mechanistic insights (Figure 4.4b). The pseudo-first-order rate constants (k_{obs}) were measured between -10 and 25 °C, and a plot of ln(k/T) versus 1/T gave a linear dependence (Figure 4.4b). The best-fit line gives activation parameters: $\Delta H^{\ddagger}$ = 13.2(1.6) kcal mol^{-1} and $\Delta S^{\ddagger}$ = –22.1(0.4) cal mol^{-1} K^{-1}, yielding an activation barrier at 298 K of $\Delta G^{\ddagger}$ = 19.7(1.7) kcal mol^{-1}. These values are consistent with a bimolecular rate-determining step.

To support the experimental studies we performed a series of density functional theory calculations on ^{6}[Fe(OCH$_3$)(N3PyO^{2Ph})]$^{+}$ (**1**) and ^{6}[Fe(OH)(N3PyO^{2Ph})]$^{+}$ (**2**) and their reactivities with (4-X-C$_6$H$_4$)$_3$C• with X = OMe, tBu, Ph, H, Cl and NO$_2$. Optimized geometries of ^{6}**1** and ^{6}**2** are given in Figure 3 and in agreement with experiment have a sextet spin ground state. The Fe-OH/Fe-OCH$_3$ bond lengths are 1.82 and 1.79 Å and match experimental crystal structure coordinates well (Figure 4.5). Moreover, replacing the OH ligand by OCH$_3$ appears to have little stereochemical effects on the structure.

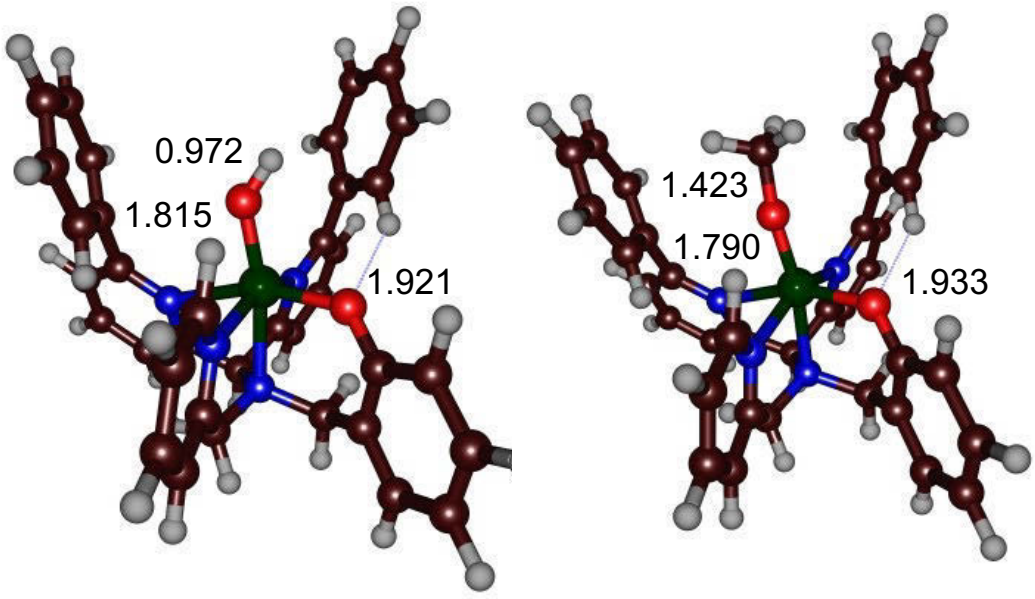

Figure 4.5. Optimized geometries of ^{6}**1** and ^{6}**2** with bond lengths in angstroms.

Subsequently, we calculated the OH/OCH_3 transfer of ^{5,7}**1** and ^{5,7}**2** to (4-X-C_6H_4)$_3$C• with X = OMe, tBu, Ph, H, Cl and NO_2 from a reactant complex (**Re**) of the two reactants via a C–O bond formation transition state (**TS**) to form an alcohol product complex (**Pr**). No charge-transfer in the reactant complexes is observed and the charges of the individual components stay virtually similar to those in the isolated complexes. Attempts to swap molecular orbitals to generate the charge-transfer state for ^{5}**Re**$_{OH,Cl}$, i.e. a complex ^{5}[Fe(OH)(N3PyO^{2Ph})]^0---(4-Cl-C_6H_4)$_3$C$^+$, converged back to the structure with a radical on the methyl moiety. Hence, no initial long-range charge-transfer takes place during or prior to the rebound reaction and each individual moiety keeps its original charge distribution. This lack of charge-transfer agrees with the experimental conclusion that the reaction occurs in a concerted fashion.

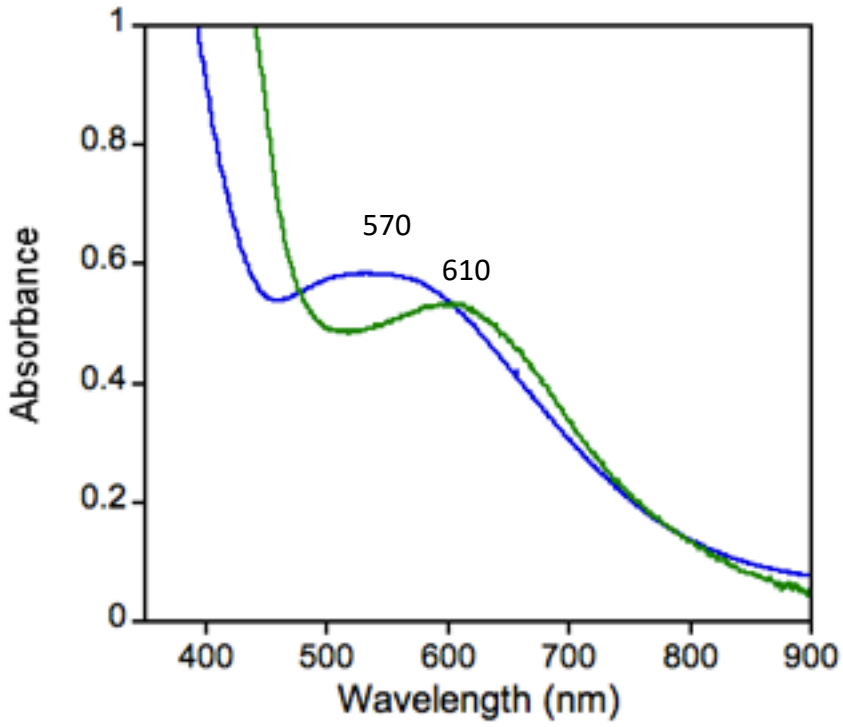

Figure 4.6. Reaction of **1** and $Ph_3C(BF_4)$ in THF at 23 °C, monitored by UV-vis spectroscopy. **1** (570 nm) is rapidly consumed. Initial spectrum (blue): **1**. Final spectrum (green): **1** has been reacted and a new species (610 nm) has been formed.

Interestingly, reaction of **1** and trityl cation, Ph_3C^+, exhibited very different reactivity. Combining **1** and $Ph_3C^+BF_4$ (4 equiv) in THF at 23 °C led to a reaction that was over within seconds as seen by UV-vis (Figure 4.6). The ether product (Ph_3COCH_3) was formed in 80% yield by ^{1}H NMR spectroscopy (Figure 4.7),[21] and the iron complex did not change oxidation state, as seen by UV-vis and Mössbauer spectroscopy (Figure 4.3, Table 4.1).

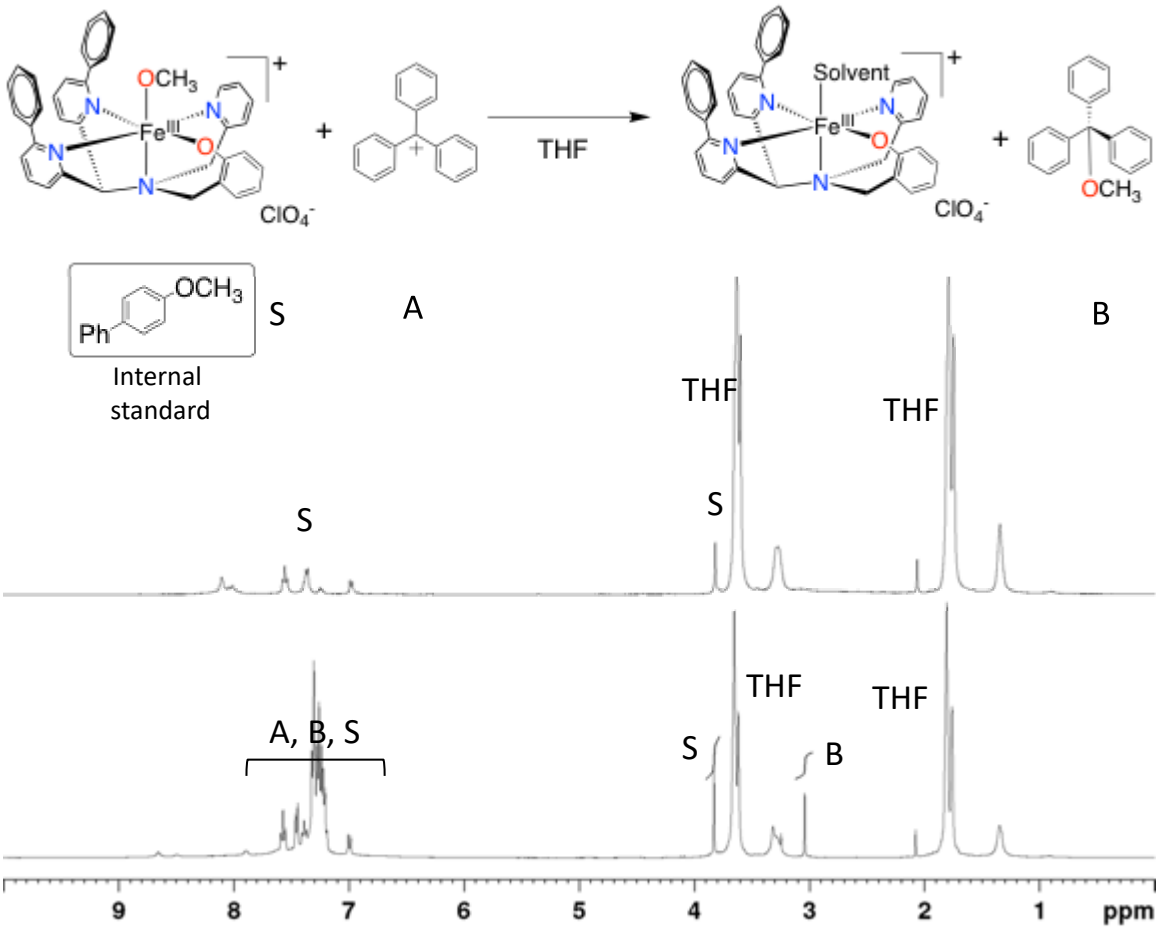

Figure 4.7. Reaction of **1** and Ph_3C^+ in THF-d_8 for 5 min at 23 °C as monitored by ^1H NMR spectroscopy. Top: **1** and 4-Ph-C_6H_4-OCH_3 (internal standard S) before addition of Ph_3C^+. Bottom: **1** and Ph_3C^+ after 5 min. Following the reaction, the –OCH_3 peak of the product Ph_3COCH_3 at 3.04 ppm was integrated against the internal standard (4-Ph-C_6H_4-OCH_3) –OCH_3 peak at 3.83 ppm.

The rapid rate is concurrent with previous observed metal-alkoxide reactions,[35] and shows that two-electron chemistry involving heterolytic cleavage of the Fe-O bond proceeds via a much smaller activation barrier than homolytic cleavage.

4.4. Conclusions

With the first observation of the key rebound step in both heme and nonheme complexes,[2, 21] the question was raised as to whether the rebound step occurs in a concerted or stepwise manner. While the mechanism in heme-type systems was determined to occur in a concerted fashion, only now has it been determined that the above rebound in a nonheme system occurs also in a concerted fashion. These experimental and computational mechanistic investigations have produced valuable information regarding the rebound reaction between radical species and a nonheme ferric complex **1**. The nature of the rebound reaction mechanism now better understood, investigations continue in order to increase understanding of the rebound paradigm in nonheme complexes, with respect to halogenase or desaturase reactivity.

4.5. Supporting Information

Contents

I. Supporting figures and tables

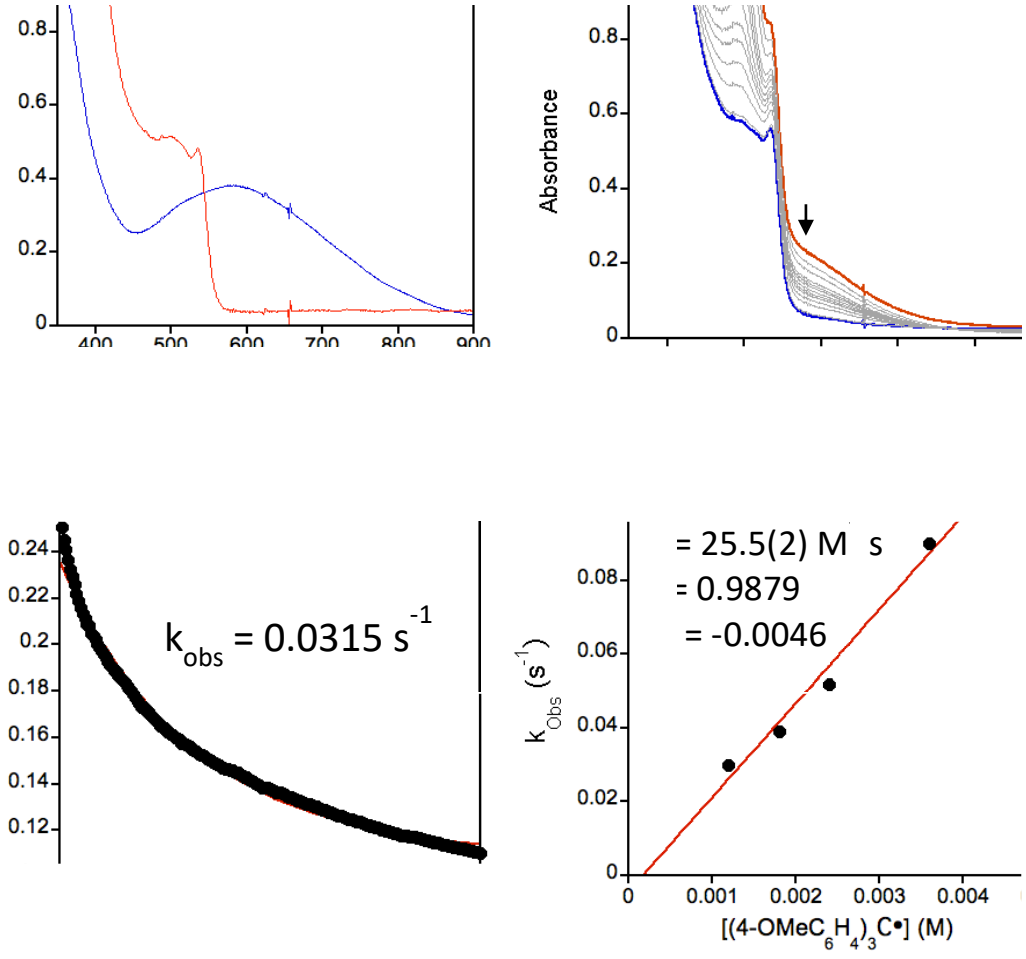

Figure 4.8. a) Overlay of UV-vis spectrum c [4)3C• (red). b) Time-resolved UV-vis spectral change for the reaction between **1** (200 μM) and (4-OMe-$C_6H_4)_3$-C• (1.22 mM) at 23 °C. c) Change in absorbance vs time for the consumption of **1** (black circles). d) Plot of k_{obs} vs [(4-OMe-$C_6H_4)_3$C•].

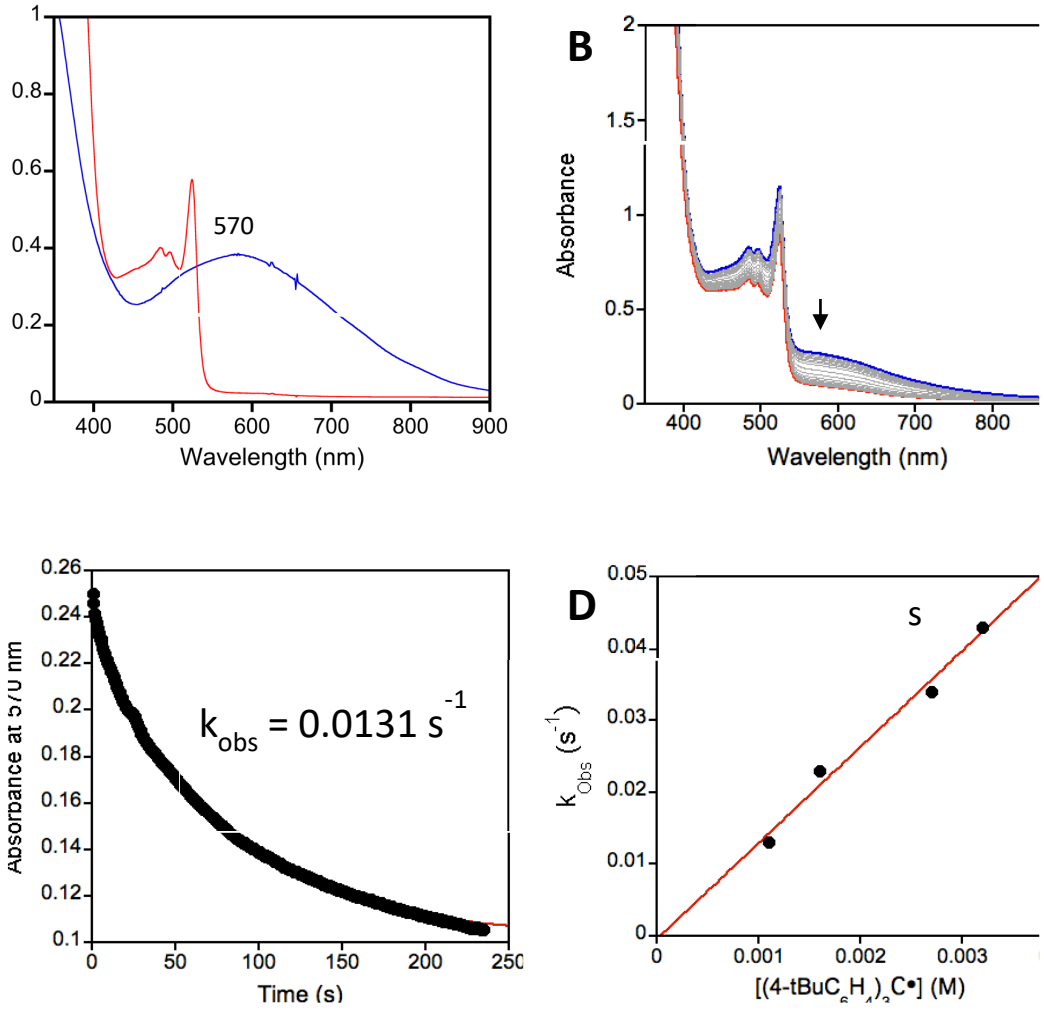

Figure 4.9. a) Overlay of UV-vis spectrum of **1** (blue) and spectrum of (4-tBu-C_6H_4)$_3$C• (red). b) Time-resolved UV-vis spectral change for the reaction between **1** (200 μM) and (4-tBu-C_6H_4)$_3$-C• (1.24 mM) at 23 °C. c) Change in absorbance vs time for the consumption of **1** (black circles). d) Plot of k_{obs} vs [(4-tBu-C_6H_4)$_3$C•].

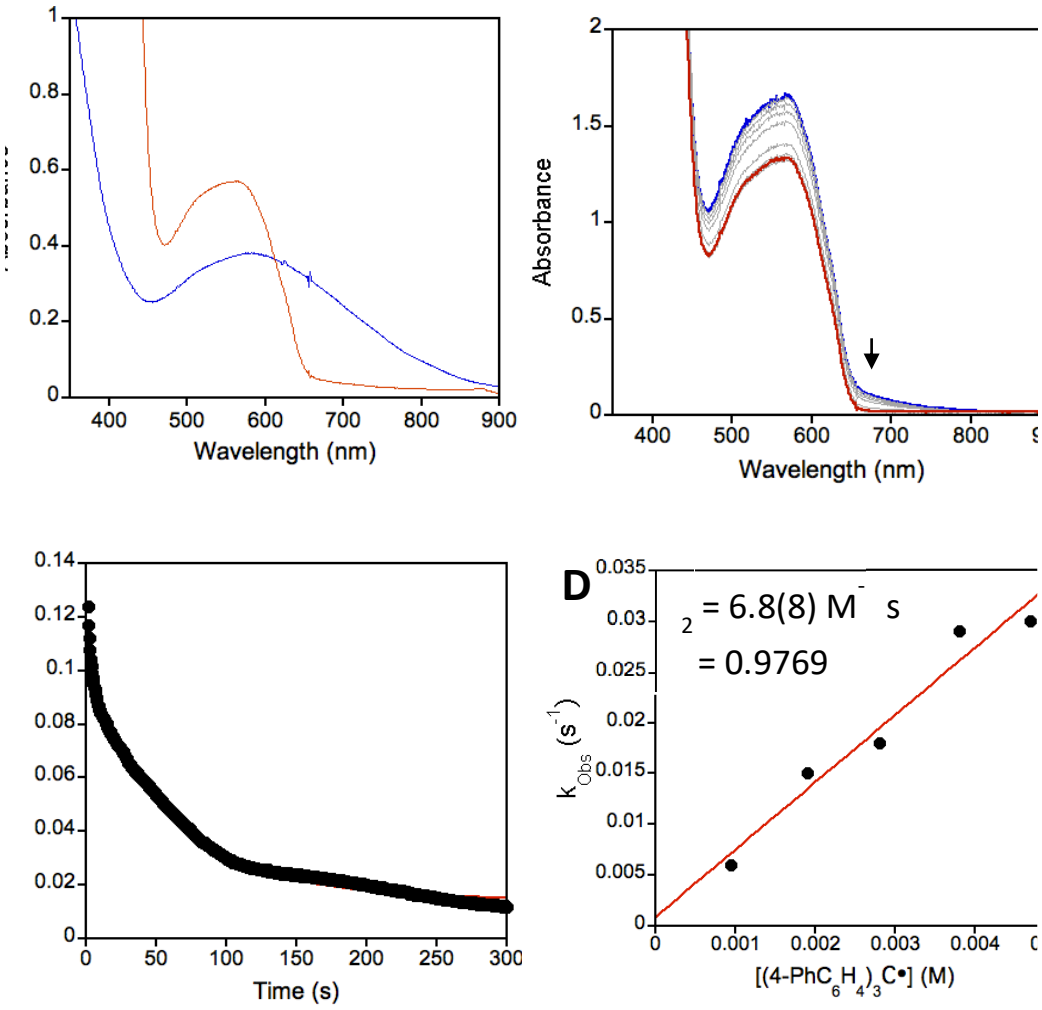

Figure 4.10. a) Overlay of UV-vis spectrum of **1** (blue) and spectrum of (4-Ph-$C_6H_4)_3C$• (orange). b) Time-resolved UV-vis spectral change for the reaction between **1** (200 μM) and (4-Ph-$C_6H_4)_3$-C• (2.93 mM) at 23 °C. c) Change in absorbance vs time for the consumption of **1** (black circles). d) Plot of k_{obs} vs [(4-Ph-$C_6H_4)_3C$•].

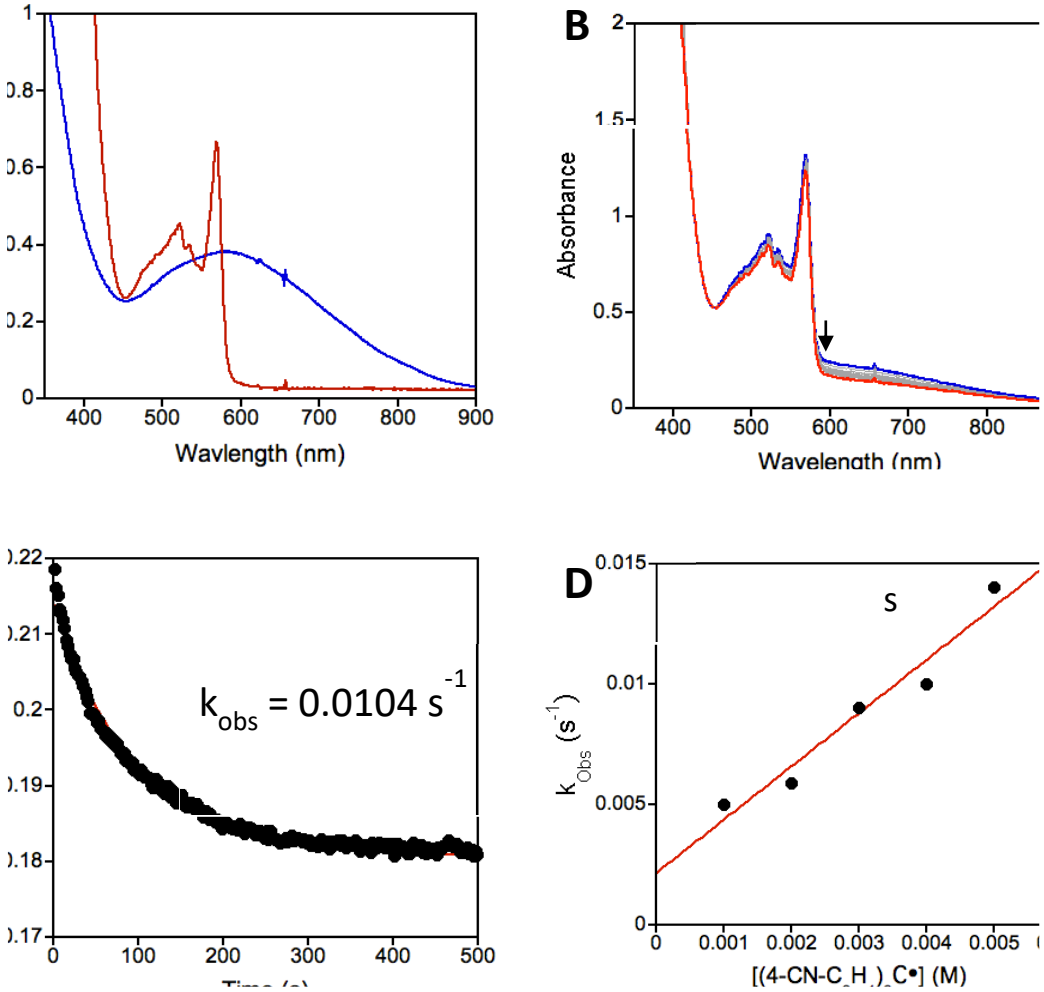

Figure 4.11. a) Overlay of UV-vis spectrum of **1** (blue) and spectrum of (4-CN-$C_6H_4)_3C$• (orange). b) Time-resolved UV-vis spectral change for the reaction between **1** (200 μM) and (4-CN-$C_6H_4)_3$-C• (4.0 mM) at 23 °C. c) Change in absorbance vs time for the consumption of **1** (black circles). d) Plot of k_{obs} vs [(4-CN-$C_6H_4)_3C$•].

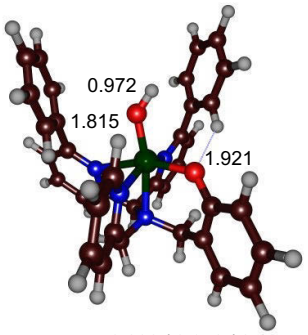

Fe-N_{eq}: 2.282 / 2.378 / 2.165
Fe-N_{ax}: 2.303

^{6}[Fe(OH)(N3PyO^{2Ph})]$^{+}$

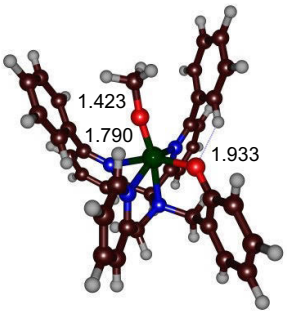

Fe-N_{eq}: 2.290 / 2.445 / 2.181
Fe-N_{ax}: 2.283

^{6}[Fe(OCH_3)(N3PyO^{2Ph})]$^{+}$

Figure 4.12. Optimized geometries of **^{6}[Fe(OH)(N3PyO^{2Ph})]$^{+}$** and **^{6}[Fe(OCH_3)(N3PyO^{2Ph})]$^{+}$** as obtained at UB3LYP/BS1 in Gaussian-09. Bond lengths are in angstroms.

Table 4.3. Group spin densities of UB3LYP/BS1 optimized transition state geometries as obtained in Gaussian-09.

	ρ_{Fe}	ρ_{ligand}	ρ_{OH}	ρ_{SubX}
^{5}**TS**$_{OMe}$	3.71	0.27	0.10	-0.08
^{5}**TS**$_{tBu}$	3.71	0.26	0.09	-0.06
^{5}**TS**$_{Ph}$	3.56	0.36	0.02	0.07
^{5}**TS**$_{H}$	3.71	0.24	0.05	0.00
^{5}**TS**$_{Cl}$	3.74	0.30	0.14	-0.18
^{5}**TS**$_{NO2}$	3.59	0.38	-0.02	0.01

Table 4.4. Group spin densities of UB3LYP/BS1 optimized product complexes as obtained in Gaussian-09.

	ρ_{Fe}	ρ_{ligand}	ρ_{OH}	ρ_{SubX}
^{5}**Pr**$_{OMe}$	3.67	0.32	0.00	0.00
^{5}**Pr**$_{tBu}$	3.67	0.33	0.00	0.00
^{5}**Pr**$_{Ph}$	3.65	0.35	0.00	0.00
^{5}**Pr**$_{H}$	3.67	0.30	0.02	0.01
^{5}**Pr**$_{Cl}$	3.67	0.33	0.00	0.00
^{5}**Pr**$_{NO2}$	3.64	0.36	0.00	0.00

Table 4.5. Group spin densities of UB3LYP/BS1 optimized geometries of ^{6}**[Fe(OH)(N3PyO2Ph)]**$^+$ and ^{6}**[Fe(OMe)(N3PyO2Ph)]**$^+$ isolated complexes as obtained in Gaussian-09.

	ρ_{Fe}	ρ_{ligand}	ρ_{OH}/ρ_{OMe}	ρ_{Total}
^{6}[Fe(OH)(N3PyO^{2Ph})]$^+$	3.99	0.54	0.46	5.00
^{6}[Fe(OCH$_3$)(N3PyO^{2Ph})]$^+$	3.94	0.43	0.62	5.00

Table 4.6. Absolute energies, zero-point energies and free energies (in au) of optimized geometries for the reaction of ^{6}**[Fe(OH)(N3PyO^{2Ph})]**$^{+}$ with radical substrate (4-X-$C_6H_4)_3C^{\bullet}$ (X = OMe, tBu, Ph, H, Cl or NO_2) as obtained in Gaussian-09.

	E [au]	ZPE [au]	G [au]	E [au]	E_{solv} [au]
	B3LYP/BS1	B3LYP/BS1	B3LYP/BS1	B3LYP/BS2	B3LYP/BS2
^{6}[Fe(OH)(N3PyO^{2Ph})]$^{+}$	-1882.278538	0.586526	-1881.759489	-1883.123834	-1883.185227
^{2}(*p*-OMe-$C_6H_4)_3C^{\bullet}$	-1076.319695	0.378323	-1075.995028	-1076.845695	-1076.858571
^{2}(*p*-tBu-$C_6H_4)_3C^{\bullet}$	-1204.519363	0.621799	-1203.960126	-1205.043302	-1205.050155
^{2}(*p*-Ph-$C_6H_4)_3C^{\bullet}$	-1425.891738	0.527489	-1425.427317	-1426.503028	-1426.515392
^{2}(*p*-H-$C_6H_4)_3C^{\bullet}$	-732.871412	0.281502	-732.632973	-733.187737	-733.193758
^{2}(*p*-Cl-$C_6H_4)_3C^{\bullet}$	-2111.594199	0.251930	-2111.391251	-2112.060718	-2112.067235
^{2}(*p*-NO_2-$C_6H_4)_3C^{\bullet}$	-1346.129247	0.286608	-1345.897618	-1346.871095	-1346.897405
^{5}**Re**$_{OMe}$	-2958.610224	0.968517	-2957.746329	-2959.974646	-2960.038182
^{5}**Re**$_{tBu}$	-3086.811406	1.210331	-3085.716782	-3088.177115	-3088.238536
^{5}**Re**$_{Ph}$	-3308.182506	1.116351	-3307.178674	-3309.632400	-3309.696065
^{5}**Re**$_{H}$	-2615.160977	0.870183	-2614.384171	-2616.318419	-2616.380630
^{5}**Re**$_{Cl}$	-3993.885858	0.840252	-3993.147419	-3995.189716	-3995.254633
^{5}**Re**$_{NO2}$	-3228.422405	0.875335	-3227.650665	-3230.002587	-3230.085269
^{5}**TS**$_{OMe}$	-2958.610685	0.967511	-2957.743993	-2959.974894	-2960.037645
^{5}**TS**$_{tBu}$	-3086.803794	1.210175	-3085.705407	-3088.165068	-3088.222379
^{5}**TS**$_{Ph}$	-3308.173605	1.116285	-3307.168733	-3309.625001	
^{5}**TS**$_{H}$	-2615.145163	0.869995	-2614.365596	-2616.298979	-2616.357523
^{5}**TS**$_{Cl}$	-3993.862927	0.840385	-3993.118221	-3995.163832	-3995.227326
^{5}**TS**$_{NO2}$	-3228.381941	0.875071	-3227.606798	-3229.963906	-3230.053807
^{5}**Pr**$_{OMe}$	-2958.631013	0.970711	-2957.760769	-2959.990370	-2960.062811
^{5}**Pr**$_{tBu}$	-3086.831916	1.213366	-3085.729300	-3088.192269	-3088.258293
^{5}**Pr**$_{Ph}$	-3308.197683	1.119173	-3307.189584	-3309.644642	-3309.700216
^{5}**Pr**$_{H}$	-2615.178549	0.873675	-2614.396344	-2616.329419	-2616.389302
^{5}**Pr**$_{Cl}$	-3993.901665	0.843577	-3993.156054	-3995.199421	-3995.271148
^{5}**Pr**$_{NO2}$	-3228.416781	0.878903	-3227.640834	-3229.995139	-3230.083891

Table 4.7. Relative energies, zero-point energies and free energies (in kcal mol^{-1}) of optimized geometries for the reaction of ^{6}**[Fe(OH)(N3PyO^{2Ph})]**$^{+}$ with radical substrate (4-X-$C_6H_4)_3C$• (X = OMe, t-Bu, Ph, H, Cl or NO_2) as obtained in Gaussian-09.

	ΔE	ΔE+ZPE	ΔG	ΔE	ΔE+ZPE	ΔG	ΔE_{solv}
	BS1	BS1	BS1	BS2	BS2	BS2	BS2
^{5}**Re**$_{OMe}$	-7.52	-5.22	5.14	-3.21	-0.91	9.45	3.52
^{5}**Re**$_{tBu}$	-8.47	-7.22	1.78	-6.26	-5.00	3.99	-1.98
^{5}**Re**$_{Ph}$	-7.67	-6.21	5.10	-3.48	-2.01	9.30	2.86
^{5}**Re**$_{H}$	-6.92	-5.57	5.20	-4.30	-2.94	7.83	-1.03
^{5}**Re**$_{Cl}$	-8.23	-7.11	2.08	-3.24	-2.11	7.08	-1.36
^{5}**Re**$_{NO2}$	-9.17	-7.79	4.04	-4.81	-3.42	8.41	-1.65
^{5}**TS**$_{OMe}$	-7.81	-6.14	6.60	-3.37	-1.70	11.05	3.86
^{5}**TS**$_{tBu}$	-3.70	-2.54	8.92	1.30	2.46	13.91	8.16
^{5}**TS**$_{Ph}$	-2.09	-0.66	11.34	1.17	2.59	14.60	
^{5}**TS**$_{H}$	3.00	4.24	16.86	7.90	9.14	21.76	13.47
^{5}**TS**$_{Cl}$	6.16	7.37	20.41	13.00	14.21	27.25	15.77
^{5}**TS**$_{NO2}$	16.22	17.43	31.57	19.47	20.68	34.82	18.09
^{5}**Pr**$_{OMe}$	-20.57	-16.89	-3.92	-13.08	-9.40	3.57	-11.93
^{5}**Pr**$_{tBu}$	-21.34	-18.18	-6.08	-15.77	-12.61	-0.50	-14.38
^{5}**Pr**$_{Ph}$	-17.20	-13.96	-1.74	-11.16	-7.92	4.30	0.25
^{5}**Pr**$_{H}$	-17.95	-14.40	-2.44	-11.20	-7.66	4.31	-6.47
^{5}**Pr**$_{Cl}$	-18.15	-14.94	-3.33	-9.33	-6.12	5.49	-11.73
^{5}**Pr**$_{NO2}$	-5.65	-2.03	10.21	-0.13	3.49	15.72	-0.79

Table 4.8. Absolute energies, zero-point energies and free energies (in au) of optimized geometries for the reaction of **^{6}[Fe(OMe)(N3PyO^{2Ph})]$^{+}$** with radical substrate (*p*-Cl-$C_6H_4)_3C^{\bullet}$ as obtained in Gaussian-09.

	E [au]	ZPE [au]	G [au]	E [au]	E_{solv} [au]
	B3LYP/BS1	B3LYP/BS1	B3LYP/BS1	B3LYP/BS2	B3LYP/BS2
^{6}[Fe(OCH$_3$)(N3PyO^{2Ph})]$^{+}$	-1921.573786	0.616778	-1921.027713	-1922.429436	-1922.489349
^{5}Re$_{Cl,OMe}$	-4033.175592	0.868985	-4032.413975	-4034.498072	-4034.562716
^{5}Pr$_{Cl,OMe}$	-4033.191224	0.872016	-4032.421669	-4034.508459	-4034.577266

Table 4.9. Relative energies, zero-point energies and free energies (in kcal mol^{-1}) of optimized geometries for the reaction of **^{6}[Fe(OMe)(N3PyO^{2Ph})]$^{+}$** with radical substrate (p-Cl-$C_6H_4)_3C\bullet$ as obtained in Gaussian-09.

	ΔE	ΔE+ZPE	ΔG	ΔE	ΔE+ZPE	ΔG	ΔE_{solv}
	BS1	BS1	BS1	BS2	BS2	BS2	BS2
^{5}Re$_{Cl,OMe}$	-4.77	-4.60	3.13	-4.97	-4.80	2.93	-3.85
^{5}Pr$_{Cl,OMe}$	-14.58	-12.51	-1.70	-11.49	-9.41	1.40	-12.98

Cartesian coordinates:

Table 4.10. ^{6}[Fe(OH)(N3PyO^{2Ph})]$^{+}$:

26	-2.779077000	-0.194090000	0.075916000
6	-4.949669000	-2.055930000	3.897068000
1	-5.919476000	-2.478832000	3.653605000
6	-4.165662000	-2.650383000	4.889035000
1	-4.535091000	-3.522884000	5.417068000
6	-2.907726000	-2.119697000	5.199709000
1	-2.302564000	-2.574463000	5.976837000
6	-2.437662000	-0.995198000	4.509477000
1	-1.471435000	-0.569016000	4.759187000
6	-3.212860000	-0.402286000	3.506511000
1	-2.839884000	0.466802000	2.976129000
6	-4.477577000	-0.932899000	3.188567000
6	-5.356372000	-0.300192000	2.175116000
6	-6.706540000	-0.044196000	2.497297000
1	-7.063777000	-0.298369000	3.486943000
6	-7.549549000	0.561847000	1.571670000
1	-8.581134000	0.777340000	1.826334000
6	-7.043928000	0.900270000	0.310867000
1	-7.670943000	1.373091000	-0.436116000
6	-5.710779000	0.613924000	0.032252000
6	-5.121971000	0.819764000	-1.361849000
1	-5.797202000	1.462444000	-1.944888000
6	-5.050611000	-0.558782000	-2.006528000
6	-6.056740000	-1.010058000	-2.858305000
1	-6.848173000	-0.340411000	-3.175081000
6	-6.028839000	-2.345544000	-3.273875000
1	-6.797745000	-2.734220000	-3.932127000
6	-4.992308000	-3.164917000	-2.835188000
1	-4.931598000	-4.199715000	-3.148022000
6	-3.976270000	-2.648311000	-2.004861000
6	-2.855067000	-3.538681000	-1.611478000
6	-1.532210000	-3.242712000	-1.975425000
1	-1.318640000	-2.325479000	-2.510457000
6	-0.500245000	-4.133361000	-1.670140000
1	0.517303000	-3.903197000	-1.969355000
6	-0.777145000	-5.325552000	-0.990735000
1	0.025377000	-6.015797000	-0.752928000
6	-2.094817000	-5.630618000	-0.630293000
1	-2.316250000	-6.554462000	-0.106523000
6	-3.130706000	-4.748649000	-0.950260000
1	-4.151497000	-4.987957000	-0.668245000
6	-3.016737000	1.501902000	-2.541956000
1	-3.093986000	2.512666000	-2.961762000

1	-3.486121000	0.819124000	-3.258244000
6	-1.561915000	1.115132000	-2.390294000
6	-0.562360000	1.610227000	-3.235479000
1	-0.809612000	2.339713000	-3.998391000
6	0.751033000	1.163050000	-3.071274000
1	1.539705000	1.539732000	-3.712830000
6	1.039127000	0.232939000	-2.063458000
1	2.048171000	-0.127224000	-1.905006000
6	0.001504000	-0.218577000	-1.251134000
1	0.148621000	-0.933486000	-0.452106000
6	-3.794874000	2.756952000	-0.542944000
1	-4.406149000	2.620758000	0.353189000
1	-4.306934000	3.483419000	-1.192473000
6	-2.439069000	3.279293000	-0.148788000
6	-2.005453000	4.554498000	-0.534584000
1	-2.633192000	5.155720000	-1.187629000
6	-0.787598000	5.068783000	-0.075417000
1	-0.466320000	6.059084000	-0.378378000
6	0.006000000	4.299810000	0.787735000
1	0.947618000	4.695854000	1.153845000
6	-0.407627000	3.026595000	1.183422000
1	0.193377000	2.420249000	1.851668000
6	-1.629102000	2.503442000	0.718977000
7	-4.878482000	0.033823000	0.939662000
7	-4.023739000	-1.347570000	-1.590675000
7	-3.758031000	1.417834000	-1.246248000
7	-1.271449000	0.213939000	-1.422958000
8	-2.129059000	-1.694634000	0.863554000
1	-1.877047000	-1.951134000	1.766426000
8	-2.022055000	1.254792000	1.084074000

Table 4.11. $^{6}[Fe(OCH_3)(N3PyO^{2Ph})]^{+}$:

26	-2.642980000	-0.528450000	-0.348958000
6	-5.277425000	-1.174314000	3.629331000
1	-6.192514000	-1.721376000	3.423504000
6	-4.644388000	-1.327542000	4.865054000
1	-5.074333000	-1.984771000	5.613443000
6	-3.461709000	-0.627828000	5.136850000
1	-2.977164000	-0.734282000	6.101832000
6	-2.910286000	0.210712000	4.161216000
1	-1.997820000	0.759679000	4.369103000
6	-3.529979000	0.356724000	2.915905000
1	-3.086947000	0.999351000	2.163785000
6	-4.724733000	-0.334058000	2.640410000
6	-5.471340000	-0.120421000	1.377528000
6	-6.859503000	0.130747000	1.441160000
1	-7.339469000	0.158328000	2.410808000
6	-7.585605000	0.386980000	0.283414000
1	-8.647160000	0.601050000	0.335963000
6	-6.921248000	0.384113000	-0.948347000
1	-7.450581000	0.588888000	-1.871665000
6	-5.556705000	0.111236000	-0.965036000
6	-4.795494000	-0.039464000	-2.279552000
1	-5.385611000	0.416655000	-3.087504000
6	-4.660329000	-1.533796000	-2.537696000
6	-5.554677000	-2.199638000	-3.374609000
1	-6.289844000	-1.643180000	-3.944690000
6	-5.488668000	-3.594428000	-3.446152000
1	-6.169043000	-4.147456000	-4.083919000
6	-4.525937000	-4.260211000	-2.692777000
1	-4.434023000	-5.337967000	-2.739868000
6	-3.622385000	-3.535099000	-1.888311000
6	-2.570324000	-4.284234000	-1.156039000
6	-1.209003000	-3.983459000	-1.328151000
1	-0.925322000	-3.147923000	-1.954569000
6	-0.228229000	-4.772239000	-0.720574000
1	0.820890000	-4.542225000	-0.876051000
6	-0.594398000	-5.867263000	0.072776000
1	0.168542000	-6.481152000	0.539622000
6	-1.948922000	-6.171671000	0.253366000
1	-2.240357000	-7.016616000	0.868033000
6	-2.930615000	-5.391549000	-0.364959000
1	-3.979584000	-5.632415000	-0.222411000
6	-2.561630000	0.363587000	-3.336637000
1	-2.605979000	1.213427000	-4.029244000
1	-2.929014000	-0.514412000	-3.878270000
6	-1.130765000	0.109572000	-2.919427000

6	-0.042510000	0.428196000	-3.739943000
1	-0.207208000	0.921472000	-4.691144000
6	1.249216000	0.117782000	-3.308836000
1	2.105027000	0.362034000	-3.927977000
6	1.426682000	-0.497806000	-2.062430000
1	2.415515000	-0.739772000	-1.692650000
6	0.303301000	-0.784276000	-1.290712000
1	0.369209000	-1.246559000	-0.314592000
6	-3.577977000	2.083015000	-1.857151000
1	-4.275491000	2.169789000	-1.020121000
1	-4.030394000	2.581286000	-2.728284000
6	-2.276695000	2.745580000	-1.496495000
6	-1.815897000	3.876467000	-2.184026000
1	-2.377397000	4.245738000	-3.038815000
6	-0.657293000	4.544331000	-1.773145000
1	-0.314241000	5.421372000	-2.310640000
6	0.047379000	4.077942000	-0.653771000
1	0.942067000	4.596010000	-0.323660000
6	-0.394626000	2.952285000	0.043450000
1	0.137325000	2.581929000	0.912605000
6	-1.557982000	2.273495000	-0.368314000
7	-4.839829000	-0.138446000	0.164898000
7	-3.705251000	-2.173615000	-1.812445000
7	-3.452559000	0.603447000	-2.158809000
7	-0.948788000	-0.494600000	-1.721310000
8	-2.110957000	-1.712571000	0.883492000
8	-1.977841000	1.167495000	0.297974000
6	-1.769868000	-2.514871000	2.008709000
1	-2.673970000	-2.766739000	2.575055000
1	-1.289914000	-3.440741000	1.672980000
1	-1.086326000	-1.968009000	2.669266000

Table 4.12. $^{5}TS_{OMe}$:

26	-2.381123000	-0.164772000	0.727719000
6	-5.472570000	-1.756375000	3.754142000
1	-6.026613000	-2.573812000	3.302842000
6	-5.207786000	-1.773307000	5.126085000
1	-5.555151000	-2.603317000	5.732476000
6	-4.515286000	-0.709072000	5.718167000
1	-4.342452000	-0.704057000	6.789814000
6	-4.053364000	0.348034000	4.924400000
1	-3.509569000	1.171392000	5.373055000
6	-4.293257000	0.357388000	3.547394000
1	-3.920171000	1.174927000	2.940836000
6	-5.029973000	-0.684603000	2.952104000
6	-5.486274000	-0.565446000	1.546296000
6	-6.832158000	-0.826603000	1.246474000
1	-7.489896000	-1.181188000	2.029534000
6	-7.325650000	-0.556385000	-0.029870000
1	-8.368449000	-0.736252000	-0.266613000
6	-6.465353000	-0.013380000	-0.979290000
1	-6.818685000	0.238901000	-1.972442000
6	-5.120124000	0.190791000	-0.648761000
6	-4.199878000	0.767761000	-1.720307000
1	-4.709250000	1.663073000	-2.116234000
6	-4.098772000	-0.194470000	-2.905956000
6	-4.056408000	0.296255000	-4.218473000
1	-4.077470000	1.363154000	-4.412695000
6	-4.015339000	-0.622709000	-5.272787000
1	-4.000934000	-0.276527000	-6.300685000
6	-4.023899000	-1.988102000	-4.991635000
1	-4.032606000	-2.706665000	-5.801374000
6	-4.071854000	-2.419024000	-3.649977000
6	-4.109811000	-3.853667000	-3.272745000
6	-4.579745000	-4.229311000	-1.999029000
1	-4.897856000	-3.452706000	-1.314525000
6	-4.645338000	-5.575226000	-1.633723000
1	-5.026093000	-5.848441000	-0.654540000
6	-4.234477000	-6.571474000	-2.528684000
1	-4.291265000	-7.617913000	-2.246940000
6	-3.753109000	-6.209401000	-3.792127000
1	-3.425755000	-6.973561000	-4.489489000
6	-3.691438000	-4.863060000	-4.161340000
1	-3.298261000	-4.604375000	-5.138753000
6	-1.713077000	1.129261000	-2.020148000
1	-0.941757000	1.766941000	-1.572466000
1	-1.900173000	1.521453000	-3.030535000
6	-1.204473000	-0.289463000	-2.103071000

6	-0.531885000	-0.780180000	-3.227230000
1	-0.379535000	-0.137632000	-4.087521000
6	-0.084798000	-2.105213000	-3.232336000
1	0.436303000	-2.503518000	-4.096154000
6	-0.330778000	-2.912051000	-2.116090000
1	-0.012413000	-3.946815000	-2.090967000
6	-0.999964000	-2.358220000	-1.025544000
1	-1.220014000	-2.904081000	-0.120087000
6	-3.083395000	2.630852000	-0.568915000
1	-3.881120000	2.537442000	0.177371000
1	-3.452689000	3.290077000	-1.371935000
6	-1.856687000	3.240467000	0.052684000
6	-1.346361000	4.461500000	-0.417251000
1	-1.823396000	4.938909000	-1.270456000
6	-0.253556000	5.077985000	0.198817000
1	0.123148000	6.024573000	-0.172912000
6	0.338719000	4.460293000	1.310215000
1	1.182891000	4.932960000	1.804184000
6	-0.149372000	3.245096000	1.792096000
1	0.292296000	2.765404000	2.659382000
6	-1.249868000	2.610323000	1.173805000
7	-4.629174000	-0.098560000	0.581375000
7	-4.116678000	-1.515806000	-2.636932000
7	-2.893843000	1.232614000	-1.130423000
7	-1.416403000	-1.071967000	-1.017190000
8	-1.707050000	1.426474000	1.637547000
8	-1.763666000	-1.697864000	1.882115000
6	0.225377000	-2.147478000	3.032616000
6	-0.832763000	-0.136649000	6.060545000
6	0.255394000	0.746229000	6.205219000
1	-1.642813000	-0.073100000	6.775434000
6	-0.858153000	-1.046148000	5.019051000
1	-1.716263000	-1.696029000	4.905594000
6	0.199555000	-1.115442000	4.074804000
6	1.281157000	-0.217275000	4.241360000
6	1.318816000	0.699849000	5.290033000
1	2.176985000	1.351082000	5.396223000
1	2.128088000	-0.269890000	3.569662000
6	1.068089000	-1.918425000	1.855808000
6	1.117491000	-0.638321000	1.253401000
1	1.973779000	0.616465000	-0.254483000
6	1.969465000	-0.373064000	0.185113000
1	0.443397000	0.135304000	1.606942000
6	2.802468000	-1.393013000	-0.309216000
6	1.910372000	-2.932195000	1.331819000
6	2.766719000	-2.674106000	0.270764000

1	1.922046000	-3.912163000	1.793225000
1	3.434505000	-3.434581000	-0.115645000
6	-0.036580000	-3.973305000	4.748777000
6	-0.154299000	-3.520528000	3.407643000
6	-0.588810000	-4.457412000	2.441963000
6	-0.905768000	-5.769130000	2.782831000
6	-0.779853000	-6.188618000	4.119899000
6	-0.337412000	-5.281563000	5.098398000
1	-0.227619000	-5.633295000	6.116906000
1	0.330758000	-3.299047000	5.511786000
1	-1.253872000	-6.449904000	2.016150000
1	-0.707688000	-4.131460000	1.418998000
1	-2.416753000	-2.036744000	2.526028000
8	0.181729000	1.603049000	7.275676000
6	1.248650000	2.573135000	7.503265000
1	2.202101000	2.068054000	7.689565000
1	1.342290000	3.255825000	6.652495000
1	0.941255000	3.123805000	8.390051000
8	-1.058840000	-7.457982000	4.567487000
6	-1.491326000	-8.482035000	3.623203000
1	-2.440379000	-8.204782000	3.152137000
1	-1.624737000	-9.378812000	4.225104000
1	-0.727748000	-8.656513000	2.857887000
8	3.685647000	-1.238038000	-1.353747000
6	3.832404000	0.068495000	-1.984746000
1	4.599761000	-0.070999000	-2.743925000
1	2.893901000	0.383027000	-2.454057000
1	4.158063000	0.820491000	-1.258674000

Table 4.13. $^{5}TS_{tBu}$:

26	-2.397015000	-0.158927000	0.820549000
6	-5.556752000	-1.773357000	3.759634000
1	-6.202293000	-2.497475000	3.272496000
6	-5.245860000	-1.923091000	5.113380000
1	-5.653082000	-2.759926000	5.671325000
6	-4.427321000	-0.981878000	5.750576000
1	-4.215560000	-1.078190000	6.811042000
6	-3.892124000	0.084284000	5.017592000
1	-3.250303000	0.812176000	5.500205000
6	-4.182498000	0.227473000	3.657633000
1	-3.751534000	1.051787000	3.099345000
6	-5.039337000	-0.690282000	3.020401000
6	-5.520745000	-0.434885000	1.641368000
6	-6.891229000	-0.564982000	1.367531000
1	-7.557851000	-0.905233000	2.149428000
6	-7.390528000	-0.188970000	0.120779000
1	-8.450349000	-0.267159000	-0.094839000
6	-6.508528000	0.322593000	-0.826008000
1	-6.860624000	0.649425000	-1.797769000
6	-5.143716000	0.398009000	-0.522211000
6	-4.202555000	0.928409000	-1.598555000
1	-4.663645000	1.853244000	-1.985800000
6	-4.173419000	-0.032823000	-2.789426000
6	-4.129283000	0.461171000	-4.100741000
1	-4.093111000	1.528358000	-4.290867000
6	-4.161746000	-0.454037000	-5.158351000
1	-4.147983000	-0.104818000	-6.185267000
6	-4.241062000	-1.818127000	-4.882021000
1	-4.304211000	-2.529713000	-5.695271000
6	-4.285145000	-2.252668000	-3.541333000
6	-4.388221000	-3.684868000	-3.164994000
6	-4.789085000	-4.037034000	-1.861085000
1	-5.006448000	-3.245044000	-1.155331000
6	-4.911206000	-5.377811000	-1.491691000
1	-5.234719000	-5.631199000	-0.486972000
6	-4.627666000	-6.393830000	-2.413360000
1	-4.727609000	-7.435937000	-2.127583000
6	-4.216527000	-6.056413000	-3.708022000
1	-3.988016000	-6.836159000	-4.427244000
6	-4.097714000	-4.714892000	-4.080782000
1	-3.760988000	-4.479029000	-5.084550000
6	-1.705664000	1.165351000	-1.927541000
1	-0.892512000	1.743949000	-1.473872000
1	-1.882059000	1.593298000	-2.925486000
6	-1.285315000	-0.278771000	-2.050065000

6	-0.695877000	-0.798230000	-3.207282000
1	-0.538318000	-0.156745000	-4.067118000
6	-0.337739000	-2.149615000	-3.243263000
1	0.113300000	-2.571739000	-4.134999000
6	-0.586121000	-2.951816000	-2.123881000
1	-0.341544000	-4.007159000	-2.125811000
6	-1.170591000	-2.369438000	-0.999580000
1	-1.397516000	-2.903921000	-0.087720000
6	-2.982726000	2.709009000	-0.435385000
1	-3.783547000	2.644949000	0.310655000
1	-3.317744000	3.400007000	-1.227052000
6	-1.728411000	3.243857000	0.197680000
6	-1.146196000	4.437027000	-0.259018000
1	-1.585646000	4.944253000	-1.115193000
6	-0.029039000	4.989808000	0.373795000
1	0.404356000	5.915588000	0.011544000
6	0.512303000	4.336763000	1.490743000
1	1.372862000	4.761164000	1.999993000
6	-0.048274000	3.147694000	1.960097000
1	0.353905000	2.644417000	2.833248000
6	-1.172050000	2.574649000	1.322339000
7	-4.650504000	0.013560000	0.680324000
7	-4.260385000	-1.351963000	-2.525270000
7	-2.867831000	1.313494000	-1.018991000
7	-1.501504000	-1.058736000	-0.964342000
8	-1.699402000	1.413913000	1.770539000
8	-1.798286000	-1.745561000	1.867945000
6	0.430076000	-2.252059000	3.076219000
6	-0.736235000	-0.622786000	6.291760000
6	0.277582000	0.322113000	6.546786000
1	-1.562417000	-0.728961000	6.981774000
6	-0.716356000	-1.429237000	5.156968000
1	-1.535615000	-2.115057000	4.979650000
6	0.329099000	-1.334022000	4.209500000
6	1.343790000	-0.372403000	4.457873000
6	1.315119000	0.424654000	5.595405000
1	2.125383000	1.127126000	5.755257000
1	2.182943000	-0.291766000	3.778923000
6	1.209298000	-1.836227000	1.913361000
6	1.144631000	-0.500002000	1.441791000
1	1.902274000	0.963593000	0.096256000
6	1.983388000	-0.067296000	0.422975000
1	0.397884000	0.169670000	1.855717000
6	2.932592000	-0.928021000	-0.176795000
6	2.129724000	-2.711260000	1.291909000
6	2.973528000	-2.260589000	0.275943000

1	2.227118000	-3.730640000	1.647015000
1	3.686634000	-2.956298000	-0.147140000
6	0.162659000	-4.271288000	4.546536000
6	0.087911000	-3.662387000	3.270916000
6	-0.275012000	-4.489879000	2.178809000
6	-0.566177000	-5.834237000	2.362621000
6	-0.499384000	-6.442410000	3.637995000
6	-0.120103000	-5.626456000	4.719126000
1	-0.029481000	-6.047772000	5.711817000
1	0.488063000	-3.690312000	5.400495000
1	-0.860516000	-6.424463000	1.501812000
1	-0.358470000	-4.047473000	1.197383000
1	-2.413505000	-2.077605000	2.550471000
6	0.294291000	1.213917000	7.800843000
6	0.296895000	2.707616000	7.368856000
1	1.170588000	2.953681000	6.756717000
1	-0.601537000	2.950979000	6.790685000
1	0.317813000	3.350361000	8.256204000
6	-0.930374000	0.971325000	8.712076000
1	-1.872191000	1.194771000	8.197314000
1	-0.968488000	-0.061057000	9.078331000
1	-0.869342000	1.628522000	9.585686000
6	1.581241000	0.912726000	8.621189000
1	1.603160000	-0.133592000	8.946267000
1	2.488851000	1.107911000	8.040756000
1	1.610058000	1.548333000	9.513424000
6	-0.828005000	-7.938048000	3.794524000
6	-2.289435000	-8.190773000	3.326242000
1	-2.532633000	-9.254618000	3.427571000
1	-2.434969000	-7.911100000	2.277644000
1	-2.999646000	-7.618481000	3.933712000
6	0.145513000	-8.772068000	2.914284000
1	-0.087095000	-9.838545000	3.012150000
1	1.184455000	-8.619337000	3.227096000
1	0.066285000	-8.507534000	1.854567000
6	-0.695848000	-8.419464000	5.257103000
1	-1.380670000	-7.885282000	5.925570000
1	0.325678000	-8.298186000	5.634839000
1	-0.943957000	-9.484527000	5.313027000
6	4.809190000	-1.482460000	-1.834606000
1	5.459637000	-1.918878000	-1.068249000
1	5.455266000	-1.046690000	-2.603858000
1	4.233230000	-2.289513000	-2.302255000
6	3.890094000	-0.383969000	-1.252920000
6	4.783488000	0.718925000	-0.615953000
1	5.382487000	0.310441000	0.205586000

1	4.184518000	1.546678000	-0.222152000
1	5.468228000	1.125365000	-1.369236000
6	3.071680000	0.234229000	-2.420497000
1	2.423425000	-0.517529000	-2.884086000
1	3.753401000	0.621017000	-3.186564000
1	2.443601000	1.065311000	-2.083193000

Table 4.14. $^{5}TS_{Ph}$:

26	-1.576546000	-0.710159000	1.025846000
6	-4.239258000	-3.726591000	3.769039000
1	-4.274900000	-4.653156000	3.205133000
6	-4.132130000	-3.772650000	5.162045000
1	-4.093013000	-4.730510000	5.669584000
6	-4.075797000	-2.586469000	5.903537000
1	-4.006418000	-2.624215000	6.985338000
6	-4.116383000	-1.352280000	5.241793000
1	-4.090918000	-0.429089000	5.812014000
6	-4.213056000	-1.303347000	3.848394000
1	-4.257610000	-0.351259000	3.332840000
6	-4.284383000	-2.491190000	3.092610000
6	-4.508487000	-2.418296000	1.627946000
6	-5.315242000	-3.368760000	0.973693000
1	-5.730113000	-4.200212000	1.529669000
6	-5.622747000	-3.194354000	-0.372996000
1	-6.239661000	-3.919953000	-0.892006000
6	-5.177837000	-2.045654000	-1.037668000
1	-5.439187000	-1.856537000	-2.068550000
6	-4.385401000	-1.133183000	-0.339633000
6	-3.962958000	0.232664000	-0.869148000
1	-4.259892000	0.924344000	-0.072153000
6	-4.684766000	0.705952000	-2.125900000
6	-5.453466000	1.878336000	-2.090471000
1	-5.555603000	2.441801000	-1.169615000
6	-6.093813000	2.299602000	-3.260588000
1	-6.710864000	3.191543000	-3.255891000
6	-5.940452000	1.558511000	-4.431111000
1	-6.452763000	1.860078000	-5.335784000
6	-5.138493000	0.400654000	-4.416049000
6	-4.914219000	-0.430549000	-5.624734000
6	-4.504397000	-1.772171000	-5.493030000
1	-4.358275000	-2.177630000	-4.499053000
6	-4.299493000	-2.568895000	-6.621155000
1	-3.998410000	-3.605048000	-6.502480000
6	-4.489628000	-2.039026000	-7.903693000
1	-4.330078000	-2.658168000	-8.780222000
6	-4.884675000	-0.704322000	-8.047805000
1	-5.022917000	-0.281646000	-9.037375000
6	-5.095726000	0.092725000	-6.919579000
1	-5.377522000	1.131294000	-7.055013000
6	-1.767165000	-0.297576000	-2.044495000
1	-0.783272000	0.180736000	-2.126580000
1	-2.300004000	-0.138849000	-2.986143000
6	-1.557963000	-1.773954000	-1.820306000

6	-1.497634000	-2.685752000	-2.881807000
1	-1.684584000	-2.343773000	-3.893419000
6	-1.203575000	-4.026042000	-2.615604000
1	-1.148919000	-4.745052000	-3.425850000
6	-0.983097000	-4.429511000	-1.292221000
1	-0.749799000	-5.459934000	-1.051734000
6	-1.071894000	-3.476894000	-0.278537000
1	-0.920671000	-3.705278000	0.768983000
6	-2.112667000	1.863782000	-0.839749000
1	-2.586883000	2.223008000	0.082762000
1	-2.583811000	2.383383000	-1.686026000
6	-0.645497000	2.184012000	-0.816428000
6	-0.088650000	3.069120000	-1.753190000
1	-0.720432000	3.463850000	-2.545818000
6	1.250372000	3.461440000	-1.673849000
1	1.664576000	4.148568000	-2.403467000
6	2.044407000	2.964406000	-0.630427000
1	3.082908000	3.271461000	-0.547890000
6	1.512152000	2.079399000	0.308347000
1	2.117598000	1.707104000	1.127337000
6	0.165279000	1.663407000	0.226119000
7	-4.007649000	-1.348814000	0.949741000
7	-4.541181000	-0.011054000	-3.265273000
7	-2.453015000	0.380956000	-0.900299000
7	-1.352787000	-2.178470000	-0.542961000
8	-0.342720000	0.782596000	1.119531000
8	-1.130765000	-1.894855000	2.513583000
6	0.814407000	-1.909349000	3.939801000
6	-0.530158000	1.322849000	5.371843000
6	0.585617000	2.186684000	5.275034000
1	-1.450538000	1.692193000	5.810481000
6	-0.463747000	0.007530000	4.936690000
1	-1.342187000	-0.622762000	4.989943000
6	0.721758000	-0.511331000	4.361404000
6	1.837068000	0.354809000	4.258315000
6	1.770523000	1.666981000	4.714705000
1	2.639494000	2.307219000	4.613512000
1	2.767517000	-0.016844000	3.846988000
6	1.763116000	-2.270834000	2.888289000
6	1.931753000	-1.428683000	1.760585000
1	2.974328000	-1.067113000	-0.067793000
6	2.861110000	-1.739304000	0.775636000
1	1.289809000	-0.559293000	1.651686000
6	3.678933000	-2.888699000	0.870201000
6	2.573709000	-3.429871000	2.980688000
6	3.512728000	-3.723132000	1.997820000

1	2.490851000	-4.078897000	3.844156000
1	4.117079000	-4.618196000	2.094135000
6	0.159455000	-2.772781000	6.207279000
6	0.272194000	-2.961594000	4.809607000
6	-0.088216000	-4.227788000	4.286469000
6	-0.529809000	-5.248183000	5.118062000
6	-0.630734000	-5.063991000	6.516472000
6	-0.276883000	-3.801984000	7.037199000
1	-0.358088000	-3.621400000	8.103203000
1	0.445626000	-1.823782000	6.644005000
1	-0.779497000	-6.212153000	4.688564000
1	-0.035674000	-4.383193000	3.216367000
1	-1.812167000	-2.256067000	3.110536000
6	4.680120000	-3.206573000	-0.174722000
6	4.441921000	-2.881399000	-1.526485000
6	5.896037000	-3.840321000	0.156738000
6	5.384722000	-3.183130000	-2.511536000
1	3.503918000	-2.415400000	-1.809694000
6	6.839840000	-4.137192000	-0.828915000
1	6.117657000	-4.071388000	1.193422000
6	6.587551000	-3.811533000	-2.167016000
1	5.179772000	-2.932754000	-3.547291000
1	7.774480000	-4.613897000	-0.552418000
1	7.321041000	-4.042862000	-2.932170000
6	0.511975000	3.587426000	5.750558000
6	-0.682443000	4.328190000	5.632890000
6	1.634132000	4.213296000	6.332061000
6	-0.750319000	5.649892000	6.078685000
1	-1.549039000	3.878508000	5.159313000
6	1.562891000	5.533390000	6.782247000
1	2.555590000	3.654680000	6.459588000
6	0.371133000	6.257264000	6.656428000
1	-1.674091000	6.208374000	5.968355000
1	2.433602000	5.994432000	7.236718000
1	0.317160000	7.283461000	7.004239000
6	-1.093998000	-6.158195000	7.402655000
6	-2.049214000	-7.095586000	6.956695000
6	-0.590907000	-6.289051000	8.713737000
6	-2.489373000	-8.123318000	7.794015000
1	-2.466109000	-7.006441000	5.958547000
6	-1.028617000	-7.319762000	9.548458000
1	0.169097000	-5.601461000	9.069757000
6	-1.980598000	-8.239808000	9.093047000
1	-3.231358000	-8.829434000	7.435869000
1	-0.621093000	-7.410155000	10.549873000
1	-2.320494000	-9.039587000	9.742321000

Table 4.15. $^{5}TS_{H}$:

26	-2.203705000	0.025717000	0.512414000
6	-5.364416000	-1.076602000	3.976848000
1	-6.107243000	-1.791310000	3.636652000
6	-5.005216000	-1.046761000	5.325950000
1	-5.474343000	-1.732531000	6.023862000
6	-4.055619000	-0.121039000	5.775929000
1	-3.799261000	-0.074318000	6.828980000
6	-3.437469000	0.741501000	4.863483000
1	-2.687881000	1.447920000	5.202746000
6	-3.786265000	0.711154000	3.509790000
1	-3.298260000	1.387441000	2.815966000
6	-4.775047000	-0.184843000	3.055903000
6	-5.320213000	-0.078480000	1.680835000
6	-6.713856000	-0.148723000	1.503930000
1	-7.346432000	-0.336559000	2.361423000
6	-7.275087000	0.093225000	0.252364000
1	-8.349891000	0.057075000	0.114010000
6	-6.431714000	0.424356000	-0.805489000
1	-6.829261000	0.651380000	-1.788164000
6	-5.050785000	0.454489000	-0.591124000
6	-4.148125000	0.772114000	-1.777420000
1	-4.633339000	1.582109000	-2.347364000
6	-4.094817000	-0.433698000	-2.716339000
6	-4.212031000	-0.269768000	-4.102227000
1	-4.308717000	0.718285000	-4.539049000
6	-4.229146000	-1.414298000	-4.907785000
1	-4.337306000	-1.325228000	-5.983351000
6	-4.136188000	-2.671349000	-4.313404000
1	-4.191968000	-3.563202000	-4.924334000
6	-4.018426000	-2.769585000	-2.911096000
6	-3.946411000	-4.073382000	-2.206279000
6	-4.262562000	-4.145571000	-0.835285000
1	-4.534677000	-3.234613000	-0.316826000
6	-4.242542000	-5.370487000	-0.164426000
1	-4.509883000	-5.411970000	0.886755000
6	-3.894682000	-6.544480000	-0.846347000
1	-3.892274000	-7.498298000	-0.328495000
6	-3.559454000	-6.481468000	-2.204131000
1	-3.280459000	-7.383659000	-2.738361000
6	-3.585795000	-5.257843000	-2.878164000
1	-3.308656000	-5.231049000	-3.926536000
6	-1.724827000	1.187933000	-2.308531000
1	-0.968941000	1.924666000	-2.012102000
1	-2.060184000	1.464361000	-3.318730000
6	-1.091439000	-0.181476000	-2.326564000

6	-0.449582000	-0.682543000	-3.463668000
1	-0.425081000	-0.091593000	-4.372446000
6	0.143448000	-1.947059000	-3.414075000
1	0.643723000	-2.351335000	-4.287347000
6	0.073419000	-2.684145000	-2.227578000
1	0.512059000	-3.671265000	-2.151098000
6	-0.579684000	-2.125734000	-1.129798000
1	-0.661928000	-2.640966000	-0.187077000
6	-2.992748000	2.714602000	-0.808391000
1	-3.754469000	2.660361000	-0.024204000
1	-3.399782000	3.324380000	-1.630933000
6	-1.741218000	3.358295000	-0.274938000
6	-1.263486000	4.559574000	-0.824205000
1	-1.780718000	4.991879000	-1.677885000
6	-0.152861000	5.214288000	-0.284030000
1	0.198604000	6.144130000	-0.717161000
6	0.490336000	4.658665000	0.830926000
1	1.347261000	5.162534000	1.267822000
6	0.035162000	3.463317000	1.389994000
1	0.517304000	3.035049000	2.262372000
6	-1.079765000	2.789972000	0.846814000
7	-4.493567000	0.186258000	0.618495000
7	-4.006262000	-1.650720000	-2.142245000
7	-2.814931000	1.286517000	-1.305498000
7	-1.143674000	-0.896732000	-1.174892000
8	-1.506902000	1.622427000	1.389349000
8	-1.705543000	-1.464640000	1.827391000
6	0.193344000	-2.173603000	2.902611000
6	-0.861147000	-1.272696000	6.419585000
6	0.036046000	-0.242732000	6.735025000
1	-1.578235000	-1.614109000	7.157383000
6	-0.835206000	-1.862351000	5.158610000
1	-1.537294000	-2.653067000	4.922232000
6	0.097593000	-1.442591000	4.176632000
6	0.997464000	-0.401605000	4.515804000
6	0.960764000	0.191691000	5.777483000
1	1.669072000	0.975711000	6.021772000
1	1.755345000	-0.092700000	3.809075000
6	1.102396000	-1.694462000	1.845532000
6	1.123124000	-0.333695000	1.457112000
1	2.046284000	1.163271000	0.227819000
6	2.051277000	0.117936000	0.518395000
1	0.374748000	0.345624000	1.851380000
6	2.976883000	-0.771376000	-0.046816000
6	2.022943000	-2.586288000	1.247774000
6	2.957265000	-2.123170000	0.318336000

1	2.027548000	-3.629727000	1.539722000
1	3.674344000	-2.814213000	-0.112102000
6	0.544765000	-4.403891000	3.972982000
6	-0.094460000	-3.641786000	2.968184000
6	-0.900986000	-4.307744000	2.025634000
6	-1.054705000	-5.695228000	2.079104000
6	-0.396556000	-6.444481000	3.062371000
6	0.403296000	-5.794038000	4.008659000
1	0.914301000	-6.364598000	4.776885000
1	1.171549000	-3.910073000	4.707143000
1	-1.694759000	-6.186242000	1.353848000
1	-1.451018000	-3.714904000	1.308068000
1	-2.347949000	-1.590318000	2.554854000
1	0.021989000	0.208495000	7.721642000
1	3.706233000	-0.413443000	-0.766287000
1	-0.511896000	-7.522759000	3.096515000

Table 4.16. $^{5}TS_{Cl}$:

26	-2.223588000	-0.006821000	0.451595000
6	-5.287667000	-0.959486000	4.046404000
1	-6.029561000	-1.696697000	3.755876000
6	-4.899597000	-0.865099000	5.384633000
1	-5.347454000	-1.522630000	6.122554000
6	-3.951676000	0.090079000	5.773130000
1	-3.676228000	0.190908000	6.817622000
6	-3.363758000	0.917816000	4.809612000
1	-2.620633000	1.651788000	5.101913000
6	-3.742318000	0.822638000	3.467273000
1	-3.280650000	1.473590000	2.733505000
6	-4.729451000	-0.103091000	3.073830000
6	-5.304074000	-0.060156000	1.707427000
6	-6.697785000	-0.173039000	1.555489000
1	-7.312085000	-0.351536000	2.428062000
6	-7.285391000	0.016625000	0.306784000
1	-8.360843000	-0.053499000	0.188308000
6	-6.470235000	0.341937000	-0.775360000
1	-6.890924000	0.530724000	-1.756419000
6	-5.088006000	0.415609000	-0.585117000
6	-4.207294000	0.730387000	-1.788933000
1	-4.708115000	1.527670000	-2.362573000
6	-4.142620000	-0.487402000	-2.710087000
6	-4.292573000	-0.349810000	-4.095090000
1	-4.426411000	0.627451000	-4.546184000
6	-4.293033000	-1.508326000	-4.881030000
1	-4.425031000	-1.441130000	-5.955463000
6	-4.153677000	-2.751356000	-4.267235000
1	-4.198274000	-3.655232000	-4.861109000
6	-4.004816000	-2.823025000	-2.865774000
6	-3.889049000	-4.113924000	-2.144090000
6	-4.197625000	-4.178478000	-0.771065000
1	-4.489700000	-3.269376000	-0.260463000
6	-4.145343000	-5.395569000	-0.087596000
1	-4.410210000	-5.433236000	0.964347000
6	-3.769891000	-6.568051000	-0.757874000
1	-3.742276000	-7.515800000	-0.229710000
6	-3.438911000	-6.510993000	-2.117215000
1	-3.137773000	-7.411497000	-2.642010000
6	-3.499522000	-5.296034000	-2.804425000
1	-3.226755000	-5.273295000	-3.854069000
6	-1.803949000	1.195542000	-2.369500000
1	-1.066269000	1.960958000	-2.101710000
1	-2.177600000	1.449737000	-3.371327000
6	-1.123423000	-0.150790000	-2.390645000

6	-0.475667000	-0.637420000	-3.530211000
1	-0.477092000	-0.051970000	-4.442685000
6	0.160654000	-1.880573000	-3.476684000
1	0.669093000	-2.272409000	-4.350655000
6	0.125533000	-2.612975000	-2.285103000
1	0.597747000	-3.584442000	-2.208696000
6	-0.535365000	-2.070558000	-1.184410000
1	-0.598739000	-2.580623000	-0.236857000
6	-3.063315000	2.686227000	-0.826403000
1	-3.805448000	2.615227000	-0.025506000
1	-3.499497000	3.294099000	-1.634630000
6	-1.809313000	3.347742000	-0.319533000
6	-1.390496000	4.580803000	-0.845634000
1	-1.953527000	5.024482000	-1.663409000
6	-0.279184000	5.252088000	-0.327425000
1	0.026114000	6.205757000	-0.743010000
6	0.426604000	4.681603000	0.740475000
1	1.285324000	5.197088000	1.159137000
6	0.030872000	3.454081000	1.275179000
1	0.560743000	3.013167000	2.112868000
6	-1.083501000	2.765829000	0.752836000
7	-4.505167000	0.194797000	0.621667000
7	-4.006286000	-1.690695000	-2.116157000
7	-2.872983000	1.264461000	-1.337862000
7	-1.138504000	-0.860125000	-1.234810000
8	-1.448321000	1.564568000	1.274216000
8	-1.823701000	-1.481185000	1.682248000
6	0.337163000	-2.255400000	2.991070000
6	-0.897650000	-1.311729000	6.429348000
6	-0.049916000	-0.242515000	6.728054000
1	-1.632786000	-1.643983000	7.150704000
6	-0.787470000	-1.935115000	5.191386000
1	-1.456499000	-2.752352000	4.951864000
6	0.172304000	-1.511733000	4.232075000
6	1.016661000	-0.422683000	4.581502000
6	0.906913000	0.209556000	5.816775000
1	1.569156000	1.025034000	6.079425000
1	1.796746000	-0.105189000	3.902673000
6	1.164645000	-1.742228000	1.902781000
6	1.132098000	-0.376461000	1.521379000
1	1.941548000	1.151526000	0.238863000
6	1.987983000	0.110409000	0.534474000
1	0.381828000	0.283980000	1.941524000
6	2.887300000	-0.764972000	-0.077786000
6	2.071000000	-2.604945000	1.235329000
6	2.939472000	-2.118915000	0.258436000

1	2.122828000	-3.650429000	1.514875000
1	3.651634000	-2.776540000	-0.224585000
6	0.559299000	-4.516974000	4.044582000
6	0.016900000	-3.705889000	3.020168000
6	-0.765985000	-4.318375000	2.019627000
6	-0.985526000	-5.696773000	2.027073000
6	-0.409701000	-6.470842000	3.034477000
6	0.359891000	-5.899577000	4.047259000
1	0.796347000	-6.518477000	4.821381000
1	1.167474000	-4.069842000	4.822982000
1	-1.605633000	-6.154614000	1.266534000
1	-1.266440000	-3.684243000	1.299158000
1	-2.401088000	-1.608845000	2.458789000
17	-0.192981000	0.571222000	8.339206000
17	4.006463000	-0.130949000	-1.359282000
17	-0.683339000	-8.266813000	3.035958000

Table 4.17. $^{5}TS_{NO2}$:

26	-2.098441000	0.027501000	0.487493000
6	-5.014240000	-0.777984000	4.258976000
1	-5.688776000	-1.602464000	4.050354000
6	-4.639635000	-0.512885000	5.577676000
1	-5.028272000	-1.128901000	6.381926000
6	-3.779700000	0.556237000	5.864490000
1	-3.502650000	0.770403000	6.891453000
6	-3.268715000	1.333564000	4.818361000
1	-2.598110000	2.159294000	5.030636000
6	-3.637215000	1.071177000	3.495483000
1	-3.247601000	1.691117000	2.697166000
6	-4.533360000	0.023064000	3.200320000
6	-5.120352000	-0.101386000	1.843982000
6	-6.498698000	-0.349323000	1.723137000
1	-7.083826000	-0.528736000	2.615195000
6	-7.118585000	-0.282583000	0.476855000
1	-8.184155000	-0.458826000	0.382810000
6	-6.355328000	0.068369000	-0.634476000
1	-6.808209000	0.177137000	-1.613154000
6	-4.982818000	0.274531000	-0.476498000
6	-4.160079000	0.653262000	-1.702957000
1	-4.713687000	1.444588000	-2.233825000
6	-4.073985000	-0.528957000	-2.666943000
6	-4.200451000	-0.340168000	-4.048266000
1	-4.339732000	0.651711000	-4.464810000
6	-4.172354000	-1.467236000	-4.878943000
1	-4.284051000	-1.359359000	-5.952296000
6	-4.036165000	-2.731646000	-4.309551000
1	-4.062303000	-3.616084000	-4.933656000
6	-3.923452000	-2.855424000	-2.908293000
6	-3.834252000	-4.175734000	-2.241382000
6	-4.338814000	-4.337170000	-0.936195000
1	-4.770293000	-3.479655000	-0.433595000
6	-4.309368000	-5.588178000	-0.314988000
1	-4.728965000	-5.706811000	0.679022000
6	-3.756010000	-6.694568000	-0.975563000
1	-3.726393000	-7.662584000	-0.486668000
6	-3.236613000	-6.539412000	-2.266896000
1	-2.800340000	-7.388644000	-2.781859000
6	-3.280020000	-5.292663000	-2.896921000
1	-2.862498000	-5.187492000	-3.893143000
6	-1.774834000	1.207568000	-2.320316000
1	-1.050913000	1.986494000	-2.054628000
1	-2.163675000	1.459764000	-3.315689000
6	-1.071798000	-0.125368000	-2.354668000

6	-0.423896000	-0.592553000	-3.501995000
1	-0.436167000	0.003379000	-4.407297000
6	0.226751000	-1.828449000	-3.466339000
1	0.737154000	-2.203882000	-4.346123000
6	0.203185000	-2.575836000	-2.283322000
1	0.684142000	-3.543781000	-2.220529000
6	-0.454419000	-2.051774000	-1.172907000
1	-0.498299000	-2.580369000	-0.234648000
6	-3.075421000	2.665466000	-0.779086000
1	-3.800177000	2.574972000	0.035849000
1	-3.552246000	3.241817000	-1.586516000
6	-1.840091000	3.389267000	-0.309428000
6	-1.524458000	4.660235000	-0.816413000
1	-2.151855000	5.091632000	-1.592221000
6	-0.430192000	5.382562000	-0.331344000
1	-0.204358000	6.364091000	-0.732159000
6	0.366477000	4.827616000	0.678946000
1	1.215502000	5.381306000	1.066033000
6	0.074715000	3.562812000	1.193250000
1	0.677813000	3.127074000	1.982276000
6	-1.022506000	2.829813000	0.704420000
7	-4.362383000	0.154373000	0.726687000
7	-3.942899000	-1.753485000	-2.113961000
7	-2.836483000	1.244884000	-1.277115000
7	-1.068496000	-0.844777000	-1.203111000
8	-1.285242000	1.587101000	1.203609000
8	-1.730572000	-1.345946000	1.827439000
6	0.140002000	-2.250682000	2.913188000
6	-1.124200000	-1.305915000	6.344910000
6	-0.226429000	-0.290699000	6.685623000
1	-1.900006000	-1.588153000	7.042497000
6	-1.001829000	-1.921902000	5.106572000
1	-1.698969000	-2.706191000	4.837979000
6	0.011101000	-1.536432000	4.188378000
6	0.917931000	-0.519301000	4.586819000
6	0.803672000	0.100396000	5.826934000
1	1.498635000	0.868225000	6.140859000
1	1.736900000	-0.239004000	3.938967000
6	1.106899000	-1.807511000	1.895791000
6	1.201169000	-0.445990000	1.514401000
1	2.194992000	0.999059000	0.251727000
6	2.132589000	-0.035307000	0.563888000
1	0.499881000	0.277068000	1.912393000
6	2.982729000	-0.985484000	-0.007497000
6	1.984052000	-2.742227000	1.290368000
6	2.927354000	-2.335143000	0.350417000

1	1.942698000	-3.785470000	1.577897000
1	3.614059000	-3.037349000	-0.103904000
6	0.299797000	-4.552955000	3.898892000
6	-0.251407000	-3.697403000	2.916148000
6	-1.100049000	-4.249172000	1.936777000
6	-1.381429000	-5.614411000	1.924559000
6	-0.806944000	-6.432867000	2.896765000
6	0.032023000	-5.922143000	3.888670000
1	0.457806000	-6.587574000	4.628370000
1	0.953882000	-4.148149000	4.662607000
1	-2.039903000	-6.041497000	1.180644000
1	-1.583230000	-3.588281000	1.231098000
1	-2.275014000	-1.364452000	2.638511000
7	-0.383557000	0.392129000	7.970989000
8	-1.427383000	0.143475000	8.644971000
8	0.517509000	1.200594000	8.327264000
7	3.940340000	-0.560202000	-1.033615000
8	4.690132000	-1.440498000	-1.543445000
8	3.951959000	0.660763000	-1.360698000
7	-1.105945000	-7.871051000	2.880127000
8	-1.885314000	-8.300813000	1.981799000
8	-0.569456000	-8.595699000	3.762326000

Table 4.18. $^{5}Re_{OMe}$:

26	-1.463741000	-1.077218000	1.214147000
6	-4.139965000	-3.311263000	4.367364000
1	-4.326989000	-4.305055000	3.974506000
6	-3.943116000	-3.140446000	5.739877000
1	-3.999502000	-3.997124000	6.403275000
6	-3.677052000	-1.867749000	6.260961000
1	-3.543179000	-1.734590000	7.329683000
6	-3.599570000	-0.768438000	5.396145000
1	-3.406907000	0.223882000	5.791064000
6	-3.791896000	-0.938017000	4.022369000
1	-3.747025000	-0.086012000	3.353942000
6	-4.068240000	-2.212455000	3.489011000
6	-4.353481000	-2.360987000	2.042334000
6	-5.266818000	-3.321811000	1.571768000
1	-5.740037000	-4.005322000	2.265423000
6	-5.595592000	-3.349142000	0.218864000
1	-6.290084000	-4.091483000	-0.159537000
6	-5.069673000	-2.377810000	-0.641204000
1	-5.343690000	-2.346417000	-1.685187000
6	-4.179973000	-1.436278000	-0.122317000
6	-3.690860000	-0.195054000	-0.868382000
1	-4.030301000	0.628043000	-0.228782000
6	-4.319123000	0.054233000	-2.232675000
6	-4.978685000	1.265503000	-2.487561000
1	-5.069022000	2.017169000	-1.711317000
6	-5.531827000	1.476317000	-3.754880000
1	-6.064552000	2.395402000	-3.973654000
6	-5.405474000	0.489626000	-4.731069000
1	-5.855825000	0.632337000	-5.704934000
6	-4.713322000	-0.699432000	-4.427992000
6	-4.526458000	-1.790719000	-5.417061000
6	-4.175270000	-3.083455000	-4.979492000
1	-4.042938000	-3.255080000	-3.918302000
6	-4.006389000	-4.124638000	-5.894324000
1	-3.749169000	-5.117552000	-5.538838000
6	-4.176359000	-3.895003000	-7.265469000
1	-4.046172000	-4.704360000	-7.976238000
6	-4.513351000	-2.612748000	-7.713463000
1	-4.636350000	-2.421960000	-8.774397000
6	-4.686626000	-1.570455000	-6.799051000
1	-4.925219000	-0.580814000	-7.172832000
6	-1.429273000	-0.767892000	-1.899299000
1	-0.442202000	-0.289946000	-1.931733000
1	-1.891346000	-0.642994000	-2.882972000
6	-1.231546000	-2.236157000	-1.611001000

6	-1.122912000	-3.197179000	-2.623598000
1	-1.269854000	-2.911601000	-3.658734000
6	-0.841567000	-4.521947000	-2.273357000
1	-0.750846000	-5.280394000	-3.043927000
6	-0.686452000	-4.861763000	-0.922863000
1	-0.469443000	-5.880602000	-0.624210000
6	-0.827202000	-3.862594000	0.040913000
1	-0.752886000	-4.015995000	1.112362000
6	-1.816885000	1.414196000	-0.749852000
1	-2.362872000	1.796810000	0.121603000
1	-2.195843000	1.934638000	-1.642373000
6	-0.351444000	1.709658000	-0.589328000
6	0.311157000	2.527372000	-1.519251000
1	-0.232106000	2.868692000	-2.397788000
6	1.637187000	2.925767000	-1.328964000
1	2.129918000	3.561143000	-2.056703000
6	2.309408000	2.508463000	-0.171752000
1	3.332545000	2.828253000	0.004783000
6	1.672953000	1.691364000	0.763584000
1	2.183060000	1.389786000	1.671954000
6	0.339907000	1.258522000	0.570575000
7	-3.783495000	-1.472591000	1.180809000
7	-4.193846000	-0.898196000	-3.186201000
7	-2.181297000	-0.058310000	-0.823092000
7	-1.088079000	-2.580690000	-0.310065000
8	-0.249974000	0.440238000	1.471305000
8	-1.073386000	-2.421447000	2.605700000
6	1.476844000	-2.176759000	4.736532000
6	0.386136000	0.994348000	6.465974000
6	1.445442000	1.861207000	6.131721000
1	-0.452181000	1.344413000	7.054466000
6	0.410099000	-0.320296000	6.019078000
1	-0.425995000	-0.971587000	6.244367000
6	1.470733000	-0.809145000	5.210098000
6	2.524144000	0.094585000	4.882515000
6	2.518062000	1.397672000	5.341550000
1	3.326983000	2.082951000	5.120938000
1	3.365918000	-0.262038000	4.301918000
6	2.116452000	-2.515968000	3.489955000
6	2.087959000	-1.616304000	2.389768000
1	2.648437000	-1.230609000	0.367468000
6	2.718426000	-1.927741000	1.192809000
1	1.472740000	-0.724410000	2.443599000
6	3.405050000	-3.150253000	1.065466000
6	2.786189000	-3.764255000	3.320600000
6	3.431708000	-4.069248000	2.137754000

1	2.835818000	-4.458848000	4.150829000
1	3.980239000	-4.994273000	2.009451000
6	0.985898000	-3.238028000	6.960722000
6	0.878551000	-3.228671000	5.541675000
6	0.167283000	-4.283466000	4.913078000
6	-0.395494000	-5.312381000	5.661752000
6	-0.242858000	-5.319190000	7.060786000
6	0.448355000	-4.272375000	7.706133000
1	0.555368000	-4.313910000	8.783124000
1	1.541507000	-2.451629000	7.458737000
1	-0.959609000	-6.088686000	5.160483000
1	-0.018489000	-4.208013000	3.846009000
1	-1.553552000	-2.339980000	3.450608000
8	1.531395000	3.166423000	6.529358000
6	0.478972000	3.757866000	7.353558000
1	0.799848000	4.784261000	7.518039000
1	-0.479453000	3.745044000	6.825202000
1	0.394238000	3.233806000	8.310739000
8	4.073453000	-3.546092000	-0.061715000
6	4.143981000	-2.655823000	-1.219312000
1	4.752963000	-3.191312000	-1.944759000
1	3.145506000	-2.471841000	-1.628240000
1	4.622101000	-1.708634000	-0.952075000
8	-0.737847000	-6.292854000	7.890615000
6	-1.426366000	-7.451702000	7.329070000
1	-1.677518000	-8.070033000	8.188446000
1	-2.340049000	-7.148233000	6.807471000
1	-0.769425000	-8.003446000	6.649217000

Table 4.19. $^{5}\mathbf{Re}_{\mathbf{tBu}}$:

26	-2.887578000	-0.065814000	-0.105213000
6	-5.849345000	-1.422650000	3.292234000
1	-6.888125000	-1.291881000	3.005676000
6	-5.487088000	-2.502829000	4.101081000
1	-6.247425000	-3.194290000	4.448404000
6	-4.146232000	-2.693258000	4.455419000
1	-3.864094000	-3.529741000	5.086479000
6	-3.170278000	-1.800791000	3.992535000
1	-2.131011000	-1.939271000	4.271839000
6	-3.527069000	-0.721075000	3.175931000
1	-2.760416000	-0.043527000	2.814683000
6	-4.873850000	-0.525020000	2.814830000
6	-5.300190000	0.637912000	1.998170000
6	-6.418239000	1.391406000	2.405306000
1	-6.937242000	1.110052000	3.312537000
6	-6.818513000	2.506695000	1.674128000
1	-7.667561000	3.099382000	1.995687000
6	-6.098026000	2.859983000	0.530586000
1	-6.376292000	3.724615000	-0.060781000
6	-5.008551000	2.074766000	0.154186000
6	-4.276082000	2.355337000	-1.154390000
1	-4.399334000	3.423846000	-1.388540000
6	-4.937236000	1.553312000	-2.270133000
6	-5.764476000	2.197111000	-3.193084000
1	-5.911371000	3.270487000	-3.148471000
6	-6.402276000	1.420625000	-4.165698000
1	-7.075724000	1.877807000	-4.882280000
6	-6.161670000	0.051849000	-4.197213000
1	-6.664240000	-0.571432000	-4.924932000
6	-5.278795000	-0.540940000	-3.265711000
6	-4.977581000	-1.988659000	-3.353274000
6	-4.661252000	-2.742360000	-2.209081000
1	-4.576800000	-2.269411000	-1.238692000
6	-4.411925000	-4.114335000	-2.316800000
1	-4.170710000	-4.677743000	-1.421420000
6	-4.470540000	-4.754554000	-3.559309000
1	-4.280644000	-5.820367000	-3.636694000
6	-4.768760000	-4.009241000	-4.707352000
1	-4.799461000	-4.491633000	-5.678848000
6	-5.020424000	-2.640199000	-4.605874000
1	-5.220487000	-2.073915000	-5.509602000
6	-2.073634000	2.032160000	-2.318232000
1	-1.346138000	2.851587000	-2.318503000
1	-2.772538000	2.228154000	-3.138880000
6	-1.351183000	0.730030000	-2.602840000

6	-0.462587000	0.610857000	-3.678696000
1	-0.245697000	1.471954000	-4.301650000
6	0.132905000	-0.626144000	-3.935926000
1	0.821377000	-0.737500000	-4.766364000
6	-0.172275000	-1.720181000	-3.114624000
1	0.262547000	-2.695506000	-3.295165000
6	-1.055131000	-1.535377000	-2.053299000
1	-1.352687000	-2.326563000	-1.377137000
6	-2.170561000	2.971149000	-0.017305000
1	-2.775811000	2.914128000	0.891933000
1	-2.239947000	3.998504000	-0.407342000
6	-0.740053000	2.635233000	0.302941000
6	0.292467000	3.560289000	0.102711000
1	0.064279000	4.522771000	-0.349411000
6	1.605480000	3.272639000	0.494747000
1	2.394163000	3.999455000	0.334697000
6	1.885444000	2.043359000	1.109878000
1	2.898696000	1.816316000	1.426991000
6	0.871261000	1.108724000	1.321750000
1	1.073013000	0.160134000	1.805687000
6	-0.451660000	1.383247000	0.912279000
7	-4.611465000	0.988594000	0.868510000
7	-4.700299000	0.220054000	-2.288072000
7	-2.818401000	2.030730000	-1.018878000
7	-1.622446000	-0.328301000	-1.809608000
8	-1.431869000	0.473855000	1.090063000
8	-3.185323000	-1.856661000	0.265684000
6	2.476934000	-3.873931000	4.159876000
6	-0.042812000	-2.255194000	6.491241000
6	0.288297000	-0.887696000	6.413124000
1	-0.860570000	-2.578687000	7.123293000
6	0.658368000	-3.220901000	5.769236000
1	0.360903000	-4.260732000	5.844999000
6	1.732002000	-2.869143000	4.912378000
6	2.056808000	-1.487926000	4.828375000
6	1.359353000	-0.535645000	5.561867000
1	1.661983000	0.502854000	5.481708000
1	2.891866000	-1.178065000	4.210556000
6	3.035873000	-3.534480000	2.853095000
6	2.370868000	-2.643481000	1.968934000
1	2.364173000	-1.633603000	0.091115000
6	2.916796000	-2.310609000	0.734366000
1	1.403861000	-2.241627000	2.251109000
6	4.159493000	-2.828820000	0.306703000
6	4.272820000	-4.067816000	2.413252000
6	4.818051000	-3.716271000	1.179190000

1	4.824730000	-4.733632000	3.066986000
1	5.778051000	-4.134788000	0.904636000
6	2.807839000	-5.424406000	6.110001000
6	2.678184000	-5.208510000	4.714465000
6	2.759723000	-6.355057000	3.878611000
6	2.948242000	-7.624137000	4.411795000
6	3.082611000	-7.836074000	5.802256000
6	3.010286000	-6.700576000	6.632308000
1	3.123743000	-6.805047000	7.703924000
1	2.785738000	-4.574380000	6.782427000
1	2.984370000	-8.470311000	3.734014000
1	2.640691000	-6.238582000	2.807304000
1	-3.103055000	-2.281403000	1.137156000
6	-0.446259000	0.201549000	7.217302000
6	-1.021877000	1.269161000	6.244775000
1	-0.236717000	1.739579000	5.643878000
1	-1.751387000	0.820368000	5.560921000
1	-1.526224000	2.058037000	6.815041000
6	-1.615153000	-0.372087000	8.050704000
1	-2.369339000	-0.850337000	7.414795000
1	-1.269194000	-1.102900000	8.790561000
1	-2.107328000	0.440400000	8.596149000
6	0.560476000	0.882052000	8.187890000
1	0.976675000	0.153629000	8.892821000
1	1.393265000	1.344892000	7.648076000
1	0.054038000	1.665460000	8.763931000
6	3.298322000	-9.260455000	6.347485000
6	2.091125000	-10.153227000	5.943051000
1	2.239828000	-11.173480000	6.315182000
1	1.970471000	-10.206703000	4.855933000
1	1.159002000	-9.765770000	6.369876000
6	4.601363000	-9.852155000	5.739912000
1	4.760371000	-10.869724000	6.115376000
1	5.471368000	-9.245811000	6.016189000
1	4.555021000	-9.901002000	4.646876000
6	3.425425000	-9.285967000	7.887700000
1	2.521363000	-8.905017000	8.376468000
1	4.282702000	-8.697889000	8.234756000
1	3.573965000	-10.317477000	8.224439000
6	6.106639000	-3.075674000	-1.342902000
1	6.856173000	-2.794678000	-0.594536000
1	6.476368000	-2.748125000	-2.320613000
1	6.032396000	-4.168873000	-1.365658000
6	4.739109000	-2.413717000	-1.059267000
6	4.928122000	-0.870812000	-1.090002000
1	5.630405000	-0.550205000	-0.312267000

1	3.982211000	-0.341282000	-0.932658000
1	5.331439000	-0.561813000	-2.061790000
6	3.753096000	-2.831945000	-2.186017000
1	3.604001000	-3.917797000	-2.189614000
1	4.155805000	-2.538295000	-3.162922000
1	2.775626000	-2.352694000	-2.064171000

Table 4.20. $^{5}\mathbf{Re}_{\mathrm{Ph}}$:

26	-2.733845000	-0.477996000	1.492149000
6	-5.335317000	-1.606698000	5.235754000
1	-6.270608000	-2.090236000	4.972422000
6	-4.673103000	-1.976594000	6.408749000
1	-5.105819000	-2.732569000	7.055595000
6	-3.455516000	-1.372659000	6.746102000
1	-2.944695000	-1.651349000	7.661894000
6	-2.899261000	-0.407283000	5.898464000
1	-1.956288000	0.062720000	6.152879000
6	-3.553053000	-0.040277000	4.716878000
1	-3.105884000	0.704449000	4.066399000
6	-4.783305000	-0.634530000	4.375793000
6	-5.538950000	-0.220270000	3.169282000
6	-6.931600000	-0.035249000	3.251882000
1	-7.426890000	-0.181589000	4.202952000
6	-7.651482000	0.374761000	2.132527000
1	-8.722185000	0.533640000	2.195292000
6	-6.970080000	0.595609000	0.934260000
1	-7.495599000	0.917387000	0.042492000
6	-5.590828000	0.389025000	0.895148000
6	-4.844152000	0.532174000	-0.425253000
1	-5.333492000	1.328734000	-1.007816000
6	-4.968125000	-0.758240000	-1.232101000
6	-5.423522000	-0.726183000	-2.553708000
1	-5.674332000	0.213966000	-3.032843000
6	-5.545612000	-1.940167000	-3.239697000
1	-5.873427000	-1.956497000	-4.273488000
6	-5.247162000	-3.127215000	-2.578070000
1	-5.326495000	-4.070155000	-3.102587000
6	-4.832507000	-3.099006000	-1.227100000
6	-4.585666000	-4.345958000	-0.464201000
6	-3.815886000	-4.329037000	0.715356000
1	-3.388187000	-3.402935000	1.083165000
6	-3.591522000	-5.511550000	1.425952000
1	-2.986450000	-5.482229000	2.326763000
6	-4.136329000	-6.724014000	0.987274000
1	-3.962839000	-7.638559000	1.544652000
6	-4.916080000	-6.747089000	-0.175212000
1	-5.360038000	-7.677003000	-0.515678000
6	-5.138243000	-5.571112000	-0.893904000
1	-5.773394000	-5.610112000	-1.772142000
6	-2.536469000	0.823077000	-1.372515000
1	-1.859541000	1.684481000	-1.354099000
1	-3.117313000	0.890695000	-2.300721000
6	-1.687702000	-0.429175000	-1.378847000

6	-1.031519000	-0.869169000	-2.534182000
1	-1.171999000	-0.342469000	-3.471875000
6	-0.196088000	-1.986779000	-2.458439000
1	0.322329000	-2.340865000	-3.342809000
6	-0.040192000	-2.644492000	-1.231644000
1	0.596758000	-3.515756000	-1.139856000
6	-0.731430000	-2.166499000	-0.120229000
1	-0.690729000	-2.630125000	0.856850000
6	-3.396184000	2.349918000	0.400036000
1	-4.007272000	2.319249000	1.306160000
1	-3.888691000	3.024219000	-0.317641000
6	-2.017768000	2.857538000	0.716793000
6	-1.540380000	4.047470000	0.149251000
1	-2.169037000	4.588069000	-0.554612000
6	-0.280304000	4.555542000	0.484233000
1	0.071693000	5.479896000	0.039924000
6	0.518251000	3.855247000	1.400363000
1	1.499927000	4.236427000	1.663866000
6	0.064736000	2.669267000	1.976427000
1	0.680704000	2.120780000	2.678411000
6	-1.209781000	2.150006000	1.651691000
7	-4.884161000	-0.004093000	1.987319000
7	-4.672104000	-1.907373000	-0.587862000
7	-3.418626000	0.935010000	-0.170400000
7	-1.533732000	-1.076606000	-0.202228000
8	-1.649342000	1.004603000	2.212232000
8	-2.315171000	-2.051404000	2.437991000
6	2.275339000	-5.940662000	2.900958000
6	0.703613000	-2.659901000	3.970073000
6	1.746869000	-2.052613000	4.707974000
1	-0.246888000	-2.154797000	3.837366000
6	0.867022000	-3.913930000	3.394022000
1	0.042265000	-4.345450000	2.837457000
6	2.097345000	-4.621237000	3.489510000
6	3.154625000	-3.985263000	4.196577000
6	2.976313000	-2.746785000	4.796211000
1	3.806334000	-2.298768000	5.330805000
1	4.104969000	-4.495880000	4.300470000
6	3.574388000	-6.319915000	2.355888000
6	4.417639000	-5.362386000	1.729756000
1	6.271302000	-4.961007000	0.740759000
6	5.651976000	-5.721371000	1.203770000
1	4.078598000	-4.336511000	1.642195000
6	6.128311000	-7.049519000	1.284656000
6	4.055889000	-7.654955000	2.430183000
6	5.298349000	-8.003293000	1.916179000

1	3.454264000	-8.409304000	2.923719000
1	5.629283000	-9.033563000	1.986797000
6	0.185520000	-6.902305000	3.904620000
6	1.169253000	-6.889238000	2.878324000
6	1.039678000	-7.859391000	1.847507000
6	0.004187000	-8.784745000	1.852030000
6	-0.957985000	-8.807977000	2.886793000
6	-0.840828000	-7.838584000	3.908680000
1	-1.570555000	-7.819081000	4.710800000
1	0.260074000	-6.190140000	4.717891000
1	-0.050364000	-9.519702000	1.056541000
1	1.754739000	-7.865777000	1.033123000
1	-2.658683000	-2.268243000	3.322788000
6	7.448283000	-7.427451000	0.729866000
6	7.952999000	-6.800026000	-0.428540000
6	8.233445000	-8.424544000	1.346056000
6	9.196846000	-7.158651000	-0.952342000
1	7.355151000	-6.051257000	-0.937839000
6	9.478917000	-8.779039000	0.823329000
1	7.881544000	-8.900858000	2.255220000
6	9.965449000	-8.148792000	-0.328389000
1	9.563014000	-6.671824000	-1.850337000
1	10.072818000	-9.540367000	1.318305000
1	10.932423000	-8.425842000	-0.734783000
6	1.562712000	-0.744347000	5.376939000
6	0.668297000	0.219674000	4.862907000
6	2.274649000	-0.432986000	6.556114000
6	0.504033000	1.451412000	5.505181000
1	0.111564000	0.027715000	3.951303000
6	2.104836000	0.796334000	7.196042000
1	2.941781000	-1.168262000	6.993285000
6	1.219479000	1.746195000	6.672446000
1	-0.176280000	2.183479000	5.082210000
1	2.656657000	1.009460000	8.105807000
1	1.088728000	2.702800000	7.167596000
6	-2.042656000	-9.817145000	2.903879000
6	-2.600197000	-10.304030000	1.701870000
6	-2.540295000	-10.323823000	4.123107000
6	-3.618232000	-11.260630000	1.720421000
1	-2.252473000	-9.913199000	0.751104000
6	-3.555998000	-11.282332000	4.139401000
1	-2.106322000	-9.991424000	5.060277000
6	-4.100013000	-11.754421000	2.938789000
1	-4.037534000	-11.617948000	0.785452000
1	-3.915531000	-11.668231000	5.087656000
1	-4.887961000	-12.499980000	2.952446000

Table 4.21. $^{5}Re_{H}$:

26	-2.951230000	-0.889579000	0.994993000
6	-4.711124000	-2.448332000	5.138675000
1	-5.741063000	-2.774891000	5.033336000
6	-3.869687000	-3.098392000	6.045112000
1	-4.255109000	-3.914033000	6.647702000
6	-2.535579000	-2.693669000	6.177378000
1	-1.884351000	-3.188870000	6.889971000
6	-2.045922000	-1.641604000	5.392424000
1	-1.013429000	-1.325090000	5.490520000
6	-2.882136000	-0.993271000	4.476959000
1	-2.493076000	-0.182362000	3.871718000
6	-4.225188000	-1.393044000	4.340522000
6	-5.161122000	-0.677531000	3.440459000
6	-6.431504000	-0.307471000	3.929310000
1	-6.688217000	-0.552566000	4.951684000
6	-7.318580000	0.401340000	3.125928000
1	-8.287525000	0.701293000	3.508751000
6	-6.933642000	0.738585000	1.824197000
1	-7.593961000	1.297600000	1.171572000
6	-5.677259000	0.338899000	1.376279000
6	-5.255360000	0.568863000	-0.068964000
1	-5.862834000	1.383961000	-0.487826000
6	-5.518581000	-0.700904000	-0.864512000
6	-6.521512000	-0.752942000	-1.830357000
1	-7.139577000	0.115525000	-2.027920000
6	-6.701931000	-1.946671000	-2.538549000
1	-7.478197000	-2.030055000	-3.290956000
6	-5.870894000	-3.024783000	-2.256780000
1	-5.996606000	-3.968228000	-2.772390000
6	-4.867399000	-2.919824000	-1.267288000
6	-3.999243000	-4.089335000	-1.002863000
6	-3.753772000	-4.542901000	0.303802000
1	-4.152271000	-3.994056000	1.145065000
6	-2.978471000	-5.686275000	0.517736000
1	-2.791813000	-6.029285000	1.529062000
6	-2.439311000	-6.386870000	-0.566685000
1	-1.834326000	-7.270019000	-0.390800000
6	-2.680820000	-5.944945000	-1.874350000
1	-2.263060000	-6.482843000	-2.718978000
6	-3.462749000	-4.808993000	-2.092138000
1	-3.639969000	-4.464504000	-3.106721000
6	-3.245685000	0.953311000	-1.528244000
1	-2.968326000	1.982428000	-1.780275000
1	-4.028956000	0.653431000	-2.233748000
6	-2.045876000	0.048900000	-1.731498000

6	-1.214207000	0.179893000	-2.849641000
1	-1.386606000	0.978266000	-3.563031000
6	-0.164082000	-0.724394000	-3.028378000
1	0.491350000	-0.635030000	-3.887505000
6	0.034415000	-1.742551000	-2.086990000
1	0.837566000	-2.460503000	-2.196693000
6	-0.818422000	-1.815685000	-0.988564000
1	-0.721578000	-2.567086000	-0.216195000
6	-3.497278000	2.192838000	0.615006000
1	-3.930903000	2.080919000	1.612349000
1	-4.013247000	3.025242000	0.112872000
6	-2.025116000	2.481376000	0.723243000
6	-1.477593000	3.693009000	0.282022000
1	-2.124245000	4.431364000	-0.185531000
6	-0.115994000	3.969492000	0.451695000
1	0.294082000	4.913443000	0.110535000
6	0.709948000	3.020277000	1.070013000
1	1.766401000	3.227920000	1.204761000
6	0.183501000	1.806498000	1.515566000
1	0.812224000	1.061399000	1.989006000
6	-1.185861000	1.526702000	1.349306000
7	-4.805561000	-0.355016000	2.158754000
7	-4.708934000	-1.752906000	-0.571659000
7	-3.795394000	0.909195000	-0.133685000
7	-1.832618000	-0.930510000	-0.823188000
8	-1.702094000	0.342538000	1.777366000
8	-2.404244000	-2.449213000	1.767670000
6	1.874094000	-5.690312000	3.317115000
6	0.867596000	-2.031609000	3.036417000
6	1.899576000	-1.402482000	3.748481000
1	0.079308000	-1.434450000	2.587255000
6	0.855674000	-3.421379000	2.894676000
1	0.060426000	-3.896901000	2.328967000
6	1.881597000	-4.227560000	3.453442000
6	2.920910000	-3.564972000	4.156795000
6	2.925413000	-2.177916000	4.305286000
1	3.725539000	-1.701705000	4.863348000
1	3.711939000	-4.155021000	4.605395000
6	3.143950000	-6.408994000	3.157629000
6	4.226410000	-5.834451000	2.441127000
1	6.241170000	-6.055229000	1.725407000
6	5.434631000	-6.514140000	2.288715000
1	4.100796000	-4.856610000	1.989503000
6	5.608725000	-7.785888000	2.851392000
6	3.343241000	-7.697939000	3.717851000
6	4.555999000	-8.370652000	3.568233000

1	2.546046000	-8.153634000	4.294271000
1	4.685316000	-9.348939000	4.020361000
6	-0.483036000	-5.968359000	4.152826000
6	0.608587000	-6.426827000	3.367534000
6	0.426952000	-7.640250000	2.650955000
6	-0.769209000	-8.354445000	2.725019000
6	-1.829156000	-7.887562000	3.516331000
6	-1.675645000	-6.688232000	4.227495000
1	-2.482428000	-6.321961000	4.855402000
1	-0.371896000	-5.057546000	4.730304000
1	-0.875491000	-9.280354000	2.167885000
1	1.232995000	-8.009400000	2.027195000
1	-1.970154000	-2.649850000	2.615113000
1	1.905370000	-0.323127000	3.867615000
1	6.550624000	-8.311801000	2.735468000
1	-2.752971000	-8.452844000	3.584903000

Table 4.22. $^{5}\mathbf{Re}_{Cl}$:

26	-2.893970000	-0.307985000	-0.147365000
6	-5.745168000	-2.089605000	3.145613000
1	-6.578266000	-2.619973000	2.694636000
6	-5.188216000	-2.562704000	4.336373000
1	-5.595754000	-3.450842000	4.806770000
6	-4.104949000	-1.893501000	4.918184000
1	-3.676420000	-2.257788000	5.845507000
6	-3.579190000	-0.751641000	4.300061000
1	-2.750568000	-0.219394000	4.755564000
6	-4.124412000	-0.280606000	3.100778000
1	-3.706291000	0.599894000	2.626480000
6	-5.212300000	-0.950830000	2.509543000
6	-5.854948000	-0.446148000	1.272605000
6	-7.258736000	-0.321528000	1.224478000
1	-7.836924000	-0.592509000	2.098434000
6	-7.882317000	0.184007000	0.088065000
1	-8.960071000	0.297434000	0.057111000
6	-7.097210000	0.561317000	-1.006943000
1	-7.547433000	0.965681000	-1.906011000
6	-5.716250000	0.403541000	-0.923382000
6	-4.821684000	0.672953000	-2.126828000
1	-5.351678000	1.341730000	-2.820192000
6	-4.542910000	-0.648586000	-2.827284000
6	-5.000500000	-0.901039000	-4.118540000
1	-5.570651000	-0.151792000	-4.656036000
6	-4.701650000	-2.139598000	-4.699758000
1	-5.041862000	-2.374765000	-5.702026000
6	-3.978073000	-3.069847000	-3.962330000
1	-3.765060000	-4.050542000	-4.368040000
6	-3.548562000	-2.767693000	-2.650221000
6	-2.837223000	-3.805292000	-1.870492000
6	-3.215141000	-4.107530000	-0.550893000
1	-3.978011000	-3.515327000	-0.064161000
6	-2.606572000	-5.165434000	0.130501000
1	-2.909925000	-5.397474000	1.145561000
6	-1.604919000	-5.921420000	-0.489164000
1	-1.135135000	-6.740481000	0.045195000
6	-1.212985000	-5.620700000	-1.800259000
1	-0.434296000	-6.200946000	-2.284028000
6	-1.832351000	-4.576965000	-2.490546000
1	-1.525434000	-4.347510000	-3.506680000
6	-2.506500000	1.408958000	-2.769968000
1	-2.301980000	2.467610000	-2.960813000
1	-2.914717000	0.992254000	-3.698164000
6	-1.204030000	0.699730000	-2.456471000

6	-0.045169000	0.936815000	-3.205539000
1	-0.052911000	1.681617000	-3.993846000
6	1.113175000	0.209513000	-2.920103000
1	2.023618000	0.383055000	-3.482752000
6	1.089271000	-0.745713000	-1.895101000
1	1.970529000	-1.323403000	-1.647530000
6	-0.089980000	-0.930201000	-1.179037000
1	-0.188812000	-1.642077000	-0.370119000
6	-3.757440000	2.617283000	-0.992749000
1	-4.518797000	2.445701000	-0.227323000
1	-4.167687000	3.329753000	-1.724408000
6	-2.513458000	3.178587000	-0.359718000
6	-2.051874000	4.467241000	-0.657076000
1	-2.577521000	5.064653000	-1.397792000
6	-0.936666000	4.999759000	0.000601000
1	-0.592725000	6.000446000	-0.235845000
6	-0.274741000	4.234294000	0.970998000
1	0.587189000	4.643492000	1.487627000
6	-0.718361000	2.947297000	1.280753000
1	-0.219170000	2.342466000	2.029201000
6	-1.837058000	2.408325000	0.618644000
7	-5.102794000	-0.090076000	0.187287000
7	-3.826589000	-1.547760000	-2.102447000
7	-3.527129000	1.286600000	-1.679742000
7	-1.206853000	-0.212258000	-1.457820000
8	-2.265534000	1.151498000	0.909046000
8	-2.373130000	-1.718887000	0.910877000
6	3.406231000	-2.232108000	3.370409000
6	4.171654000	-0.876108000	6.834193000
6	5.559818000	-0.755602000	6.760867000
1	3.645403000	-0.586466000	7.735617000
6	3.474052000	-1.361415000	5.728931000
1	2.393922000	-1.435228000	5.779938000
6	4.142609000	-1.728866000	4.531466000
6	5.555234000	-1.586966000	4.504491000
6	6.261172000	-1.108431000	5.607466000
1	7.340397000	-1.021681000	5.576217000
17	6.475004000	-0.124793000	8.201219000
1	6.104014000	-1.882300000	3.617751000
6	3.884409000	-1.943248000	2.013684000
6	4.503190000	-0.706837000	1.693659000
1	5.388838000	0.536670000	0.167328000
6	4.934026000	-0.419078000	0.397905000
1	4.622109000	0.043642000	2.466472000
6	4.760522000	-1.377777000	-0.599713000
17	5.295226000	-0.998944000	-2.305950000

6	3.740756000	-2.890319000	0.966461000
6	4.179672000	-2.617806000	-0.330011000
1	3.305066000	-3.858904000	1.182669000
1	4.090153000	-3.363618000	-1.111202000
6	2.024760000	-3.908078000	4.646485000
6	2.182143000	-3.019038000	3.551677000
6	1.104212000	-2.922113000	2.633374000
6	-0.065497000	-3.666328000	2.790094000
6	-0.167634000	-4.528895000	3.881224000
17	-1.691937000	-5.514210000	4.098824000
6	0.862004000	-4.661474000	4.812257000
1	0.764858000	-5.348520000	5.644073000
1	2.834535000	-4.026158000	5.356876000
1	-0.876015000	-3.569893000	2.076776000
1	1.180550000	-2.234811000	1.798692000
1	-2.250103000	-1.671128000	1.877045000

Table 4.23. $^{5}\mathbf{Re}_{NO2}$:

26	-1.970514000	-0.504441000	0.690889000
6	-4.414960000	-3.931884000	2.874587000
1	-4.991956000	-4.515998000	2.164525000
6	-3.893711000	-4.550919000	4.011964000
1	-4.075196000	-5.606655000	4.181593000
6	-3.140348000	-3.808392000	4.929370000
1	-2.752099000	-4.284710000	5.823855000
6	-2.893451000	-2.451384000	4.690593000
1	-2.312665000	-1.870377000	5.399271000
6	-3.397297000	-1.830573000	3.544205000
1	-3.188505000	-0.782759000	3.364559000
6	-4.172327000	-2.564986000	2.627496000
6	-4.826349000	-1.910171000	1.470644000
6	-6.178934000	-2.200323000	1.194638000
1	-6.700748000	-2.905385000	1.828238000
6	-6.844485000	-1.550401000	0.160655000
1	-7.889443000	-1.760142000	-0.037944000
6	-6.152752000	-0.603528000	-0.601181000
1	-6.640871000	-0.066261000	-1.405975000
6	-4.812259000	-0.363306000	-0.310690000
6	-3.988739000	0.568489000	-1.189394000
1	-4.662755000	1.304715000	-1.651164000
6	-3.328697000	-0.246529000	-2.291714000
6	-3.615253000	-0.018020000	-3.637414000
1	-4.318139000	0.754426000	-3.929057000
6	-2.973946000	-0.812027000	-4.595982000
1	-3.175064000	-0.670990000	-5.652108000
6	-2.090560000	-1.798739000	-4.170896000
1	-1.612658000	-2.454594000	-4.887428000
6	-1.843552000	-1.988380000	-2.792806000
6	-0.941108000	-3.075594000	-2.353335000
6	-1.279505000	-3.900226000	-1.265643000
1	-2.185870000	-3.697659000	-0.708612000
6	-0.466927000	-4.983439000	-0.918197000
1	-0.740707000	-5.608380000	-0.076339000
6	0.701171000	-5.246693000	-1.644141000
1	1.329108000	-6.089574000	-1.374731000
6	1.054634000	-4.424835000	-2.721617000
1	1.961365000	-4.621956000	-3.283952000
6	0.235869000	-3.351088000	-3.078900000
1	0.519627000	-2.713947000	-3.911025000
6	-1.955033000	2.039860000	-1.179724000
1	-1.936567000	3.074230000	-0.822106000
1	-2.273899000	2.072097000	-2.228328000
6	-0.546785000	1.483564000	-1.107199000

6	0.516193000	2.114630000	-1.765502000
1	0.341863000	3.024699000	-2.329150000
6	1.795631000	1.560961000	-1.682013000
1	2.630346000	2.039452000	-2.181982000
6	1.988103000	0.383739000	-0.946423000
1	2.966505000	-0.073823000	-0.867949000
6	0.893481000	-0.195902000	-0.311295000
1	0.954221000	-1.105117000	0.272099000
6	-3.611761000	2.166011000	0.673210000
1	-4.310712000	1.534462000	1.227585000
1	-4.196509000	2.937632000	0.150220000
6	-2.632184000	2.808182000	1.616400000
6	-2.601552000	4.196616000	1.805119000
1	-3.273645000	4.827639000	1.228864000
6	-1.732242000	4.776902000	2.735959000
1	-1.721751000	5.852184000	2.874098000
6	-0.880808000	3.957316000	3.490157000
1	-0.205649000	4.400661000	4.214677000
6	-0.895589000	2.572500000	3.315412000
1	-0.245539000	1.924034000	3.891678000
6	-1.766429000	1.984357000	2.378480000
7	-4.154749000	-1.002369000	0.695845000
7	-2.463246000	-1.199795000	-1.868431000
7	-2.949417000	1.270217000	-0.362530000
7	-0.343270000	0.355524000	-0.392821000
8	-1.773403000	0.636512000	2.208072000
8	-1.162023000	-2.019490000	1.219269000
6	3.392533000	-2.027014000	6.423072000
6	4.427435000	1.621959000	6.369503000
6	4.692180000	1.786819000	5.006281000
1	4.533287000	2.465471000	7.039091000
6	4.018206000	0.374649000	6.829992000
1	3.790368000	0.247792000	7.881377000
6	3.853533000	-0.721119000	5.941238000
6	4.146574000	-0.510693000	4.566922000
6	4.566339000	0.728891000	4.100360000
1	4.806266000	0.892022000	3.058208000
1	4.068567000	-1.339225000	3.873521000
6	2.522674000	-2.842223000	5.582666000
6	1.606943000	-2.241785000	4.672573000
1	0.083978000	-2.525525000	3.179708000
6	0.781423000	-3.004061000	3.856619000
1	1.527263000	-1.162707000	4.630996000
6	0.864457000	-4.402210000	3.930643000
6	2.562186000	-4.265053000	5.632250000
6	1.750161000	-5.037677000	4.814175000

1	3.265186000	-4.756578000	6.293212000
1	1.797809000	-6.118478000	4.834483000
6	5.092904000	-2.183492000	8.263054000
6	3.808757000	-2.501557000	7.744921000
6	2.942489000	-3.286560000	8.552483000
6	3.334758000	-3.730629000	9.810372000
6	4.610628000	-3.400575000	10.276631000
6	5.496749000	-2.632420000	9.515754000
1	6.479812000	-2.408353000	9.908568000
1	5.783541000	-1.605603000	7.661024000
1	2.674035000	-4.314317000	10.437697000
1	1.945305000	-3.517960000	8.198059000
1	-1.090743000	-2.965893000	1.444131000
7	5.103793000	3.099085000	4.509605000
8	5.298828000	3.225819000	3.264779000
8	5.234492000	4.036923000	5.346941000
7	0.028613000	-5.222154000	3.076019000
8	0.112256000	-6.479493000	3.169143000
8	-0.763340000	-4.650903000	2.253884000
7	5.028380000	-3.871281000	11.599435000
8	6.179507000	-3.544461000	12.006106000
8	4.213115000	-4.577711000	12.258778000

Table 4.24. $^{5}\mathbf{Pr}_{\mathrm{OMe}}$:

26	-2.474417000	-0.002184000	-0.097955000
6	-5.608645000	-1.338216000	3.082341000
1	-6.553917000	-1.697571000	2.687635000
6	-5.126407000	-1.843349000	4.291804000
1	-5.706202000	-2.580156000	4.837569000
6	-3.899194000	-1.396338000	4.799241000
1	-3.524373000	-1.778809000	5.741969000
6	-3.156977000	-0.444215000	4.089049000
1	-2.215219000	-0.083393000	4.487729000
6	-3.633729000	0.065207000	2.874233000
1	-3.064511000	0.836586000	2.362915000
6	-4.865335000	-0.383121000	2.358095000
6	-5.416653000	0.155449000	1.092684000
6	-6.772616000	0.518759000	1.002997000
1	-7.400752000	0.434352000	1.880454000
6	-7.282172000	1.017266000	-0.193686000
1	-8.321594000	1.317183000	-0.265074000
6	-6.433535000	1.136151000	-1.298177000
1	-6.800867000	1.512285000	-2.245944000
6	-5.098247000	0.755558000	-1.168656000
6	-4.178204000	0.751419000	-2.386715000
1	-4.527333000	1.525914000	-3.085828000
6	-4.296607000	-0.596005000	-3.099016000
6	-4.553148000	-0.668720000	-4.472061000
1	-4.653580000	0.231090000	-5.069065000
6	-4.696204000	-1.936108000	-5.051083000
1	-4.913184000	-2.032684000	-6.109232000
6	-4.581706000	-3.071417000	-4.251765000
1	-4.732143000	-4.053092000	-4.682312000
6	-4.311302000	-2.930607000	-2.873838000
6	-4.196221000	-4.094950000	-1.963335000
6	-4.405321000	-3.929315000	-0.579884000
1	-4.641613000	-2.942417000	-0.201594000
6	-4.332358000	-5.021382000	0.287235000
1	-4.510112000	-4.878742000	1.348119000
6	-4.044633000	-6.299175000	-0.210734000
1	-4.001460000	-7.149410000	0.462090000
6	-3.821923000	-6.473907000	-1.581842000
1	-3.591008000	-7.458234000	-1.975340000
6	-3.896450000	-5.382173000	-2.450653000
1	-3.700923000	-5.536524000	-3.506381000
6	-1.698517000	0.659936000	-2.917338000
1	-0.896250000	1.402654000	-2.833467000
1	-2.046876000	0.678762000	-3.957756000
6	-1.109174000	-0.701229000	-2.591092000

6	-0.354697000	-1.406365000	-3.532168000
1	-0.233699000	-1.009995000	-4.534344000
6	0.247432000	-2.614064000	-3.163319000
1	0.843995000	-3.166274000	-3.881079000
6	0.077374000	-3.095132000	-1.861439000
1	0.539507000	-4.017549000	-1.533989000
6	-0.696954000	-2.356823000	-0.968010000
1	-0.853415000	-2.660423000	0.058743000
6	-2.679769000	2.565445000	-1.621292000
1	-3.502934000	2.751851000	-0.922532000
1	-2.878284000	3.150855000	-2.531914000
6	-1.372953000	3.004227000	-1.009482000
6	-0.632828000	4.044415000	-1.596525000
1	-0.979478000	4.476728000	-2.532185000
6	0.520621000	4.548619000	-0.989175000
1	1.073278000	5.357459000	-1.453817000
6	0.942160000	4.008080000	0.233409000
1	1.826647000	4.402197000	0.724102000
6	0.228485000	2.967440000	0.831844000
1	0.539376000	2.545106000	1.780810000
6	-0.926968000	2.447107000	0.219497000
7	-4.595763000	0.286440000	0.007384000
7	-4.179885000	-1.694864000	-2.325854000
7	-2.766815000	1.084749000	-1.967942000
7	-1.275504000	-1.184311000	-1.330904000
8	-1.605873000	1.418946000	0.806536000
8	-1.013341000	-2.343483000	2.224564000
6	0.284017000	-2.833270000	2.808423000
6	-0.528707000	-2.416277000	6.536924000
6	0.329161000	-1.373062000	6.926526000
1	-1.178387000	-2.857386000	7.284137000
6	-0.506312000	-2.879318000	5.226109000
1	-1.148535000	-3.710810000	4.951973000
6	0.357968000	-2.315884000	4.259178000
6	1.213289000	-1.286173000	4.671395000
6	1.206624000	-0.812152000	5.991137000
1	1.890441000	-0.020362000	6.271212000
1	1.906611000	-0.845121000	3.966399000
6	1.357170000	-2.235127000	1.886668000
6	1.247852000	-0.896313000	1.471581000
1	2.087990000	0.730716000	0.351861000
6	2.211741000	-0.304249000	0.646828000
1	0.390868000	-0.308653000	1.778759000
6	3.312415000	-1.058838000	0.217818000
6	2.468702000	-2.973921000	1.439157000
6	3.434867000	-2.397349000	0.615687000

1	2.584980000	-4.010009000	1.731303000
1	4.293386000	-2.963949000	0.274563000
6	1.183463000	-5.101801000	3.585718000
6	0.280728000	-4.371659000	2.783689000
6	-0.579333000	-5.088592000	1.943974000
6	-0.548171000	-6.489631000	1.887865000
6	0.363307000	-7.193318000	2.683344000
6	1.230364000	-6.491256000	3.536315000
1	1.921207000	-7.055650000	4.151358000
1	1.850104000	-4.575046000	4.260227000
1	-1.235064000	-7.006725000	1.228688000
1	-1.301872000	-4.554485000	1.339072000
1	-1.690540000	-2.314054000	2.932038000
8	0.233331000	-0.984565000	8.251584000
6	1.119505000	0.056555000	8.750080000
1	2.169886000	-0.239925000	8.653311000
1	0.951157000	1.003880000	8.225302000
1	0.862511000	0.166997000	9.802271000
8	0.485848000	-8.575173000	2.711383000
6	-0.382798000	-9.377051000	1.868691000
1	-1.437659000	-9.223419000	2.125980000
1	-0.102194000	-10.409523000	2.071381000
1	-0.224933000	-9.152303000	0.807151000
8	4.324353000	-0.577356000	-0.601744000
6	4.306738000	0.821469000	-0.993406000
1	5.208056000	0.961382000	-1.588551000
1	3.422763000	1.055892000	-1.598501000
1	4.334891000	1.479490000	-0.117427000

Table 4.25. $^{5}Pr_{tBu}$:

26	-3.059196000	0.264988000	0.372507000
6	-6.225377000	0.788381000	4.091969000
1	-7.277288000	0.862801000	3.834120000
6	-5.853823000	0.234038000	5.319044000
1	-6.618529000	-0.099490000	6.012664000
6	-4.498330000	0.104226000	5.647925000
1	-4.206765000	-0.326410000	6.600008000
6	-3.517129000	0.538570000	4.747751000
1	-2.467317000	0.458191000	5.009106000
6	-3.882110000	1.094335000	3.515448000
1	-3.111219000	1.466055000	2.845499000
6	-5.244083000	1.214523000	3.172734000
6	-5.672059000	1.770853000	1.867223000
6	-6.772429000	2.649369000	1.777856000
1	-7.264157000	2.974743000	2.685765000
6	-7.198634000	3.108741000	0.535085000
1	-8.035803000	3.793801000	0.461540000
6	-6.532510000	2.679131000	-0.620773000
1	-6.848128000	3.009581000	-1.603660000
6	-5.445505000	1.820409000	-0.478911000
6	-4.722872000	1.221616000	-1.688274000
1	-5.072921000	1.721873000	-2.602185000
6	-5.074604000	-0.264279000	-1.749219000
6	-5.895923000	-0.822198000	-2.726750000
1	-6.301308000	-0.208012000	-3.522520000
6	-6.181061000	-2.193021000	-2.654070000
1	-6.817871000	-2.657761000	-3.398429000
6	-5.657429000	-2.950413000	-1.607848000
1	-5.901613000	-4.000756000	-1.511437000
6	-4.836031000	-2.335294000	-0.642842000
6	-4.302548000	-3.072302000	0.523688000
6	-4.242993000	-2.446739000	1.784697000
1	-4.612892000	-1.432603000	1.903734000
6	-3.786461000	-3.149590000	2.905083000
1	-3.778813000	-2.659787000	3.873742000
6	-3.373037000	-4.482299000	2.776959000
1	-3.020881000	-5.032734000	3.642851000
6	-3.423652000	-5.109877000	1.524937000
1	-3.098955000	-6.139447000	1.421503000
6	-3.890374000	-4.414059000	0.407370000
1	-3.912336000	-4.905493000	-0.560107000
6	-2.427924000	0.666722000	-2.566364000
1	-1.983788000	1.407978000	-3.241503000
1	-3.097955000	0.047268000	-3.174212000
6	-1.328186000	-0.219722000	-2.004371000

6	-0.203896000	-0.533285000	-2.774804000
1	-0.085786000	-0.099556000	-3.761845000
6	0.766765000	-1.392276000	-2.251668000
1	1.648132000	-1.638615000	-2.833466000
6	0.595941000	-1.910243000	-0.964034000
1	1.338754000	-2.553751000	-0.510028000
6	-0.543288000	-1.557665000	-0.239548000
1	-0.688320000	-1.904110000	0.778248000
6	-2.781584000	2.782025000	-1.284579000
1	-3.470037000	3.208542000	-0.549564000
1	-2.895376000	3.347119000	-2.222160000
6	-1.364743000	2.906760000	-0.778770000
6	-0.429039000	3.686930000	-1.476415000
1	-0.716469000	4.134401000	-2.425323000
6	0.849941000	3.917726000	-0.962582000
1	1.558000000	4.528363000	-1.511796000
6	1.197197000	3.366252000	0.278663000
1	2.181161000	3.554125000	0.697936000
6	0.285567000	2.581128000	0.987174000
1	0.542361000	2.153127000	1.949587000
6	-1.000417000	2.333328000	0.470414000
7	-5.015366000	1.385350000	0.737212000
7	-4.547881000	-1.010193000	-0.743873000
7	-3.235553000	1.356273000	-1.513973000
7	-1.491784000	-0.734654000	-0.756876000
8	-1.878566000	1.551038000	1.159109000
8	-0.418655000	-2.379674000	2.892829000
6	0.682243000	-2.590686000	3.881906000
6	-1.226194000	-1.769261000	7.123821000
6	-0.640049000	-0.569317000	7.566992000
1	-2.022039000	-2.230632000	7.696159000
6	-0.784130000	-2.409074000	5.960732000
1	-1.237918000	-3.355839000	5.679974000
6	0.262023000	-1.879629000	5.184533000
6	0.845086000	-0.678771000	5.617702000
6	0.402246000	-0.042271000	6.780469000
1	0.891760000	0.877673000	7.082886000
1	1.658651000	-0.241224000	5.052690000
6	1.913021000	-1.956512000	3.219324000
6	1.771477000	-0.816172000	2.407928000
1	2.727173000	0.659292000	1.195013000
6	2.885326000	-0.212994000	1.821370000
1	0.784292000	-0.405906000	2.234910000
6	4.189938000	-0.706794000	2.024627000
6	3.205136000	-2.456490000	3.424915000
6	4.320294000	-1.840832000	2.841903000

1	3.354132000	-3.337721000	4.037849000
1	5.297730000	-2.266197000	3.033131000
6	1.377994000	-4.638159000	5.276702000
6	0.866878000	-4.104304000	4.085118000
6	0.584329000	-4.995041000	3.035755000
6	0.795358000	-6.366555000	3.183625000
6	1.306608000	-6.913954000	4.377855000
6	1.593718000	-6.015085000	5.418186000
1	1.989668000	-6.378318000	6.358455000
1	1.608202000	-3.980731000	6.108109000
1	0.565221000	-7.021181000	2.348595000
1	0.194530000	-4.603080000	2.103645000
1	-1.260688000	-2.688089000	3.285117000
6	-1.070171000	0.151345000	8.862432000
6	-1.524154000	1.599283000	8.528765000
1	-0.722000000	2.177545000	8.058535000
1	-2.382048000	1.595098000	7.846182000
1	-1.819965000	2.121587000	9.446275000
6	-2.235169000	-0.569986000	9.577449000
1	-3.131693000	-0.621947000	8.947576000
1	-1.961984000	-1.588828000	9.874509000
1	-2.502727000	-0.020518000	10.486448000
6	0.136528000	0.206876000	9.840901000
1	0.474604000	-0.802706000	10.100332000
1	0.984556000	0.746411000	9.406536000
1	-0.151361000	0.720333000	10.765964000
6	1.529710000	-8.436037000	4.496267000
6	0.179234000	-9.175122000	4.285639000
1	0.326273000	-10.258960000	4.361933000
1	-0.248698000	-8.963076000	3.299640000
1	-0.551770000	-8.875272000	5.045530000
6	2.540595000	-8.895297000	3.409163000
1	2.704802000	-9.977157000	3.479874000
1	3.506000000	-8.393181000	3.538540000
1	2.177644000	-8.675329000	2.399479000
6	2.090980000	-8.839945000	5.878933000
1	1.406645000	-8.568147000	6.690894000
1	3.062891000	-8.372706000	6.074291000
1	2.232694000	-9.925703000	5.913721000
6	6.735535000	-0.687945000	1.707734000
1	6.929319000	-0.681013000	2.786288000
1	7.556859000	-0.151941000	1.219445000
1	6.761890000	-1.726511000	1.358364000
6	5.393314000	-0.002958000	1.363310000
6	5.460946000	1.470741000	1.851588000
1	5.589609000	1.514660000	2.939016000

1	4.550199000	2.023606000	1.596545000
1	6.309628000	1.985298000	1.385169000
6	5.219731000	-0.023158000	-0.180649000
1	5.183995000	-1.053654000	-0.553193000
1	6.063174000	0.485428000	-0.662842000
1	4.298868000	0.483354000	-0.489750000

Table 4.26. $^{5}\mathbf{Pr}_{Ph}$:

26	-2.501627000	-0.068452000	0.529314000
6	-5.481726000	-1.566130000	3.773737000
1	-6.097735000	-2.366038000	3.374036000
6	-5.135584000	-1.567832000	5.126292000
1	-5.480398000	-2.369026000	5.771204000
6	-4.355508000	-0.529378000	5.650554000
1	-4.107609000	-0.517823000	6.706885000
6	-3.901289000	0.493076000	4.809416000
1	-3.297738000	1.300318000	5.210038000
6	-4.225959000	0.488443000	3.449065000
1	-3.870237000	1.287903000	2.807835000
6	-5.032896000	-0.536774000	2.921374000
6	-5.542412000	-0.458489000	1.531796000
6	-6.920534000	-0.617600000	1.308292000
1	-7.565481000	-0.840418000	2.148339000
6	-7.450500000	-0.424663000	0.034262000
1	-8.515809000	-0.525055000	-0.140583000
6	-6.590664000	-0.067631000	-1.002509000
1	-6.966601000	0.110566000	-2.003429000
6	-5.221529000	0.042542000	-0.746980000
6	-4.295218000	0.363784000	-1.915178000
1	-4.778598000	1.159822000	-2.502877000
6	-4.194108000	-0.843716000	-2.849385000
6	-4.206040000	-0.673618000	-4.239668000
1	-4.264677000	0.316115000	-4.679701000
6	-4.170546000	-1.816238000	-5.048245000
1	-4.200148000	-1.723098000	-6.128454000
6	-4.125145000	-3.075579000	-4.453170000
1	-4.136730000	-3.965549000	-5.069355000
6	-4.110164000	-3.179996000	-3.045991000
6	-4.065453000	-4.484325000	-2.342082000
6	-4.478079000	-4.571045000	-0.997742000
1	-4.827070000	-3.672828000	-0.503030000
6	-4.449293000	-5.792483000	-0.322445000
1	-4.783120000	-5.846825000	0.708863000
6	-4.001253000	-6.949324000	-0.972975000
1	-3.979672000	-7.898034000	-0.447269000
6	-3.581460000	-6.873980000	-2.306117000
1	-3.226736000	-7.763653000	-2.815760000
6	-3.613312000	-5.653178000	-2.985197000
1	-3.263402000	-5.614259000	-4.011325000
6	-1.797620000	0.650618000	-2.275026000
1	-1.032672000	1.375998000	-1.972438000
1	-2.003416000	0.824221000	-3.339609000
6	-1.263214000	-0.748941000	-2.070926000

6	-0.583656000	-1.434513000	-3.080490000
1	-0.450067000	-0.969618000	-4.050523000
6	-0.094425000	-2.719249000	-2.826686000
1	0.430513000	-3.267170000	-3.601536000
6	-0.299128000	-3.291547000	-1.567347000
1	0.059453000	-4.285913000	-1.334757000
6	-0.981512000	-2.556848000	-0.599908000
1	-1.157244000	-2.956288000	0.389102000
6	-3.164435000	2.402742000	-1.120440000
1	-4.016081000	2.455413000	-0.432473000
1	-3.455383000	2.909082000	-2.053620000
6	-1.970476000	3.101007000	-0.523381000
6	-1.404263000	4.215040000	-1.165947000
1	-1.798276000	4.524295000	-2.131127000
6	-0.363549000	4.939924000	-0.579025000
1	0.057325000	5.800135000	-1.087273000
6	0.120140000	4.548611000	0.676916000
1	0.921679000	5.108673000	1.147901000
6	-0.422946000	3.441444000	1.331821000
1	-0.060717000	3.135835000	2.307687000
6	-1.465011000	2.702527000	0.740888000
7	-4.696969000	-0.160257000	0.491952000
7	-4.157192000	-2.063122000	-2.274552000
7	-2.980627000	0.919102000	-1.414681000
7	-1.449572000	-1.309148000	-0.845630000
8	-1.976701000	1.606483000	1.375399000
8	-1.204683000	-0.647692000	2.367690000
6	-0.013768000	-1.352886000	2.958168000
6	-0.105487000	0.452796000	6.338956000
6	1.180807000	1.020960000	6.454271000
1	-0.815805000	0.575507000	7.150115000
6	-0.463554000	-0.302049000	5.224184000
1	-1.449252000	-0.749316000	5.174233000
6	0.444956000	-0.513365000	4.169229000
6	1.730040000	0.039061000	4.282160000
6	2.088231000	0.793106000	5.404331000
1	3.080911000	1.228031000	5.452239000
1	2.459662000	-0.110284000	3.496426000
6	1.069830000	-1.424256000	1.862460000
6	1.342594000	-0.276134000	1.093618000
1	2.555181000	0.628996000	-0.436022000
6	2.355786000	-0.273876000	0.132933000
1	0.767185000	0.629781000	1.249870000
6	3.137599000	-1.421357000	-0.097200000
6	1.842823000	-2.570906000	1.625740000
6	2.859443000	-2.568542000	0.661936000

1	1.662543000	-3.475390000	2.192946000
1	3.449013000	-3.466314000	0.504616000
6	0.294200000	-3.507931000	4.283096000
6	-0.503453000	-2.731423000	3.422339000
6	-1.738195000	-3.258026000	3.016996000
6	-2.148660000	-4.528785000	3.431777000
6	-1.345527000	-5.319774000	4.272654000
6	-0.115486000	-4.776176000	4.695131000
1	0.509675000	-5.338209000	5.380853000
1	1.231806000	-3.107291000	4.654188000
1	-3.100637000	-4.916816000	3.083868000
1	-2.397992000	-2.660867000	2.401456000
1	-1.175100000	0.323093000	2.552757000
6	4.241121000	-1.411516000	-1.109020000
6	3.997041000	-1.779066000	-2.443995000
6	5.544136000	-1.033008000	-0.739150000
6	5.030213000	-1.769148000	-3.387411000
1	2.993861000	-2.072740000	-2.738616000
6	6.577429000	-1.022913000	-1.682435000
1	5.744940000	-0.748203000	0.288950000
6	6.323283000	-1.390775000	-3.008681000
1	4.827745000	-2.056770000	-4.414495000
1	7.578051000	-0.729271000	-1.381927000
1	7.125313000	-1.383490000	-3.739493000
6	1.564103000	1.821746000	7.645489000
6	0.633090000	2.672505000	8.273985000
6	2.867574000	1.749254000	8.175889000
6	0.993447000	3.425757000	9.394446000
1	-0.368810000	2.764542000	7.866514000
6	3.227469000	2.502425000	9.296478000
1	3.592802000	1.079166000	7.725402000
6	2.292099000	3.343715000	9.910359000
1	0.264416000	4.081755000	9.859326000
1	4.233848000	2.425941000	9.695397000
1	2.571762000	3.928059000	10.780739000
6	-1.781370000	-6.671157000	4.711266000
6	-3.135071000	-6.938310000	4.997439000
6	-0.850196000	-7.719289000	4.852075000
6	-3.543681000	-8.209933000	5.408603000
1	-3.864506000	-6.137368000	4.927521000
6	-1.258720000	-8.990629000	5.264190000
1	0.194162000	-7.542768000	4.614914000
6	-2.607215000	-9.241648000	5.543495000
1	-4.589340000	-8.392683000	5.635404000
1	-0.526485000	-9.785773000	5.361268000
1	-2.923875000	-10.228225000	5.865408000

Table 4.27. $^{5}Pr_{H}$:

26	-2.852632000	-0.152447000	1.192200000
6	-3.695701000	-2.913644000	4.834364000
1	-3.611382000	-3.942393000	4.500382000
6	-3.267789000	-2.571363000	6.119936000
1	-2.859842000	-3.335756000	6.771631000
6	-3.353569000	-1.245211000	6.561575000
1	-3.028091000	-0.982935000	7.562147000
6	-3.861986000	-0.259136000	5.706233000
1	-3.942695000	0.767608000	6.046319000
6	-4.284129000	-0.595074000	4.415305000
1	-4.699225000	0.165759000	3.763680000
6	-4.209754000	-1.930980000	3.963810000
6	-4.761125000	-2.294522000	2.636830000
6	-5.447799000	-3.507717000	2.451922000
1	-5.526691000	-4.210966000	3.271005000
6	-6.069890000	-3.763538000	1.233431000
1	-6.597977000	-4.697186000	1.073886000
6	-6.061465000	-2.782453000	0.235450000
1	-6.581871000	-2.937565000	-0.697465000
6	-5.370822000	-1.591228000	0.461876000
6	-5.504023000	-0.361945000	-0.439274000
1	-6.108762000	0.322541000	0.168832000
6	-6.281460000	-0.566336000	-1.732406000
6	-7.360384000	0.272778000	-2.041883000
1	-7.677572000	1.044564000	-1.349336000
6	-8.031239000	0.082659000	-3.255621000
1	-8.881231000	0.704541000	-3.514132000
6	-7.608523000	-0.924118000	-4.121036000
1	-8.139776000	-1.101983000	-5.047348000
6	-6.507788000	-1.729146000	-3.763720000
6	-6.005716000	-2.819019000	-4.635610000
6	-5.266933000	-3.881933000	-4.079042000
1	-5.073561000	-3.879303000	-3.013178000
6	-4.802382000	-4.923885000	-4.884362000
1	-4.250417000	-5.745341000	-4.438378000
6	-5.057453000	-4.919244000	-6.261763000
1	-4.697977000	-5.729786000	-6.886919000
6	-5.779579000	-3.862325000	-6.827800000
1	-5.972483000	-3.845352000	-7.895179000
6	-6.250618000	-2.821805000	-6.022771000
1	-6.788434000	-2.000928000	-6.484914000
6	-3.355634000	-0.003889000	-1.773795000
1	-2.607266000	0.792755000	-1.876909000
1	-3.928002000	-0.041256000	-2.705759000
6	-2.640552000	-1.312432000	-1.559252000

6	-2.363709000	-2.189995000	-2.612422000
1	-2.736904000	-1.971169000	-3.604865000
6	-1.627157000	-3.349915000	-2.362051000
1	-1.404728000	-4.038975000	-3.169165000
6	-1.187787000	-3.613139000	-1.059338000
1	-0.609613000	-4.499348000	-0.828553000
6	-1.505021000	-2.706529000	-0.051125000
1	-1.178008000	-2.849718000	0.968135000
6	-4.468498000	1.887086000	-0.602169000
1	-5.094624000	2.059367000	0.280963000
1	-5.054424000	2.151471000	-1.494742000
6	-3.249380000	2.761464000	-0.513440000
6	-2.986588000	3.747199000	-1.477823000
1	-3.630151000	3.818970000	-2.351517000
6	-1.928705000	4.647248000	-1.318771000
1	-1.738830000	5.405639000	-2.070207000
6	-1.128113000	4.568173000	-0.170250000
1	-0.313628000	5.272078000	-0.029851000
6	-1.368665000	3.593203000	0.800741000
1	-0.762907000	3.531419000	1.697716000
6	-2.420934000	2.672111000	0.635597000
7	-4.676291000	-1.384141000	1.620933000
7	-5.870389000	-1.541105000	-2.576448000
7	-4.194972000	0.389285000	-0.605328000
7	-2.214785000	-1.577885000	-0.295894000
8	-2.642763000	1.695828000	1.560798000
8	-1.435298000	-0.831086000	2.766782000
6	0.046143000	-0.640735000	3.100772000
6	-0.514622000	2.764430000	4.826774000
6	0.777428000	3.298455000	4.816154000
1	-1.332634000	3.328606000	5.262767000
6	-0.767008000	1.506849000	4.264645000
1	-1.780329000	1.131324000	4.252183000
6	0.268926000	0.767410000	3.678444000
6	1.565134000	1.317215000	3.660634000
6	1.818379000	2.569299000	4.228643000
1	2.824291000	2.975430000	4.205789000
1	2.377554000	0.768567000	3.196114000
6	0.771840000	-0.790811000	1.756643000
6	0.549550000	0.182321000	0.762370000
1	1.016050000	0.863547000	-1.223780000
6	1.191517000	0.097128000	-0.475471000
1	-0.104685000	1.021934000	0.970517000
6	2.079039000	-0.955259000	-0.738097000
6	1.671951000	-1.833699000	1.489867000
6	2.320183000	-1.914743000	0.249199000

1	1.886436000	-2.575936000	2.248760000
1	3.023366000	-2.720768000	0.065503000
6	1.180147000	-1.511206000	5.248243000
6	0.378400000	-1.750277000	4.119434000
6	-0.114298000	-3.055489000	3.917761000
6	0.192745000	-4.088245000	4.808130000
6	0.999173000	-3.837300000	5.924593000
6	1.488245000	-2.545765000	6.140154000
1	2.110650000	-2.336746000	7.003904000
1	1.567160000	-0.518465000	5.437356000
1	-0.192397000	-5.087160000	4.628270000
1	-0.746375000	-3.262950000	3.062515000
1	-1.927065000	-1.001309000	3.596984000
1	0.970872000	4.272722000	5.252572000
1	1.242944000	-4.637825000	6.615146000
1	2.590168000	-1.013606000	-1.693570000

Table 4.28. $^{5}Pr_{Cl}$:

26	-2.962512000	-0.000870000	-0.288809000
6	-6.112739000	-0.244785000	3.512380000
1	-7.166373000	-0.315274000	3.260438000
6	-5.649774000	-0.810715000	4.702609000
1	-6.348368000	-1.299450000	5.373464000
6	-4.288708000	-0.745897000	5.028751000
1	-3.929442000	-1.171274000	5.960078000
6	-3.395629000	-0.113092000	4.155084000
1	-2.344060000	-0.042407000	4.412639000
6	-3.850432000	0.453701000	2.958475000
1	-3.151441000	0.977409000	2.312177000
6	-5.218096000	0.388322000	2.624140000
6	-5.740651000	0.985833000	1.372522000
6	-6.961256000	1.694440000	1.369067000
1	-7.485644000	1.847422000	2.303673000
6	-7.464128000	2.214256000	0.180473000
1	-8.394376000	2.771118000	0.175693000
6	-6.752123000	2.015191000	-1.009938000
1	-7.122031000	2.399122000	-1.953657000
6	-5.549530000	1.315670000	-0.953793000
6	-4.765739000	0.960275000	-2.219448000
1	-5.191004000	1.507176000	-3.072489000
6	-4.918683000	-0.544160000	-2.444983000
6	-5.679846000	-1.097535000	-3.472629000
1	-6.174956000	-0.460571000	-4.196427000
6	-5.788257000	-2.493438000	-3.543943000
1	-6.375312000	-2.955273000	-4.329785000
6	-5.153700000	-3.283412000	-2.586581000
1	-5.263037000	-4.360388000	-2.601075000
6	-4.397453000	-2.672592000	-1.567786000
6	-3.748443000	-3.451815000	-0.489773000
6	-3.721066000	-2.948147000	0.825848000
1	-4.202099000	-2.001076000	1.054302000
6	-3.156044000	-3.698858000	1.862933000
1	-3.170043000	-3.306622000	2.874517000
6	-2.607374000	-4.960762000	1.595157000
1	-2.192256000	-5.559259000	2.399757000
6	-2.621350000	-5.465193000	0.287195000
1	-2.194229000	-6.439656000	0.076777000
6	-3.190751000	-4.719439000	-0.747302000
1	-3.185242000	-5.114125000	-1.758120000
6	-2.436541000	0.831638000	-3.161251000
1	-2.118726000	1.701421000	-3.748511000
1	-3.027117000	0.195725000	-3.831387000
6	-1.211696000	0.052368000	-2.714441000

6	-0.060059000	0.018836000	-3.507970000
1	-0.016145000	0.599796000	-4.422617000
6	1.031023000	-0.752935000	-3.100244000
1	1.934223000	-0.782389000	-3.699493000
6	0.947039000	-1.469035000	-1.901632000
1	1.778077000	-2.060243000	-1.537917000
6	-0.225386000	-1.391709000	-1.149867000
1	-0.310941000	-1.905790000	-0.199850000
6	-3.036666000	2.704298000	-1.622458000
1	-3.760520000	2.943727000	-0.838514000
1	-3.239132000	3.362170000	-2.481072000
6	-1.637171000	2.948423000	-1.108951000
6	-0.827337000	3.928785000	-1.704456000
1	-1.190185000	4.448066000	-2.588592000
6	0.418534000	4.266003000	-1.168662000
1	1.027459000	5.029807000	-1.639134000
6	0.860074000	3.620629000	-0.005231000
1	1.816111000	3.889873000	0.433291000
6	0.075401000	2.636444000	0.599326000
1	0.399535000	2.136653000	1.505465000
6	-1.172866000	2.278682000	0.056242000
7	-5.046551000	0.819669000	0.210671000
7	-4.282300000	-1.318595000	-1.528694000
7	-3.307190000	1.271367000	-2.028841000
7	-1.288452000	-0.649164000	-1.552536000
8	-1.917888000	1.298499000	0.643165000
8	0.227430000	-2.826467000	1.742566000
6	1.310224000	-3.007770000	2.748047000
6	-0.895582000	-3.374171000	5.874723000
6	-0.643398000	-2.170967000	6.532315000
1	-1.588316000	-4.094091000	6.293469000
6	-0.224817000	-3.637604000	4.677833000
1	-0.395947000	-4.588585000	4.182949000
6	0.687685000	-2.714404000	4.128841000
6	0.925365000	-1.520735000	4.826585000
6	0.264766000	-1.243282000	6.031210000
1	0.461323000	-0.322483000	6.566720000
1	1.631309000	-0.796859000	4.439956000
6	2.384152000	-1.988077000	2.338161000
6	2.004821000	-0.779864000	1.726484000
1	2.661554000	1.089510000	0.867935000
6	2.962683000	0.168643000	1.352037000
1	0.958083000	-0.582246000	1.536041000
6	4.306804000	-0.092946000	1.606208000
6	3.747660000	-2.218346000	2.581443000
6	4.715134000	-1.272827000	2.221362000

1	4.072453000	-3.142947000	3.042606000
1	5.764910000	-1.459903000	2.410488000
6	2.443528000	-5.095681000	3.736569000
6	1.837389000	-4.450024000	2.645079000
6	1.770352000	-5.126440000	1.416132000
6	2.284528000	-6.419256000	1.276043000
6	2.876676000	-7.032621000	2.378182000
6	2.966985000	-6.387923000	3.609316000
1	3.431463000	-6.881040000	4.454375000
1	2.506660000	-4.597614000	4.697752000
1	2.230013000	-6.937559000	0.326331000
1	1.307747000	-4.635919000	0.568617000
1	-0.552865000	-3.359312000	2.002050000
17	-1.523405000	-1.812049000	8.088495000
17	5.559498000	1.138557000	1.117107000
17	3.544570000	-8.718019000	2.204321000

Table 4.29. $^{5}\mathbf{Pr}_{NO2}$:

26	-1.646189000	-0.359766000	1.684655000
6	-3.992275000	-2.565630000	5.039430000
1	-4.269987000	-3.563979000	4.718696000
6	-3.714496000	-2.331618000	6.388699000
1	-3.797020000	-3.144578000	7.101781000
6	-3.338267000	-1.052669000	6.820493000
1	-3.141700000	-0.867602000	7.871034000
6	-3.230411000	-0.009997000	5.891401000
1	-2.949658000	0.984753000	6.219132000
6	-3.512776000	-0.237918000	4.538919000
1	-3.468888000	0.585787000	3.834548000
6	-3.904885000	-1.520796000	4.095872000
6	-4.329654000	-1.729491000	2.690427000
6	-5.386618000	-2.603147000	2.386361000
1	-5.865458000	-3.165145000	3.177443000
6	-5.846103000	-2.694848000	1.075041000
1	-6.657042000	-3.370033000	0.825726000
6	-5.292039000	-1.869744000	0.092376000
1	-5.667177000	-1.891638000	-0.919635000
6	-4.247724000	-1.007648000	0.435528000
6	-3.780204000	0.105230000	-0.507612000
1	-4.348101000	0.978256000	-0.160433000
6	-4.158171000	-0.083186000	-1.970316000
6	-4.770227000	0.956256000	-2.681636000
1	-5.025365000	1.889942000	-2.192639000
6	-5.065201000	0.755394000	-4.036138000
1	-5.554919000	1.534000000	-4.610434000
6	-4.743675000	-0.461159000	-4.633747000
1	-4.998913000	-0.640805000	-5.670297000
6	-4.119033000	-1.468315000	-3.868252000
6	-3.757257000	-2.788513000	-4.437598000
6	-3.618896000	-3.905822000	-3.590303000
1	-3.775891000	-3.775104000	-2.526381000
6	-3.300380000	-5.160340000	-4.114266000
1	-3.217078000	-6.016290000	-3.452052000
6	-3.102823000	-5.320284000	-5.492048000
1	-2.858483000	-6.295651000	-5.899325000
6	-3.224390000	-4.214691000	-6.341912000
1	-3.063125000	-4.328137000	-7.408562000
6	-3.550022000	-2.959797000	-5.820563000
1	-3.618932000	-2.111915000	-6.493709000
6	-1.334670000	-0.044774000	-1.252107000
1	-0.425997000	0.556538000	-1.120149000
1	-1.651982000	0.075608000	-2.292710000
6	-1.013327000	-1.492208000	-0.974783000

6	-0.649771000	-2.387140000	-1.986240000
1	-0.643485000	-2.058915000	-3.017939000
6	-0.326335000	-3.703455000	-1.652878000
1	-0.048682000	-4.408571000	-2.427761000
6	-0.387117000	-4.106391000	-0.311796000
1	-0.157843000	-5.124699000	-0.022222000
6	-0.756358000	-3.170989000	0.649900000
1	-0.824113000	-3.419130000	1.700185000
6	-2.241212000	2.032570000	-0.208317000
1	-2.989944000	2.321604000	0.538496000
1	-2.540521000	2.459835000	-1.176121000
6	-0.901004000	2.583609000	0.193837000
6	-0.232137000	3.512412000	-0.620636000
1	-0.654020000	3.765384000	-1.590169000
6	0.948575000	4.128165000	-0.196594000
1	1.451449000	4.844204000	-0.836470000
6	1.466790000	3.819536000	1.068273000
1	2.375928000	4.300926000	1.413627000
6	0.821244000	2.894728000	1.892891000
1	1.214634000	2.655226000	2.874355000
6	-0.359583000	2.261754000	1.464150000
7	-3.740101000	-0.985831000	1.703283000
7	-3.842103000	-1.262193000	-2.552580000
7	-2.329573000	0.512044000	-0.285512000
7	-1.049289000	-1.886646000	0.324965000
8	-0.969804000	1.324362000	2.258312000
8	-0.657428000	-1.395956000	3.540306000
6	0.630776000	-1.765039000	4.242377000
6	0.779887000	1.597887000	6.110537000
6	1.714965000	1.297609000	7.099470000
1	0.360234000	2.594218000	6.057782000
6	0.411760000	0.605183000	5.197596000
1	-0.275128000	0.853189000	4.396063000
6	0.972772000	-0.680221000	5.285153000
6	1.934502000	-0.947144000	6.279070000
6	2.307812000	0.036941000	7.192912000
1	3.041544000	-0.154519000	7.964756000
1	2.397617000	-1.925129000	6.344848000
6	1.746658000	-1.734464000	3.187510000
6	1.747780000	-0.713411000	2.220161000
1	2.795072000	0.176870000	0.548278000
6	2.782960000	-0.608613000	1.292434000
1	0.953641000	0.021556000	2.215508000
6	3.833230000	-1.525863000	1.349558000
6	2.842707000	-2.614234000	3.248964000
6	3.887886000	-2.517957000	2.327711000

1	2.893693000	-3.378738000	4.014076000
1	4.732680000	-3.193460000	2.359284000
6	-0.153824000	-3.260873000	6.166994000
6	0.340284000	-3.147422000	4.854470000
6	0.416314000	-4.312624000	4.064411000
6	0.027436000	-5.553192000	4.567471000
6	-0.452878000	-5.626280000	5.875656000
6	-0.546825000	-4.496849000	6.685699000
1	-0.920257000	-4.592755000	7.696831000
1	-0.234189000	-2.383955000	6.796085000
1	0.091135000	-6.454384000	3.971824000
1	0.794865000	-4.255242000	3.052056000
1	-1.365826000	-1.330768000	4.217620000
7	2.095569000	2.338413000	8.063902000
8	2.948971000	2.041002000	8.945366000
8	1.544275000	3.469722000	7.957354000
7	4.913885000	-1.437218000	0.359415000
8	5.869056000	-2.257311000	0.452613000
8	4.820140000	-0.550751000	-0.536079000
7	-0.882521000	-6.927713000	6.406870000
8	-1.336815000	-6.961296000	7.583952000
8	-0.780991000	-7.933403000	5.650298000

Table 4.30. $^{2}(p\text{-OMe-C}_6\text{H}_4)_3\text{C}\bullet$:

6	0.981287000	-2.035428000	4.129316000
6	0.223873000	1.038187000	6.233067000
6	1.219732000	1.923982000	5.793081000
1	-0.489645000	1.334825000	6.993707000
6	0.136046000	-0.239353000	5.676633000
1	-0.653861000	-0.900639000	6.014576000
6	1.039855000	-0.691939000	4.674282000
6	2.025959000	0.246184000	4.240940000
6	2.112462000	1.519332000	4.783900000
1	2.875159000	2.218312000	4.458776000
1	2.745085000	-0.056787000	3.488596000
6	1.618833000	-2.380115000	2.839874000
6	1.452483000	-1.615198000	1.665381000
1	1.800958000	-1.431668000	-0.448754000
6	1.983269000	-2.030234000	0.436189000
1	0.867805000	-0.701851000	1.707796000
6	2.721330000	-3.219470000	0.363143000
6	2.396599000	-3.564613000	2.733355000
6	2.945623000	-3.973704000	1.526347000
1	2.563368000	-4.162702000	3.622342000
1	3.537007000	-4.878836000	1.448106000
6	0.416821000	-3.332739000	6.244443000
6	0.326483000	-3.145752000	4.839158000
6	-0.373369000	-4.135579000	4.106601000
6	-0.911808000	-5.269318000	4.715659000
6	-0.756106000	-5.449924000	6.096894000
6	-0.107772000	-4.464805000	6.860189000
1	0.005675000	-4.628980000	7.926195000
1	0.950867000	-2.603805000	6.844446000
1	-1.437072000	-5.997884000	4.109365000
1	-0.491566000	-4.007620000	3.036005000
8	1.410489000	3.211908000	6.287976000
6	0.656731000	3.629891000	7.458593000
1	1.046363000	4.614957000	7.713586000
1	-0.416076000	3.702735000	7.240447000
1	0.816421000	2.939532000	8.295687000
8	-1.189894000	-6.574058000	6.793052000
6	-1.655524000	-7.721964000	6.033905000
1	-2.578828000	-7.495774000	5.486136000
1	-0.888761000	-8.065062000	5.328677000
1	-1.850363000	-8.495087000	6.776218000
8	3.271479000	-3.750933000	-0.801406000
6	2.921781000	-3.157320000	-2.080496000
1	3.282542000	-2.124499000	-2.156085000
1	3.423531000	-3.773173000	-2.825314000

1	1.837549000	-3.184655000	-2.243783000

Table 4.31. $^{2}(p\text{-tBu-}C_6H_4)_3C\bullet$:

6	1.170074000	-2.142461000	3.828553000
6	-0.084583000	0.562236000	6.155154000
6	0.883636000	1.583311000	6.049702000
1	-0.931388000	0.690373000	6.822287000
6	0.013389000	-0.618313000	5.432113000
1	-0.752196000	-1.376012000	5.552761000
6	1.087977000	-0.857668000	4.531356000
6	2.048386000	0.177732000	4.410282000
6	1.947076000	1.359290000	5.153943000
1	2.727324000	2.103372000	5.037722000
6	0.741976000	2.848956000	6.918823000
1	2.905822000	0.036431000	3.760136000
6	1.734023000	-2.303607000	2.498336000
6	1.874716000	-1.227417000	1.580177000
1	2.492125000	-0.553389000	-0.348187000
6	2.414689000	-1.414633000	0.306338000
1	1.523069000	-0.241507000	1.861911000
6	2.841891000	-2.679718000	-0.141774000
6	3.448944000	-2.928656000	-1.538046000
6	2.165354000	-3.580700000	2.034928000
6	2.691071000	-3.755592000	0.760734000
1	2.094945000	-4.433484000	2.700423000
1	3.005000000	-4.751273000	0.461554000
6	0.972407000	-3.584553000	5.881107000
6	0.602035000	-3.312285000	4.544074000
6	-0.382078000	-4.142052000	3.970077000
6	-1.010546000	-5.147946000	4.714431000
6	-0.667639000	-5.394595000	6.056407000
6	-1.352394000	-6.477829000	6.918684000
6	0.364490000	-4.606314000	6.606997000
1	0.694836000	-4.785266000	7.625159000
1	1.739621000	-2.975783000	6.349023000
1	-1.790923000	-5.728678000	4.236829000
1	-0.692638000	-3.962035000	2.945384000
6	3.587346000	-1.625346000	-2.357697000
1	4.230411000	-0.898533000	-1.847953000
1	4.041859000	-1.847653000	-3.330658000
1	2.614377000	-1.155908000	-2.543603000
6	2.544159000	-3.914919000	-2.329636000
1	2.987746000	-4.138167000	-3.308297000
1	2.419464000	-4.861226000	-1.792108000
1	1.549114000	-3.485093000	-2.493497000
6	4.865876000	-3.553520000	-1.384265000
1	5.530808000	-2.875581000	-0.836932000
1	4.835445000	-4.503646000	-0.840493000

1	5.302513000	-3.744415000	-2.372269000
6	-2.602091000	-7.073444000	6.226749000
1	-2.345553000	-7.596267000	5.298352000
1	-3.078515000	-7.803085000	6.891816000
1	-3.339516000	-6.297104000	5.993550000
6	-0.337160000	-7.624890000	7.186016000
1	0.551477000	-7.251318000	7.707218000
1	-0.796116000	-8.401503000	7.811481000
1	-0.008894000	-8.086589000	6.247392000
6	-1.805347000	-5.873381000	8.280400000
1	-2.530326000	-5.066037000	8.128954000
1	-2.281100000	-6.649678000	8.892757000
1	-0.964700000	-5.465067000	8.851125000
6	1.891444000	3.852025000	6.682669000
1	1.757541000	4.726237000	7.330114000
1	2.864687000	3.404424000	6.919851000
1	1.916410000	4.206545000	5.645213000
6	-0.608423000	3.557970000	6.613054000
1	-0.667041000	3.865514000	5.562527000
1	-1.458868000	2.900494000	6.825245000
1	-0.710551000	4.452724000	7.238328000
6	0.750353000	2.443259000	8.420442000
1	-0.053795000	1.737432000	8.652606000
1	1.700975000	1.968669000	8.692349000
1	0.610424000	3.330333000	9.051371000

Table 4.32. $^{2}(p\text{-Ph-}C_6H_4)_3C\bullet$:

6	1.454097000	-2.328049000	3.997916000
6	0.780383000	0.555286000	6.372034000
6	1.815781000	1.466763000	6.066418000
1	0.024803000	0.829655000	7.100995000
6	0.672245000	-0.669268000	5.721997000
1	-0.152714000	-1.328498000	5.969218000
6	1.590448000	-1.057627000	4.708341000
6	2.635359000	-0.140770000	4.413465000
6	2.746121000	1.076125000	5.077074000
1	3.585714000	1.723492000	4.844592000
1	3.382236000	-0.411461000	3.675708000
6	1.869290000	-2.452954000	2.599685000
6	1.794862000	-1.364165000	1.689698000
1	2.042089000	-0.657661000	-0.314828000
6	2.161686000	-1.504056000	0.354330000
1	1.399863000	-0.415254000	2.034500000
6	2.631462000	-2.733242000	-0.156819000
6	2.354833000	-3.682961000	2.079553000
6	2.722430000	-3.815595000	0.745909000
1	2.468893000	-4.530098000	2.746235000
1	3.124627000	-4.762220000	0.400512000
6	1.109012000	-3.746329000	6.054282000
6	0.868765000	-3.487941000	4.680677000
6	0.031127000	-4.404159000	3.994470000
6	-0.529694000	-5.501603000	4.639915000
6	-0.285543000	-5.754590000	6.006569000
6	0.551740000	-4.850260000	6.693965000
1	0.756507000	-5.007373000	7.748265000
1	1.751556000	-3.075284000	6.614092000
1	-1.151540000	-6.186002000	4.071982000
1	-0.190079000	-4.232999000	2.946708000
6	-2.155827000	-7.412009000	6.303032000
6	-2.725378000	-8.518680000	6.937890000
6	-0.891083000	-6.923591000	6.690767000
1	-3.698061000	-8.879307000	6.617460000
6	-2.049410000	-9.158418000	7.984232000
6	-0.220969000	-7.581615000	7.743203000
1	-2.494583000	-10.014761000	8.480876000
1	0.765636000	-7.243390000	8.042616000
6	-0.795661000	-8.682100000	8.385357000
1	-0.257435000	-9.177209000	9.187988000
1	-2.707433000	-6.904890000	5.518122000
6	2.494815000	3.891878000	6.097815000
6	1.916551000	2.780726000	6.747921000
6	2.584207000	5.134153000	6.730573000

1	3.031431000	5.972613000	6.205319000
6	1.431238000	2.966310000	8.059705000
6	2.089171000	5.302756000	8.029038000
1	1.006862000	2.125765000	8.599426000
1	2.153939000	6.268247000	8.521247000
6	1.511543000	4.211676000	8.688776000
1	1.127375000	4.329915000	9.697431000
1	2.855937000	3.787069000	5.080236000
6	3.784455000	-3.233825000	-4.282595000
6	3.213965000	-4.297719000	-3.573768000
6	3.961678000	-1.998408000	-3.646609000
1	3.055817000	-5.254494000	-4.062651000
1	4.406505000	-1.168364000	-4.187144000
6	2.833242000	-4.129597000	-2.240368000
6	3.582601000	-1.830656000	-2.311835000
1	2.367528000	-4.953246000	-1.709716000
1	3.756940000	-0.878066000	-1.821783000
6	3.015596000	-2.895262000	-1.580493000
1	4.090013000	-3.368029000	-5.315584000

Table 4.33. $^{2}(p\text{-H-C}_6\text{H}_4)_3\text{C}\bullet$:

6	0.630461000	-2.003122000	3.827277000
6	-0.423578000	0.960041000	5.954477000
6	0.621461000	1.866650000	5.726749000
1	-1.252742000	1.242745000	6.596586000
6	-0.414248000	-0.296646000	5.349562000
1	-1.236289000	-0.981543000	5.526208000
6	0.640534000	-0.690948000	4.479919000
6	1.692032000	0.242858000	4.272921000
6	1.682110000	1.494318000	4.889234000
1	2.505932000	2.181234000	4.718783000
1	2.528622000	-0.035109000	3.641751000
6	1.227345000	-2.203136000	2.503854000
6	1.286038000	-1.157595000	1.542309000
1	1.863647000	-0.546906000	-0.435867000
6	1.841879000	-1.363867000	0.279645000
1	0.861378000	-0.191096000	1.788124000
6	2.357352000	-2.618709000	-0.074693000
6	1.764055000	-3.464205000	2.122176000
6	2.314399000	-3.665240000	0.856391000
1	1.760073000	-4.277744000	2.838567000
1	2.725904000	-4.635808000	0.595453000
6	0.179032000	-3.368946000	5.897280000
6	-0.003377000	-3.147037000	4.510030000
6	-0.811893000	-4.069143000	3.799169000
6	-1.407015000	-5.156016000	4.443037000
6	-1.200142000	-5.366583000	5.812981000
6	-0.400108000	-4.469341000	6.533787000
1	-0.216067000	-4.635288000	7.591491000
1	0.799639000	-2.682755000	6.464322000
1	-2.032914000	-5.838912000	3.876469000
1	-0.984173000	-3.909069000	2.739924000
1	0.609412000	2.844674000	6.197159000
1	2.790182000	-2.780402000	-1.056990000
1	-1.655273000	-6.216102000	6.312218000

Table 4.34. $^{2}(p\text{-Cl-}C_6H_4)_3C\bullet$:

6	0.630461000	-2.003122000	3.827277000
6	-0.423578000	0.960041000	5.954477000
6	0.621461000	1.866650000	5.726749000
1	-1.252742000	1.242745000	6.596586000
6	-0.414248000	-0.296646000	5.349562000
1	-1.236289000	-0.981543000	5.526208000
6	0.640534000	-0.690948000	4.479919000
6	1.692032000	0.242858000	4.272921000
6	1.682110000	1.494318000	4.889234000
1	2.505932000	2.181234000	4.718783000
1	2.528622000	-0.035109000	3.641751000
6	1.227345000	-2.203136000	2.503854000
6	1.286038000	-1.157595000	1.542309000
1	1.863647000	-0.546906000	-0.435867000
6	1.841879000	-1.363867000	0.279645000
1	0.861378000	-0.191096000	1.788124000
6	2.357352000	-2.618709000	-0.074693000
6	1.764055000	-3.464205000	2.122176000
6	2.314399000	-3.665240000	0.856391000
1	1.760073000	-4.277744000	2.838567000
1	2.725904000	-4.635808000	0.595453000
6	0.179032000	-3.368946000	5.897280000
6	-0.003377000	-3.147037000	4.510030000
6	-0.811893000	-4.069143000	3.799169000
6	-1.407015000	-5.156016000	4.443037000
6	-1.200142000	-5.366583000	5.812981000
6	-0.400108000	-4.469341000	6.533787000
1	-0.216067000	-4.635288000	7.591491000
1	0.799639000	-2.682755000	6.464322000
1	-2.032914000	-5.838912000	3.876469000
1	-0.984173000	-3.909069000	2.739924000
17	-1.942320000	-6.752849000	6.625594000
17	0.601671000	3.464170000	6.488614000
17	3.054809000	-2.878239000	-1.680650000

Table 4.35. $^{2}(p\text{-}NO_2\text{-}C_6H_4)_3C\bullet$:

6	0.730986000	-2.099503000	3.922246000
6	-0.185170000	0.873565000	6.091988000
6	0.826196000	1.771595000	5.729472000
1	-0.940379000	1.182301000	6.803230000
6	-0.208657000	-0.387943000	5.509212000
1	-1.009660000	-1.070044000	5.766822000
6	0.774259000	-0.785040000	4.556211000
6	1.795087000	0.156274000	4.236243000
6	1.821848000	1.420155000	4.810504000
1	2.597243000	2.134857000	4.567289000
1	2.583193000	-0.124297000	3.549099000
6	1.301398000	-2.299121000	2.586942000
6	1.262584000	-1.273136000	1.602958000
1	1.813063000	-0.669459000	-0.400685000
6	1.846231000	-1.445596000	0.353153000
1	0.747746000	-0.345515000	1.821548000
6	2.486528000	-2.655903000	0.065977000
6	1.937516000	-3.523179000	2.240184000
6	2.532105000	-3.700596000	0.995522000
1	1.997631000	-4.319983000	2.971912000
1	3.043152000	-4.618688000	0.737408000
6	0.273685000	-3.408765000	6.022442000
6	0.118586000	-3.236544000	4.621650000
6	-0.656348000	-4.195545000	3.916127000
6	-1.263461000	-5.260735000	4.574850000
6	-1.082584000	-5.392752000	5.955732000
6	-0.310788000	-4.482619000	6.685610000
1	-0.176346000	-4.632614000	7.749014000
1	0.879884000	-2.706881000	6.582881000
1	-1.876773000	-5.978851000	4.045777000
1	-0.807193000	-4.076695000	2.849147000
7	3.122601000	-2.832685000	-1.237041000
8	3.706284000	-3.932206000	-1.466677000
8	3.058936000	-1.876338000	-2.064834000
7	-1.716884000	-6.508199000	6.658180000
8	-2.474135000	-7.275386000	5.995443000
8	-1.473964000	-6.645907000	7.892830000
7	0.842714000	3.106970000	6.318311000
8	-0.018199000	3.376936000	7.207173000
8	1.714357000	3.927938000	5.905158000

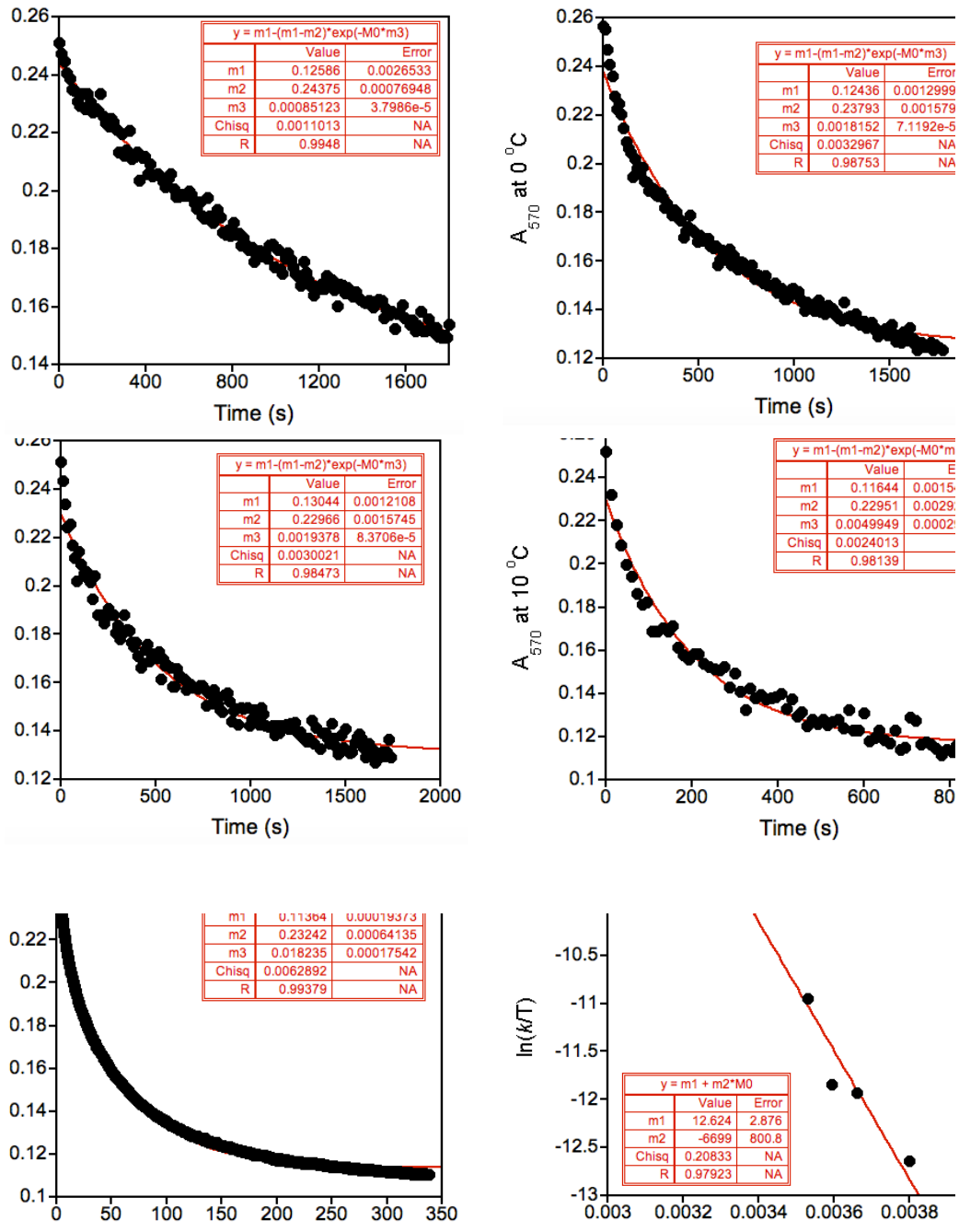

Figure 4.13. Pseudo-first-order fittings of the plots of A_{570} versus time for reactions of **1** (0.2 mM) with (p-tBu-C_6H_4)$_3$C• (2 mM) at different temperatures (-10 °C to 25 °C) and Eyring plot (ln(k/T) versus 1/T).

Table 4.36. Hammett parameters, rate constants, and redox potentials for the reaction of **1** with *para*-substituted radicals used during this study.

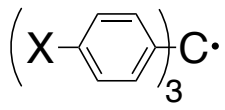	$3\sigma^{+}_{para}$[36]	***k*** **(M^{-1} s^{-1})**	**$E_{1/2}$, (V vs $Fc^{+/0}$)[a]**
-OMe	-2.33	25.5(2)	-0.58
-tBu	-0.77	13.4(1)	-0.25
-Ph	-0.54	6.8(8)	-0.19
-CN	1.98	2.2(3)	0.07

[a] For the reaction: $Ar_3C^+ + e^- \rightarrow Ar_3C\bullet$ in CH_3CN at 25 °C.[37]

Derivation of Marcus Plot Analysis[2, 38]

For a given redox reaction:

$$Red_a + \mathrm{Ox}_b \rightarrow \mathrm{Ox}_a + \mathrm{Red}_b \qquad (1)$$

The rate constant k_{ab} can be stated in terms of the free energy (ΔG^*_{ab}) of this reaction:

$$k_{ab} = Z_{ab} e^{\frac{-\Delta G^*_{ab}}{RT}} \qquad (2)$$

$$\ln k_{ab} = \frac{-\Delta G^*_{ab}}{RT} + \ln Z_{ab} \qquad (3)$$

Z_{ab} is the frequency of collisions between a and b when in solution. ΔG^*_{ab} contains the sum of a series of 3 terms: a) the electrostatic work required to draw two ions together (w_{elec}), b) required energy to alter the solvent structure (ΔG^*_{solv}), and c) the necessary energy for the distortion of a metal-ligand bond-length (ΔG^*_{lig}):

$$\Delta G^*_{ab} = \omega_{elec} + \Delta G^*_{solv} + \Delta G^*_{lig} \qquad (4)$$

When a reaction involves a molecule that is neutral, and an ion, w_{elec} is 0. Terms concerning ligand and solvent energy have been quantified by Marcus,[39] and the derivation of such brought about the Marcus cross-relation:

$$k_{ab} = (k_{aa} k_{bb} K_{ab} f)^{1/2} \qquad (5)$$

Elements k_{aa} and k_{bb} represent rate constants for exchange of electrons between oxidized and reduced states of an element ("self-exchange"), and K_{ab} is the defined equilibrium constant for the redox reaction between a and b. The element f is a function of the three terms k_{aa}, k_{bb}, and K_{ab}.

$$Red_a + Ox^*_a \rightarrow \mathrm{Ox}_a + \mathrm{Red}^*_a \qquad (k_{aa}) \quad (6)$$

$$Red_b + Ox^*_b \rightarrow \mathrm{Ox}_b + \mathrm{Red}^*_b \qquad (k_{bb}) \quad (7)$$

$$Red_a + \mathrm{Ox}_b \rightleftarrows \mathrm{Ox}_a + \mathrm{Red}_b \qquad (K_{ab}) \quad (8)$$

$$\ln f = \frac{0.25\,(\ln K_{ab})^2}{ln\frac{k_{aa}k_{bb}}{z^2}} \qquad (9)$$

With these definitions, equation 5 can then be re-written in the following:

$$\ln k_{ab} = 0.5\ \ln K_{ab} + 0.5[\ln k_{aa} + \ln k_{bb} + \ln f] \quad (10)$$

The Nernst equation can then be used to relate equilibrium constants K_{ab} to the standard redox potential E°:

$$\Delta G° = -nRt \ln K = -nFE° \qquad (11)$$

$$\ln K = \frac{F}{RT}(E^\circ_{red} - E^\circ_{ox}) \qquad (12)$$

When substituting equations 9 and 12 into equation 10, while holding E°_{red} constant,

$$\frac{RT}{F}\ln k = -0.5\,E^{\circ}_{ox} +$$

$$[0.5\,E^{\circ}_{red} + 0.5\frac{RT}{F}\ln k_{aa} + 0.5\frac{RT}{F}\ln k_{bb} + 0.5\frac{RT}{F}(\frac{0.25\,(\ln K_{ab})^2}{ln\frac{k_{aa}k_{bb}}{z^2}})] \quad (13)$$

The term E°_{ox} refers to the redox potential for the substrate undergoing oxidation. At the equilibrium conditions, $\Delta G° \approx 0$, and $K_{ab} \approx 1$, the final term in equation 13 is cancelled. Because of that, when under limiting conditions, a simple linear free energy relationship is revealed by the Marcus theory, with a slope of (RT/F) ln k vs. E° of approximately -0.5 for a reaction having an ET rate-determining step. This slope of -0.5 is expected when $\Delta G°$ is small, otherwise large values of $\Delta G°$ bring about a ln(f) term that would no longer be ~0. For strongly endergonic reactions, the slope seen in a Marcus plot would approach -1.

4.6. References

1. Huang, X.; Groves, J. T., *JBIC, J. Biol. Inorg. Chem.* **2017,** *22*, 185-207.

2. Zaragoza, J. P. T.; Yosca, T. H.; Siegler, M. A.; Moënne-Loccoz, P.; Green, M. T.; Goldberg, D. P., *J. Am. Chem. Soc.* **2017,** *139*, 13640-13643.

3. Tamanaha, E.; Zhang, B.; Guo, Y.; Chang, W.-c.; Barr, E. W.; Xing, G.; Clair, J. S.; Ye, S.; Neese, F.; J. Martin Bollinger, J.; Krebs, C., *J. Am. Chem. Soc.* **2016,** *138*, 8862-8874.

4. Cho, K. B.; Hirao, H.; Shaik, S.; Nam, W., *Chem. Soc. Rev.* **2016,** *45*, 1197-210.

5. Liao, H.-J.; Li, J.; Huang, J.-L.; Davidson, M.; Kurnikov, I.; Lin, T.-S.; Lee, J. L.; Kurnikova, M.; Guo, Y.; Chan, N.-L.; Chang, W.-c., *Angew. Chem. Int. Ed.* **2018,** *57*, 1831-1835.

6. Dunham, N. P.; Chang, W.-c.; Mitchell, A. J.; Martinie, R. J.; Zhang, B.; Bergman, J. A.; Rajakovich, L. J.; Wang, B.; Silakov, A.; Krebs, C.; Boal, A. K.; J. Martin Bollinger, J., *J. Am. Chem. Soc.* **2018,** *140*, 7116-7126.

7. Hsieh, C. H.; Huang, X.; Amaya, J. A.; Rutland, C. D.; Keys, C. L.; Groves, J. T.; Austin, R. N.; Makris, T. M., *Biochemistry* **2017,** *56*, 3347-3357.

8. Rude, M. A.; Baron, T. S.; Brubaker, S.; Alibhai, M.; Cardayre, S. B. D.; Schirmer, A., *Appl. Environ. Microbiol.* **2011,** *77*, 1718-1727.

9. Liu, Y.; Wang, C.; Yan, J.; Zhang, W.; Guan, W.; Lu, X.; Li, S., *Biotechnol. Biofuels* **2014,** *7*, 28-40.

10. Dennig, A.; Kuhn, M.; Tassoti, S.; Thiessenhusen, A.; Gilch, S.; Bülter, T.; Haas, T.; Hall, M.; Faber, K., *Angew. Chem. Int. Ed.* **2015,** *54*, 8819-8822.

11. Matthews, S.; Belcher, J. D.; Tee, K. L.; Girvan, H. M.; McLean, K. J.; Rigby, S. E. J.; Levy, C. W.; Leys, D.; Parker, D. A.; Blankley, R. T.; Munro, A. W., *J. Biol. Chem.* **2017,** *292*, 5128-5143.

12. Rui, Z.; Li, X.; Zhu, X.; Liu, J.; Domigan, B.; Barr, I.; Cate, J. H. D.; Zhang, W., *Proc. Natl. Acad. Sci.* **2014,** *111*, 18237-18242.

13. Mitchell, A. J.; Zhu, Q.; Maggiolo, A. O.; Anath, N. R.; Hillwig, M. L.; Liu, X.; Boal, A. K., *Nat. Chem. Biol.* **2016,** *12*, 636-640.

14. Matthews, M. L.; Neumann, C. S.; Miles, L. A.; Grove, T. L.; Booker, S. J.; Krebs, C.; Walsh, C. T.; Bollinger, J. M., Jr., *Proc. Natl. Acad. Sci.* **2009,** *106*, 17723-17728.

15. Martinie, R. J.; Livada, J.; Chang, W.; Green, M. T.; Krebs, C.; Bollinger, J. M., Jr.; Silakov, A., *J. Am. Chem. Soc.* **2015,** *137*, 6912-6919.

16. Wong, C.; Fujimori, D. G.; Walsh, C. T.; Drennan, C. L., *J. Am. Chem. Soc.* **2009,** *131*, 4872-4879.

17. Planas, O.; Clemancey, M.; Latour, J.-M.; Company, A.; Costas, M., *Chem. Commun.* **2014,** *50*, 10887-10890.

18. Puri, M.; Biswas, A. N.; Fan, R.; Guo, Y.; Que, L., Jr., *J. Am. Chem. Soc.* **2016,** *138*, 2484-2487.

19. Rana, S.; Dey, A.; Maiti, D., *Chem. Commun.* **2015,** *51*, 14469-14472.

20. Price, J. C.; Barr, E. W.; Hoffart, L. M.; Krebs, C.; Bollinger, J. M. J., *Biochemistry* **2005,** *44*, 8138-8147.

21. Pangia, T. M.; Davies, C. G.; Prendergast, J. R.; Gordon, J. B.; Siegler, M. A.; Jameson, G. N. L.; Goldberg, D. P., *J. Am. Chem. Soc.* **2018,** *140*, 4191-4194.

22. Jang, E. S.; McMullin, C. L.; Kass, M.; Meyer, K.; Cundari, T. R.; Warren, T. H., *J. Am. Chem. Soc.* **2014,** *136*, 10930-10940.

23. Dünnebacke, D.; Neumann, W. P.; Penenory, A.; Stewen, U., *Chem. Ber.* **1989,** *122*, 533-535.

24. Gaussian 09, R. A.; Frisch, M. J.; Trucks, G. W.; Schlegel, H. B.; Scuseria, G. E.; Robb, M. A.; Cheeseman, J. R.; Scalmani, G.; Barone, V.; Mennucci, B.; Petersson, G. A.; Nakatsuuji, H.; Caricato, M.; Li, X.; Hratchian, H. P.; Izmaylov, A. F.; Bloino, J.; Zheng, G.; Sonnenberg, J. L.; Hada, M.; Ehara, M.; Toyota, K.; Fukuda, R.; Hasegawa, J.; Ishida, M.; Nakajima, T.; Honda, Y.; Kitao, O.; Nakai, H.; Vreven, T.; Montgomery Jr., J. A.; Peralta, J. E.; Ogliaro, F.; Bearpark, M.; Heyd, J. J.; Brothers, E.; Kudin, K. N.; Staroverov, V. N.; Kobayashi, R.; Normand, J.; Raghavachari, K.; Rendell, A.; Burant, J. C.; Iyengar, S. S.; Tomasi, J.; Cossi, M.; Rega, N.; Milliam, J. M.; Klene, M.; Knox, J. E.; Cross, J. B.; Bakken, V.; Adamo, C.; Jaramillo, J.; Gomperts, R.; Stratmann, R. E.; Yazyev, O.; Austin, A. J.; Cammi, R.; Pomelli, C.; Ochterski, J. W.; Martin, R. L.; Morokuma, K.; Zakrzewski, V. G.; Voth, G. A.; Salvador, P.; Dannenberg, J. J.; Dapprich, S.; Daniels, A. D.; Farkas, Ö.; Foresman, J. B.; Ortiz, J. V.; Cioslowski, J.; Fox, D. J.

25. Becke, A. D., *J. Chem. Phys.* **1993,** *98*, 5648-5652.

26. Lee, C.; Yang, W.; Parr, R. G., *Phys. Rev. B* **1988,** *37*, 785-789.

27. Hay, P. J.; Wadt, W. R., *J. Chem. Phys.* **1985,** *82*, 270-283.

28. Ditchfield, R.; Hehre, W. J.; Pople, J. A., *J. Chem. Phys.* **1971,** *54*, 724-728.

29. Tomasi, J.; Mennucci, B.; Cammi, R., *Chem. Rev.* **2005,** *105*, 2999-3093.

30. Li, G.; Han, A.; Pulling, M. E.; Estes, D. P.; Norton, J. R., *J. Am. Chem. Soc.* **2012,** *134*, 14662-14665.

31. Colclough, N.; Smith, J. R. L., *J. Chem. Soc. Perkin Trans. 2* **1994**, 1139-1149.

32. Marcus, R. A.; Sutin, N., *Biochim. Biophys. Acta., Rev. Bioenerg.* **1985,** *811*, 265-322.

33. Osako, T.; Ohkubo, K.; Taki, M.; Tachi, Y.; Fukuzumi, S.; Itoh, S., *J. Am. Chem. Soc.* **2003,** *125*.

34. Lee, J. Y.; Peterson, R. L.; Ohkubo, K.; Garcia-Bosch, I.; Himes, R. A.; Woertink, J.; Moore, C. D.; Solomon, E. I.; Fukuzumi, S.; Karlin, K. D., *J. Am. Chem. Soc.* **2014,** *136*, 9925-9937.

35. Blanchard, J.; In, M.; Schaudel, B.; Sanchez, C., *Eur. J. Inorg. Chem.* **1998,** *1998*, 1115-1127.

36. Brown, H. C.; Okamoto, Y., *J. Am. Chem. Soc.* **1958,** *80*, 4979-4987.

37. Volz, H.; Lotsch, W., *Tetrahedron Lett.* **1969**, 2275-2278.

38. Marcus, R. A.; Sutin, N., *Biochim. Biophys. Acta., Rev. Bioenerg.* **1985,** *811*.

39. Marcus, R. A., *J. Chem. Phys.* **1963,** *67*, 853-857.

Chapter 5 Evaluation of Oxygen Reactivity and Halogen Rebound in Additional Compounds

5.1. Introduction

This chapter continues on with previous themes, focusing initially on the proposal of ligands which were fashioned to coordinate ferrous centers in an axial fashion, in attempt to stabilize iron-oxygen intermediates. While projects to address the causes and nature of the oxygen rebound mechanism within nonheme iron model complexes have been explored to provide useful mechanistic information,[1] there still remain areas of potential future focus.[2] The mechanism of oxygen rebound in both iron enzymes and now model complexes is better known and explored than has been in the past, however other processes are observed in enzymes which may present additional rebound mechanisms for exploration in addition to oxygen rebound. There are additional reaction opportunities other than direct oxygen rebound when the radical and metal complex remain within the solvent cage. Some involve cage escape, while others involve alternative interactions between the metal and radical.[3-4] In the case of several nonheme iron/oxyglutarate enzymes such as AsqI, NapI, and VioC, there occurs a desaturation mechanism by which desaturation occurs, and rebound does not occur. The final product produced contains a C=C bond in the substrate material.[3-4] Additionally the nonheme iron halogenase enzymes such as CytC3, WelO5, and SyrB2 induce halogenation of substrates by a halogen rebound mechanism.[5-10] While both hydroxide and halogen are available for potential reaction with the radical resultant from the substrate, there remains a question as to the factors which influence halogen

rebound over oxygen rebound. During the key rebound step it is proposed that the orientation of the substrate and competing hydroxide ligand are primary factors in the determination of the halogen rebound (Scheme 5.1).

Scheme 5.1. Rebound processes observed in nonheme iron enzymes.

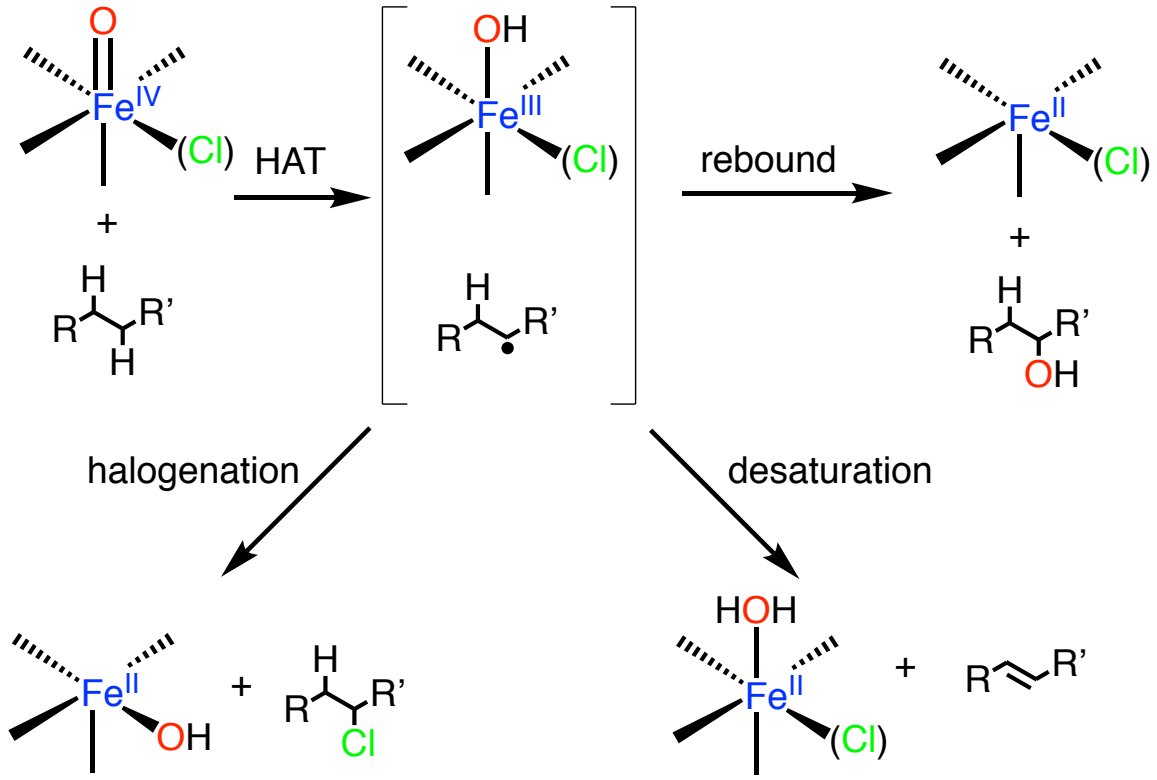

An additional complex was synthesized and investigated to research the potential for halogen rebound in a $Fe^{III}(Cl)$ complex, as opposed to $-OCH_3$ rebound previously observed.[1] Another complex bearing $Fe^{III}(F)$ was synthesized and also investigated for initial evidence of potential fluoride rebound.

5.2. Experimental

General Methods and Materials. All chemicals and reagents were purchased from Sigma- Aldrich, Fisher Scientific, Acros Organics, Merck, Fluka Analytical, or Alfa Aesar and were used without further purification unless noted otherwise. Solvents (methanol,

diethyl ether, acetonitrile, and tetrahydrofuran) used in organic synthesis were purified via Pure-Solv Solvent Purification System from Innovative Technology, Inc. Carbon tetrachloride was purchased from Fisher Scientific and used without further purification. For Mössbauer spectroscopy, ^{57}Fe (95.93% isotope-enriched) was purchased from Cambridge Isotope Laboratories. Solvents used in the reactions of the iron(II) and iron(III) complexes were subjected to additional purification after initial purification via a Pure-Solv Solvent Purification System. Acetonitrile was distilled over calcium hydride. THF was distilled from sodium/benzophenone. All solvents were degassed by freeze-pump-thaw cycles and stored in a N2 filled dry box. Reactions involving inert atmosphere were performed using either standard Schlenk techniques or in a dry box. The compounds N-phenyl-2-chloroethanamide, bis(pyridin-2-yl)methanol, and $N3PyOH^{2Ph}$ were prepared according to literature procedures.[1, 11-12] $^{57}Fe(ClO4)2$ was synthesized by reaction of perchloric acid with ^{57}Fe in distilled, degassed acetonitrile under airfree conditions, forming a solution which was used without further purification. *Caution: Perchlorate salts of metal complexes are potentially explosive. Care should be taken when handling these compounds*.

Analytical Methods. Kinetic UV-vis measurements were performed on a Hewlett-Packard Agilent 8453 diode-array spectrophotometer with a 3.5 mL quartz cuvette (path length = 1 cm) equipped with a septum. Other UV-visible spectra were recorded on a Varian Cary 50 Bio spectrophotometer. NMR spectra were collected on a Bruker Avance 400 MHz FT-NMR spectrometer. FAB-MS was obtained using a VG analytical VG-70SE magnetic sector mass spectrometer.

Scheme 5.2. Proposed synthesis of axial amidate-coordinated iron (II).

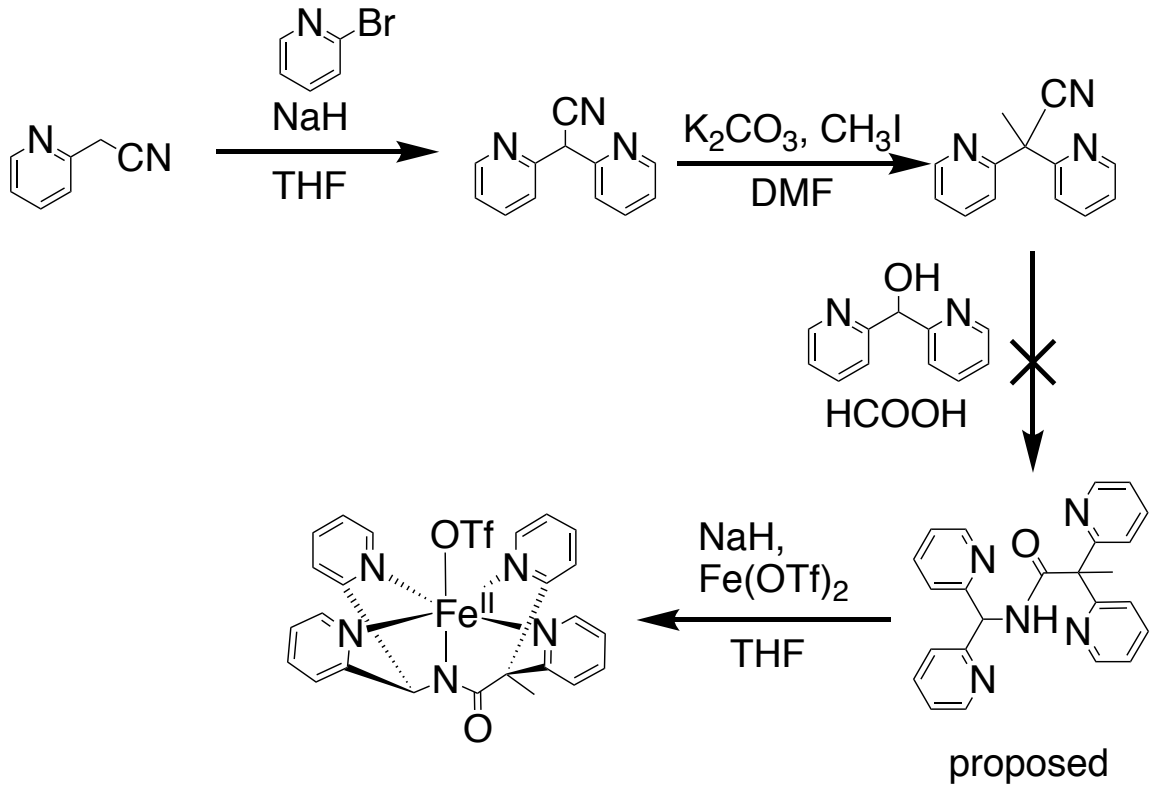

Synthesis of Bis(pyridin-2-yl)acetonitrile. The synthesis was adapted from a previous literature procedure.[13] A slurry of 60% NaH (25 mmol) was suspended in 90 mL dry THF under an argon atmosphere. To the suspension was added a solution of (pyridin-2-yl)acetonitrile (1.6429g, 12.5 mmol) dissolved in 10 mL dry THF. Following cessation of H_2 gas formation, a solution of 2-dibromopyridine (0.5 mL, 5 mmol) in 10 mL THF was added. The solution was heated at 90 °C for 20 h. The solution was cooled and quenched with saturated aqueous NH_4Cl (25 mL). The solvent was removed under reduced pressure and the resulting aqueous solution was extracted with $CHCl_3$, dried with $MgSO_4$ then concentrated under vacuum. Column chromatography (silica gel, $CHCl_3$) yielded bis(pyridin-2-yl)acetonitrile in 0.7451 g (31%). The compound was isolated as a light

brown solid. ^{1}H NMR ($CDCl_3$) (Figure 5.6): δ 16.45-16.12 (br s, 1H), δ 7.94-7.87 (m, 2H), δ 7.52-7.45 (m, 2H), δ 7.42-7.36 (m, 2H), δ 6.64-6.57 (m, 2H).

Synthesis of 2,2-Bis(pyridine-2-yl)propionitrile. The synthesis was adapted from a previous literature procedure.[13] A solution of bis(pyridin-2-yl)acetonitrile (0.500 g, 2.6 mmol) was made in dry DMF (25 mL), to which was added methyl iodide (3 mmol) and K_2CO_3 (7.8 mmol). The slurry was stirred under argon for 24 h at 23 °C. The DMF was evaporated and the residue dissolved in H_2O, then extracted with $CHCl_3$ to give 0.460 g of brown solid (85%). ^{1}H NMR ($CDCl_3$) (Figure 5.7): δ 8.65-8.58 (m, 2H), δ 7.76-7.67 (m, 2H), δ 7.59-7.53 (m, 2H), δ 7.26-7.21 (m, 2H), δ 2.31-2.25 (s, 3H). The compound was used without further purification.

Reaction of 2,2-Bis(pyridine-2-yl)propionitrile and bis(pyridin-2-yl)methanol. The synthesis was adapted from a previous literature procedure.[14] Formic acid (8 mL, 88% aqueous) was added to bis(pyridin-2-yl)methanol (0.718g, 4 mmol) and stirred. An amount of 2,2-bis(pyridine-2-yl)propionitrile (0.855 g, 4 mmol). The reaction was heated to reflux under inert atmosphere. Following 48 h, the reaction was neutralized with 10% aqueous $NaHCO_3$ and extracted with $CHCl_3$. The extract was dried with $MgSO_4$, filtered through celite, and solvent removed under reduced pressure. FAB-MS: *calcd* for $[M+H]^+$ 396.1819, observed mass: 376.1535.

Scheme 5.3. Synthesis of axial amide donor.

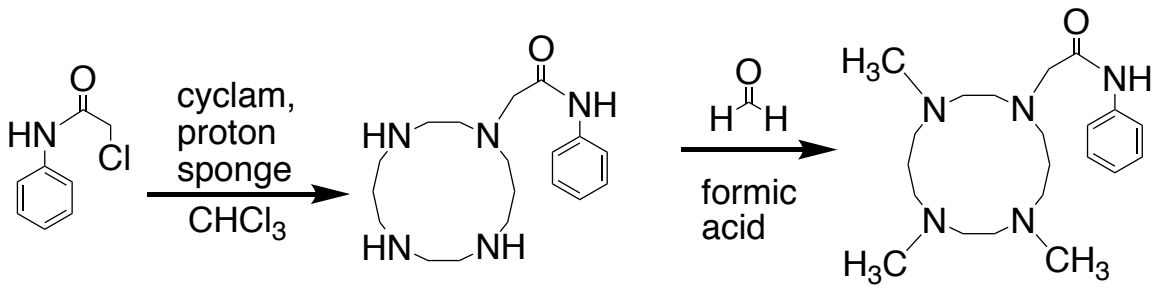

Synthesis of 2-(1,4,8,11-tetraazacyclotetradecan-1-yl)-*N*-phenylacetamide. The synthesis was adapted from a previous literature procedure.[11] Cyclam (1,4,8,11-tetraazacyclotetradecane) (0.792 g, 4 mmol) was combined with proton sponge (1,8-bis(dimethylamino)naphthalene) (0.537 g, 2.5 mmol). The compounds were dissolved in 80 mL chloroform under inert gas and heated to 60 °C. To the resulting solution was added N-phenyl-2-chloroethanamide (0.457 g, 2.7 mmol) dropwise in a solution in 20 mL chloroform. The solution was heated to reflux and help under those conditions for 24 h. Following completion of the reaction, the solvent was removed under reduced pressure. Column chromatography (basic alumina) using a mobile phase of dichloromethane with a methanol gradient (0-10%) yielded the desired 2-(1,4,8,11-tetraazacyclotetradecan-1-yl)-*N*-phenylacetamide (0.6340 g, 71%) as a brown oil. ^{1}H NMR ($CDCl_3$) (Figure 5.8): δ 7.65-7.54 (m, 2H), δ 7.37-7.27 (m, 2H), δ 7.15-7.05 (m, 1H), δ 3.25-3.16 (s, 2H), δ 2.83-2.61 (m, 16H), δ 2.83-2.61 (m, 16H), δ 1.83-1.65 (m, 4H). ^{13}C NMR ($CDCl_3$) (Figure 5.9): δ 170.7, 138.7, 128.7, 124.3, 121.8, 58.9, 57.5, 53.5, 50.4, 49.0, 48.7, 48.0, 47.8, 47.4, 28.8, 26.8.

Synthesis of *N*-phenyl-2-(4,8,11-trimethyl-1,4,8,11-tetraazacyclotetradecan-1-yl)acetamide ($TMC^{Am\text{-}Ph}$). The synthesis was adapted from a previous literature procedure.[15] An amount of 2-(1,4,8,11-tetraazacyclotetradecan-1-yl)-*N*-phenylacetamide (0.258 g, 0.77 mmol) was dissolved in 5 mL of 37% aqueous formaldehyde (50 mmol). To the solution was added aqueous formic acid (88%, 5 mL, 120 mmol), and heated to reflux for 48 h. Following completion of the time period, the reaction was made basic (pH ~8) with aqueous sodium carbonate solution. The solution was extracted with chloroform, dried with $MgSO_4$m filtered through celite, and solvent removed under reduced pressure to obtain the target *N*-phenyl-2-(4,8,11-trimethyl-1,4,8,11-tetraazacyclotetradecan-1-yl)acetamide (0.100 g) in 35% yield. The product was used without further purification. ^{1}H NMR ($CDCl_3$) (Figure 5.10): δ 10.37-10.05 (s, 1H) 7.71-7.58 (m, 2H), 7.38-7.28 (m, 2H), 7.15-7.03 (m, 1H), 3.21-3.12 (s, 2H), 2.83-2.36 (m, 16H), 2.28-2.21 (s, 3H), 2.20-2.14 (s, 3H), 2.13-2.04 (s, 3H), 1.79-1.51 (m, 4H).

Scheme 5.4. Synthesis of $[Fe^{II}(Cl)(TMC^{Am\text{-}Ph})](Cl)$.

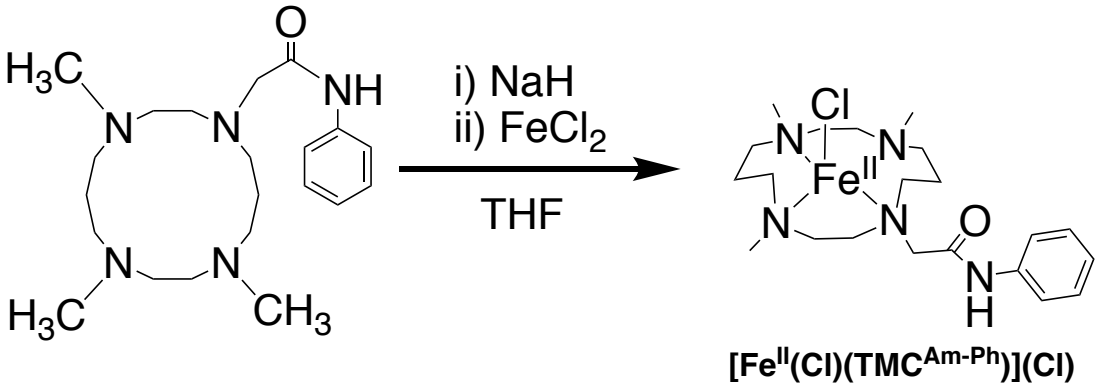

Synthesis of $[Fe^{II}(Cl)(TMC^{Am\text{-}Ph})](Cl)$. Under an inert atmosphere, $TMC^{Am\text{-}Ph}$ (100 mg, 0.27 mmol) was dissolved in THF (5 mL). To this solution was added NaH (6.5 mg, 0.27 mmol), followed by stirring for 5 min. To the resulting slurry was added $FeCl_2$ (33 mg, 0.27 mmol) and allowed to stir for 30 minutes. Following the completion of the reaction,

the mixture was filtered through celite. The THF solvent was removed under vacuum and the residue redissolved in methanol. Vapor diffusion of diethyl ether allowed formation of pale crystals of [Fe^{II}(Cl)(TMC^{Am-Ph})](Cl) after 5-7 days (21 mg, 22%) suitable for X-ray diffraction (Figure 5.1, Scheme 5.4).

Synthesis of [$Fe(Cl)_2N3PyO^{2Ph}$]. While under an inert atmosphere, $N3PyOH^{2Ph}$ (116 mg, 0.21 mmol) was dissolved in acetonitrile (5 mL). An amount of triethylamine (28 μL, 0.21 mmol) was added to the solution and stirred for 5 min. After the stirring, $FeCl_2$ (26 mg, 0.21 mmol) was added to the yellow solution, prompting a color change to dark brown. The solution was stirred for 30 min, filtered through celite, and exposed to air. The dark brown solution changed to dark green over the course of 20 h. The green solution was filtered through celite and vapor diffusion of diethyl ether formed a small amount of dark green crystals after 8 days, accompanied by a large amount of pale yellow needles. An isolated amount (4 mg, 3%) of green crystals allowed for the characterization by X-ray diffraction (Figure 5.3).

Synthesis of [Fe(F)$N3PyO^{2Ph}$](BF_4). Inside an inert atmosphere, $N3PyOH^{2Ph}$ (130 mg, 0.24 mmol) was dissolved in acetonitrile (10 mL). Triethylamine (32 μL, 0.24 mmol) was added and the solution was stirred for 5 min. Following stirring, $Fe(BF_4)_2.6H_2O$ (86 mg, 0.24 mmol) was added to the solution, forming a dark brown color. After stirring for 30 min, the solution was filtered through celite. Following filtration, the solution was exposed to air, prompting a color change from dark brown to dark blue. Vapor diffusion of diethyl ether into the acetonitrile solution produced a small amount (3 mg, 2%) of dark crystals after 7 days suitable for X-ray diffraction (Figure 5.4).

Reaction of [Fe(Cl)$_2$N3PyO^{2Ph}] with Gomberg's Dimer. UV-vis Spectroscopy. A solution of **[Fe(Cl)$_2$N3PyO^{2Ph}]** (2 mL, 0.15 mM) in CH_3CN was placed into a quartz cuvette (1 cm pathlength) under an inert atmosphere. The initial spectrum was recorded at 23 °C. Gomberg's dimer $(Ph_3C)_2$, (2 equiv in 0.1 mL THF) was added and the UV-vis bands at λ_{max} = 516 nm (triphenyl methyl radical) and λ_{max} = 590 nm (**[Fe(Cl)$_2$N3PyO^{2Ph}]**) were monitored over 5 min. Decay (~95%) of the 590 nm peak was observed over this time period at 23 °C, indicating the consumption of the Fe^{III} starting material **[Fe(Cl)$_2$N3PyO^{2Ph}]** (Figure 5.3).

Reaction of [Fe(F)N3PyO^{2Ph}](BF$_4$) with Gomberg's Dimer. UV-vis Spectroscopy. A solution of **[Fe(F)N3PyO^{2Ph}](BF$_4$)** (2 mL, 0.6 mM) in CH_3CN was placed into a quartz cuvette (1 cm pathlength) under an inert atmosphere, and an initial spectrum was recorded at 23 °C. Gomberg's dimer $(Ph_3C)_2$, (2 equiv in 0.1 mL THF) was added and the UV-vis bands at λ_{max} = 516 nm (triphenyl methyl radical) and λ_{max} = 570 nm (**[Fe(F)N3PyO^{2Ph}](BF$_4$)**) were monitored over 1 h. Decay (~90%) of the 570 nm peak was observed over this time period at 23 °C, indicating the reaction of the Fe^{III} starting material **[Fe(F)N3PyO^{2Ph}](BF$_4$)** (Figure 5.5).

Single crystal X-Ray crystallography

All reflection intensities were measured at 110(2) K using a SuperNova diffractometer (equipped with Atlas detector) with Mo *K*α radiation (λ = 0.71073 Å) under the program CrysAlisPro (Version CrysAlisPro 1.171.39.29c, Rigaku OD, 2017). The same program

was used to refine the cell dimensions and for data reduction. The structure was solved with the program SHELXS-2014/7 and was refined on F^2 with SHELXL-2014/7.[16-17] The unpublished structures may be accessed from the Johns Hopkins University X-ray Crystallography Facility at http://xray.chm.jhu.edu/, using the appropriate reference code.

Crystal structure of [Fe(Cl)TMC$^{Am\text{-}Ph}$]Cl. Analytical numeric absorption corrections based on a multifaceted crystal model were applied using CrysAlisPro (Version 1.171.36.32 Agilent Technologies, 2013). The temperature of the data collection was controlled using the system Cryojet (manufactured by Oxford Instruments). The H atoms were placed at calculated positions (unless otherwise specified) using the instructions AFIX 23, AFIX 43, AFIX 137 or AFIX 147 with isotropic displacement parameters having values 1.2 or 1.5 times *U*eq of the attached C or O atoms. The H atom attached to N5 was found from difference Fourier maps, and its coordinates and isotropic temperature factor were refined freely. The structure is ordered. Reference code: **xs0338a**.

Fw = 534.35, colorless rod, 0.37 × 0.09 × 0.08 mm^3, monoclinic, *P*21/*c* (no. 14), a = 16.9428(3), b = 18.4367(3), c = 8.55879(13) Å, β = 101.5960(15)°, V = 2618.94(8) Å^3, Z = 4, D_x = 1.355 g cm^{-3}, μ = 6.714 mm^{-1}, T_{min}-T_{max}: 0.291–0.641. 15948 Reflections were measured up to a resolution of $(\sin \theta/\lambda)_{max}$ = 0.62 Å^{-1}. 5155 Reflections were unique (R_{int} = 0.0290), of which 4656 were observed [$I > 2\sigma(I)$]. 298 Parameters were refined. $R1/wR2$ [$I > 2\sigma(I)$]: 0.0290/0.0679. $R1/wR2$ [all refl.]: 0.0336/0.0702. S = 1.022. Residual electron density found between −0.24 and 0.34 e Å^{-3}.

Crystal structure of [Fe(Cl)$_2$N3PyO^{2Ph}]. One of the two lattice acetonitrile lattice solvent molecules is found to be disordered over two orientations. The occupancy factor of the major component of the disorder refines to 0.876(3). Numerical absorption correction based on gaussian integration over a multifaceted crystal model was applied using CrysAlisPro. The temperature of the data collection was controlled using the system Cryojet (manufactured by Oxford Instruments). The H atoms were placed at calculated positions using the instructions AFIX 13, AFIX 23, AFIX 43 or AFIX 137 with isotropic displacement parameters having values 1.2 or 1.5 *U*eq of the attached C atoms. The structure is partly disordered. Reference code: **xs1433a**.

Table 5.1. Experimental crystallographic report for **[Fe(Cl)$_2$N3PyO^{2Ph}]**.

Crystal data	
Chemical formula	$C_{36}H_{29}Cl_2FeN_4O \cdot 2(C_2H_3N)$
M_r	742.49
Crystal system, space group	Triclinic, *P*-1
Temperature (K)	110
a, *b*, *c* (Å)	11.5841 (3), 13.4122 (4), 13.8909 (4)
α, β, γ (°)	110.423 (3), 104.646 (2), 108.060 (2)
V (Å^3)	1757.96 (9)
Z	2
Radiation type	Mo *K*α
μ (mm^{-1})	0.62
Crystal size (mm)	0.53 × 0.33 × 0.25
Data collection	
Diffractometer	SuperNova, Dual, Cu at zero, Atlas
Absorption correction	Gaussian *CrysAlis PRO* 1.171.39.29c (Rigaku Oxford Diffraction, 2017) Numerical absorption correction based on gaussian integration over a multifaceted crystal model Empirical absorption correction using spherical harmonics, implemented in SCALE3 ABSPACK scaling algorithm.
T_{min}, T_{max}	0.419, 1.000

No. of measured, independent and observed [$I > 2\sigma(I)$] reflections	27060, 8071, 7143
R_{int}	0.027
$(\sin \theta/\lambda)_{max}$ (Å^{-1})	0.650
Refinement	
$R[F^2 > 2\sigma(F^2)]$, $wR(F^2)$, S	0.033, 0.083, 1.04
No. of reflections	8071
No. of parameters	481
No. of restraints	66
H-atom treatment	H-atom parameters constrained
$\Delta\rho_{max}$, $\Delta\rho_{min}$ (e Å^{-3})	0.69, -0.39

Crystal structure of [Fe(F)N3PyO^{2Ph}](BF$_4$). Analytical numeric absorption correction using a multifaceted crystal model was applied using CrysAlisPro. The temperature of the data collection was controlled using the system Cryojet (manufactured by Oxford Instruments). The H atoms were placed at calculated positions using the instructions AFIX 13, AFIX 23, AFIX 43 or AFIX 137 with isotropic displacement parameters having values 1.2 or 1.5 U_{eq} of the attached C atoms. The structure is partly disordered. The BF_4^- counterion is found to be disordered over two orientations, and the occupancy factor of the major component of the disorder refines to 0.62(3). Reference code: **xs1724a**.

Table 5.2. Experimental crystallographic report for **[Fe(F)N3PyO^{2Ph}](BF$_4$)**.

Crystal data	
Chemical formula	$C_{36}H_{29}FFeN_4O \cdot BF_4 \cdot 2(C_2H_3N)$
M_r	777.40
Crystal system, space group	Triclinic, *P*-1
Temperature (K)	110
a, *b*, *c* (Å)	9.8039 (4), 11.8889 (7), 15.7998 (7)
α, β, γ (°)	84.994 (4), 85.615 (3), 77.724 (4)

V (Å^3)	1789.44 (15)
Z	2
Radiation type	Cu $K\alpha$
μ (mm^{-1})	3.97
Crystal size (mm)	0.15 × 0.06 × 0.02
Data collection	
Diffractometer	SuperNova, Dual, Cu at zero, Atlas
Absorption correction	Analytical *CrysAlis PRO* 1.171.39.29c (Rigaku Oxford Diffraction, 2017) Analytical numeric absorption correction using a multifaceted crystal model based on expressions derived by R.C. Clark & J.S. Reid. (Clark, R. C. & Reid, J. S. (1995). Acta Cryst. A51, 887-897) Empirical absorption correction using spherical harmonics, implemented in SCALE3 ABSPACK scaling algorithm.
T_{min}, T_{max}	0.678, 0.954
No. of measured, independent and observed [$I > 2\sigma(I)$] reflections	22887, 6983, 5582
R_{int}	0.052
$(\sin \theta/\lambda)_{max}$ (Å^{-1})	0.616
Refinement	
$R[F^2 > 2\sigma(F^2)]$, $wR(F^2)$, S	0.042, 0.111, 1.03
No. of reflections	6983
No. of parameters	535
No. of restraints	142
H-atom treatment	H-atom parameters constrained
$\Delta\rho_{max}$, $\Delta\rho_{min}$ (e Å^{-3})	0.39, -0.32

5.3. Results and Discussion

Efforts were targeted at gleaning additional information on the O_2-activation by mononuclear nonheme iron complexes, with a focus on the generation and isolation of ferric–superoxo or other iron-oxygen intermediates. Due to the electron-donating capabilities expounded above, the axial amidate moiety was selected as a candidate for

potential dioxygen activation. The N4Py framework was chosen as the scaffold since such a framework is readily modified to affect both steric and electronic factors.[18-20]

It was proposed to initially synthesize an unmodified framework in order to optimize the metalation, then modify the framework with additional steric or electronic factors to modulate reactivity as necessary. Synthesis of the precursors proceeded smoothly, however due to the sterically-hindered nature of the precursors, as well as the potential interference of some of the functional groups present, the key reaction meant to form the amide connection unfortunately proved intractable. Several variations of the procedure were attempted, however only yielded what appeared to be products indicating rearrangement induced by the reaction conditions.

While initial attempts to synthesize the proposed axial amidate-coordinate iron(II) complex were unsuccessful, additional experimentation was performed on an alternative complex. The axial amidate framework was maintained as a viable and potentially useful target. However, the N4Py framework was rejected for the alternative proposal of a cyclam-based framework.[20] There has been previous success in isolating O_2-derived iron intermediates in mononuclear nonheme complexes, indicating the viability of the framework.[19, 21-23] The basic cyclam (1,4,8,11-tetraazacyclotetradecane) ligand was modified with an axial amide donor on one segment, while other segments were altered by inclusion of methyl substituents in the manner of TMC (1,4,8,11-tetramethyl-1,4,8,11-tetraazacyclotetradecane) (Scheme 5.5).

Scheme 5.5. Alternative proposed synthesis of axial amidate-coordinated iron(II).

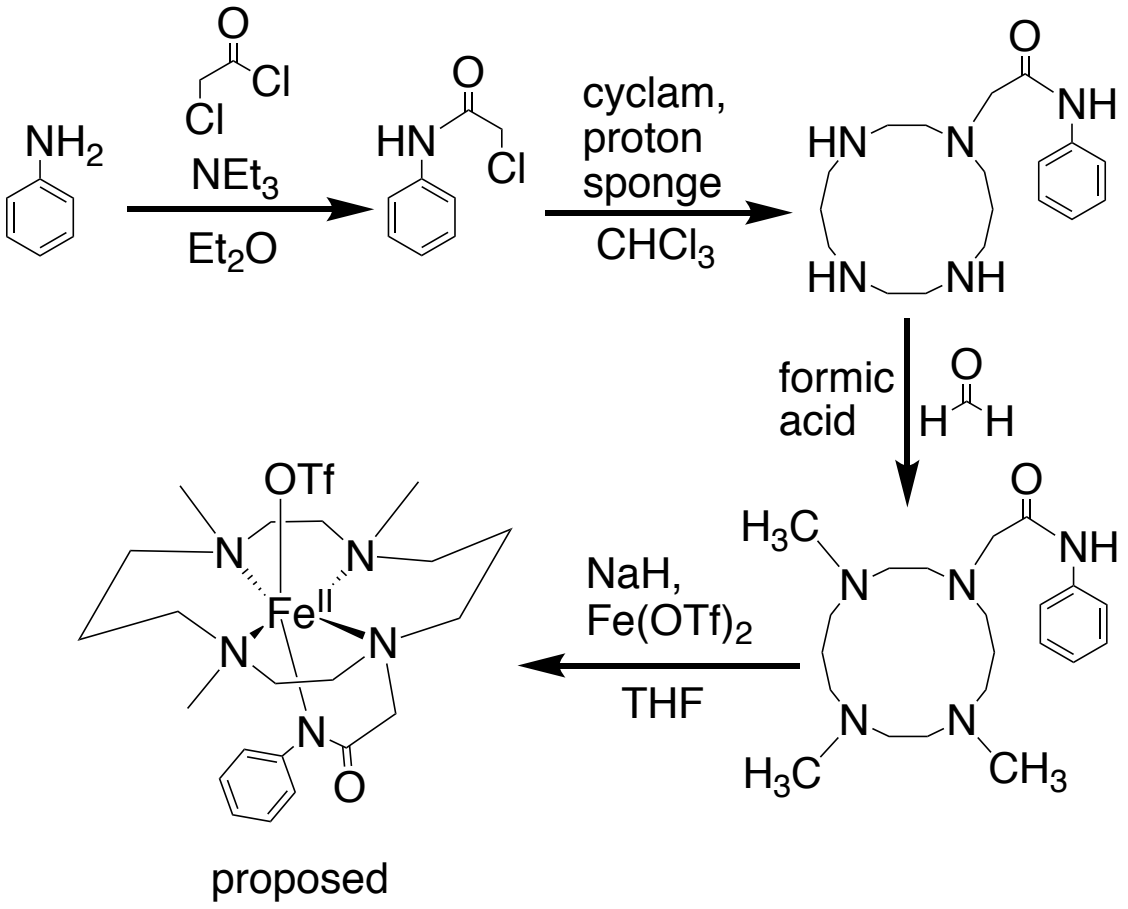

It was proposed that the steric encumbrance of methylated tertiary amines would reduce the likelihood of dimerization of the proposed iron compounds, similarly to the encumbrance achieved previously by other TMC-ligated iron complexes.[19, 22] Metalation of the complex was attempted by several methods, however the desired product was not isolated. Solutions of a complex which was oxygen-sensitive were obtained, although no crystals sufficient for X-ray crystallographic analysis were isolated. When metalation was performed utilizing $FeCl_2$, a complex was obtained wherein the TMC moiety of the ligand was bound to the metal. However, the amide remained protonated, and was unable to attach in an axially-bound manner. Thus, the target compound was not obtained.

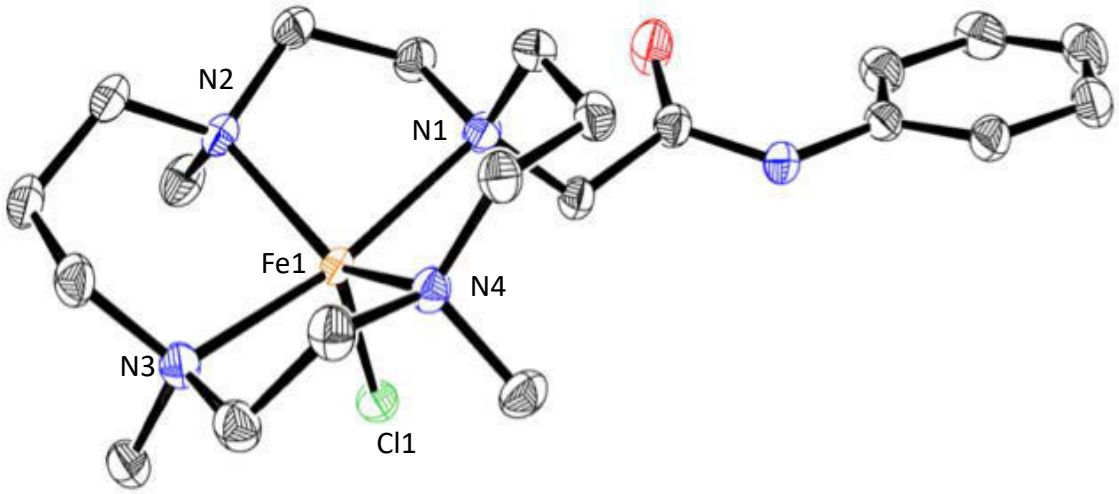

Figure 5.1. Displacement ellipsoid plot (50% probability level) of **[Fe(Cl)TMC^{Am-Ph}]Cl**. H atoms, lattice solvent molecules, and Cl counterion have been omitted for clarity. Selected bond distances (Å) and angles (°): Fe1-Cl1 2.2791(5), Fe1-N1 2.311(2), Fe1-N2 2.162(1), Fe1-N3 2.253(2), Fe1-N4 2.172(1), Cl1-Fe1-N1 96.48(4), Cl1-Fe1-N2 108.07(4), Cl1-Fe1-N3 99.46(4), Cl1-Fe1-N4 116.77(4), N1-Fe1-N2, 82.60(5), N1-Fe1-N3 164.01(5), N1-Fe1-N4 89.74(5), N2-Fe1-N3 93.62(5), N2-Fe1-N4 135.08(5), N3-Fe1-N4 81.97(5).

The crystal structure was thus 5-coordinate and a distorted square pyramidal geometry (Figure 5.1). An alternative method of deprotonation of the amide might be capable of inducing axial-ligation and potential iron-oxygen adduct formation.

It was proposed that a synthetic model might be employed in the interrogation of a direct observation of halogen rebound, in the manner of previous observations of rebound performed by this group.[1, 24] While model complexes that have been previously investigated in this research group have contained hydroxide or methoxide donors for performance of oxygen rebound, an additional compound was synthesized wherein the

presence of iron(III)-chloride species allowed for the potential to directly probe the key halogen rebound step.

Through modification and adaptation of an existing phenolate-based ligand functionalized with phenyl substituents, a ferric–halogen compound was synthesized. Reaction with an initial ferrous chloride reagent under oxygen-free conditions followed by exposure to atmospheric oxygen induced the formation of a green solution. Crystallization of the green solution was achieved by vapor diffusion of diethyl ether into an acetonitrile solution of the compound.

Scheme 5.6. Formation and isolation of an iron(III)-chloride mononuclear model complex.

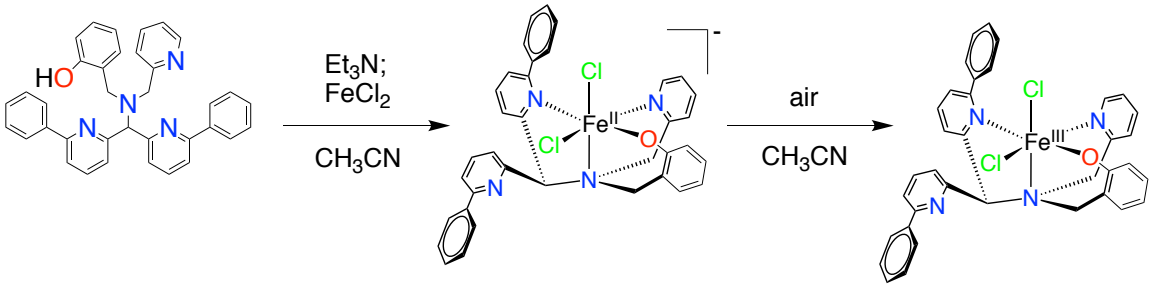

The resulting crystals contained significant amounts of side-product salts, which impeded growth of larger amounts of the target compound. However the product was characterized by X-ray diffraction, revealing a dichloride structure wherein one of the phenyl-substituted pyridyl moieties had been displaced through incorporation of a second chloride ligand.

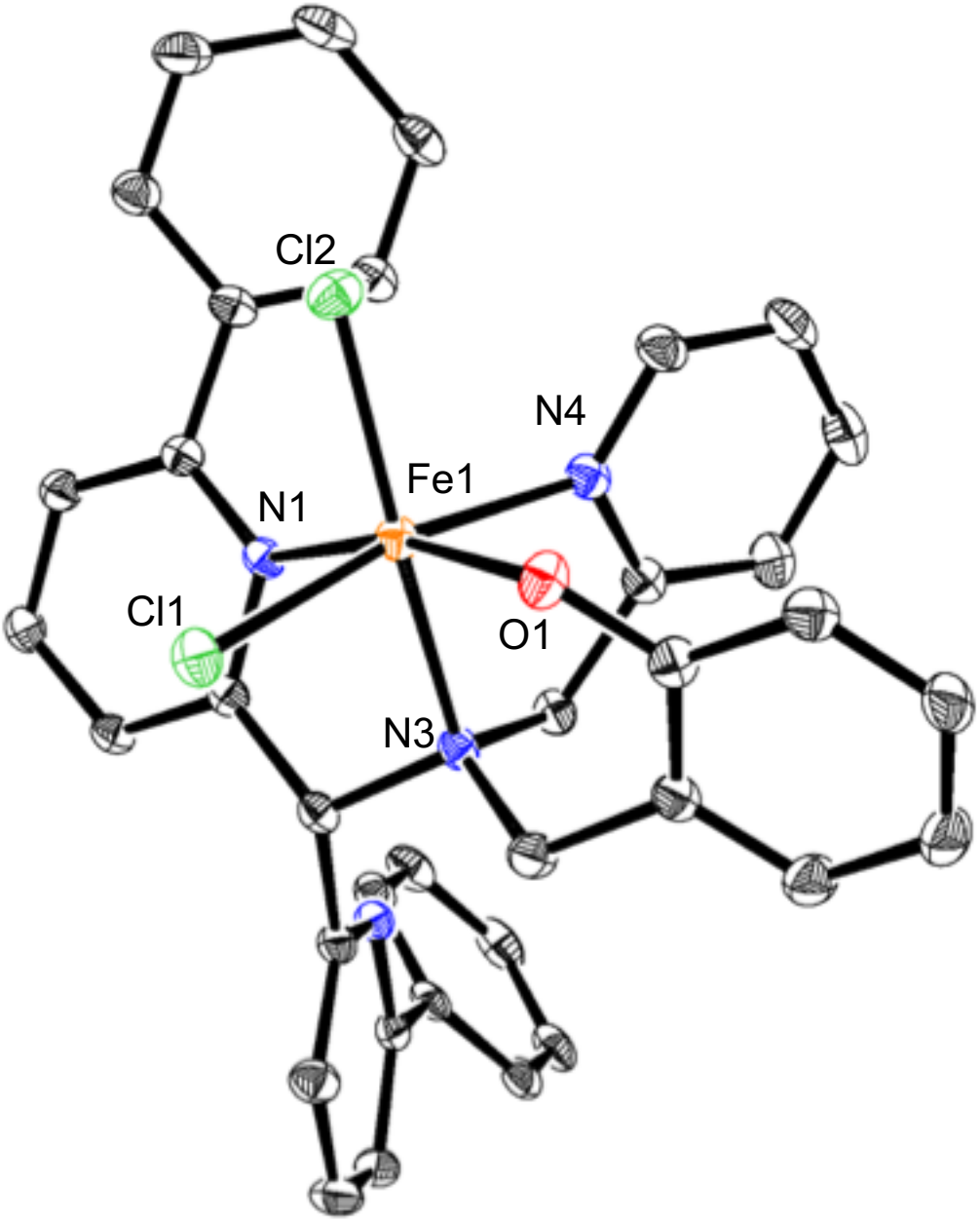

Figure 5.2. Displacement ellipsoid plot (50% probability level) of **[Fe(Cl)$_2$N3PyO^{2Ph}]**. H atoms and lattice solvent molecules have been omitted for clarity. Selected bond distances (Å) and angles (°): Fe1-N1 2.314(2), Fe1-N3 2.235(1), Fe1-N4 2.168(2), Fe1-O1 1.908(1), Fe1-Cl1 2.3313(6), Fe1-Cl2 2.2675(4), Cl1-Fe1-Cl2 97.13(2), Cl1-Fe1-N1 89.47(4), Cl1-Fe1-N3 92.27(4), Cl1-Fe1-N4 168.99(4), Cl1-Fe1-O1, 92.64(4), Cl2-Fe1-N1 97.63(4), Cl2-Fe1-N3 165.74(4), Cl2-Fe1-N4 93.82(4), Cl2-Fe1-O1 99.96(4), N1-Fe1-N3 71.67(5),

N1-Fe1-N4 90.19(5), N1-Fe1-O1 161.87(5), N3-Fe1-N4 77.19(5), N3-Fe1-O1 90.25(5), N4-Fe1-O1 84.34(6).

When Gomberg's dimer $(Ph_3C)_2$, a trityl radical source, was reacted with $[Fe(Cl)_2N3PyO^{2Ph}]$, the green color disappeared and became yellow, indicating reaction with trityl radical and likely formation of an Fe^{II} product (Figure 5.3). It was also proposed that concurrent formation of a trityl chloride material had occurred.

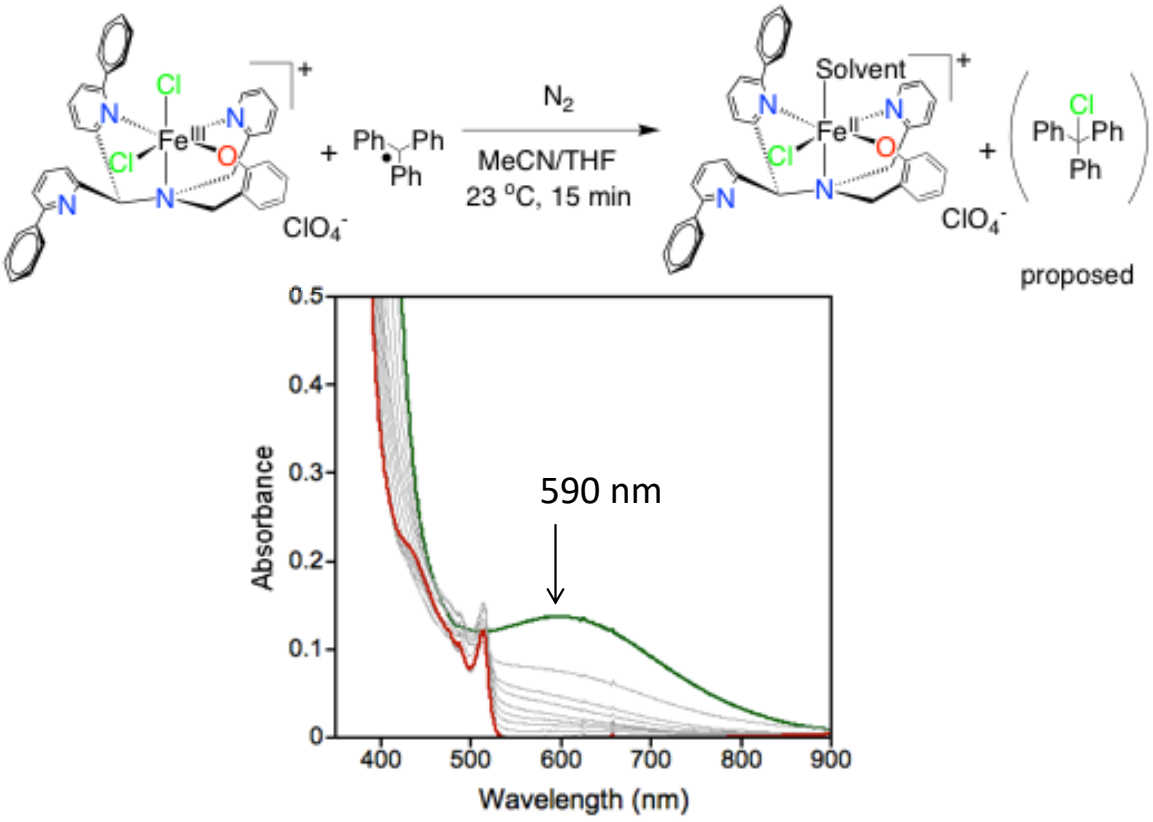

Figure 5.3. Reaction of **$[Fe^{III}(Cl)_2(N3PyO^{2Ph})]$** and $(Ph_3C)_2$ in THF/Acetonitrile at 23 °C, monitored by UV-vis spectroscopy over the course of 15 min.

These observations indicated potential rebound reactivity, and lead to future investigations into the halogen rebound process within a mononuclear nonheme complex. Although the

synthesis was reattempted, co-formation of copious accompanying salt formations prevented the isolation of additional samples of [Fe(Cl)$_2$N3PyO^{2Ph}].

The halogenase enzymes work readily with chlorine, but there is some question as to the process by which a fluorine atom might be transferred. Previously in this research group there have been observed some formation of Fe^{III}(F) complexes which might be potential platforms through which the rebound step might be directly interrogated for putative fluoride rebound, or else determination of the mechanism of fluorine transfer.[25]

Reaction of the previously-investigated [Fe^{II}(N4Py^{2Ph2F})(CH$_3$CN)](ClO$_4$)$_2$ with IBX-ester oxidant produced a side-product in a small amount that was characterized by X-ray diffraction (Scheme 5.7).

Scheme 5.7. Formation of Fe^{III}(F) side-product.[25]

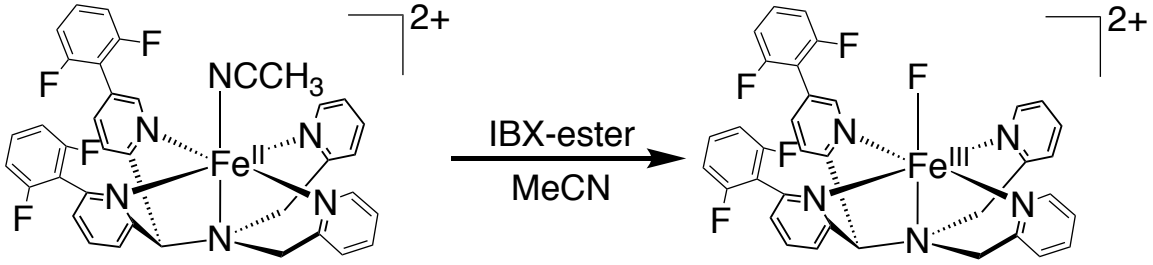

Isolation and characterization of the side product revealed [Fe^{III}(F)(N4Py^{2Ph2F})](ClO$_4$)$_2$, likely generated by errant interaction with free fluoride material from synthesis of precursors, and subsequent oxidation processes. However the material was not formed in amounts large enough to pursue further, and was not significantly investigated.

While the above compound was not a viable opportunity for pursuance of the potential for fluorine rebound in a mononuclear nonheme complex, additional work was done to generate a complex with such potential. Reaction of the known N3Py^{2Ph}OH ligand with ferrous material in the presence of a $(BF_4)^-$ counterion, followed by the exposure of

the material to atmospheric oxygen brought about formation of a deep blue solution (Scheme 5.8).

Scheme 5.8. Formation of a phenolate-bound $Fe^{III}(F)$ complex.

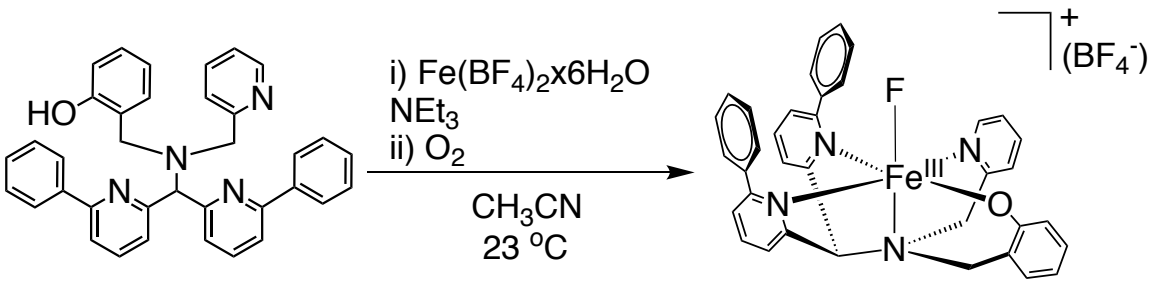

Formation of the $Fe^{III}(F)$ product was likely due to interaction with free fluoride impurity and ferrous material which may be capable of attaching onto the fluoride. While the product was generated, isolated, and characterized by XRD as $[Fe^{III}(F)(N3PyO^{2Ph})](BF_4)$ (Figure 5.4), the small amount isolated was likely evidence of existence as a side product of a secondary reaction, and was not subsequently repeated.

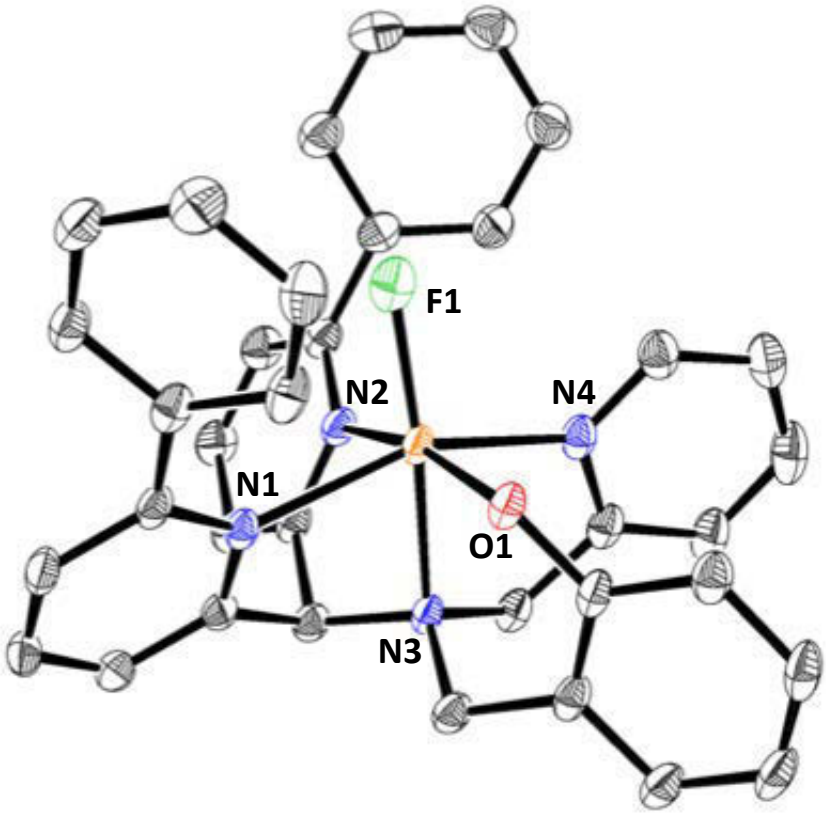

Figure 5.4. Displacement ellipsoid plot (50% probability level) of **[Fe(F)N3PyO^{2Ph}](BF$_4$)**. H atoms, lattice solvent molecules, and BF_4^- counterion have been omitted for clarity. Selected bond distances (Å) and angles (°): Fe1-N1 2.236(2), Fe1-N2 2.308(2), Fe1-N3 2.190(2), Fe1-N4 2.123(2), Fe1-O1 1.898(2), Fe1-F1 1.872(2), N1-Fe1-N2 83.61(7), N1-Fe1-N3 76.49(7), N1-Fe1-N4 154.20(7), N1-Fe1-O1, 97.03(7), N1-Fe1-F1 102.56(7), N2-Fe1-N3 73.18(7), N2-Fe1-N4 86.45(7), N2-Fe1-O1 162.69(7), N2-Fe1-F1 93.75(7), N3-Fe1-N4 77.86(7), N3-Fe1-O1 90.09(7), N3-Fe1-F1 166.93(7), N4-Fe1-O1 86.66(7), N4-Fe1-F1 101.79(7).

However, when the available ferric material was dissolved in an airfree CH_3CN solution, it was found to be capable of reacting with $(Ph_3C)_2$ at room temperature to consume the Fe^{III}(F) material (Figure 5.5). The reactivity appeared similar to that observed in both

$Fe^{III}(OCH_3)$ and $Fe^{III}(Cl)$ material, which was a possible indication of rebound-like reactivity and proposed formation of Fe^{II} and trityl fluoride.

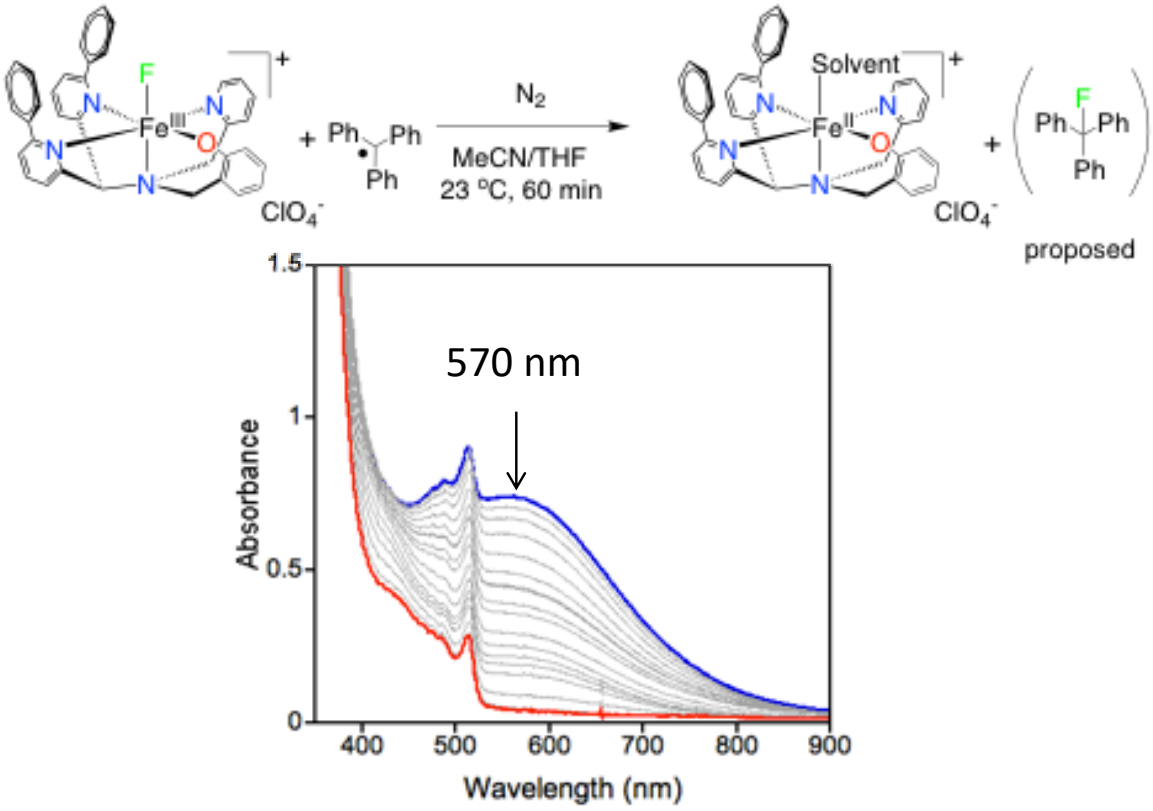

Figure 5.5. Reaction of **$[Fe^{III}(F)(N3PyO^{2Ph})](BF_4)$** and $(Ph_3C)_2$ in THF/Acetonitrile at 23 °C, monitored by UV-vis spectroscopy over the course of 60 min.

While unable to explore further without the synthesis of additional material, potential evidence for rebound reactivity to generate a new C-F bond foreshadows further advances in the understanding of the rebound mechanism in mononuclear nonheme iron complexes.

5.4. Conclusions

Several avenues of reactivity have been explored, with some compounds presenting interesting models for halogen rebound when reacted with organic radicals. Further insight into nonheme iron model halogen rebound would give a greater understanding of the

nonheme halogenase enzymes, and presents an additional method of investigating the rebound paradigm.

5.5. Supporting Information

Contents

I. Supporting Figures

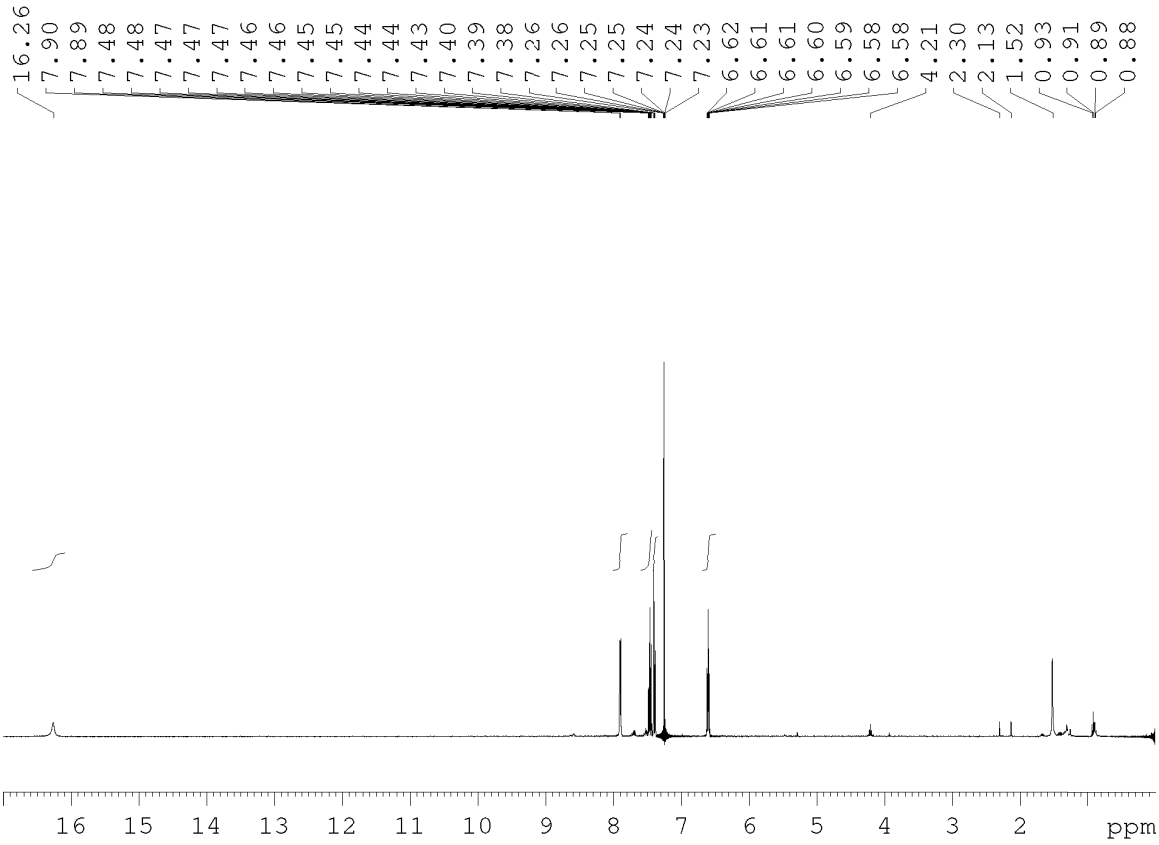

Figure 5.6. ^{1}H NMR spectrum of bis(pyridin-2-yl)acetonitrile in $CDCl_3$.

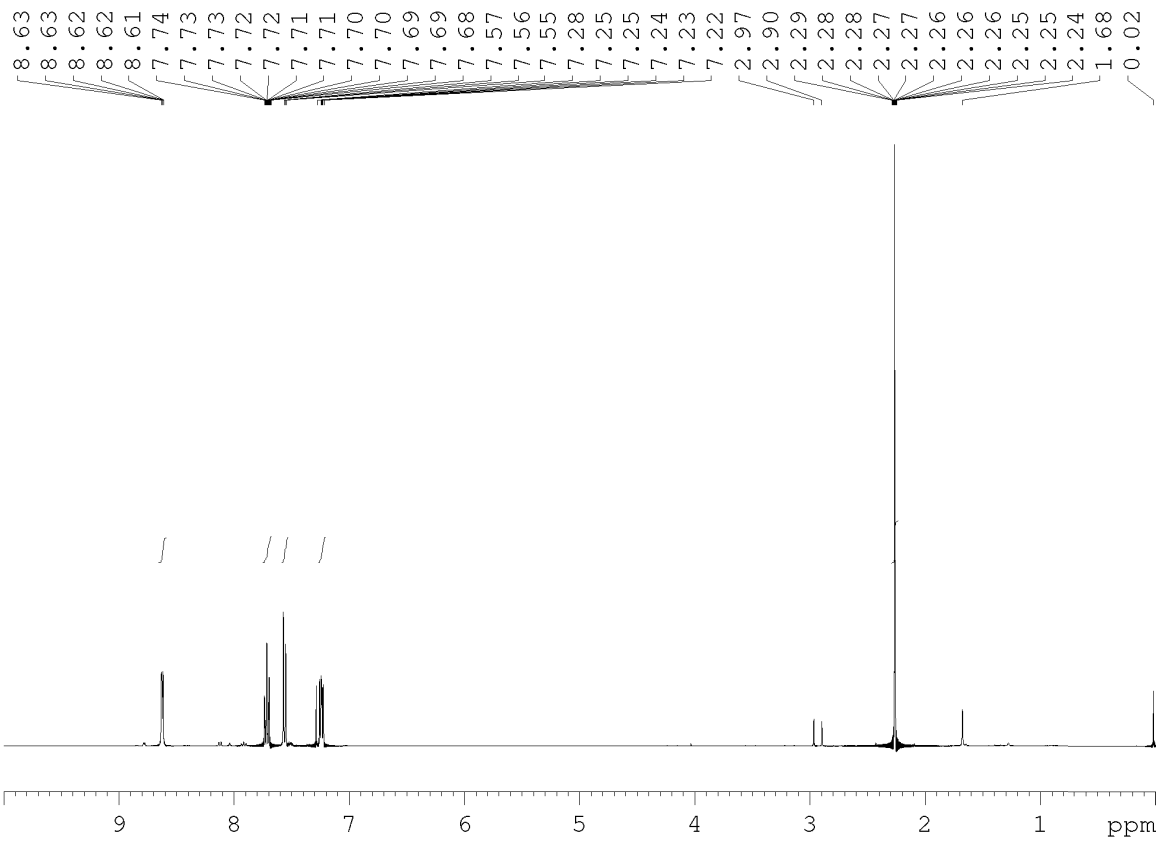

Figure 5.7. ^{1}H NMR spectrum of 2,2-bis(pyridine-2-yl)propionitrile in $CDCl_3$.

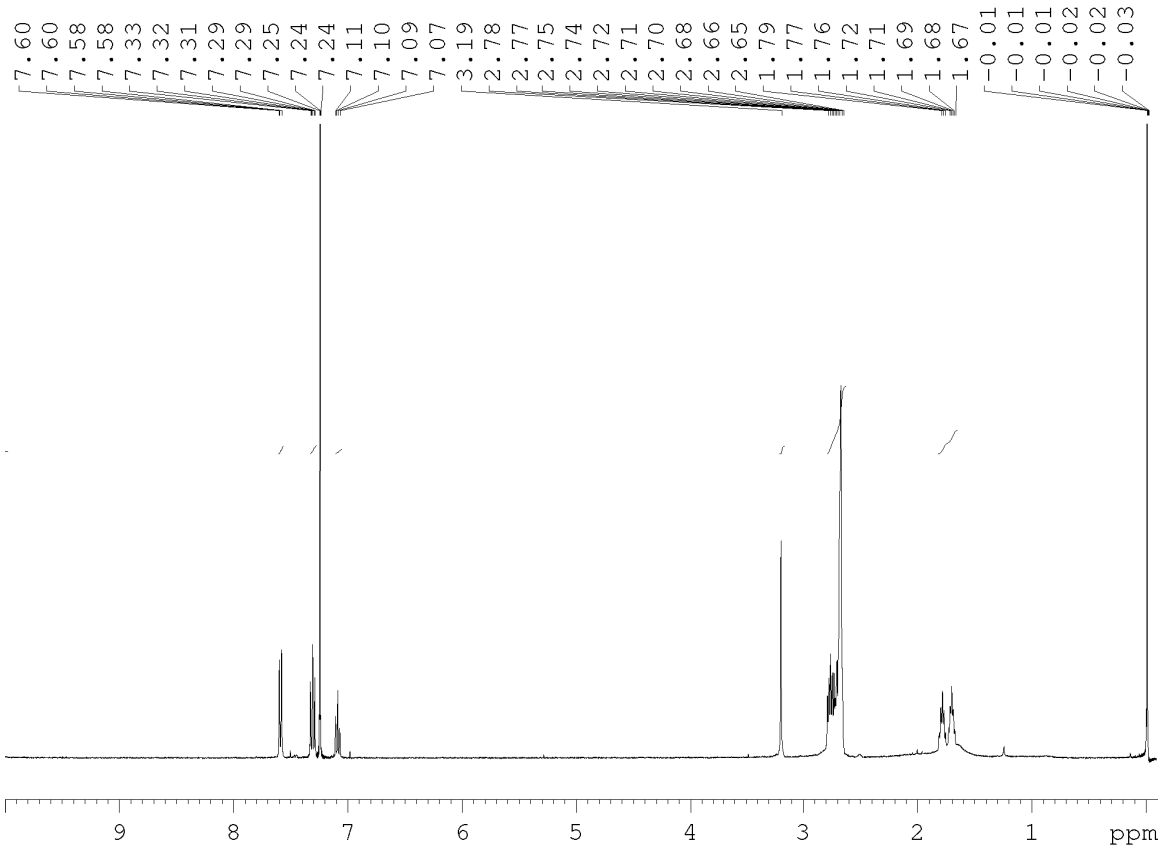

Figure 5.8. ^{1}H NMR spectrum of 2-(1,4,8,11-tetraazacyclotetradecan-1-yl)-N-phenylacetamide in $CDCl_3$.

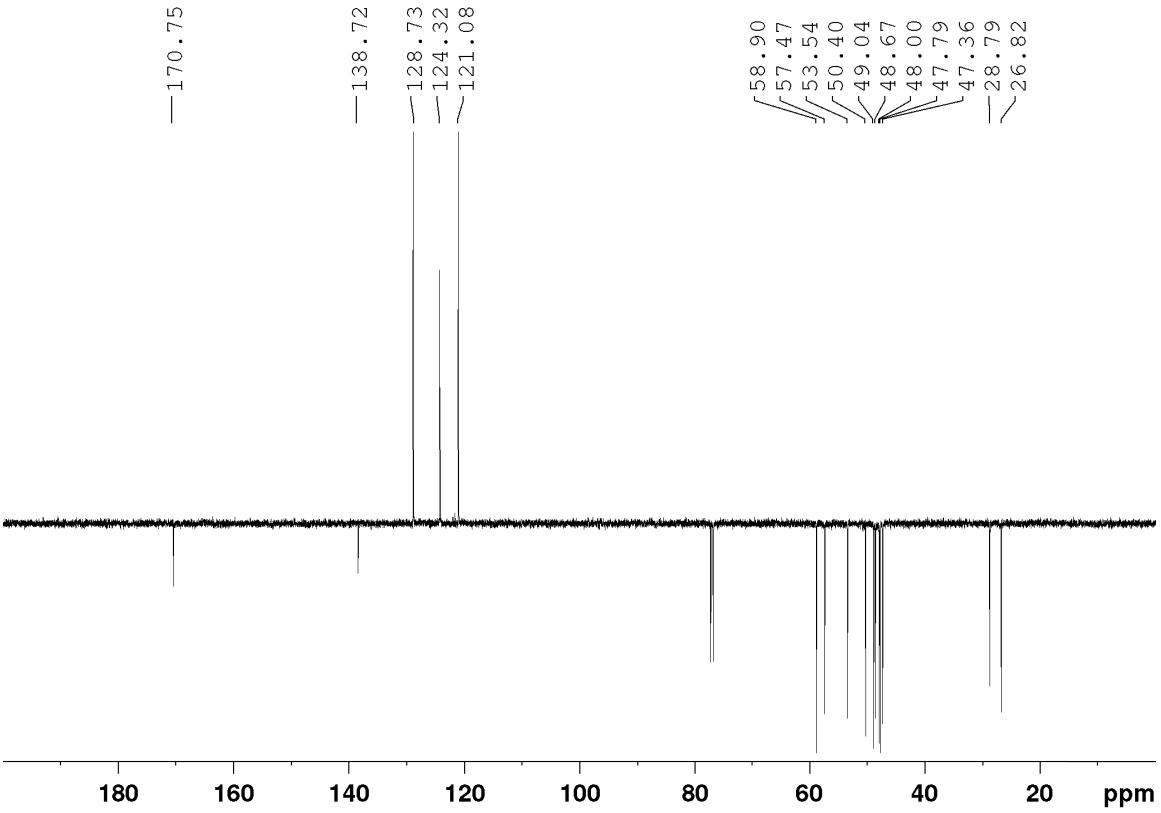

Figure 5.9. ^{13}C NMR spectrum of 2-(1,4,8,11-tetraazacyclotetradecan-1-yl)-N-phenylacetamide in $CDCl_3$.

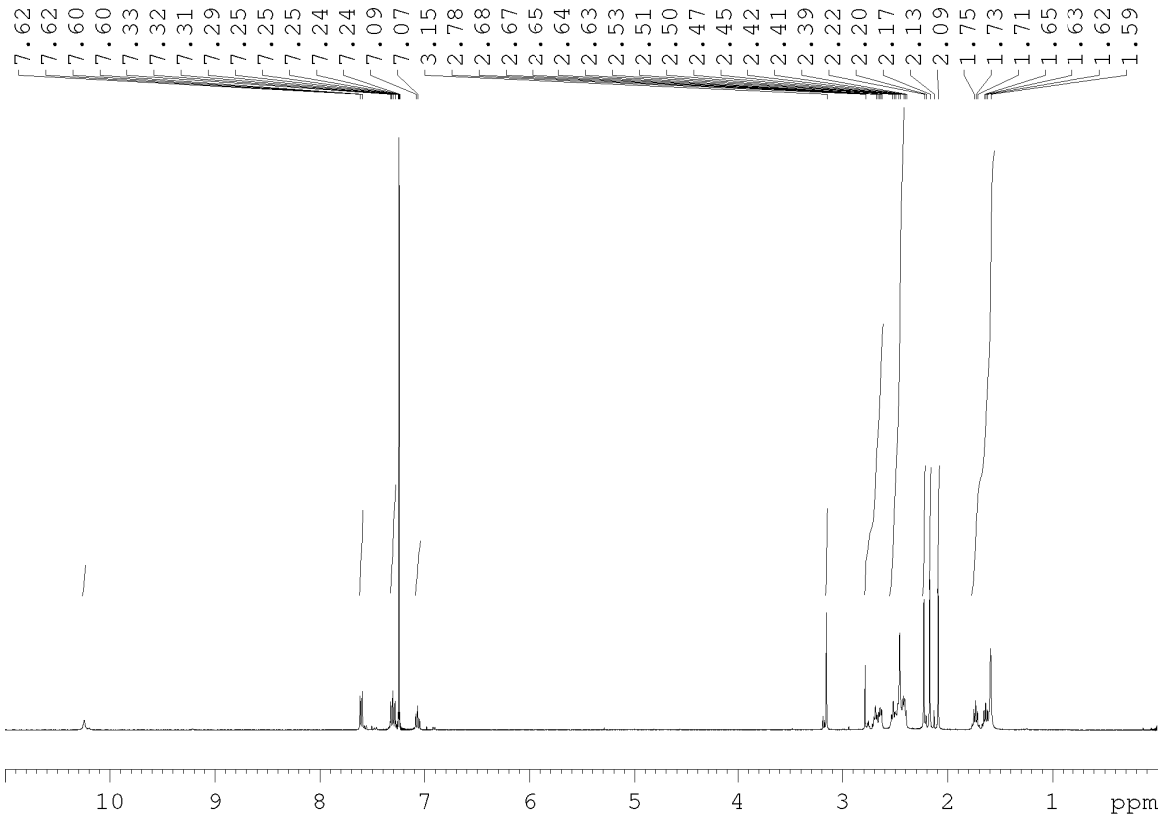

Figure 5.10. ^{1}H NMR spectrum of N-phenyl-2-(4,8,11-trimethyl-1,4,8,11-tetraazacyclotetradecan-1-yl)acetamide in $CDCl_3$.

5.6. References

1. Pangia, T. M.; Davies, C. G.; Prendergast, J. R.; Gordon, J. B.; Siegler, M. A.; Jameson, G. N. L.; Goldberg, D. P., *J. Am. Chem. Soc.* **2018,** *140*, 4191-4194.

2. Cho, K. B.; Hirao, H.; Shaik, S.; Nam, W., *Chem. Soc. Rev.* **2016,** *45*, 1197-210.

3. Dunham, N. P.; Chang, W.-c.; Mitchell, A. J.; Martinie, R. J.; Zhang, B.; Bergman, J. A.; Rajakovich, L. J.; Wang, B.; Silakov, A.; Krebs, C.; Boal, A. K.; J. Martin Bollinger, J., *J. Am. Chem. Soc.* **2018,** *140*, 7116-7126.

4. Liao, H.-J.; Li, J.; Huang, J.-L.; Davidson, M.; Kurnikov, I.; Lin, T.-S.; Lee, J. L.; Kurnikova, M.; Guo, Y.; Chan, N.-L.; Chang, W.-c., *Angew. Chem. Int. Ed.* **2018,** *57*, 1831-1835.

5. Mitchell, A. J.; Zhu, Q.; Maggiolo, A. O.; Anath, N. R.; Hillwig, M. L.; Liu, X.; Boal, A. K., *Nat. Chem. Biol.* **2016,** *12*, 636-640.

6. Matthews, M. L.; Neumann, C. S.; Miles, L. A.; Grove, T. L.; Booker, S. J.; Krebs, C.; Walsh, C. T.; Bollinger, J. M., Jr., *Proc. Natl. Acad. Sci.* **2009,** *106*, 17723-17728.

7. Martinie, R. J.; Livada, J.; Chang, W.; Green, M. T.; Krebs, C.; Bollinger, J. M., Jr.; Silakov, A., *J. Am. Chem. Soc.* **2015,** *137*, 6912-6919.

8. Wong, C.; Fujimori, D. G.; Walsh, C. T.; Drennan, C. L., *J. Am. Chem. Soc.* **2009,** *131*, 4872-4879.

9. Planas, O.; Clemancey, M.; Latour, J.-M.; Company, A.; Costas, M., *Chem. Commun.* **2014,** *50*, 10887-10890.

10. Puri, M.; Biswas, A. N.; Fan, R.; Guo, Y.; Que, L., Jr., *J. Am. Chem. Soc.* **2016,** *138*, 2484-2487.

11. Aime, S.; Botta, M.; Parker, D.; Williams, J. A. G., *J. Chem. Soc. Dalton Trans.* **1995**, 2259-2266.

12. Roelfes, G.; Vrajmasu, V.; Chen, K.; Ho, R. Y. N.; Rohde, J.-U.; Zondervan, C.; Crois, R. M. l.; Schudde, E. P.; Lutz, M.; Spek, A. L.; Hage, R.; Feringa, B. L.; Münck, E.; Lawrence Que, J., *Inorg. Chem.* **2003,** *42*, 2639-2653.

13. Newkome, G. R.; Evans, D. W.; Kiefer, G. E.; Theriot, K. J., *Organometallics* **1988,** *7*, 2537-2542.

14. Gullickson, G. C.; Lewis, D. E., *Synthesis* **2003,** *2003*, 681-684.

15. Barefield, E. K.; Wagner, F., *Inorg. Chem.* **1973,** *12*, 2435-2439.

16. Sheldrick, G. M., *Acta Cryst.* **2008,** *A64*, 112-122.

17. Sheldrick, G. M., *Acta Cryst.* **2015,** *C71*, 3-8.

18. Sahu, S. Z., Bo; Pollock, Christopher J.; Durr, Maximilian; Davies, Casey G.; Confer, Alex M.; Ivanović-Burmazović, Ivana; Siegler, Maxime A.; Jameson, Guy N. L.; Krebs, Carsten; Goldberg, David P., *J. Am. Chem. Soc.* **2016,** *138*, 12791-12802.

19. Sahu, S.; Goldberg, D. P., *J. Am. Chem. Soc.* **2016,** *138*, 11410-11428.

20. Sahu, S.; Widger, L. R.; Quesne, M. G.; de Visser, S. P.; Matsumura, H.; Moënne-Loccoz, P.; Siegler, M. A.; Goldberg, D. P., *J. Am. Chem. Soc.* **2013,** *135*, 10590-10593.

21. Thibon, A.; England, J.; Martinho, M.; Victor G. Young, J.; Frisch, J. R.; Guillot, R.; Girerd, J.-J.; Münck, E.; Lawrence Que, J.; Banse, F., *Angew. Chem. Int. Ed.* **2008,** *47*, 7064-7067.

22. Lee, Y.-M.; Hong, S.; Morimoto, Y.; Shin, W.; Fukuzumi, S.; Nam, W., *J. Am. Chem. Soc.* **2010,** *132*, 10668-10670.

23. Li, F.; Heuvelen, K. M. V.; Meyer, K. K.; Münck, E.; Lawrence Que, J., *J. Am. Chem. Soc.* **2013,** *135*, 10198-10201.

24. Zaragoza, J. P. T.; Yosca, T. H.; Siegler, M. A.; Moënne-Loccoz, P.; Green, M. T.; Goldberg, D. P., *J. Am. Chem. Soc.* **2017,** *139*, 13640-13643.

25. Sahu, S.; Quesne, M. G.; Davies, C. G.; Dürr, M.; Ivanović-Burmazović, I.; Siegler, M. A.; Jameson, G. N. L.; Visser, S. P. d.; Goldberg, D. P., *J. Am. Chem. Soc.* **2014,** *136*, 13542-13545.

Thomas Pangia
116 West University Parkway
Baltimore, MD, 21210

Education

August 2007 - May 2012	B.S. in Chemistry Georgia College & State University Milledgeville, GA
September 2012 - May 2014	M.A. in Chemistry The Johns Hopkins University Baltimore, MD
May 2014 - January 2019	Ph.D. in Chemistry The Johns Hopkins University Baltimore, MD

Objectives

Organic, organometallic, and inorganic synthesis for industrial applications or formation of useful, naturally produced molecules.
Develop or improve chemical reactions or catalysts to aid in the achievement of natural product synthesis.
Combine knowledge of investing and business with chemistry to understand corporate aspects of chemical-based companies, toward teaching the application of science to business.

Achievements

Capable of identifying useful synthetic disconnects, towards the formation of target molecules.
Can set and achieve realistic goals, as well as perform and complete multiple projects simultaneously.
Able to work well with groups, or work independently with minimal guidance.

Publications

Pangia, Thomas M.; Davies, Casey G.; Prendergast, Joshua R.; Gordon, Jesse B.; Siegler, Maxime A.; Jameson, Guy N. L.; Goldberg, David P. "Observation of Radical Rebound in a Mononuclear Nonheme Iron Model Complex". *J. Am. Chem. Soc.*, **2018**, 140, 4191-4194.

Work Experience

Teaching:

Spring 2016 Introduction to Chemistry II Laboratory Teaching Assistant, Johns Hopkins University, Baltimore, MD. Led a weekly lab section for introductory chemistry labs.

Fall 2015 Problem Solving for Introductory Chemistry I Instructor, Johns Hopkins University, Baltimore, MD. Taught a twice-weekly lecture section based around application-based learning practices, to improve material retention from the large-group lecture setting.

Fall 2015 Introductory Chemistry I Head Teaching Assistant, Johns Hopkins University, Baltimore, MD. Coordinated teaching assistants in the supplemental instruction of students to aid learning comprehension.

Fall 2014 Organic Chemistry I Teaching Assistant, Johns Hopkins University, Baltimore, MD. Led weekly lectures to supplement regular class attendance and aid students in their grasp of first-semester organic chemistry concepts.

Spring 2014 Intermediate Chemistry II Teaching Assistant, Johns Hopkins University, Baltimore, MD. Guided students in a laboratory setting to aid in their comprehension of lecture materials, using application of theories as a learning tool.

Fall 2013 Introductory Chemistry I Head Teaching Assistant, Johns Hopkins University, Baltimore, MD. Supervised teaching assistants while leading supplementary instruction sections to improve student comprehension.

Fall 2013 Introductory Chemistry I Laboratory Head Teaching Assistant, Johns Hopkins University, Baltimore, MD. Supervised teaching assistants during a weekly lab section for an introductory chemistry lab.

Spring 2013 Introduction to Chemistry II Teaching Assistant, Johns Hopkins University, Baltimore, MD. Led discussion-based instruction sessions to increase student comprehension and retention.

Spring 2013 Introduction to Chemistry II Laboratory Teaching Assistant, Johns Hopkins University, Baltimore, MD. Supervised a weekly lab section for introductory chemistry labs.

Fall 2012 Introduction to Chemistry I Teaching Assistant, Johns Hopkins University, Baltimore, MD. Led discussion-based instruction sessions to increase student comprehension and retention.

Fall 2012 Introduction to Chemistry I Laboratory Teaching Assistant, Johns Hopkins University, Baltimore, MD. Supervised a weekly lab section for introductory chemistry labs.

Spring 2012 Survey of Chemistry II Supplemental Instructor, Georgia College & State University, Milledgeville, GA. Led peer-instruction sessions based on introductory organic chemistry/biochemistry topics.

Fall 2011 Introduction to Chemistry I Supplemental Instructor, Georgia College & State University, Milledgeville, GA: Helped increase students' understanding of lecture topics with additional supplemental learning sessions.

Fall 2010 Survey of Chemistry I Supplemental Instructor, Georgia College & State University, Milledgeville, GA: Aided in student comprehension by leading supplemental sessions focusing on introductory chemistry.

Spring 2010 Organic Chemistry II Supplemental Instructor, Georgia College & State University, Milledgeville, GA: Built on professors' lecture topics by conducting additional peer - led supplemental sessions geared toward the second semester organic chemistry student.

Research:

Spring 2013 - Present Graduate Research: Worked in the Goldberg Research Group at Johns Hopkins on the proposal and synthesis of nonheme iron model complexes.

Summer 2011 REU (Research Experience for Undergraduates), University of Memphis, Memphis TN: Worked with the Burkey Research Group on designing a new photochromic system and collaborated with the Webster Research Group to computationally predict potential properties.

Summer 2010 REU (Research Experience for Undergraduates), University of Memphis, Memphis TN: Worked with the Burkey Research Group on the development of a bistable photochromic material with applications in optical storage devices.

Spring 2009 - Spring 2012 Undergraduate Research: Worked in the Cossey Research Group at Georgia College on the implementation of a multistep formal synthesis of members of a natural product series.

Awards/Scholarships

May 2014	2014 - 2015 Johns Hopkins University Ernest M. Marks Award for excellence in teaching.
April 2014	2014 - 2015 Johns Hopkins University Owen Scholars Award for outstanding graduate students.

April 2013	2013 - 2014 Johns Hopkins University Owen Scholars Award for outstanding graduate students.
April 2012	2012 - 2013 Johns Hopkins University Owen Scholars Award for outstanding entering graduate students.
April 2012	2011 - 2012 Georgia College & State University Outstanding Student in Math and Sciences Disciplines.
April 2012	2011 - 2012 Baarda-Hargaden Endowment: Georgia College & State University Chemistry, Physics and Astronomy department outstanding senior award.
April 2012	2011 - 2012 Georgia College & State University outstanding chemistry major.
October 2011	2011 - 2012 Faculty - General Scholarship: Georgia College & State University award for academic excellence
April 2011	2011 - 2012 Clyde E. Keeler Science Award: Georgia College & State University award for excellence in undergraduate research
May 2010	2010 - 2011 Ralph Norman Scholarship: Georgia College & State University award for academic excellence
May 2010	2010 - 2011 Faculty - General Scholarship: Georgia College & State University award for academic excellence
April 2010	2010 - 2011 Georgia College & State University Louise McWilliams Christian Outstanding Junior Chemistry Major Award
August 2009	2009-2010 National Phi Kappa Phi Emerging Scholar Award
April 2009	2009 - 2010 Georgia College & State University Jesse Trawick Outstanding Sophomore Chemistry Major Award
January 2009 – May 2012	Georgia College & State University Chemistry Scholar
January 2009 - May 2012	Georgia College & State University President's List

Presentations

July 20, 2016	Poster Presentation: "Evidence of Radical Rebound in a Non-Heme Iron Model Complex" University of Pennsylvania Department of Chemistry, Mid-Atlantic Seaboard Inorganic Symposium (MASIS) 2016
April 21, 2012	Oral Presentation: "Investigation of a Microwave Induced Diels Alder Reaction" Georgia College Department of Chemistry, Physics and Astronomy 7th Annual Undergraduate Showcase
April 13, 2012	Oral Presentation: "Exploration of a Microwave-Induced Diels Alder Reaction" 15th Annual Georgia College Student Research Conference
August 12, 2011	Oral Presentation: "Proposed Synthesis of a Di-functional Di-tethered Manganese Tricarbonyl"-Conclusion of 2011 Summer Undergraduate Research at the University of Memphis

April 23, 2011	Poster Presentation: "Formal Synthesis of the Schweinfurthin Series"-Georgia College & State University Department of Chemistry, Physics and Astronomy 6th Annual Undergraduate Showcase
April 15, 2011	Oral Presentation: "Formal Synthesis of the Schweinfurthin Series"-14th Annual Georgia College Student Research Conference
March 29, 2011	Poster: "Potential Characteristics and Proposed Synthesis of a Predicted Photochromic Isomeric Pair"-241st ACS National Meeting and Exposition
February 26, 2011	Oral Presentation: "Proposed Synthesis of a Predicted Photochromic Isomeric System"-31st Annual University of Memphis Undergraduate Research Conference
August 13, 2010	Oral Presentation: "Potential Characteristics and Proposed Synthesis of a Predicted Photochromic Isomeric Pair"-Conclusion of 2010 Summer Undergraduate Research at the University of Memphis
April 25, 2009	Poster Presentation: "Organic Synthesis of Natural Products Using the Diels Alder Reaction"

Professional Memberships

March 2011 - present	Kappa Mu Epsilon Mathematics Honor Society
April 2011 - present	Phi Kappa Phi Honor Society
January 2009 - present	American Chemical Society